

# An integrative perspective on extreme convective precipitation events in the southeastern Alpine forelands: Scaling relationships and damage contribution

Katharina Schröer

May 2020

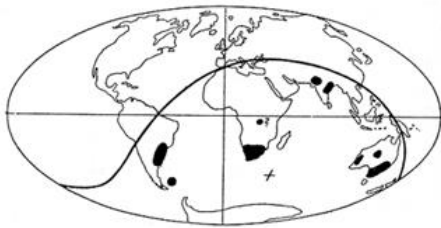


Financially supported by



The **Wegener Center for Climate and Global Change** is an interdisciplinary, internationally recognized research and graduate education institute of the University of Graz that is pooling the University's expertise in Climate, Environmental and Global Change. It brings together research teams and scientists from fields such as geophysics and climate physics, meteorology, economics, geography, and regional sciences. At the same time close links are maintained and further developed with many national and international cooperation partners. The research interests range from monitoring, analysis, and modeling of climate and environmental change to the investigation of climate change impacts and the analysis of the human dimensions of these changes related to mitigation, adaptation, and loss&damage. (more information at [www.wegcenter.at](http://www.wegcenter.at))

The present report is the result of a PhD thesis work completed in December 2018. The work was funded by the Austrian Science Fund (FWF) under research grant W 1256-G15 (Doctoral Programme Climate Change – Uncertainties, Thresholds and Coping Strategies)



**Alfred Wegener** (1880-1930), after whom the Wegener Center is named, was founding holder of the University of Graz Geophysics Chair (1924-1930). In his work in the fields of geophysics, meteorology, and climatology he was a brilliant scientist and scholar, thinking and acting in an interdisciplinary way, far ahead of his time with this style. The way of his ground-breaking research on continental drift is a shining role model—his sketch on the relations of continents based on traces of an ice age about 300 million years ago (left) as basis for the Wegener Center Logo is thus a continuous encouragement to explore equally innovative ways: *paths emerge in that we walk them* (Motto of the Wegener Center).

## Wegener Center Verlag • Graz, Austria

© 2019 All Rights Reserved.

Selected use of individual figures, tables or parts of text is permitted for non-commercial purposes, provided this report is correctly and clearly cited as the source. Publisher contact for any interests beyond such use: [wegcenter@uni-graz.at](mailto:wegcenter@uni-graz.at).

ISBN 978-3-9504717-6-2

May 2020

Contact: Dr. Katharina Schroeer  
[katharina.schroeer@posteo.net](mailto:katharina.schroeer@posteo.net)

Wegener Center for Climate and Global Change  
University of Graz  
Brandhofgasse 5  
A-8010 Graz, Austria  
[www.wegcenter.at](http://www.wegcenter.at)

Katharina SCHROEER

**An integrative perspective on extreme convective precipitation  
events in the southeastern Alpine forelands:  
Scaling relationships and damage contribution**

**PhD thesis**

to obtain the academic degree  
Doctor of Natural Sciences

submitted to the  
Faculty of Environmental and Regional Sciences and Education  
University of Graz

Supervisor

**Univ.-Prof. Dr. Gottfried Kirchengast**  
University of Graz, Austria

Co-supervisor

**Univ.-Prof. Dr. Oliver Sass**  
University of Graz, Austria and  
University of Bayreuth, Germany

External Supervisor

**Dr. Mari R. Tye**  
National Center for Atmospheric Research, Boulder, USA

This thesis was completed in November 2018 and editorially updated in December 2019.  
Chapter 4 was updated in section 4.2 (Research article 2) to the final published paper  
version (replacing the early-online published version) and minor editorial updates and  
corrections were made in the text.



## Acknowledgements

Many friends and colleagues have contributed to making the work on this thesis productive and enjoyable. My sincere gratitude goes to all of them. I thank Gottfried Kirchengast for being a reliable and supportive supervisor; I found a trustful and honest environment, with space for creativity, freedom, and debate. Special thanks go to Mari R. Tye for many discussions and scientific advice, both face-to-face and long-distance. Her nudges in the right direction and refreshing nonchalance were encouraging beyond the scientific matter. Sincere gratitude also goes to Andi Prein for facilitating my stay at NCAR, and providing support and advice both scientifically and as a friend. I want to thank James, Cindy, Erin, Greg, and all members of the C3WE and Regional Climate Group of the Mesoscale & Microscale Meteorology Laboratory at NCAR, who welcomed me warmly whenever I came or returned to Boulder.

A shout-out to the DKs, to Bettina and Regina, and particularly to the Innerkoffers in Graz, who retained their humor even in stressful times. All faculty staff and in particular my co-supervisor Oliver Sass be thanked for creating an accepting environment and providing helpful feedback in numerous colloquia and workshops. I appreciate the Austrian Science Fund giving this interdisciplinary group of doctoral students the opportunity to advance research on climate change in such integrative framework as the DK Climate Change.

I acknowledge the offices and helpful staff of the Office of the Styrian Government, the Austrian Hydrographic Services of Burgenland, Styria, Lower Austria, Tyrol, and Salzburg, and the ZAMG for providing data and information on precipitation, runoff, and damage claims to the disaster fund. The partners of the WegenerNet climate station network are thanked for making this unique climate data resource possible. I appreciate all the people who have asked *the internet* any conceivable question on programming and other issues and those people behind *the internet* who invest their time and best effort to answer them.

A heartfelt thank you to Karen for filtering awkwardness (in texts and in life, generally), and being a friend. Daniel, Scarlet, and Christian for their proofreading support and helpful comments. Thank you Christian for being a bastion of calm in the (my) craziness and my family for being the best family in the world.



## Abstract

Research on extreme convective precipitation events (ECPEs) is crucial to avoid damage and to better understand the climate system, but a lack of area-covering long-term measurements of the short-lived and localized storms hamper climatological analyses.

This thesis explores uncertainties associated with ECPEs in the Austrian southeastern Alpine forelands using sub-daily rain and stream gauge observations as well as damage data. Additional variables are used to define weather types and socioeconomic vulnerabilities. Different analytic and statistical methods are applied to quantify sampling biases and temperature sensitivities as well as damage contributions from ECPEs.

Using a novel technique to systematically thin out the  $1.4 \text{ km} \times 1.4 \text{ km}$  WegenerNet Feldbach region climate station network (WegenerNet), it is demonstrated that conventional rain gauge networks lead to severe underestimation of extreme area rainfall in convective storms. The rate of underestimation follows a power law with exponent  $-0.5$  over inter-station distances from 1 km to 30 km. It is shown that damage reported to the Austrian disaster fund under convective weather types is systematically less correlated with precipitation extremes, as compared to stratiform weather systems. These findings are particularly relevant, as higher daily mean temperature has been shown to robustly correlate with an increase in precipitation extremes. This indicates that ECPEs might become more intense with climate warming, however, temporal trends and the role of dynamic processes need further research.

The thesis underlines the need for high resolution observations and strategies to implement sampling uncertainties into model evaluation and risk reduction strategies, as ECPEs significantly contribute to total damage and the risk from such events will likely increase.





## Zusammenfassung

Um das Klimasystem besser zu verstehen und Unwetterschäden zu begrenzen, ist die Erforschung kleinräumiger konvektiver Starkniederschlagsereignisse (KSNE) essenziell. Ein Mangel flächendeckender und lange zurückreichender Aufzeichnungen erschwert die Analyse dieser räumlich wie zeitlich hoch variablen Ereignisse. Diese Dissertation erforscht KSNE im südöstlichen Alpenvorraum Österreichs und mit ihnen verbundene Unsicherheiten. Hierzu werden unter-tägliche Niederschlagsmessungen, Schadensmeldungen und Daten zur Bestimmung von Wetterlagen und sozioökonomischen Vulnerabilitäten mittels verschiedener analytischer und statistischer Methoden ausgewertet.

Ein innovativer Ansatz dünnt das Klimastationsnetzwerk WegenerNet systematisch aus und kann so nachweisen, dass konventionelle Messnetze eine Unterschätzung der maximalen Flächenniederschläge von KSNE erheblich begünstigen. Darüber hinaus wird gezeigt, dass Schäden, die während konvektiver Wetterlagen gemeldet werden, systematisch seltener mit extremen Niederschlagsmessungen in Zusammenhang gebracht werden können, als Schäden, die bei Wetterlagen mit flächigem Niederschlag auftreten. Die Ergebnisse sind besonders relevant, weil unter-stündliche bis unter-tägliche Niederschlagsextreme robust und stark positiv mit der Lufttemperatur in Zusammenhang stehen. KSNE könnten daher mit fortschreitendem Klimawandel und einhergehender Erwärmung intensiver werden, wobei zeitliche Trends und die Rolle dynamischer Prozesse weiterhin von vielen Unsicherheiten geprägt sind.

Insgesamt zeigen die Ergebnisse dieser Dissertation, wie wichtig hochaufgelöste Beobachtungsdaten sind, um Strategien zu entwickeln, mithilfe derer Messunsicherheiten bei der Modellevaluierung und in der Naturgefahrenprävention besser berücksichtigt werden können. Vor dem Hintergrund steigender Durchschnittstemperaturen und einer wahrscheinlichen Zunahme der Intensität von KSNE ist dies besonders relevant.



## Research articles and author contributions

SCHROEER, K., Kirchengast, G. and O, S. (2018) Strong dependence of extreme convective precipitation intensities on gauge network density. *Geophysical Research Letters* 45: 16. Pages 8253–8263. DOI 10.1029/2018GL077994. G.K. and K.S. conceived the approach and developed the FWTM-sampling method. K.S. designed and implemented the computational framework and performed the numerical calculations as well as the weather type analysis. S.O. prepared the WegenerNet data and performed the spatial correlation analyses. K.S. wrote the manuscript with support from G.K., who provided advice and contributed to the text. All authors helped shape the analysis and manuscript revisions and gave their final approval of the paper to be published.

SCHROEER, K. and Tye, M. R. (2019) Quantifying damage contributions from convective and stratiform weather types: how well do precipitation and discharge data indicate the risk? *Journal of Flood Risk Management* 2019;12:e12491. 13 pages. DOI 10.1111/jfr3.12491. K.S. devised the initial project idea with input from M.R.T.. K.S. collected the data, performed the analyses and calculations, designed the figures, and drafted the manuscript. M.R.T. helped in sharpening the research focus, aided in interpreting the results and worked on the manuscript. Both authors gave their final approval of the paper to be published.

SCHROEER, K. and Kirchengast, G. (2018) Sensitivity of extreme precipitation to temperature: the variability of scaling factors from a regional to local perspective. *Climate Dynamics* 50:10–12. Pages 3981–3994. DOI 10.1007/s00382-017-3857-9. K.S. and G.K. developed the idea and design of the work. K.S. collected and processed the data, performed the statistical analyses, and designed the figures. K.S. took the lead in writing the manuscript with G.K. providing guidance and contributing to the text. Both authors gave their final approval of the paper to be published.



# CONTENTS

LIST OF ABBREVIATIONS	xv
1 INTRODUCTION	1
2 RESEARCH CHALLENGES OF CONVECTIVE PRE- CIPITATION EXTREMES	5
2.1 Across scales: Localized extreme precipitation from a climatological perspective . . . . .	5
2.2 Overarching research question and scope . . . . .	10
2.2.1 Observations . . . . .	11
2.2.2 Societal Risk . . . . .	14
2.2.3 Temperature sensitivity . . . . .	16
3 DATA AND METHODOLOGY	21
3.1 Study area and choice of data . . . . .	22
3.2 Choice of methods . . . . .	27
3.2.1 From data series to individual events . . . . .	27
3.2.2 Identifying convective conditions through weather types . . . . .	28
3.2.3 Designing a method to assess sampling uncertainty: The Fishnet- Windowed Triangular Mesh (FWTM) Method . . . . .	30
3.2.4 Choosing robust methods to explore the character and risk from ECPEs . . . . .	31
4 SCALING RELATIONSHIPS AND DAMAGE CON- TRIBUTION OF CONVECTIVE PRECIPITATION	37
4.1 Research Article 1: Dependence of extreme convective precipitation intensities on gauge network density . . . . .	37
4.1.1 Introduction . . . . .	39

## CONTENTS

4.1.2	Data and methods . . . . .	40
	Precipitation data and convective events selection . . . . .	40
	Multi-scale estimation of EMAP . . . . .	41
4.1.3	Results and discussion . . . . .	43
4.1.4	Summary and conclusions . . . . .	46
4.1.5	References . . . . .	47
4.2	Research Article 2: Damage contributions from convective and stratiform weather types . . . . .	51
4.2.1	Introduction . . . . .	53
4.2.2	Data and Methods . . . . .	54
	Damage claim and municipality data . . . . .	54
	Precipitation and discharge . . . . .	56
	Weather types . . . . .	57
4.2.3	Results . . . . .	58
	Distribution of damage claims by weather types . . . . .	58
	Annual exceedance probabilities of damage-associated river discharge and precipitation . . . . .	59
4.2.4	Discussion . . . . .	61
	Discussion of uncertainties and limitations . . . . .	61
	Implications for future risk assessment . . . . .	62
4.2.5	Conclusion . . . . .	63
4.2.6	References . . . . .	63
4.3	Research Article 3: Sensitivity of extreme precipitation to temperature from a regional to local perspective . . . . .	67
4.3.1	Introduction . . . . .	69
4.3.2	Data . . . . .	70
4.3.3	Methods . . . . .	71
4.3.4	Results and discussion . . . . .	74
	Spatial variability and regional patterns of scaling factors . . . . .	74
	Seasonal and storm type patterns of scaling factors . . . . .	75
	How regional scaling factors relate to absolute rainfall intensities . . . . .	77
4.3.5	Summary and concluding remarks . . . . .	79
4.3.6	References . . . . .	80

## 5 DISCUSSION AND CONCLUSIONS 83

## CONTENTS

APPENDIX	91
A.1 Supplementary Information Research Article 1 . . . . .	91
A.2 Supplementary Information Research Article 2 . . . . .	101
LIST OF FIGURES	112
LIST OF TABLES	113
REFERENCES	115





# LIST OF ABBREVIATIONS

AEP	annual exceedance probability 32, 34, 113
AHYD	<i>Hydrographischer Dienst Österreich</i> / Austrian Hydrographic Service 22, 23, 26, 27, 30, 83–85, 87
ARF	Areal Reduction Factors 13
BM	block maxima 33
CA	cluster analysis 29, 31
CAPE	convective available potential energy 21, 28
CC	Clausius-Clapeyron 16–19, 89, 90
CPM	Convection Permitting Climate Models 7, 17, 18, 86
ECMWF	European Center for Medium-Range Weather Forecasts 24, 26
ECPEs	extreme convective precipitation events v, xi, 1–3, 5, 8–10, 12–16, 21–24, 27, 28, 30, 31, 35, 83–90
EOF	empirical orthogonal functions 31
FWTM	Fishnet-Windowed Triangular Mesh xi, 13, 23, 30, 31
GCM	General Circulation Models, also Global Climate Models 6, 7, 17
GEV	generalized extreme value distribution 32–34, 113
GMST	global mean surface temperature 16, 17, 19
GPD	generalized pareto distribution 33
i.i.d.	independent and identically distributed random 32, 33
IPCC	Intergovernmental Panel on Climate Change 6

## LIST OF ABBREVIATIONS

PCA	principal component analysis 29, 31
PDF	probability distribution function 6
POT	peak-over-threshold 33
PSL	sea level pressure 21, 28
QPE	quantitative precipitation estimate 84
RCM	Regional Climate Models 7
RX1D	annual maximum daily precipitation amount 6, 17
SCS	severe convective storms 7, 8, 24
sQX1D	annual seasonal maximum daily discharge 33, 34, 113
sRX1D	annual seasonal maximum daily precipitation amount 33, 34, 113
T/P-scaling	temperature-precipitation scaling, or temperature sensitivity of precipitation 11, 16–18, 20, 34, 35, 89, 90
$T_{2m}$	surface temperature 17
$T_{dew}$	dew point temperature 17, 18
UV700	700 hPa wind velocity 28
WegenerNet	WegenerNet Feldbach region climate station network v, 13, 22, 23, 26, 27, 30, 83–86
ZAMG	<i>Zentralanstalt für Meteorologie und Klimatologie</i> 22–24, 26–30, 83–85, 87
ZG500	500 hPa geopotential height 28

# 1 INTRODUCTION

somebody tell me the truth / and  
the rain came down / it rains on  
everyone

---

John Maus

Towering cumulonimbus clouds banking up in summer skies presage extreme convective precipitation events (ECPEs). Convective cells are often not larger than a few kilometers in diameter and last for less than a couple of hours, yet such storms harbor substantial damage potential. The sudden onset and difficult prediction of such events make it a particular delicate hazard with little time for exposed communities to prepare. Flood patterns and impacts of such events differ from large scale flooding. Demolished roads and settlements flooded by water and mud, and numerous fatalities demonstrate the disastrous consequences from ECPEs. Unfortunately, such extreme events regularly occur in the eastern Alpine region. Localized flash flooding and debris flows triggered by intense precipitation can disrupt life until long after the event has passed, for example as in Braunsbach, Germany in 2016 (*Bronstert et al.*, 2018; *Laudan et al.*, 2017), or in Oberwölz, Austria in 2011 (*hydroConsult GmbH*, 2011).

With rapid climate change the global hydrological cycle intensifies, as rates of evaporation and atmospheric water vapor content rise with increasing global mean temperatures (*Duethmann and Blöschl*, 2018; *Huntington*, 2006; *O’Gorman*, 2015; *Trenberth et al.*, 2003). Results from observations and model studies reassert the physics-based theoretical expectation that extreme precipitation increases as a consequence of warming (*Fischer and Knutti*, 2016). While society may adapt to a change in mean temperature, the potential increase in extreme hydro-meteorological events will issue significant challenges. Not only scientists, but also engineers and local decision makers thus have great interest in knowing when and where extreme events are likely to occur. Therefore, it is important to understand not only how potentially catastrophic events will change on the global

## 1 INTRODUCTION

scale, but even more so how these changes will manifest on the regional to local level, where prevention has to be actuated and impacts have to be dealt with.

Systematic research on localized ECPEs is complicated due to their high natural variability. Large uncertainties have to be taken into account even when the focus is set on present and near future challenges, and these uncertainties grow for long-term assessments. Because extreme events are rare by definition, it is technically and financially difficult to collect consistent observations, which hampers long-term analyses. As a consequence, the character and consequences of localized, sub-daily extreme convective precipitation have long been dominated by forecast- and warning-oriented research (*Allen, 2018*). Automatic weather stations and fast data transmission, ever improving remote sensing technology, and rapidly evolving computer power increasingly facilitate studies from a climatological perspective. It is, however, crucial to identify the sources of uncertainty inherent to the data used and to understand how they may affect study results.

This thesis addresses some of the uncertainties related to ECPEs in the southeastern Alpine forelands. As the sources of uncertainty are plentiful, the focus is narrowed to taking an integrative perspective on three aspects: gauge observations, damage potential, and temperature sensitivity of ECPEs. This is because it is generally acknowledged that ECPEs are misrepresented in rain gauge observations, but the extent to which this is the case is largely not quantified. Furthermore, it is not well explored how much ECPEs contribute to the socioeconomic cost caused by natural hazard impacts. Detecting damage patterns under convective and non-convective conditions, while also considering regional factors of vulnerability and exposure, can help to understand the risk and allocate funds accordingly. Through exploring how extreme precipitation intensities scale with temperature, patterns of variability on the regional-to-local level can be identified and valuable conclusions be drawn with regard to both present and potential future developments.

Studying a confined region in the Austrian southeastern Alpine forelands allows the advantage of using various sources of data that are available at high quality and resolution. Historical data of the recent decades are explored to understand patterns of ECPEs, but also identify pitfalls in observations. Insights gained on the small scale can then provide valuable reference and recommendation to issues and applications on larger scales. The core data sources used are sub-hourly precipitation observations from a comparably dense regular rain gauge network with approximately 7 km inter-station distance and from a very high-

density research rain gauge network with inter-station distances of about 1.4 km. In addition, data on natural hazard damage and a suite of environmental and socioeconomic data is used. Using a weather typing and event scale approach, all data is used to statistically and analytically analyze the character and consequences of ECPEs. The results provide empirically derived points of reference useful to a broad range of applications such as high-resolution climate models or natural hazard risk assessments.

This thesis is structured as follows: Chapter 2 opens with an introductory discussion of the literature in extreme precipitation research and embeds the research questions of this thesis in the context of recent developments. Choices of data and methods are explained in Chapter 3.

The research articles that constitute this thesis, Research Article 1 *Strong dependence of extreme convective precipitation intensities on gauge network density*, Research Article 2 *Quantifying damage contributions from convective and stratiform weather types: How well do precipitation and discharge data indicate the risk?*, and Research Article 3 *Sensitivity of extreme precipitation to temperature: the variability of scaling factors from a regional to local perspective* are included in Chapter 4. Chapter 5 discusses the overarching findings of the research and closes with concluding remarks.



## 2 RESEARCH CHALLENGES OF CONVECTIVE PRECIPITATION EXTREMES

Extreme weather events and induced natural hazards can severely impair the functioning of human-environmental systems. Consequential damages are felt even long after the actual event has passed. To avert losses, societies and individuals around the world strive to better cope with the risk from extreme weather, which will likely be exacerbated by climate change (*Easterling et al.*, 2000).

This thesis takes an integrative perspective on the character of and impact from extreme convective precipitation events (ECPEs). Extreme weather in the form of convective precipitation events occurs regularly but such storms are hard to predict (*Allen*, 2018) and often lead to catastrophic outcomes. Concentrated water masses in extreme convective events can trigger destructive flash flooding and debris flows with very short lead times. This chapter summarizes general advances and challenges in the research of extreme convective precipitation in the first part and embeds this thesis' research questions more specifically in the second part.

### 2.1 Across scales: Localized extreme precipitation from a climatological perspective

As Earth's climate is changing at unprecedented pace, we face likely shifts in the magnitude and frequency of extreme events, yet the details of how these shifts manifest on the regional-to-local scale are very uncertain (*IPCC*, 2013, ch.10). One reason for this is that current assessments of changes and robust trends in observations and climate model projections are based primarily on means. Changes in extreme weather and climate events with global warming have long been theoretically and conceptually discussed (e.g., *Fischer and Knutti*, 2016). A

common way to approach a climate variable is through visualizing its probability distribution. A change in the mean, i.e., the location parameter of its probability distribution function (PDF), is only one of the moments that govern the probability of weather outcomes in a given climate state. Changes in the variability and shape of the distributions, i.e., shape and scale parameters also determine the form of PDF and are decisive for exceedance probabilities of extreme events located at the tails of a distribution (*Alexander and Tebaldi, 2012*). While there is high confidence in the signals of changing means with climate change, robust findings are only emerging on the variability and changes of extremes.

Research on extremes must operate in the marginal space of rare high magnitude / low probability events. The climate system is naturally variable and oscillates on scales from seconds to millennia. In order to detect changes that go beyond the expected variability, it is necessary to robustly distinguish signal from noise. Short data series will naturally exhibit a low signal-to-noise ratio, and the same is valid if the spatial and temporal scales of interest are small.

General Circulation Models, also Global Climate Models (GCM) allow analyzing longer, simulated, time series from an idealized model framework. For the CMIP2<sup>1</sup> generation of GCM, *Allen and Ingram (2002)* find that the uncertainty in changes of global mean precipitation is much higher than the inter-model spread. As different GCM were not designed as an ensemble to represent natural variability, groups increasingly initiate large ensemble runs of one specific model in order to better understand the role of natural variability (e.g., *Aalbers et al., 2018; Dittus et al., 2018; McKinnon and Deser, 2018; Pendergrass et al., 2017*).

In its fifth assessment report on global climate change, the Intergovernmental Panel on Climate Change (IPCC) concludes with *high confidence* that extreme precipitation is increasing (*IPCC, 2013*), with more regions worldwide exhibiting significant positive trends than negative. Most global studies analyze the annual maximum daily precipitation amount (RX1D)<sup>2</sup>, for which reliable observational records exist on scales of several decades, with some data series reaching back to the 19<sup>th</sup> century (*Becker et al., 2013*). However, the global coverage of qualitative

---

<sup>1</sup>The Coupled Model Intercomparison Project CMIP was started 1995 to facilitate running common GCM experiments and further to coordinate, compare, and share results among different modelling groups as well as to disseminate model output to research groups who do not have own models. CMIP Phase 2 GCM are from around the year 2000. CMIP is currently in Phase 6. (*World Climate Research Program, 2018*)

<sup>2</sup>RX1D is one of several climate indices defined in order to streamline international monitoring of climate extremes (*Zhang et al., 2012*)



## 2.1 ACROSS SCALES: LOCALIZED EXTREME PRECIPITATION FROM A CLIMATOLOGICAL PERSPECTIVE

rain gauge observations is still very heterogeneous. The limited availability of precipitation data causes GCM to be less constrained by observations, and so directly influences the level of confidence we can have in their outputs (*Allen and Ingram, 2002*).

On the sub-daily scale, observations to derive precipitation indices are generally sparse and far from homogeneous, and so do not yet allow for a global assessment of changes (*Alexander, 2016; Allen, 2018*). With the spreading of automated weather stations, sub-daily to sub-hourly sampling has become more frequent, and major efforts are now underway to collect and convert data from other sources, to document and analyze sub-daily precipitation measurements on a global scale (*Blenkinsop et al., 2018*).

Research on the climatological scale of severe convective weather<sup>3</sup> has increased significantly in the past decade. This is because major hurdles such as the lack of systematic observational data are ameliorating, but also because climate models' resolution, which had long been too coarse to study convective phenomena, has increased. With rapidly evolving computer power, Convection Permitting Climate Models (CPM) allow researching patterns and processes of extreme precipitation on scales from 12 km to 1 km where convection no longer needs to be fully parameterized (*Chan et al., 2018; Prein et al., 2017a*).

Advances of CPM brought improvements from Regional Climate Models (RCM) in better representing summertime precipitation, and in particular the diurnal cycle of precipitation (*Ban et al., 2014; Prein et al., 2015*). Despite these leaps, current CPM simulations are restricted to single realizations and simulating discontinuous periods of time (e.g., one historical and one future decade (*Ban et al., 2015*)). Nevertheless, CPM will continue to advance our understanding of small scale extreme events as simulations on climatological time scales are evolving (*Wang et al., 2018*).

As fundamental and so-called *ground-truth* reference to our theory and indispensable to model validation, observational data are at the core of weather and climate science. With advancing CPM it becomes ever more important to acquire reliable reference data to scrutinize the output of simulations at unprecedentedly high resolution. However, significant uncertainties also exist in observational datasets. Large discrepancies among different datasets have been identified (*Zittis,*

---

<sup>3</sup>The term severe convective storms (SCS) includes hazards from atmospheric convective systems, which are tornadoes, large hail, thunderstorms, and excessive rain (*Allen, 2018*). This thesis focuses on extreme convective precipitation, although it is possible that hail occurred in the analyzed storms.

2017). *Prein and Gobiet (2017)* show that available gridded precipitation datasets spread in ranges comparable to the spread of precipitation in an ensemble of climate model runs. This demonstrates that observational uncertainties need better quantification.

In addition to understanding the uncertainties on the data itself, it is equally important to understand the processes they represent. Only time and close-meshed observation will increase the sample size of real-world extreme events and subsequently the robustness of statistical analysis and trend detection, particularly at sub-daily and regional-to-local scales. It is even more important, therefore, to advance our knowledge of small-scale extreme events through understanding the involved processes and to leverage all information available to research today.

Another reason climatological perspectives on convective extremes are lacking is not related to data. As *Allen (2018)* notes with regard to research on SCS under climate change, “[t]he challenge of the interdisciplinary nature of this area of research is the tendency for researchers to be focused in their training predominantly either on the mesoscale (<400km, <1 day) or on the synoptic to climate scale (>400km and on periods of days to decades)”. In this sense, also research on ECPEs is situated between two different paradigms. On the one hand, climatologists seek to understand how larger-scale patterns interact with local phenomena, and the kind of hazards we have to expect on longer time scales. On the other hand is the scale of chaotic regional-to-local weather, where “[e]ven on a day-to-day basis, severe-weather forecasters struggle to identify where and when thunderstorms may initiate, and if they do, whether they will be long-lived and severe” (*Allen, 2018*).

Both perspectives provide relevant hazard information to society. On the one end, forecasts and warnings assist people in taking immediate action. On the other end, the long-term perspective is essential to guide prevention, such as norms (e.g., building codes (*Garsaball and Markov, 2017*)), measures (e.g., structural flood protection), as well as to educate and facilitate adaptive behavior (*Kreibich et al., 2017*). Long-term perspectives are also required to allocate funds and calculate insurance premiums (*Unterberger, 2018; Unterberger et al., 2019*).

This listing of measures taken by societies already shows that the level of how severely societies are impacted by extreme weather events is only partly governed by the hazard. Socioeconomic development is a major driving force behind observed and projected increases in losses from extreme climate and weather events (e.g., *Perez-Morales et al., 2018; Strader et al., 2017a,b*). The level to which societies can reduce their vulnerability and exposure through adapting to variability and

## 2.1 ACROSS SCALES: LOCALIZED EXTREME PRECIPITATION FROM A CLIMATOLOGICAL PERSPECTIVE

change largely determines the consequences from extreme events. The concept of risk allows taking into account the different factors and processes that eventually put lives and assets in jeopardy (*Morss et al.*, 2011). Although exact definitions of terms such as vulnerability, hazard, and exposure vary across groups and disciplines (*Jurgilevich et al.*, 2017), they share a common concept of risk as the intersection of hazard and vulnerability, which describes in the broadest sense the space (not necessarily restricted to physical space) where susceptible life and property are exposed to a hazardous process.

This thesis is not only interested in the atmospheric process of ECPEs, but also in its societal relevance in terms of their damage potential. Figure 2.1 illustrates how the framework of risk is understood in the context of this thesis. ECPEs are governed by atmospheric processes and are located on the hazard side. ECPEs can trigger hydrological and geomorphological hazards, given conditions at the Earth's surface are favorable (e.g., steep topography, high sediment supply, high antecedent soil moisture). The processes can occur in different areas of the study region and may follow distinct patterns. At locations where, and times when, people and assets are both exposed and susceptible to these hazards, the risk materializes. Vulnerability here is understood as the intersection of exposure and susceptibility, acknowledging that other interpretations exist (*Jurgilevich et al.*, 2017). All risk factors are subject to spatial and temporal variability on different scales, making the risk analysis inherently complex.

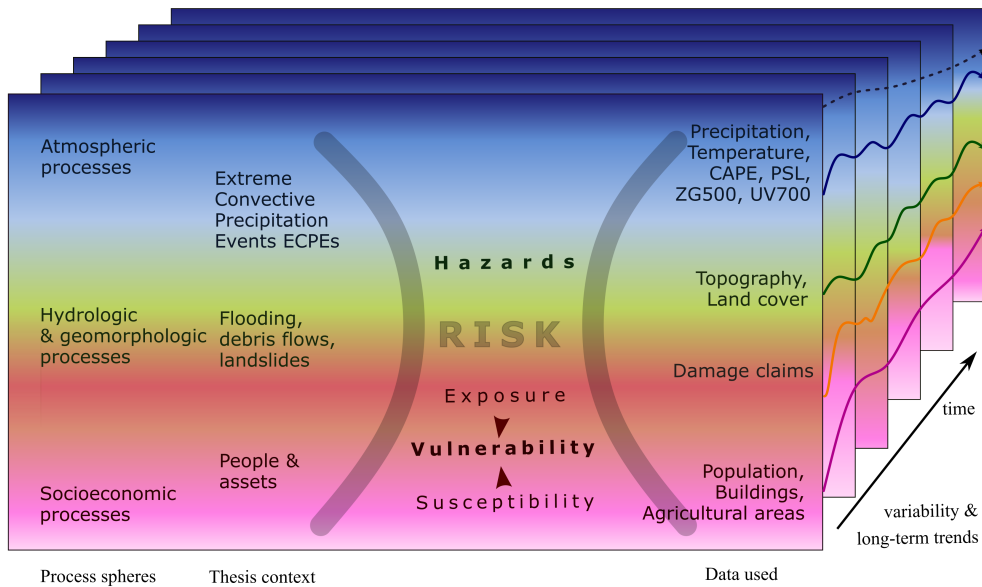


Figure 2.1: Risk framework in the context of processes and data analyzed in this thesis.

## 2.2 Overarching research question and scope

This thesis takes an integrative perspective on ECPEs not only because it explores the physical phenomenon between the scales of extreme weather and climate, but also because it investigates societal implications of ECPEs in the form of incurred damage. Building on high-resolution observations of precipitation and additional data in the southeastern Alpine forelands, it is analyzed how the most extreme precipitation events scale with temperature conditions, how they are represented in gauge observations, and what the associated vulnerabilities are on the regional-to-local level. The overarching research question is:

*What is the character and relevance of ECPEs in the Austrian south-eastern Alpine forelands and how can associated uncertainties be quantified?*

The research articles that constitute this thesis address this question from three different angles, which are (i) observations, (ii) societal risk and (iii) temperature sensitivities.

Three subordinate research questions thus accrue from the overarching research question. Each research article roots in one of the three levels, but their sub-

## 2.2 OVERARCHING RESEARCH QUESTION AND SCOPE

jects are inevitably interlinked. The scope and approach of the three chapters is laid out hereafter. Because there has been a very active debate on temperature-precipitation scaling, or temperature sensitivity of precipitation (T/P-scaling) in the recent years, the topic of temperature sensitivities is given somewhat more space to embed Research Article 3 in this research landscape.

### 2.2.1 OBSERVATIONS

Precipitation is an important aspect of the natural world for all life on Earth. It is yet a delicate one, as both shortage and excess can lead to disastrous consequences. The most relevant quantity for observers (i.e., life) on the ground is the amount of water falling over a given area. Precipitation is traditionally measured, however, at point scale<sup>4</sup>. This allows collecting standardized and comparable quantities of precipitation while containing environmental biases and disturbances, such as evaporation, in the best possible ways. However, rain gauges cannot directly measure area precipitation, and sites are not necessarily representative of the surrounding areas under all circumstances.

Remotely sensed measurements of the atmosphere taken by radar and satellite technology allow detecting spatial patterns of precipitation in two, and increasingly also in three dimensions (*Handler and Homeyer, 2018; Mroz et al., 2018*). Satellites, in particular, can sample precipitation seamlessly over land and ocean, the latter being notoriously undersampled in global observations (*Allen and Ingram, 2002*). Unfortunately, however, satellite products do not yet adequately resolve extreme events on short time scales (*Furl et al., 2018*). Ground based radar observation, despite uncertainties (*Cecinati et al., 2017; Villarini et al., 2014*), can be used to investigate structures of convective precipitation events on relevant spatiotemporal scales (approx. 5 min and 1 km) (*Eggert et al., 2015; Lochbihler et al., 2017; Marra and Morin, 2018; Peleg et al., 2018*). Because of comparably short records, and ever evolving technology that is mostly targeted towards forecasting applications, the availability of long-term, quality-controlled radar datasets is limited. Consequently, radar analyses on climatological time scales are still rare and analyze comparably short periods (10 yr to 15 yr) (*Nisi et al., 2016; Panziera et al., 2018*).

This thesis focuses on observations from rain gauge station networks. Rain gauges constitute the most fundamental way of observing precipitation in-situ and

---

<sup>4</sup>Point scale here refers to the orifice of the deployed rain gauge, which, depending on the sensor, is usually 200 cm to 500 cm (*O et al., 2018*)

on ground level. Many regions of the world rely on rain gauges and they provide the longest records of precipitation. Furthermore, advancing remote sensing technology and models need high-quality ground measurements for reference and validation.

To get information on area precipitation from point observations, most applications use gridded products of precipitation. Precipitation at unobserved sites is estimated from interpolating point measurements using geostatistical methods (e.g., *Hiebl and Frei, 2016; Isotta et al., 2014; Sideris et al., 2014*, for Alpine regions). The result is a spatially smoothed and coherent field of precipitation estimates. For these gridded precipitation products it is not usually easily traceable which rain gauge stations were used to generate the precipitation field. There exist large discrepancies among different precipitation products, which can also stem from different interpolation methods (*Herrera et al., 2018*). Although these issues are acknowledged, the potential implications of an uncertain *ground truth* often remain ignored or undisclosed, as most studies in hydrology or climate model evaluation only choose or have available one observational product to work with.

Because of the concentrated rainfall patterns in ECPEs, they are generally undersampled by conventional rain gauge observation networks. This is because the inter-station distances of operational networks are comparably large, e.g., approximately 10 km in Austria (*Schroeer and Tye, 2019*), but can be one order of magnitude larger in other parts of the world (e.g., *Gubler et al., 2017*). In order for a network to comprehensively capture ECPEs, the required spacing of rain gauges depends on the spatial extent, life span, and travel speed of convective cells. In the Netherlands, radar data show that 90% of convective storm cells are smaller than 7 km in diameter (*Lochbihler et al., 2017*). In southeastern Austria, extreme convective storms often do not last longer than a couple of hours (*Schroeer et al., 2018*). Peak precipitation rates within the storms occur on even shorter and smaller scales (*Peleg et al., 2016; Syed et al., 2003*), requiring even denser meshing in order to record the most extreme intensities.

Uncertainties from undersampling and underestimation of peak intensities of ECPEs cascade to downstream applications, with potential implications for risk assessments. Most hydrological models, for example, process interpolated precipitation data. Spatial misrepresentation of areal precipitation amounts can propagate to wrong streamflow estimates, or bias the parameter estimation when observed runoff is fit to observed precipitation. Another example is the estimation

## 2.2 OVERARCHING RESEARCH QUESTION AND SCOPE

of Areal Reduction Factors (ARF)<sup>5</sup> in hydraulic application design (*Beck et al.*, 2017; *Svensson and Jones*, 2010). Furthermore, the validation and analysis of climate models strongly depends on estimates of mean area precipitation, because models output precipitation amounts as an area mean over each gridcell (*Herrera et al.*, 2018; *Kotlarski et al.*, 2017).

Because many applications rely on spatial precipitation data and ECPEs bear high hazard potential, it is essential to quantify uncertainties in spatiotemporal resolution of observations of convective precipitation events. Globally, only very few precipitation observation networks exist that have a dense enough station network to capture convective extreme events (e.g., *Goodrich et al.*, 2008). The density of the observing network always is a trade-off of coverage and accuracy against technological and financial constraints and priorities. The WegenerNet Feldbach region climate station network (WegenerNet) in southeastern Styria, Austria, is one of the very few networks worldwide and the only one available in the European mid-latitudes with >150 rain gauges over an area of approximately 15 km × 20 km. The effects of potential undersampling of ECPEs can so be empirically investigated based on systematic, quality-controlled rain gauge measurements. Hence the first research question addressed in Research Article 1 in Section 4.1 (*Schroerer et al.*, 2018) is:

*How does the rain gauge density in an observation network influence the estimation of event maximum area precipitation of ECPEs?*

Section 4.1.1 introduces the difficulties to estimate area rainfall from extreme convective precipitation events. In Section 4.1.2, the data is introduced and it is described how the experimental sampling framework of the Fishnet-Windowed Triangular Mesh (FWTM) method is set up to empirically test the dependence of observed extreme convective precipitation intensities on the density of the rain gauge network. Results and implications are discussed in Section 4.1.3 and a concluding summary is given in Section 4.1.4.

---

<sup>5</sup>“ARF  $\eta$  is a key parameter in the design for hydrological extremes. For a basin of area  $A$ ,  $\eta(A, D, T)$  is the ratio between the area-average rainfall intensity over a duration  $D$  with return period  $T$  and the point rainfall intensity for the same  $D$  and  $T$ .” (*Veneziano and Langousis*, 2005, p 1)

### 2.2.2 SOCIETAL RISK

The quality of observations and subsequently the robustness of estimated changes of ECPEs are highly relevant from an impact perspective, as, for example, planners and decision makers are reliant on accurate hazard information. The undersampling of localized short-duration precipitation intensities might thus result in a biased picture and reduced awareness of the risk from such events. When taking an impact perspective instead of focusing on the hazard alone, many more factors and processes have to be considered, which all influence the severity of an impact. They range from runoff generation to the vulnerabilities of the exposed assets, and make any analysis inherently more complex (*Cortès et al.*, 2018).

Patterns of large-scale extreme precipitation events and consequential extensive river floods are often investigated at climatological and national to global scales (*Bloeschl et al.*, 2017; *Hofstaetter et al.*, 2018; *Unterberger et al.*, 2019; *Willner et al.*, 2018), although also uncertainties may scale high (*Trigg et al.*, 2016). Natural hazards associated with ECPEs, however, are very different in that they are spatially much more confined in time and space than large-scale river flooding. Consequentially, also the data required to map the events need to be much finer resolved, which exacerbates acquiring them in sufficient quality (*Amponsah et al.*, 2018; *Laudan et al.*, 2017). Studies often focus on individual flash flood events, single catchments, and specifically on urban environments, while findings are rarely compiled on a regional or even national scale. The smaller spatial extent of the total affected area also confines the scope socioeconomic impacts and thus may seem less relevant from an (inter-)national perspective.

However, cumulative effects of smaller-scale extremes can significantly increase the risk of damage on both the spatial and temporal scale. Recent research exploring the coastal risk of flooding showed that the total risk from small-scale events, referred to as nuisance flooding, accumulates to present financial risk in the same range as more rare events of higher magnitude (*Moftakhari et al.*, 2017). *Bernet et al.* (2017) showed that surface water flooding<sup>6</sup> is more often associated with short and intense storms and contributes significantly to flood losses in Switzerland. Furthermore, the chance that a point-scale extreme occurs rises when the considered area is enlarged. This means, point-scale recurrence intervals for a given event magnitude (i.e., the probability that the *same* spot is hit twice by such event) may

---

<sup>6</sup>Surface water flooding here refers to flooding of surfaces that is not associated with flow paths along rivers and water channels.



## 2.2 OVERARCHING RESEARCH QUESTION AND SCOPE

not reflect the frequency with which the event occurs over a larger region (i.e., the probability that such event occurs twice at *any* spot in a region). Since funds to cope with disasters are often managed on national level, localized extreme events may have to be compensated more often than recurrence intervals calculated from single site records suggest.

Given the strong evidence that extreme convective precipitation is intensifying (c.f. Section 2.2.3), understanding the patterns of vulnerability towards such events is essential to adequately plan for risk reduction measures. Also, little is known about the cumulative effects and damage contributions from ECPEs and how they relate to damage incurred under larger and longer-lasting and larger stratiform precipitation patterns.

The southeastern Alpine forelands offer a unique opportunity to study vulnerabilities to extreme precipitation on a regional scale. This is because qualitative and high resolution precipitation observations are available, and are complemented by river gauge measurements and damage claim data that indicate the severity of impacts. A multi-layered assessment allows identifying damage patterns under different weather types and municipality groups and so detect vulnerabilities to extreme precipitation. Furthermore, it is possible to learn about uncertainties associated with hazard observations and calculated recurrence intervals. Research Article 2 (*Schroerer and Tye, 2019*) addresses the following research question:

*What are damage contributions from convective and stratiform precipitation events and associated uncertainties regarding the risk from localized extreme precipitation events?*

The challenges of quantifying damage contributions from localized extreme events are introduced in Section 4.2.1. Section 4.2.2 describes how damage claim data and observations of precipitation and discharge are prepared and applied in the study and how socioeconomic, topographic, and synoptic preconditions are calculated using a clustering and weather typing approach. It is then presented in Section 4.2.3 how the claims distribute over the different weather types and how they relate to estimated hazard levels in observed daily discharge and precipitation. Section 4.2.4 discusses the complexity that integrated risk research faces and elaborates on the implications for future research on the impacts of small-scale extremes. Section 4.2.5 concludes the article.

### 2.2.3 TEMPERATURE SENSITIVITY

In light of the high damage potential of ECPEs, there is widespread demand for information on the magnitude and frequency of extreme events as well as estimates on whether these may change with global warming. The large uncertainties in assessing trends and variability of precipitation due to the lack of observations particularly apply to extreme events. To obtain more robust statements, *Allen and Ingram* (2002) proposed to constrain the magnitude of possible changes and associated uncertainties through calculating large-scale energy budget. Warmer air can hold more water vapor, and this physical principle is described by the Clausius-Clapeyron (CC) equation<sup>7</sup>. Under general conditions at the Earth’s surface, this relation predicts an increase in atmospheric water vapor content of  $6\% \text{ }^\circ\text{C}^{-1}$  to  $7\% \text{ }^\circ\text{C}^{-1}$  (*Held and Soden*, 2006).

The increase in global mean precipitation with global mean surface temperature (GMST) is bound to approximately  $2\% \text{ }^\circ\text{C}^{-1}$  by energy constraints. Because the most intense rainfall events are expected when all available moisture precipitates, the most extreme precipitation should be more directly constrained by the CC equation under constant relative humidity (*Allen and Ingram*, 2002; *Held and Soden*, 2006). Based on these principles, it is generally established that the global hydrological cycle intensifies with increasing GMST, with the consequential effect that extreme precipitation events become heavier (*Fischer and Knutti*, 2016; *Held and Soden*, 2006; *Trenberth et al.*, 2003).

The idea of constraining changes in precipitation extremes by means of the CC equation sparked widespread attention among scientists. Under the name of T/P-scaling, a large body of literature has emerged, comprising a surprisingly diverse set of approaches. This has led to considerable debate as to the drivers, implications, and correct interpretation of scaling rates (*Zhang et al.*, 2017). It is therefore important to distinguish the purpose and methodologies before interpreting and comparing results from different studies.

Although the approaches can sometimes blend into each other, three main tracks can be identified: (i) a global approach (ii) a regional-statistical approach

---

<sup>7</sup>The theoretical expectation of precipitation intensification is based on the CC equation describing the relation of pressure of a substance to temperature in a system, in meteorology most commonly approximated as  $\frac{1}{e_s} \frac{de_s}{dT} = \frac{L_v}{R_v T^2}$  where  $T$  is the temperature,  $e_s$  is the saturation vapor pressure of water,  $L_v$  the latent heat of vaporization, and  $R_v$  the gas constant for water vapor to relate atmospheric water vapor content to temperature (*American Meteorological Society*, 2018)

## 2.2 OVERARCHING RESEARCH QUESTION AND SCOPE

and a (iii) convective-process approach. The partitioning of the different categories will be briefly discussed.

(i) Studies of global scope build on *Allen and Ingram (2002)* and early models and theory (see *Fischer and Knutti, 2016*, for a review) to assess how precipitation responds to increases in GMST using regular or idealized GCM. Here, T/P-scaling is approached from a mainly conceptual and process-based perspective, where global energy budget and the CC relation serve as starting points to understand patterns of precipitation changes at global scale. The atmospheric processes associated with increasing temperature and water vapor content are analyzed, such as changes in vertical motion, condensation rates, and precipitation efficiency. Generally, dissecting the physical process is given priority over obtaining a particular scaling rate (*Muller and O’Gorman, 2011; O’Gorman and Schneider, 2009a,b; Pendergrass and Gerber, 2016; Pendergrass and Hartmann, 2014*).

One of the main findings of global studies is that because of the energetically constrained changes to global mean precipitation, the intensification of extremes happens at cost of light precipitation intensities (*Pendergrass and Hartmann, 2014; Trenberth et al., 2003*). This has since been confirmed in studies at storm scale level in both observations (*Ye et al., 2017*) and CPM (*Ban et al., 2015; Dai et al., 2017*). In an encompassing approach to T/P-scaling, *Pfahl et al. (2017)* separate RX1D response to global warming into a globally rather homogeneous thermodynamic component governed by the saturation vapor pressure and a spatially much more variable dynamic component governed by changes in vertical velocities (*Nie et al., 2018; Pfahl et al., 2017*). Following studies further explored the importance of atmospheric circulation and storm scale dynamics for extreme precipitation response (*Ali and Mishra, 2018; Nie et al., 2018; Tandon et al., 2018*). Inevitably, however, studies using GCM operate on scales much larger than convective extremes and thus cannot resolve processes that are crucial to local extreme precipitation, particularly on sub-daily scales (*Lenderink and Fowler, 2017; O’Gorman and Schneider, 2009a*).

(ii) Looking for a proxy to approximate changes in precipitation on the regional scale, a second group of T/P-scaling studies exists that relate measures of extreme precipitation, typically a high percentile, to local temperature rather than GMST. Most studies use rain gauge based observations and daily mean surface temperature ( $T_{2m}$ ), or dew point temperature ( $T_{dew}$ ) (e.g., *Berg et al., 2013; Formayer and Fritz, 2016; Lenderink and van Meijgaard, 2009; Mishra et al., 2012; Wasko and*

*Sharma, 2015; Wasko et al., 2016*), but also CPM have been used to assess local T/P-scaling (*Ban et al., 2015; Kendon et al., 2016; Prein et al., 2017b*).

Studies that follow the regional approach regress binned precipitation percentiles on local daily ambient temperature indices and interpret the slope of the regression line<sup>8</sup>. It is consistently found that the slope of the regression line exceeds  $7\% \text{ } ^\circ\text{C}^{-1}$ , and reaches up to so-called super-CC scaling rates ( $14\% \text{ } ^\circ\text{C}^{-1}$ ) for hourly to sub-hourly time scales and convective precipitation. The “puzzling variety” (*Bao et al., 2017a*) of scaling rates found across studies has motivated authors to identify effects that modulate a pure CC scaling relationship. Among these are positive deviations through statistical artifacts and transition from stratiform to convective precipitation (*Berg and Haerter, 2013*) and negative deviations through storm-type effects (*Bao et al., 2017a; Molnar et al., 2015; Wasko et al., 2015*). Furthermore, also climatological moisture limitations in more arid regions and future increase in drier weather patterns during summer have been discussed (*Chan et al., 2016; Drobinski et al., 2016; Prein et al., 2017b*).

Some authors strongly advocate the use of  $T_{\text{dew}}$  as regressor, because it incorporates moisture content of the air mass and so “removes” the so-called “hook shape” from temperature-precipitation relation graphs (*Lenderink and Fowler, 2017; Lenderink et al., 2018; Wasko et al., 2018*). While this helps to isolate the thermodynamic CC scaling component, using  $T_{\text{dew}}$  does not allow to identify dynamic processes that modify precipitation extremes, nor does it allow direct causal inference of changes induced by climate warming.

It is important to note that the regional approach does not allow to make inferences about the behavior of precipitation extremes in the future. In the mid-latitudes, scaling rates are governed by the climatology of the considered location and influenced by, e.g., the seasonal cycle (*Wang et al., 2017; Zhang et al., 2012*). The regional scaling approach can be used, however, to assess changes in temperature sensitivity by determining T/P-scaling for two or more separate time periods separately and assessing whether they differ in statistically significant ways (*Bao et al., 2017a*).

(iii) A third group of authors studies how the processes of convective initialization and storm development cause intensification of extreme precipitation within

---

<sup>8</sup>Usually an exponential regression is applied through log-transforming precipitation and fitting a linear regression model to binned precipitation quantiles (*Hardwick Jones et al., 2010*). Another approach is to use quantile regression (*Wasko and Sharma, 2014*) (see also Section 3.2 d))

## 2.2 OVERARCHING RESEARCH QUESTION AND SCOPE

individual convective cells (*Loriaux et al.*, 2013, 2016a,b; *Singleton and Toumi*, 2012) and which role convective organization and cell interaction at regional to global scales play for extreme rain rates (*Bao et al.*, 2017b; *Haerter et al.*, 2017; *Moseley et al.*, 2016; *Pendergrass et al.*, 2016). They show that updrafts and entrainment rates as well as the initiation of convective cells in the cold pools of preceding cells are important contributors to instantaneous precipitation rates to scale beyond the CC rate.

The different nature of approaches and pitfalls in interpreting scaling rates have been discussed by *Zhang et al.* (2017) and by *Pendergrass* (2018). *Pendergrass* (2018) stresses that it is important to be aware and communicate the differences in the definition of extreme precipitation (see also *Schär et al.*, 2016) before jumping to conclusions. Authors consistently note that thermodynamic forcing, or CC scaling alone, cannot provide the simple answer to our questions of extreme precipitation changes.<sup>9</sup> Yet, divisiveness on the topic and disagreement on the role of statistical effects of local scaling rates have not ceased, as the recent debate on direction, magnitude, and physical reasons for statistical scaling rates in Australia demonstrates (c.f. *Bao et al.*, 2017a, 2018; *Barbero et al.*, 2017; *Lenderink et al.*, 2018). While dispute is essential to scientific debate, it should be reminded that the goal is to better understand the physical mechanisms and processes that lead to deviations from the CC rate rather than to find proof for the CC equation itself.

With long records of sub-daily observations becoming available on continental scale, approaches (i) and (iii) can be merged to assess the precipitation response of sub-daily rainfall extremes with GMST. Comparing observations from the most recent climatological period to the preceding 30-year period, *Guerreiro et al.* (2018) find a robust increase in the k largest extreme events over Australia, which is outside of expectations from natural variability.

An advantage of regional studies is that they can explore sub-daily and even sub-hourly precipitation data. If adequately interpreted, temperature-precipitation

---

<sup>9</sup>For example, “However, local temperature changes may not be a good proxy for global warming because they tend to co-vary with other meteorological factors (such as humidity, atmospheric stability, or wind direction) in ways that are uncharacteristic of changes in the mean temperature” (*IPCC*, 2013, p 626f).

“[...] at higher surface temperatures and small spatiotemporal scales, extreme precipitation can strengthen at rates beyond the Clausius–Clapeyron rate ( $\sim 7\% \text{ K}^{-1}$ ). The ‘null hypothesis’, where thermodynamic limits alone cap increases of intensity, is thereby likely ruled out, and dynamical effects have been brought into discussion.” (*Haerter et al.*, 2017).

“One major drawback of scaling relationships is that they aggregate a range of climate dynamics, and hence, there are questions on how they may apply in the future.” (*Wasko et al.*, 2015)

scaling provides means to better understand extreme precipitation, given it is considered that the behavior and development of extreme precipitation are also influenced by dynamic processes on the large scale .

Research Article 3 uses sub-hourly precipitation observations in a dense rain gauge network with average inter-station distances of 7 km to 10 km to analyze how the temperature sensitivities vary on a local-to-regional scale. Opposed to studies based on less dense networks or only one single rain gauge (e.g., *Drobinski et al.*, 2016; *Formayer and Fritz*, 2016; *Scherrer et al.*, 2016), this allows to identify the variability and to interpret the meaningfulness of T/P-scaling on the regional-to-local level. The research questions addressed in *Schroerer and Kirchengast* (2018) are:

- (1) Which factors control the spatial and temporal variability seen in the temperature sensitivities on a regional scale? (2) How applicable and useful is the scaling approach on the regional-to-local scale considering regional climate variability? (3) What do scaling factors tell us about changes in absolute rainfall intensities?*

Section 4.3.1 reviews the temperature-precipitation scaling literature and motivates the endeavor to assess scaling factors from a regional-to-local scale perspective. Section 4.3.2 describes the rain gauge network and data used for the scaling study and Section 4.3.3 explains the quantile regression method to establish the regional-to-local scaling factors. The variability and patterns of scaling factors and implications of percentage sensitivities for the interpretation of absolute precipitation amounts are discussed in Section 4.3.4. A summary and concluding remarks are given in Section 4.3.5.

### 3 DATA AND METHODOLOGY

This thesis sets out to explore the character of and risk from extreme convective precipitation events (ECPEs) in the southeastern Alpine forelands. All three of the research articles presented consider ECPEs on various spatial and temporal scales, and are therefore limited by the extent to which point scale observations from rain gauges represent these processes. Data and methods were chosen to allow quantifying the uncertainties associated with the sampling mode. Other sources of uncertainty exist in precipitation observations, however, they are not within the scope of this thesis (see *Sun et al.*, 2018, for a review). These include technical errors and biases on the instrumental side, but also aleatory uncertainty. This is because we can only observe one state of weather, however, due to chaotic and complex processes, the present is one realization out of many possible paths within certain boundary conditions. It is important to keep in mind that these other factors are also an integral part of any data analyzed.

The data at the core of this thesis are rain gauge-based precipitation observations from operational weather service stations as well as from one hydrological and one research rain gauge network. In addition, data on larger-scale atmospheric conditions (i.a., sea level pressure (PSL) and convective available potential energy (CAPE)), topography (i.a., slope, exposure), and socioeconomic factors (i.a., population, buildings) are considered. This allows a multi-layered analysis of atmospheric, hydrospheric, and anthropospheric elements. It is crucial to choose the methodology that best serves the research purpose and also fits the various kinds and sources of data. Several statistical methods are combined to analyze how ECPEs relate to temperature, damages, and the station density of observing networks. All data were processed and algorithms implemented using Python (Python Software Foundation, [www.python.org](http://www.python.org)). In some cases, geospatial processing methods were integrated through the python module *arcpy* of the geographic information system ArcGIS ([www.esri.com/arcgis](http://www.esri.com/arcgis)).

This chapter discusses in particular the underlying methodology to the thesis

as a whole and elaborates on the choice of data and methods relevant to the three research articles. Detailed descriptions of data and methods used in each individual article can be found in the data and methods sections of the research articles (Data Sections 4.1.2, 4.2.2, 4.1 and 4.3.2; Methods Sections 4.1.2, 4.2.3, 4.2.2, and 4.3.3), and in the supplementary information to the Research Articles 1 and 2 in Appendices A.1 and A.2.

### 3.1 Study area and choice of data

As previously discussed (c.f. Section 2), ECPEs are likely misrepresented in gauge-based precipitation observations and derived gridded datasets but the extent of misrepresentation is largely unknown. This hampers analyses of localized extreme events at regional and climatological scales. A sufficiently dense rain gauge station network and complementary data are required to quantify these uncertainties. The study region in the southeastern Alpine forelands of Austria offers an ideal setting for several reasons. Long-term high-quality records of precipitation and other data are available at high resolution. The region is prone to intense convective precipitation events during the summer months (*Seibert et al.*, 2006), and has experienced considerable warming during the last decades, suggesting a particular sensitivity to global climate change (*Hohmann et al.*, 2018; *Kabas et al.*, 2011). In spite of the strong warming trend, no statistically significant or coherent trends could be identified in the annual mean and maximum daily precipitation and for the summer season in the southeastern Alpine region (*CCCA*, 2016).

The central datasets used here are point-scale precipitation observations from gauges operated by the Austrian weather service *Zentralanstalt für Meteorologie und Klimatologie* (ZAMG), the *Hydrographischer Dienst Österreich* / Austrian Hydrographic Service (AHYD), and the research network WegenerNet Feldbach region climate station network (WegenerNet). WegenerNet data is available under open data policy ([www.wegenernet.org](http://www.wegenernet.org)), and the network is explicitly designed for research purposes (see *Kirchengast et al.*, 2014, for more information on the WegenerNet).

Daily and sub-daily precipitation data from ZAMG is made available to the Wegener Center at the University of Graz for research purposes through a data sharing agreement. The 10 min recordings of precipitation used in this thesis were provided by the federal office of ZAMG in Styria through station-by-station



### 3.1 STUDY AREA AND CHOICE OF DATA

inquires. Sub-daily precipitation data from AHYD were also collected through personal inquiries directed to five federal departments of the AHYD (i.e., the states of Styria, Tyrol, Lower Austria, Salzburg, and Carinthia, respectively). The different access policies and restrictions on the data showcase one common barrier to research on high resolution observations.

AHYD provides daily observations of precipitation and discharge through the platform [www.ehyd.gv.at](http://www.ehyd.gv.at) hosted by the Austrian Federal Ministry of Sustainability and Tourism (before 8 January 2018: Federal Ministry of Agriculture, Forestry, Environment and Water Management (BMLFUW)).

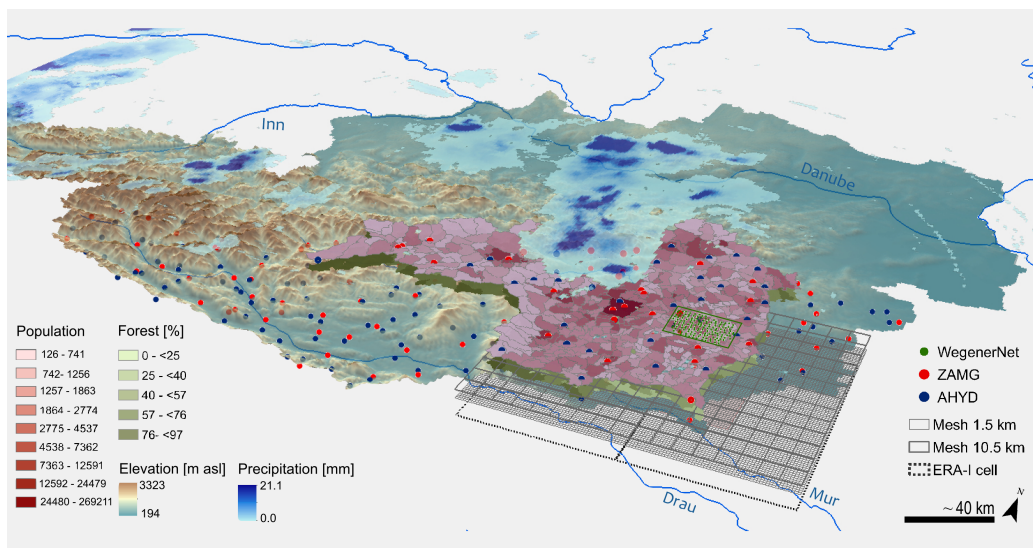


Figure 3.1: The study area in the Austrian southeastern Alpine forelands. The edges of the digital elevation model demarcate Austria. Green, blue, and red dots show the gauge locations of WegenerNet, AHYD, and ZAMG networks used in the southeastern Austrian study area, respectively. Green and red shaded data layers show examples of land cover (here: forested area) and population data for the municipalities analyzed in Research Article 2. The blue data layer is a snapshot of INCA gridded precipitation dataset from 2011-07-07 15:45. Grids in the southeastern region visualize grid resolutions of the ERA-Interim data and 1.5 km and 10.5 km fishnet meshes used in the Fishnet-Windowed Triangular Mesh (FWTM). Note that the layers are vertically displaced and the illustration is not equidistant, equal of area, or angle.

The goal of collecting different datasets is to use as much information on ECPEs in the study region as possible. Given the uncertainties associated with observational records, using data from various sources comes with limitations, such

as using data that is not homogenized<sup>1</sup>. Some of the pitfalls can be alleviated through careful research design. The following aspects are considered throughout the analyses. First, the magnitude of instrumental uncertainty (e.g., *O et al.*, 2018) is smaller than the targeted sampling uncertainty of extreme precipitation. Further, the core interest lies in the character of largest events. These are described using percentiles, but absolute thresholds are also considered. All data are checked against neighboring stations and existing quality controlled gridded daily precipitation products. This procedure applies especially to outliers, which are individually checked for plausibility. Additional information is collected from, e.g., the ZAMG daily weather reports and media outlets, such as online archives of local newspapers. The winter months are excluded from the analysis which avoids most uncertainties due to frozen precipitation. Hail cannot be excluded since no systematic observations of hail are available for Austria, and hail can occur particularly in severe convective storms (SCS). Hail damage is, however, excluded from the damage data analysis, because hail damage is not covered by the disaster fund. Because of short and homogenized records, sub-daily data are not used for time series analysis or trend detection. Spatial interpolation of sub-daily precipitation data is avoided because of the stark spatio-temporal precipitation gradients. Last, sources of uncertainties and confidence intervals are shown and discussed throughout the analysis.

Through identifying synoptic conditions that govern precipitation generation, the use of weather types can increase confidence in the type of precipitation despite fragmentary ground-based measurements. To characterize larger-scale atmospheric conditions, global reanalysis data from ERA-Interim with a horizontal resolution of  $0.75^\circ$  (approx. 80 km) (*Dee et al.*, 2011) is used. The data is well documented and freely available through the European Center for Medium-Range Weather Forecasts (ECMWF). The procedure of weather type classification is described in detail in Section 3.2.2.

The atmospheric process of precipitation is only one element of risk from ECPEs. In Research Article 2, the scope is widened to taking a climate-impact perspective through assessing incurred damages reported to the Austrian disaster

---

<sup>1</sup>Data homogenization describes the process of identifying inhomogeneities and breakpoints in observational records caused by non-weather and climate related factors and adjusting for them where possible. Reasons for inhomogeneities are, for example, station relocations, changes in the land surface and built structures in the vicinity of the station. Rigorous quality claims and the necessity for well-documented metadata on the station history leads to drastic reduction of available homogenized gauge records (*Auer et al.*, 2005).

### 3.1 STUDY AREA AND CHOICE OF DATA

fund (*Katastrophenfonds*). Complexity in the dynamic human-environment system so becomes a further source of uncertainty. Because of this, it is necessary to include more layers of data. Case studies are often able to use finer-grained data of land cover and exposed assets (*Ettlinger et al.*, 2016; *Fuchs et al.*, 2015; *Spekkers et al.*, 2017), and it is generally desirable to have as exact information as possible. However, data above a catchment scale are usually not readily available. The required level of detail is further affected by the sensitivity of the analysis to a respective resolution. The scale of analysis in Research Article 2 is preset by the resolution of the damage data. These are available daily and at the municipality scale. An advantage of using coarser data is that information comes from the same data source over the entire study region. The resolution of the data chosen as risk indicators described below is thus considered appropriate for the initial assessment of damage contributions from convective and stratiform weather types.

Table 3.1 lists all data and respective resolution used in this study. On the hazard side, precipitation and atmospheric observations are used. Also runoff is considered, for which stream gauge observations are employed. Both natural and anthropogenic factors of land surface and subsurface properties influence runoff generation. Land cover data and a digital elevation model allow considering the basic disposition of the Austrian municipalities. A third level is given by the susceptibility of people and infrastructure to be adversely affected by the hazard. Census data and building inventories are considered as a proxy for the spatial distribution of vulnerabilities in the study region.

Table 3.1: Properties and usage of data used in the research articles

Variable <sup>a</sup>	Type/Product	Original spatial resolution	Original temporal resolution	Source <sup>b</sup>	Usage
<i>rr</i>	gauge	point	10 min, 1 d	ZAMG	Temperature sensitivities, testing and validation, precipitation recurrence intervals, Research Articles 1, 2, 3
	grid/gpard1	1 km × 1 km	1 d		
	grid/INCA	1 km × 1 km	15 min		
	grid/WegenerNet	1 km × 1 km	1 d	Wegener Center, University of Graz	
<i>Q</i>	gauge	point	5 min, 10 min, 1 d	AHYD	Flood recurrence intervals, Research Article 2
	gauge	point	1 d		
<i>CAPE</i>	grid/ERA-I	0.75° × 0.75°	1 d	ECMWF	Weather typing, Research Articles 1, 2, 3
<i>PSL</i>	grid/ERA-I	0.75° × 0.75°	1 d		
<i>ZG500</i>	grid/ERA-I	0.75° × 0.75°	1 d		
<i>u700, v700</i>	grid/ERA-I	0.75° × 0.75°	1 d		
<i>SynopticAT</i>	text, identifier	national (Austria)	1 d	ZAMG	
<i>Damage</i>	table	municipality	1 d		
<i>Population</i>	table	municipality	effective 2001	STYR	Municipality clustering, Research Article 2
<i>Topography</i>	grid	10 m × 10 m	effective 2010		
<i>Landcover</i>	grid/CORINE	100 m × 100 m	effective 2006	EAA	
<i>Buildings</i>	vector data	–	effective 2016	OSM	

<sup>a</sup>*rr*: precipitation, *Q*: discharge, *CAPE*: Convective available potential energy, *PSL*: sea level pressure, *ZG500*: 500 hPa geopotential height, *u700, v700*: 700 hPa wind speed, *SynopticAT*: written weather reports

<sup>b</sup>ZAMG: Austrian weather service, AHYD: Austrian hydrographic service, STYR: Office of the Styrian Government, Graz, Austria, EEA: European Environmental Agency, OSM: openstreetmap.org

## 3.2 Choice of methods

Given the heterogeneity of the data used in this study, statistical and analytic methods need to be flexible and allow adequate reporting on the associated uncertainties. The applied methods should be traceable and facilitate conclusive interpretation of the results. In the following paragraphs, the methodical choices are discussed.

### 3.2.1 FROM DATA SERIES TO INDIVIDUAL EVENTS

The typical spatial scale of ECPEs is in the order of a few kilometers, and precipitation occurs on temporal scales from minutes to a few hours. Highly concentrated peak intensities precipitate over even smaller scales (*Peleg et al., 2016*). At daily resolution extreme intensities are thus not well resolved, but consecutive days can mostly be assumed to be independent events. Sub-daily sampling allows a better representation of the peak intensities, however, consecutive sub-daily recordings are more likely to come from the same storm and so be dependent. Studies that assess the temperature sensitivity of extreme precipitation often use all sub-daily samples to calculate extreme percentiles. This likely violates the statistically premised independence. However, potential sensitivities of the results are rarely discussed. To avoid dependencies, calculations in this thesis base on samples of individual storms. An event detection algorithm is run on the full precipitation data series to identify consecutive wet episodes separated by dry intervals.<sup>2</sup> For each event, peak intensities for 10 min to 3 h time integration, total accumulated precipitation, and duration are calculated. This allows for robust statistical analyses based on physically plausible events and also reduces the amount of data for faster processing. The event statistics derived from the ZAMG and AHYD rain gauge records show good agreement with expected precipitation patterns under the weather types extracted from independent data sources (see description of weather typing below). Furthermore, also the convective precipitation classification automated in the WegenerNet quality control largely agrees with the timing of events delineated in the region, indicating that the procedure is robust.

---

<sup>2</sup>To avoid segmentation by very small observations (minimum sampling resolution amounts to 0.1 mm), an observation is counted as wet only if the accumulated 1 h precipitation total around any 10 min observation exceeds a given threshold (1 mm). This removes very small values surrounded by dry records and accepts occasional dry observations within longer events if the total hour sum is large enough. Sensitivity tests supported plausible dissociation for a wet-hour threshold of 1 mm.

### 3.2.2 IDENTIFYING CONVECTIVE CONDITIONS THROUGH WEATHER TYPES

ECPEs are at the center of all three research articles, and the difficulties in reliably observing such events have been discussed in Sections 2 and 3.1. Because under-sampling of localized extreme events is a known issue, precipitation data alone cannot be used to robustly distinguish between convective and non-convective precipitation. Environmental approaches are an established method that help to identify conditions that favor the emergence of severe convective weather (e.g., *Allen et al.*, 2015; *Gensini and Allen*, 2018; *Madonna et al.*, 2018; *Mohr et al.*, 2015). Higher confidence in the state of the atmosphere at larger scales can so narrow down uncertainties in observations of the phenomenon itself.

Weather typing is one common environmental approach to explore the connections of larger-scale circulation and smaller-scale hazards, such as landslides or flooding (e.g., *Messeri et al.*, 2015; *Wood et al.*, 2016). Two basic approaches can be distinguished (*Philipp et al.*, 2016). Approach 1 uses predefined weather type classifications, while approach 2 more flexibly identifies patterns relevant to a particular atmospheric phenomenon. Approach 1 is useful, e.g., to detect changes in general circulation patterns over time or in the context of weather forecasts, where given weather type classifications have been used for long times (*Hoffmann*, 2018; *Nilsen et al.*, 2017). Approach 2 allows to target the pattern identification to a particular predictand (*Schiemann and Frei*, 2010; *Vallorani et al.*, 2017), which in this thesis are conditions favoring ECPEs. Here, the two types are combined to obtain a tailored classification for studying ECPEs in the southeastern Alpine forelands. First, an automated classification is obtained (approach 2), which is then refined using weather classes operationalized by the ZAMG (approach 1).

For the classification procedure, the COST 733 Circulation Type Classification software is employed (*Philipp et al.*, 2016). Variables known to be relevant predictors of convective weather are chosen prior to running the pattern detection algorithms. The variables used are PSL, CAPE, 500 hPa geopotential height (ZG500), and 700 hPa wind velocity (UV700) from ERA-Interim reanalysis (1979-2016) (*Dee et al.*, 2011) over the Greater Alpine Region (see also Section 4.2.3). The variables considered are measures of the general flow direction governed by the large-scale pressure distribution, of atmospheric instability, and the velocity of the weather systems. Several sensitivity tests were done by varying the number and type of input variables, the domain, the time over which the clusters are identified,

## 3.2 CHOICE OF METHODS

and by changing the number of prescribed output weather types to 9, 12, or 27. The chosen classification scheme is a combination of principal component analysis (PCA) and cluster analysis (CA) with the number of weather types prescribed to 27 and is described in detail in *Prein et al. (2016)*. The final setup was found to be the most appropriate for distinguishing between stratiform and convective precipitation patterns.

The combination of four predictive variables and a high number of weather types used in the classification leads to a differentiated clustering where some patterns are populated by less than 10 occurrences. Although the overall target is to distinguish only between primarily convective or stratiform precipitation weather types, a detailed first clustering is beneficial. This is because the region of interest in the southeastern Alpine forelands is significantly smaller than the region over which the clustering needs to be run in order to identify the large-scale flows. The study area is furthermore located in immediate vicinity to the Alps, which constitute a major climatic divide. The peculiarities of the Alpine ridges and valleys are insufficiently resolved in the ERA-Interim dataset with resolution of approx. 80 km (ERA-Interim gridcells are visualized in Figure 3.1 for comparison).

To eventually arrive at a diagnostic delineation of weather patterns over the study region, charts of the predictive variables under the 27 weather types are analyzed together with high-resolution precipitation observations in the study region and a catalogue of written Austrian weather reports issued by the ZAMG. For each day, the reports contain a written statement on the synoptic situation and an identifier assigning one of 18 weather classes<sup>3</sup>. The final six weather types used for the analysis are described in Section 4.2.3.

The chosen procedure trades off the immediate transferability of the method against a robust identification of weather types that cause convective precipitation events in the southeastern Alpine foreland region. For example, days on which main weather patterns transitioned from one to another cannot be adequately resolved by the automated COST 733 method at daily resolution. The written weather reports allows identifying such days and considering them in the final classification.

---

<sup>3</sup>The circulation types are 1) High over western and middle Europe 2) Interim high 3) Zonal high pressure ridge 4) High centered over Fennoscandia 5) High centered over Eastern Europe 6) Northerly flow 7) Northwesterly flow 8) Westerly flow 9) Southwesterly flow 10) Southerly flow 11) Low gradient situation 12) Low south of the Alps 13) Low centered over the western Mediterranean Sea 14) Low centered over southwestern Europe 15) Low over the British Islands 16) Meridional low pressure trough 17) Continental low 18) Low on trajectory Adria-Poland (“Vb”)

Furthermore, the written reports provide highly valuable information for the outlier verification.

### 3.2.3 DESIGNING A METHOD TO ASSESS SAMPLING UNCERTAINTY: THE FWTM METHOD

Many methods exist to estimate area precipitation from gauge measurements through interpolating observations to unobserved sites (*Chen et al.*, 2008; *Hiebl and Frei*, 2016; *Isotta et al.*, 2014). Such estimates can be cross-validated using gauges that were excluded from the interpolation process. This assessment is always either limited to the point scale or limited by the inter-station distances of the rain gauges, which determine the size of the area over which precipitation is estimated. Most operational rain gauge networks have station spacings of 10 km and more, therefore it is largely unknown how sampling uncertainties materialize on the often much smaller scales characteristic to peak convective precipitation intensities. These uncertainties become particularly relevant when evaluating high resolution climate models, which output precipitation (and any other variable) as gridcell averages.

The WegenerNet is a research climate station network that simultaneously fulfills the criteria of very dense gauge spacing (1.4 km), a high number of gauges (154 as of 2018), and being operationally run for a comparably long time (since 2007). For the first time, this set-up allows to empirically assess uncertainties in observed peak precipitation intensities in convective events using ground-based observations. The idea is to downsample the high resolution network to estimate how lower-resolution networks measure the same ECPEs. So far, no method exists to systematically reduce the rain gauge station density. Hence the goal of the FWTM method presented in Research Article 1 was to develop an algorithm to thin out a very high density network step-by-step, strictly controlling the inter-station distances between each group of any three neighboring edge gauges. Triangulation unambiguously defines the area spanned between the gauges. Keeping inter-station distances fixed avoids interpolation biases from unevenly spaced gauges. The meshing controls for balanced representation of sampling areas despite varying initial densities of the ZAMG + AHYD and WegenerNet networks. The procedure of FWTM is described in detail in Section 4.1.2 (see also Figure 4.1.3). As a result, a cascade of networks with approximately equally spaced nodes is created. Applying the event detection scheme and identification of convective environments



## 3.2 CHOICE OF METHODS

described above, peak event intensities and estimated mean area precipitation were calculated for sub-hourly to sub-daily time scales at spatial scales from 1.5 km to 30 km. In principle, the results obtained from FWTM method can so be interpreted equivalently to climate model output, offering new opportunities for testing and validation on convective scales.

### 3.2.4 CHOOSING ROBUST METHODS TO EXPLORE THE CHARACTER AND RISK FROM ECPEs

In addition to the methods discussed, further statistical procedures were applied. In contrast to the methods discussed above, they are not designed and developed individually but rather used “out of the box” without specific adaptations: a) principal component analysis (PCA), also empirical orthogonal functions (EOF), b) cluster analysis (CA), c) extreme value statistics, and d) quantile regression.

a) PCA and b) CA: In atmospheric sciences, PCA is mostly used to “identify patterns of simultaneous variation” (*Storch and Zwiers, 1999, p 293*), such as identifying global teleconnections from global gridded climate data. Methods a) and b) are also applied in the weather typing, but the dimension reduction and clustering procedure is automated by the COST 733 classification software and, besides the sensitivity tests described above, used without further adjustments. PCA is applied in a different context in Research Article 2. Dealing with many different data on various scales simultaneously calls for a reduction to the most essential factors that best explain the variability in the data. Damage data are reported for 480 municipalities in southeastern Austria, and each municipality is associated with certain topography, land cover, population, and number of buildings. These are used to identify vulnerability factors that have an effect on the risk from ECPEs. It would be possible to run an isolated analysis for each municipality, but this would lead to unclear results. This is because many municipalities have similar preconditions and effects would be difficult to distinguish. Also the statistical robustness decreases, as the number of claims per analyzed instance is drastically reduced. Instead, indicators are used to pool the municipalities into similar groups. This can be achieved through PCA and CA. In a first step, principal components explaining most of the variance in the multi-dimensional data are identified (the data used for clustering are indicated in Table 3.1). In a second step, the municipalities are grouped by means of k-means clustering. Each municipality

is randomly assigned to one of a predefined number of clusters to which a centroid is defined as the average location of all points. Each instance is then iteratively assigned to its closest cluster, whose centroid is then recalculated until all samples are clustered to their closest, i.e. most similar, centroid (*Hooshyar et al.*, 2015; *Sharghi et al.*, 2018). Sensitivity tests varying the total amount of explained variability by the principal components, and the target number of clusters showed that the four clusters of alpine, agricultural, urban, and city character is a distinctive, yet overseable pooling of the municipalities.

c) extreme value statistics: In climate sciences, extreme value statistics is widely used to model the tails of a climate variable’s probability distribution  $F$  (the parent distribution, *Gilleland and Katz* (2016)) by fitting a distribution  $F^n$  to the extrema and use its quantiles to make inferences about exceedance probabilities of rare extreme events. Extreme value theory is frequently applied to rainfall and streamflow data (*Towler et al.*, 2010; *Villarini et al.*, 2011). The results often have direct practical implications, e.g. for dimensioning flood protection measures according to a defined protection level, such as a *100-year flood*. In probabilistic terms, a *100-year flood* is to be understood as a flood event with annual exceedance probability (AEP) of  $1/100 = 0.01$  whose magnitude  $z$  (the return level) is exceeded on average once in 100 years (the recurrence interval or return period).

To model the extreme value distribution, the maxima  $M_n = \max\{X_1, \dots, X_n\}$  are assumed to be of an infinite sequence of independent and identically distributed random (i.i.d.) variables  $X_1, \dots, X_n$ , and so the probability  $\Pr\{M_n \leq z\} = F^n(z)$ . However,  $F^n(z) \rightarrow 0$  as  $n \rightarrow \infty$  if  $F$  does not have a finite upper limit smaller than  $z$  (*Gilleland and Katz*, 2016). The Fisher–Tippett–Gnedenko theorem, analogous to the central limit theorem<sup>4</sup>, states that if the maxima  $M_n$  converge, then they asymptotically follow one of three distributions from the generalized extreme value distribution (GEV) family. The GEV family comprises the Gumbel (type I), Fréchet (type II), and Weibull (type III) distributions, which can be subsumed in the form:

$$G(z) = \exp\left[-\left\{1 + \xi \left(\frac{z - \mu}{\sigma}\right)\right\}_+^{-1/\xi}\right],$$

---

<sup>4</sup>The central limit theorem states that the distribution of sums of an infinite series of i.i.d. variables asymptotically follows a normal distribution, regardless of the distribution of the variables. It is also relevant for the analysis of precipitation, e.g., while the distribution of daily precipitation is not normally distributed, annual sums of precipitation converge to a normal distribution for large samples. (*Storch and Zwiers*, 1999)

### 3.2 CHOICE OF METHODS

where  $y_+ = \max\{y, 0\}$ ,  $\sigma > 0$  and  $-\infty < \mu, \xi < \infty$  (Coles, 2001; Gilleland and Katz, 2016).  $\mu$  and  $\sigma$  are commonly called the location and scale parameter, respectively. The shape parameter  $\xi$  determines the behaviour of the tail and thus the type of the distribution. Fréchet  $\xi > 0$ , Weibull for  $\xi < 0$ . If  $\xi \rightarrow 0$ , the GEV reduces to the Gumbel type:

$$G(z) = \exp\left[-\exp\left\{-\left(\frac{z-\mu}{\sigma}\right)\right\}\right], -\infty < z < \infty.$$

This approach is commonly referred to as block maxima (BM) approach<sup>5</sup>, as the maxima are taken from sequence of data blocks, usually one year of daily data. Research Article 2 uses the annual seasonal maxima of daily precipitation totals (annual seasonal maximum daily precipitation amount (sRX1D)) and discharge (annual seasonal maximum daily discharge (sQX1D)) to estimate their recurrence intervals on days where damages from hydro-meteorological hazards were reported (see Section 4.1).

The Gumbel or GEV Type-I distribution is commonly applied in flood frequency analysis, but it is sometimes argued that the light-tailed Gumbel distribution underestimates rare extremes and thus a three parameter GEV is recommended (Koutsoyiannis, 2004; Phillips et al., 2018). However, fitting three parameters is less robust for small sample sizes, as is the case for some of the catchments. The sensitivity of the results presented in Research Article 2 was thoroughly tested and also fit to a three-parameter general GEV for comparison. Using the estimates from GEV, the relative share of major events increases at cost of minor events, but also the share of extremes (recurrence interval >20 yr) decreases. This is explained by the fat-tailed shape of the GEV.

Table 3.2 schematically summarizes the effects of using either of the two methods on the results. The shifted limits between minor, major, and extreme events do not significantly change the relative shares of the hazard levels associated with damage and thus do not alter the conclusions drawn from the analysis. Furthermore, uncertainty intervals from GEV (estimated through a bootstrapping procedure as described in Section 4.1) are much larger and include or overlap those estimated for the Gumbel fits. In summary, the results cannot be interpreted as significantly different or superior. The positive goodness of fit tests and the fact that data are

---

<sup>5</sup>A second approach is the peak-over-threshold (POT) approach, where extremes are defined by values exceeding a high threshold. The extrema of a sequence of i.i.d. variables then converge to the generalized pareto distribution (GPD) (Gilleland and Katz, 2016).

### 3 DATA AND METHODOLOGY

Table 3.2: Qualitative description of results from the sensitivity tests comparing the estimated AEP using GEV versus GEV type-I (Gumbel) fitted to sRX1D and sQX1D for the empirically observed events of magnitude  $z$

Parts of empirical distribution	classification through GEV	classification through GEV type-I (Gumbel)
left part (small $z$ )	lower probability, events more likely classified major than minor	higher probability, events more likely classified minor than major
middle part (medium $z$ )	lower probability, events more likely classified major than minor	higher probability, events more likely classified minor than major
right part (large $z$ , tail)	higher probability, events more likely classified major than extreme	lower probability, events more likely to be classified extreme than major

not extrapolated over the observation period, support that the choice to fit Gumbel distributions sufficiently serves the purpose of the analysis. The high uncertainty ranges nevertheless show the general caveats of applying extreme value statistics to comparatively short real-world data and underline the need for further research.

d) quantile regression: Research Article 3 analyses the temperature sensitivity of extreme precipitation to local temperatures in the southeastern Alpine forelands. It is thus a form of the regional-statistical approach (ii) of estimating instantaneous scaling rates. Most authors employ a “standard binning approach” (*Westra et al.*, 2014). In addition, quantile regression has been proposed. Unlike in ordinary linear regression, not the mean, but a given quantile of the predictand is modeled (*Koenker*, 2005; *Villarini and Slater*, 2018). *Wasko and Sharma* (2014) argue that quantile regression is a superior method for estimating temperature-precipitation scaling, or temperature sensitivity of precipitation (T/P-scaling) rates, because it is insensitive to sample size and allows to flexibly integrate co-variates. The first point is important, since naturally the sample of extremes becomes smaller towards the high end of the temperature scale particularly in the midlatitudes. Furthermore, estimating slopes using standard linear regression methods as employed in the binning approach, is generally sensitive to outliers. Given a large sample, the results from both methods are statistically robust and comparable among the

### 3.2 CHOICE OF METHODS

two methods (*Molnar et al.*, 2015). Although uncertainty estimates from quantile calculation in the standard method could be considered in the regression analysis, confidence intervals around obtained scaling rates are often not shown or discussed. The distribution of samples is implicitly considered in quantile regression and allows a straightforward reporting of the associated model uncertainty.

Furthermore, the robustness of the T/P-scaling is increased through using precipitation event indicators as described above. This avoids a potential issue where several sub-daily precipitation samples of the same storm are repeatedly paired with the daily temperature. This reduces the influence of temporal dependence, but does not consider spatial dependence of neighboring stations. Analyses of spatial correlation and general results from Research Article 1 show that peak intensities in ECPEs rapidly decorrelate in space with an estimated correlation distance of 7.8 km (see Figure 4.1.4). Since rain gauges used in Research Article 3 are 7 km to 10 km apart, the sampling method is appropriate for convective events. When scaling factors are calculated for each station individually (see Figure 4.1.2), this is not directly relevant. However, the patterns of scaling factors emerging at longer integration times indicate the much larger correlation distances in non-convective precipitation events. Hence statistical effects may arise from mixing observations across climatically different zones. To limit such effects, pooled scaling factor analyses are done for climatically coherent sub-regions in the eastern and western part of the study domain, respectively.



## 4 SCALING RELATIONSHIPS AND DAMAGE CONTRIBUTION OF CONVECTIVE PRECIPITATION

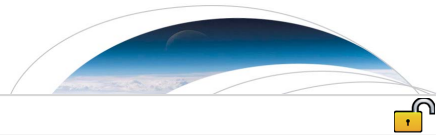
### 4.1 Research Article 1: Strong dependence of extreme convective precipitation intensities on gauge network density

Published as:

**Katharina Schroeer**, Gottfried Kirchengast and Sungmin O (2018). Strong dependence of extreme convective precipitation intensities on gauge network density. *Geophysical Research Letters* **45**, pages 8253–8263. DOI: 10.1029/2018GL077994. Original article and supporting information available at: <https://doi.org/10.1029/2018GL077994>







RESEARCH LETTER

10.1029/2018GL077994

Key Points:

- A dense 1-km-scale rain gauge network is used to quantify maximum area precipitation from convective storms on subhourly scales
- Point-scale extreme precipitation is underestimated by approximately 20% by less resolving 10-km-scale operational networks
- Extreme convective rainfall intensity decays over distance  $d$  [km] by a  $d^{-0.5}$  power law, that is, by  $\sim 50\%$  from 1 to 5 km

Supporting Information:

- Supporting Information S1

Correspondence to:

K. Schroeer,  
katharina.schroeer@uni-graz.at

Citation:

Schroeer, K., Kirchengast, G., & O, S. (2018). Strong dependence of extreme convective precipitation intensities on gauge network density. *Geophysical Research Letters*, 45, 8253–8263. <https://doi.org/10.1029/2018GL077994>

Received 19 MAR 2018

Accepted 15 JUL 2018

Accepted article online 20 JUL 2018

Published online 21 AUG 2018

©2018. The Authors.

This is an open access article under the terms of the Creative Commons Attribution License, which permits use, distribution and reproduction in any medium, provided the original work is properly cited.

## Strong Dependence of Extreme Convective Precipitation Intensities on Gauge Network Density

Katharina Schroeer<sup>1,2,3</sup> , Gottfried Kirchengast<sup>1,2,4</sup> , and Sungmin O<sup>2,4,5</sup> 

<sup>1</sup>Wegener Center for Climate and Global Change (WEGC), University of Graz, Austria, <sup>2</sup>FWF-DK Climate Change, University of Graz, Austria, <sup>3</sup>Now at Federal Office of Meteorology and Climatology MeteoSwiss, Zurich, Switzerland, <sup>4</sup>Institute for Geophysics, Astrophysics, and Meteorology/Institute of Physics, NAWI Graz, University of Graz, Austria, <sup>5</sup>Now at Department of Biogeochemical Integration, Max Planck Institute for Biogeochemistry, Jena, Germany

**Abstract** Extreme convective precipitation on subhourly scales is notoriously misrepresented in rain gauge-based observations, but uncertainties are weakly quantified at the 1 to 30 km scale. We employ a unique observing network, the high-density WegenerNet and surrounding operational rain gauge network in southeastern Austria, to sample convective precipitation extremes at these scales. By systematically constructing lower-density networks, we explore how estimated maximum area precipitation depends on observing station density. Using subhourly to hourly temporal resolution, we find a  $d^{-0.5(\pm 0.1)}$  power law decay of the event maximum area precipitation over distances  $d$  from 1 to 30 km, showing that operational gauge networks underrate extreme convective precipitation falling over small areas. Furthermore, extremes at point scale are found underestimated by operational networks by about 20%. We consider the dependencies representative for short-duration convective events over similar regions at midlatitudes and the results valuable for high-resolution climate model evaluation.

**Plain Language Summary** Precipitation is commonly measured using rain gauge networks. For many applications it is relevant how much precipitation fell over a given area, which is often approximated from point-scale gauge observations. In operational networks, gauges are usually 10 km or more apart. This spacing is not sufficient to observe extreme rain intensities in summer convective events, which occur on subhourly time scales and over small areas. Sparse gauge observations lead to high uncertainty in the estimated area precipitation from such events, hampering, for example, damage risk assessments. The WegenerNet Feldbach region in southeastern Austria is one of the densest networks worldwide, with 150 rain gauges within an area of just 300 km<sup>2</sup>. We use this as core network to explore how maximum area precipitation in convective events depends on the density of the gauge network. We find strong spatial dependence showing that maximum area precipitation observed at 5–6 km gauge separation distance is less than 50% of the maximum intensity observed at point scale. We demonstrate that extreme convective precipitation is underestimated in operational networks. The derived spatial dependence curves illustrate the concentrated nature of convective extremes and are valuable for evaluating climate models and interpreting rain gauge-derived precipitation data sets.

### 1. Introduction

Convective storms at midlatitudes cause the most intense precipitation on short time and small spatial scales (minutes to hours and meters to a few kilometers, respectively). Knowing the spatial distribution, timing, and magnitude of convective extreme precipitation is crucial to understand flash floods (Archer & Fowler, 2018; Cristiano et al., 2017; Rogelis & Werner, 2013) or debris flow initialization (Marra et al., 2016). Concurrent with socioeconomic changes, risks from such events might change as heavy convective precipitation intensifies with global warming (e.g., Ban et al., 2015; Dai et al., 2017; Prein et al., 2017; Westra et al., 2014; Ye et al., 2017).

Rain gauges deliver the only direct measurement of surface precipitation and, with data available on climatological time scales, constitute the fundamental source and reference for precipitation studies despite inevitable uncertainties (McMillan et al., 2012; Sun et al., 2018). Often, area rather than point precipitation

is desired, and deriving area estimates from gauge observations is a long-standing challenge in hydrometeorology. Usually, gauge data are deterministically or geostatistically interpolated (Dirks et al., 1998; Lebel & Laborde, 1988; Ly et al., 2011; Syed et al., 2003; Verworn & Haberlandt, 2011). Spatial correlation measures of gauge observations help estimating area precipitation (Ciach & Krajewski, 2006; Sivapalan & Blöschl, 1998; Sunilkumar et al., 2016; Tokay et al., 2014; Villarini et al., 2008). On small scales, however, this is a challenge because usually very few data pairs exist at small station separation distances, weakening the robustness of the estimated correlogram, semivariogram, or covariance function (Lebel & Laborde, 1988).

For coherent precipitation fields over flat terrain, interpolation yields acceptable results even in low density networks (Dingman, 2015; McMillan et al., 2012), but intense convective precipitation in the midlatitudes unfolds on smaller scales than most operational networks cover at scales of 10 km or larger. Because of the scale mismatch between point observations and precipitation process (cf. Blöschl & Sivapalan, 1995), convective extremes are poorly represented in widely applied gauge-derived precipitation grids.

Radar data provide valuable insights to spatial precipitation structures. Eggert et al. (2015) found that convective precipitation dominates precipitation extremes in Germany at scales below 10 km and shorter than 45 min. Over the Netherlands, 90% of summertime convective events were <7 km in cell diameters, and peak precipitation intensities declined rapidly within 5 km from the storm center (Lochbihler et al., 2017). Yet, considerable uncertainties remain in radar-derived quantitative estimates of precipitation intensities at surface level (Berne & Krajewski, 2013). In convective events and on subhourly to hourly time scales, extreme intensities are often severely underestimated (Bárdossy & Pegram, 2017; Haberlandt & Berndt, 2016; Kann et al., 2015).

In infrastructure design and climate model evaluation (Mishra et al., 2012; Tripathi & Dominguez, 2013), area reduction factors (ARFs; Ly et al., 2011), relating point to area precipitation, are often employed. Area reduction is larger in summer due to increased convective precipitation and in rare extreme events (Eggert et al., 2015; Svensson & Jones, 2010). Although characteristic differences between ARFs for convective and stratiform precipitation have long been recognized (Bell, 1976), little reliable research exists of how extreme area precipitation scales in the 1 to 10 km range. On subhourly to hourly time scales, little or no reduction is assumed over areas of 5 to 10 km<sup>2</sup> (Langousis, 2005). Again, low rain gauge density hampers a robust evaluation of ARFs (e.g., Barbero et al., 2014).

Precipitation at very small scales below 1 km can be studied in confined, campaign-type study settings (Goodrich et al., 1995; Pedersen et al., 2010; Peleg et al., 2013), and at large scales, uncertainties generally decrease. But on the 1 to 10 km scale, just below most operational rain gauge network densities and in the gray zone of climate models, extreme convective surface area precipitation is still subject to large uncertainties (Lind et al., 2016). This restrains evaluation of climate model skill to represent precipitation intensities, particularly for rare extreme events relevant to society (Prein & Gobiet, 2017; Sunyer et al., 2013). Regional climate models at comparably high spatial resolution of 6 km still show considerable negative precipitation biases in summer compared to point precipitation statistics (Olsson et al., 2014). Deeper knowledge of observational uncertainties is crucial to evaluate and interpret such simulations.

Rain gauges provide close to *ground-truth* precipitation observations, but very few networks with >50 gauges, densities of >0.1 gauges/1 km<sup>2</sup>, and subhourly recordings required to study convective area precipitation exist around the globe (e.g., Moore et al., 2000; Singer & Michaelides, 2017; Yoon & Lee, 2017). The very high density, long-term climate station network WegenerNet Feldbach Region (WEGN) in southeastern Austria provides a unique setting with 150 gauges (density 0.5 gauges/1 km<sup>2</sup>). Here we empirically explore the dependence of event maximum area precipitation (EMAP) estimates in extreme convective storms on the observing station density to quantify observational uncertainty associated with convective extreme precipitation at the critical 1 to 30 km scale.

## 2. Data and Methods

### 2.1. Precipitation Data and Convective Events Selection

The study area of 60 km × 60 km is located in southeastern Austria (Figure 1). It is characterized by low-elevation topography except for its north-western most area. The region is considered to be climatologically homogeneous regarding synoptic patterns of heavy precipitation (Seibert et al., 2007). Precipitation observations from 170 rain gauges in the extended convective season (April–September) are used over the years from 2007 to 2015. The 11 and 9 gauges are operated by the Austrian national weather service (ZAMG)

# 4.1 RESEARCH ARTICLE 1: DEPENDENCE OF EXTREME CONVECTIVE PRECIPITATION INTENSITIES ON GAUGE NETWORK DENSITY

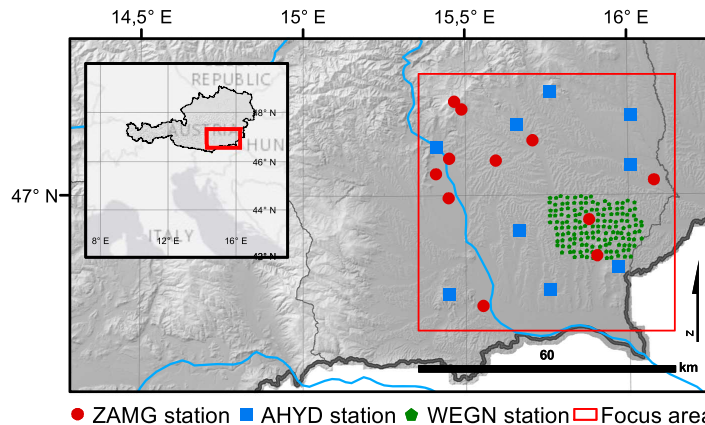


**Figure 1.** Study area and rain gauge locations in southeastern Austria. ZAMG = Austrian national weather service; AHYD = Austrian hydrographic service; WEGN = WegenerNet Feldbach Region.

and the Austrian hydrographic service (AHYD), respectively. The WEGN, operated by the Wegener Center of the University of Graz, comprises 150 gauges approximately aligned on a grid with 1.4 km  $\times$  1.4 km station spacing.

The WEGN network is located over the southeast quadrant of the study domain covering an area of about 20 km  $\times$  15 km. Interstation distances range from 0.7 to 23.4 km. For a detailed introduction of the WEGN and its data quality control and data products generation, see Kirchengast et al. (2014) and Kabas et al. (2011). Raw precipitation amount is sampled at 5-min intervals. O et al. (2018) recently performed a thorough validation and bias estimation of the gauge data and we here use the bias-corrected WEGN level 2 version 6 precipitation data. All WEGN observations are aggregated to 10-min temporal resolution to match AHYD and ZAMG data resolution.

Summertime convective precipitation events are identified a priori. WEGN data processing automatically flags time intervals as convective based on the interstation variability of precipitation. Based on the flagged observations, convective events are classified individual events if they are separated by  $\geq 5$  hr of no or nonconvective precipitation. This way 429 convective events were identified, with a mean duration of 1.2 hr, and less than 1% of events longer than 5 hr. To allow for advection time over the study domain, 2 hr before and after each event are included as margins in the analysis.

To complement the WEGN classification, larger-scale synoptic conditions favoring convection were identified from ERA-Interim reanalysis data (Dee et al., 2011) using the COST Action 733 CT classification software (Philipp et al., 2016; Schiemann & Frei, 2010) and synoptic classifications issued by the Austrian weather service ZAMG. Technical details on the weather typing are provided in the supporting information Text S1.

An event detection algorithm (cf. Schroeer & Kirchengast, 2018) run over all convective days identified 98 precipitation events not flagged by WEGN over the study region. After visual validation using radar-rain gauge-blended integrated nowcasting through comprehensive analysis (INCA) nowcasting precipitation grids (Haiden et al., 2010), these were added to the sample, resulting in a total of 527 convective precipitation events  $E_{1-527}$ . Snapshots of two characteristic storm patterns are displayed for illustration in Figure 2.

## 2.2. Multi-Scale Estimation of EMAP

The spatial correlation of precipitation provides a first measure to characterize precipitation patterns. Pearson's correlation coefficient is calculated from gauge observations after Villarini et al. (2008), and root-mean-square deviation (RMSD) of precipitation (Mishra, 2013) is calculated at increasing station separation distances. For computing the RMSD, pairs of zero rainfall are omitted to avoid overestimating the spatial homogeneity of the rainfall field due to many zero-zero pairs in the network, which are naturally common in convective events. All measures are assessed for 10-min, 30-min, 1-hr, and 3-hr time integrations ( $\tau$ ).

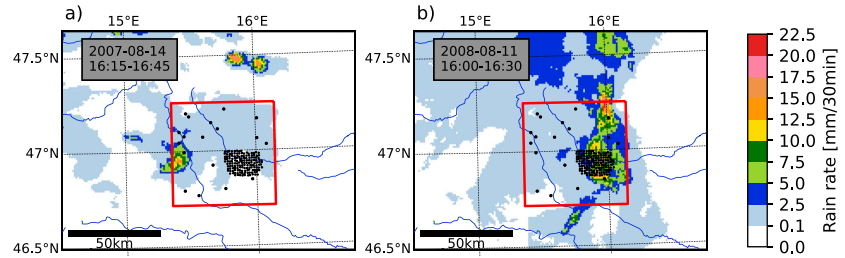


**Figure 2.** Typical examples of sampled convective events over the study region (red square). Both events occurred after very hot days (daily max  $T > 30^{\circ}\text{C}$ ) in low gradient synoptic weather conditions. Data are from the radar/rain gauge-blended integrated nowcasting through comprehensive analysis (INCA). Rain gauges are indicated as black dots. (a) Single-cell convective storm, (b) multicell convective storm.

The equations used are summarized in Table S2. Correlation analyses, however, do not measure area precipitation and are not targeted to event peak intensities. Results are sensitive to the selection of time frames and uncertainties can arise from averaging over different precipitation intensities (Wood et al., 2000).

In convective precipitation events, highest intensities and main runoff are generated by the storm core (Lochbihler et al., 2017; Syed et al., 2003). Extreme intensities are a key uncertainty in observations of convective precipitation and peaks are relevant for infrastructure design. WEGN allows us to empirically explore how estimates of gauge-derived, subhourly EMAP in extreme convective events depend on the station density.

We approach this endeavor in two steps (see Figure 3). First, subnetworks of decreasing resolution are extracted from the high-density network and second, convective area precipitation is estimated for each of the subnetworks.

To systematically generate subnetworks of predefined station separation distance  $d$ , we introduce the fishnet-windowed triangular mesh (FWTM) method. We increase  $d$  stepwise by 1.5 km from 1.5 to 49.5 km and at each step apply a search tolerance of  $s(d) = \pm 0.75$  km. As intergauge distances in a real network are never exactly the same, such a search tolerance  $s$  must be applied (gray circles in Figure 3). While too low search

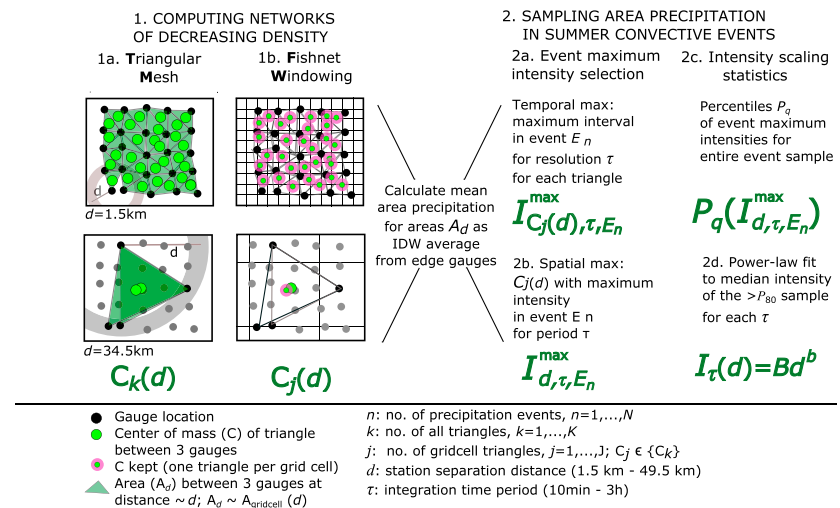


**Figure 3.** Schematic description of the fishnet-windowed triangular mesh (FWTM) subnetwork sampling method including inverse-distance-weighted area rainfall estimation per triangle.

# 4.1 RESEARCH ARTICLE 1: DEPENDENCE OF EXTREME CONVECTIVE PRECIPITATION INTENSITIES ON GAUGE NETWORK DENSITY



tolerance decreases statistical robustness through reducing the number of station pairs, too high search tolerance leads to overlapping distance bin boundaries; we find  $s(d) = \pm 0.75$  km the best choice to maximize search tolerance while avoiding bin overlap.

For each  $d$ , all rain gauges are paired with those neighboring gauges at distance  $d \pm s(d)$  with which they form an approximately equilateral triangle  $C$  with side length  $d$ . At each distance  $d$ , a total number of  $k$  triangular areas among three gauges A, B, and C with  $\overline{AB} \approx \overline{BC} \approx \overline{CA} \approx d$  is found ( $C_k(d)$ , Figure 3, 1a). Although rainfall cells are naturally not triangular in shape, triangles constitute the most elementary and robust way to construct an area over which mean area precipitation can be uniquely defined. Constructing equilateral triangles also eliminates issues arising from irregular rain gauge spacing.

Because of the very high density of stations in the WEGN area, triangles may spatially overlap, for example, when two gauges are so close that both qualify as edge station for a triangle at larger  $d$  (c.f. Figure 3, 1b). If both areas were kept, information is used which would not be available in a real network with separation distance  $d$ . We avoid such potential biases by superimposing a regular *fishnet* grid with cell area  $A_{\text{gridcell}}(d)$ , corresponding to the area  $A_d$  of  $C_k(d)$  over the study domain to filter redundant triangular areas. That is, only one triangle with its center of mass closest to each fishnet cell's center is kept. This fishnet-windowing reduces the number of triangles from  $C_k(d)$  to  $C_j(d)$  (Figure 3, 1b). We tested the sensitivity of the analysis to this filtering by shifting the fishnet's origin in latitude and longitude, to *randomize* the gauges selected as edge stations, and found our results robust over the different testing scenarios (see Figure S1).

In each of the subnetworks of interstation distances  $d \in [1.5, 49.5]$ , precipitation intensity  $I_{C_j(d),\tau,E_n}$  over all triangular areas  $C_j$  is estimated as the arithmetic mean weighted by the gauge distances to the triangle's center of mass (linear inverse-distance-weighting, IDW). Testing the sensitivity of calculations using squared IDW (exponent 2) showed little effect on the results (see Figure S1). For all convective events  $E_n$ , area rainfall estimation is done for integration times  $\tau \in (10, 30, 60, 180$  min), obtaining time series for all triangular areas  $C_j(d)$  at each  $d$  and  $\tau$ .

Next, we select the maximum intensity during each event in both time and space. Only the largest precipitation observation at  $\tau$  is kept:  $I_{C_j(d),\tau,E_n}^{\max}$  (temporal selection, Figure 3, 2a). Of all temporal event maxima over the study domain, we select the area with the highest estimated precipitation:  $I_{d,\tau,E_n}^{\max}$  (spatial selection). This selects the highest estimated mean area precipitation in each individual convective event  $E_n$ , done for all subnetworks with the different station separation distances  $d$  (Figure 3, 2b).

Of the  $n = 527$  convective events, extreme events are defined as those in which the maximum subhourly area intensity at  $d = 1.5$  km exceeds the 80th percentile ( $P_{80}$  events, Figure 3, 2c). The selected summertime convective storms already sample the most intense subdaily precipitation of the years (Schroerer & Kirchengast, 2018), so that this threshold allows analyzing a robust ensemble of extreme events.

The extreme EMAP  $I_\tau(d)$ , called EMAP hereafter, is then adopted to be the median of the  $P_{80}$  events and is obtained for each time resolution  $\tau$ : EMAP\_10, EMAP\_30, EMAP\_60, EMAP\_180. The upper and lower boundaries of the 90% confidence interval of EMAP are estimated as the  $\frac{n}{2} - \frac{1.645\sqrt{n}}{2}$  and  $(\frac{n}{2} + 1) + \frac{1.645\sqrt{n}}{2}$  ranked values of the sample, respectively.

Finally, a two-parameter power law of the form  $I_\tau(d) = Bd^{-b}$  is fitted to the observed EMAP over the 1.5 to 33.0 km range (Figure 3, 2d). The chosen outer scale is considered the limit to reasonable inferences in the 60 km  $\times$  60 km study domain, with sampling up to  $d = 33.0$  km being nearly seamless despite the strict bin separation (only three bins 20.5, 22.5, and 30.5 km are not populated), whereas above, areas can no longer be seamlessly covered with triangles due to the large interstation distances combined with few stations in this large-scale domain.

### 3. Results and Discussion

Figure 4 shows rapidly decorrelating precipitation at 10-min resolution (correlation distance  $d_0 = 7.8$  km), which decreases for longer integration times (3 hr:  $d_0 = 26.5$  km). The relative RMSD of precipitation amounts between gauges (Figure 4b) increases rapidly up to around 10 to 15 km for subhourly scales and eventually levels off, while 1-hourly and 3-hourly curves increase even beyond 20 km. These short correlation distances of convective precipitation are consistent with other studies (e.g., Dzotsi et al., 2014). The results indicate

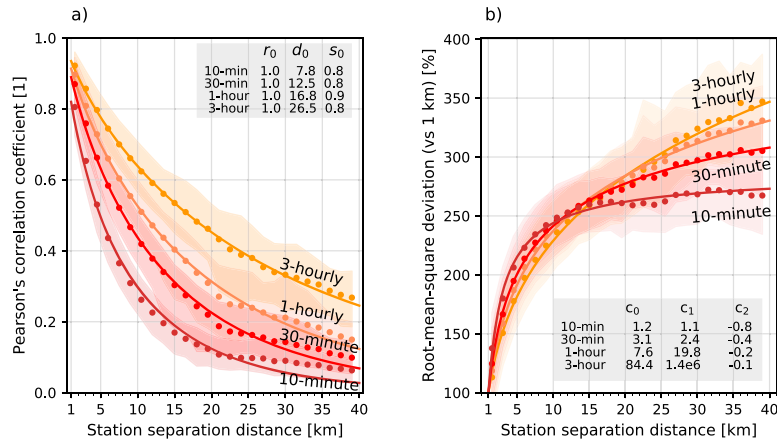


**Figure 4.** (a) Correlogram (spatial correlation) and (b) root-mean-square deviation of precipitation (pairs of zero rainfall are omitted) in 1.5 km bins (dots), using all station series at time integrations from 10 min to 3 hr. Solid lines show three-parameter exponential models fitted to the paired correlations, parameters are shown in the boxes. Shaded areas show the 5th–95th percentile range in each bin. Parameter uncertainties are provided in Table S3.

that an operational coverage of ground observations at 7 to 10-km distance scales cannot provide reliable estimates of area precipitation on smaller spatial scales.

Figure 5 shows the maximum estimated area precipitation in extreme convective precipitation events (EMAP) depending on station separation distance (i.e., the density) of the rain gauge network. Figure 5a shows the EMAP intensity  $I_{\text{area}}(d)$  relative to gauge observations  $I_{\text{point}}$ , which describes an empirical area reduction  $I_{\text{area}}/I_{\text{point}}$ .

Two measures are shown for comparison. First, theoretical ARFs,  $ARF_{\text{theor}}$ , are calculated from maximum point observations following Leclerc and Schaake (1972, equation given in Table S2). Among many methods of ARF calculation, this was chosen because it has repeatedly been used to evaluate precipitation in regional climate models (e.g., Mishra et al., 2012; Tripathi & Dominguez, 2013). Second, using the 20 operational ZAMG + AHYD rain gauges only, precipitation fields are interpolated onto regular grids of cell size  $C(d)$  applying standard squared IDW interpolation with no further restrictions. For each  $E_p(d, \tau)$ , maxima are saved to obtain a best estimate of EMAP from the fixed-density operational network if no further information on the rainfall field was available.

The smallest observable area in the full network is  $\sim 1 \text{ km}^2$  for a triangular area with station separation distance  $\sim 1.5 \text{ km}$ . At this scale, EMAP is 94% (10 and 30 min) to 85% (3 hr) of the point observation. At  $d = 3 \text{ km}$ , EMAP drops to 69% (3 hr) to 66% (10 min). Near operational network scales of  $d = 10 \text{ km}$ , the observed EMAP is 37% (3 hr) to 33% (10 min). With decreasing change rates, EMAPs reach 25% (3 hr) to 20% (10 min) at  $d = 30 \text{ km}$ . These results underline the small scales of extreme convective intensities, as integrating over 3 hr at 1 km scale significantly decreases observed intensities, while enlarging the area but sampling at short temporal intervals also strongly decreases the EMAP estimates.

Between  $d = 1.5 \text{ km}$  and  $d = 35 \text{ km}$  (areas from 1 to  $500 \text{ km}^2$ , respectively), the observed EMAP decays at a rate well approximated by a two-parameter power law  $I_a(d) = Bd^b$ , with an exponent  $b$  (dimensionless) and a reference intensity  $B$  (in intensity units), the latter describing the reference EMAP at a distance  $d$  (in units [km]) of 1 km. We find exponents  $b \approx -0.5(\pm 0.1)$  up to the hourly time scale, that is, a decrease by 50% from 1 to 5 km, and a lower but not significantly different  $b \approx -0.45(\pm 0.1)$  at  $\tau = 3 \text{ hr}$ . All parameters are given in Figure 5, parameter uncertainties are provided in Table S4.

The  $ARF_{\text{theor}}$  used in climate model evaluation studies decreases at a much lower rate to 80–90% within the first 10 km, to reach constant values of 50–75% at 20 to 30 km. This underlines that properties of convective extremes are not sufficiently considered by such ARFs, as emphasized also by Wright et al. (2014),

# 4.1 RESEARCH ARTICLE 1: DEPENDENCE OF EXTREME CONVECTIVE PRECIPITATION INTENSITIES ON GAUGE NETWORK DENSITY

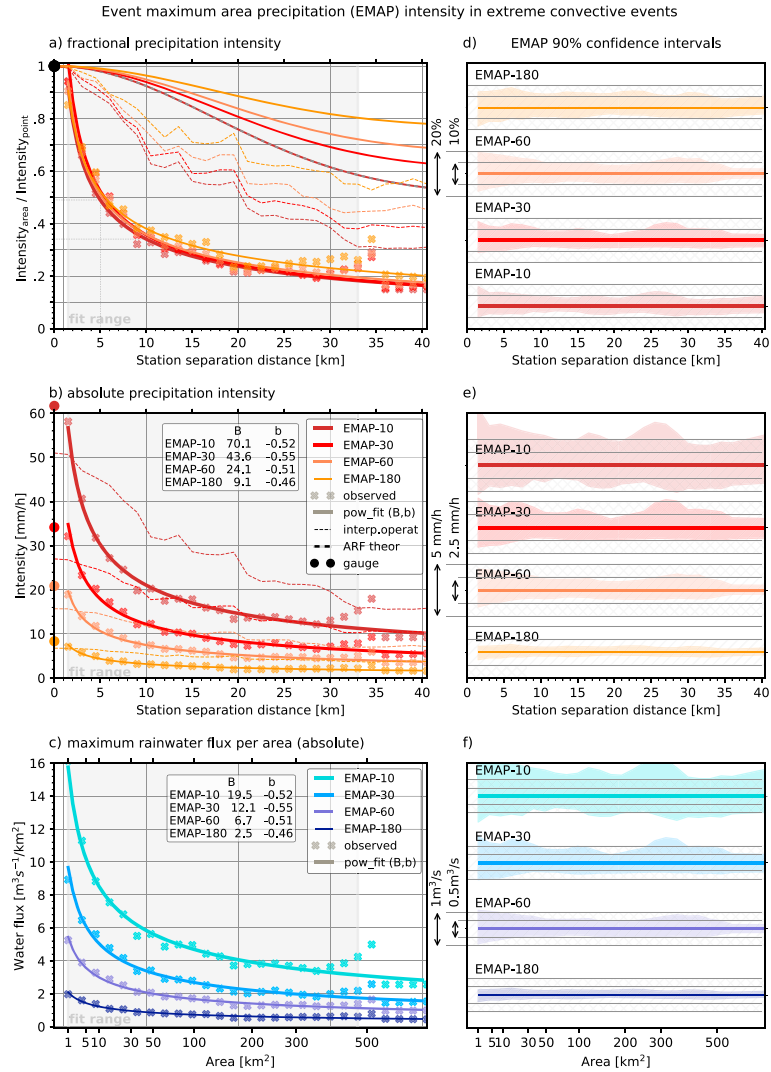


**Figure 5.** Observed (marker symbols) and power law fits (continuous lines) of EMAP intensities in extreme convective precipitation events observed at interstation distances  $d$  for different integration times: 10 min (dark red), 30 min (red), 1 hr (orange), 3 hr (yellow). EMAP point observations are also indicated (circles at distance zero). (a) EMAP relative to the point observation scale, ARF after Leclerc and Schaacke (1972; dashed bicolored lines) and estimates from ZAMG + AHYD operational gauge interpolation only (thin dashed colored lines) are shown for comparison; (b) Absolute EMAP intensities [mm/hr] in the high-density WegenerNet Feldbach Region (markers and heavy lines) and low density ZAMG + AHYD operational network (light dashed lines), respectively; (c) EMAP converted to the rainwater flux per area. (d–f) Shaded areas show the magnitude of the 90% confidence intervals around the corresponding EMAP estimates in (a), (b), and (c), shown in separate panels to avoid graphical confusion in (a), (b), and (c). The legend in (b) is valid also for panel (a). Boxes show parameters of the power law fits. x axis scales of distances  $d$  in (a) and (b) are consistent in scale with the x axis of (c), showing the corresponding areas between three gauges at distance  $d$ . EMAP = event maximum area precipitation; ARF = area reduction factor; ZAMG = Austrian national weather service; AHYD = Austrian hydrographic service.

who explored storm-centered, event-based radar estimates of area reduction down to hourly scales in North Carolina, United States, demonstrating underestimation of reduction by the traditional U.S. Weather Bureau method.

The estimates from interpolated rainfall grids lie in between estimates from  $ARF_{\text{theor}}$  and the empirically sampled EMAPs. The 80th percentile of point precipitation sampled from the operational network is 17–25% lower than in the ensemble including WEGN stations, showing that operational network sampling underestimates the magnitude of extreme point rainfall. However, from  $d = 3$  km, extreme area estimates from the operational network are 12% to 50% larger than estimates from the FWTM network sampling. This indicates that the area of maximum precipitation intensity is overestimated in the operational network, because no area precipitation estimate of such magnitude is observed for the same event despite sampling with much denser networks (station separation distances of 1.5 to 9 km). A potential reason for this is the radial estimation around the rain gauge, leading to characteristic bull's eye effects around local maxima. This statement is only robust for  $d$  smaller than 7–10 km, because at larger  $d$ , the operational station density exceeds that of the less dense FWTM subnetworks.

Figure 5b shows EMAP intensities in WEGN and operational station network in millimeter per hour. EMAP curves of different time integrations stay separated over  $d$ . The 10-min intensities are highest even over large areas. Hence, peak precipitation rates in convective storms are usually not sustained for 30 min or longer, 30-min extreme rates are not sustained over 1 hr, and so forth. This is substantiated by the usually short duration of events at individual station locations (median: 1.5 hr, interquartile range: 0.9 to 2.6 hr).

The estimated EMAP intensities are finally converted to units of total rainwater flux per area (i.e., EMAP intensities are multiplied by the area over which the EMAP is calculated (Figure 5c)). This leans toward hydrological applications and illustrates the magnitude of maximum total rainwater volume precipitating over the given areas in extreme convective storms. One may view this as catchment water influx estimates, while actual runoff water fluxes will clearly depend on factors such as topography, land cover, and soil properties.

#### 4. Summary and Conclusions

We showed that EMAP in extreme convective storms occurs over small areas; hence, the EMAP estimation depends on the density of any observing station network. The results here are based on 9 years of precipitation observations from the very dense WegenerNet rain gauge network (WEGN) and surrounding stations of operational networks (ZAMG and AHYD).

We found a power law decay of observed EMAP with increasing interstation distance  $d$  of the rain gauges over 1 to 35 km and areas of 1 to 500 km<sup>2</sup>, respectively, following  $d^{-0.5(\pm 0.1)}$ , which corresponds to a decay of ~50% from 1 to 5 km distance. Extremes at the point scale (the rain gauge location), however, stay well below the values extrapolated to the point from the power law for small (1 km scale) distances. This indicates that the spatial extent of the most extreme intensity in convective storm cells (i.e., the area over which there would be no EMAP reduction from the point location) is smaller than 1 km<sup>2</sup> but clearly not zero, that is, needs to be addressed at subkilometer scale (e.g., Pedersen et al., 2010).

When deriving areas of maximum precipitation from interpolation of the operational network only, a simple interpolation method such as IDW results in overestimating the area affected by most extreme precipitation intensities at scales below the operational resolution. The presented scaling rates can assist in choosing interpolation parameters, for example, when adjusting the power value of IDW to precipitation type for confining the range of influence as suggested by Kann et al. (2015).

Irrespective of interpolation, the frequency of extreme peak precipitation is significantly undersampled in the operational network. While the maximum point-scale intensities recorded in both data sets are of similar magnitude, the distribution of extreme intensities in convective events shows significant differences, with the 80th percentile being approximately 20% lower when sampled from ZAMG-AHYD as compared to WEGN.

Unadjusted traditional ARFs strongly underestimate area reduction of convective extremes on small scales, since storm type differences are not explicitly considered (Pavlovic et al., 2016). Extremes at point scale are caused by different storm types than extremes at larger scales (Eggert et al., 2015). Comparative studies show that applying unadjusted ARF methods (e.g., review by Svensson & Jones, 2010) may significantly overestimate or underestimate area rainfall and that storm-centered, radar-based approaches better capture area



# 4.1 RESEARCH ARTICLE 1: DEPENDENCE OF EXTREME CONVECTIVE PRECIPITATION INTENSITIES ON GAUGE NETWORK DENSITY



reduction in thunderstorm environments (Mineo et al., 2018; Wright et al., 2014). Advantages and drawbacks of ARF methods should thus not only be carefully considered in engineering but also in evaluating climate models.

Our empirically substantiated spatial scaling can serve as a reference for improved evaluations of convective storm types in climatologically similar regions, that is, in warm temperate, fully humid, and warm summer climates at midlatitudes, such as most of Central Europe and southeastern parts of United States, Australia, or South-America (e.g., Kottek et al., 2006).

Radar data will further grow in quality and relevance for precipitation observation but rain gauges remain the primary source for ground-truth reference data sets. Most data sets of past climate rely on gauge data alone, and insufficient coverage by ground stations is responsible for persisting uncertainty. Our study quantified part of these uncertainties for summertime convective precipitation events at midlatitudes.

Peak area precipitation in convective events decays on spatial scales much smaller than operational network interstation distances, leading to severe underestimation at scales below 10 km, which can conversely result in interpolating too low intensity over too large areas. With growing evidence that midlatitude convective precipitation extremes are intensifying with climate change (e.g., Barbero et al., 2017; Dai et al., 2017; Fischer & Knutti, 2016; Ye et al., 2017), it is increasingly relevant to interpret and evaluate climate model and gauge-derived precipitation intensities at kilometer-scales. By providing a fundamental scaling dependence of convective extreme area precipitation on station density derived from high-quality, ground-truth gauge observations, our results can assist these tasks.

## Acknowledgments

This project was funded by the Austrian Science Fund (FWF) under research grant W 1256-G15 (Doctoral Programme Climate Change Uncertainties, Thresholds and Coping Strategies). WegenerNet funding is provided by the Austrian Ministry for Science and Research, the University of Graz, the state of Styria (which also included European Union regional development funds), and the city of Graz; detailed information is found at [www.wegcenter.at/wegenernet](http://www.wegcenter.at/wegenernet) and the data are available through the WegenerNet data portal ([www.wegenernet.org](http://www.wegenernet.org)). We thank the Austrian national weather service ZAMG for access to rain gauge and gridded (INCA and gpard1) precipitation data (available through <https://www.zamg.ac.at/cms/en/climate/climate>) and the offices of the Austrian hydrographic service AHYD for access to their gauge precipitation data (available through <http://www.wasserwirtschaft.steiermark.at/cms/beitrag/10742148/22349571/>). We thank ECMWF Reading for access to ERA-Interim reanalysis data (available at <http://apps.ecmwf.int/datasets/data/interim-full-daily>).

## References

- Archer, D., & Fowler, H. (2018). Characterising flash flood response to intense rainfall and impacts using historical information and gauged data in Britain. *Journal of Flood Risk Management*, 11, 121–133. <https://doi.org/10.1111/jfr3.12187>
- Ban, N., Schmidli, J., & Schär, C. (2015). Heavy precipitation in a changing climate: Does short-term summer precipitation increase faster? *Geophysical Research Letters*, 42, 1165–1172. <https://doi.org/10.1002/2014GL062588>
- Barbero, R., Fowler, H. J., Lenderink, G., & Blenkinsop, S. (2017). Is the intensification of precipitation extremes with global warming better detected at hourly than daily resolutions? *Geophysical Research Letters*, 44, 974–983. <https://doi.org/10.1002/2016GL071917>
- Barbero, G., Moissello, U., & Todeschini, S. (2014). Evaluation of the areal reduction factor in an urban area through rainfall records of limited length: A case study. *Journal of Hydrologic Engineering*, 19, 05014016. [https://doi.org/10.1061/\(ASCE\)HE.1943-5584.0001022](https://doi.org/10.1061/(ASCE)HE.1943-5584.0001022)
- Bárdossy, A., & Pegram, G. (2017). Combination of radar and daily precipitation data to estimate meaningful sub-daily point precipitation extremes. *Journal of Hydrology*, 544(Supplement C), 397–406. <https://doi.org/10.1016/j.jhydrol.2016.11.039>
- Bell, F. C. (1976). The areal reduction factor in rainfall frequency estimation (IH Report No.35). Wallingford: Institute of Hydrology. <http://nora.nerc.ac.uk/id/eprint/5751>
- Berne, A., & Krajewski, W. F. (2013). Radar for hydrology: Unfulfilled promise or unrecognized potential? *Advances in Water Resources*, 51, 357–366. <https://doi.org/10.1016/j.advwatres.2012.05.005>
- Blöschl, G., & Sivapalan, M. (1995). Scale issues in hydrological modelling: A review. *Hydrological Processes*, 9(3-4), 251–290. <https://doi.org/10.1002/hyp.3360090305>
- Ciach, G., & Krajewski, W. (2006). Analysis and modeling of spatial correlation structure of small-scale rainfall in central Oklahoma. *Advances in Water Resources*, 1450–1463. <https://doi.org/10.1016/j.advwatres.2005.11.003>
- Cristiano, E., ten Veldhuis, M.-C., & van de Giesen, N. (2017). Spatial and temporal variability of rainfall and their effects on hydrological response in urban areas – A review. *Hydrology and Earth System Science*, 21(7), 3859–3878. <https://doi.org/10.5194/hess-21-3859-2017>
- Dai, A., Rasmussen, R. M., Liu, C., Ikeda, K., & Prein, A. F. (2017). A new mechanism for warm-season precipitation response to global warming based on convection-permitting simulations. *Climate Dynamics*, 1–26. <https://doi.org/10.1007/s00382-017-3787-6>
- Dee, D. P., Uppala, S. M., Simmons, A. J., Berrisford, P., Poli, P., Kobayashi, S., et al. (2011). The ERA-Interim reanalysis: Configuration and performance of the data assimilation system. *Quarterly Journal of the Royal Meteorological Society*, 137(656), 553–597. <https://doi.org/10.1002/qj.828>
- Dingman, S. L. (2015). *Physical hydrology* (3rd ed.). Long Grove, IL: Waveland Press.
- Dirks, K., Hay, J., Stow, C., & Harris, D. (1998). High-resolution studies of rainfall on Norfolk island: Part II: Interpolation of rainfall data. *Journal of Hydrology*, 208(3), 187–193. [https://doi.org/10.1016/S0022-1694\(98\)00155-3](https://doi.org/10.1016/S0022-1694(98)00155-3)
- Dzotsi, K. A., Matyas, C. J., Jones, J. W., Baigorria, G., & Hoogenboom, G. (2014). Understanding high resolution space-time variability of rainfall in southwest Georgia, United States. *International Journal of Climatology*, 34(11), 3188–3203. <https://doi.org/10.1002/joc.3904>
- Eggert, B., Berg, P., Haerter, J. O., Jacob, D., & Moseley, C. (2015). Temporal and spatial scaling impacts on extreme precipitation. *Atmospheric Chemistry and Physics*, 15(10), 5957–5971. <https://doi.org/10.5194/acp-15-5957-2015>
- Fischer, E. M., & Knutti, R. (2016). Observed heavy precipitation increase confirms theory and early models. *Nature Climate Change*, 6, 986–991. <https://doi.org/10.1038/nclimate3110>
- Goodrich, D. C., Faurès, J.-M., Woolhiser, D. A., Lane, L. J., & Sorooshian, S. (1995). Measurement and analysis of small-scale convective storm rainfall variability. *Journal of Hydrology*, 173(1), 283–308. [https://doi.org/10.1016/0022-1694\(95\)02703-R](https://doi.org/10.1016/0022-1694(95)02703-R)
- Haberlandt, U., & Berndt, C. (2016). The value of weather radar data for the estimation of design storms – An analysis for the Hannover region. *Spatial Dimensions of Water Management - Redistribution of Benefits and Risks*, 373, 81–85. <https://doi.org/10.5194/piabs-373-81-2016>
- Haiden, T., Kann, A., Wittmann, C., Pistotnik, G., Bica, B., & Gruber, C. (2010). The integrated nowcasting through comprehensive analysis (INCA) system and its validation over the eastern Alpine region. *Weather and Forecasting*, 26(2), 166–183. <https://doi.org/10.1175/2010WAF2222451.1>

- Kabas, T., Leuprecht, A., Bichler, C., & Kirchengast, G. (2011). WegenerNet climate station network region Feldbach, Austria: Network structure, processing system, and example results. *Advances in Science and Research*, 6, 49–54. <https://doi.org/10.5194/asr-6-49-2011>
- Kann, A., Meirold-Mautner, I., Schmid, F., Kirchengast, G., Fuchsberger, J., Meyer, V., et al. (2015). Evaluation of high-resolution precipitation analyses using a dense station network. *Hydrology and Earth System Sciences*, 19(3), 1547–1559. <https://doi.org/10.5194/hess-19-1547-2015>
- Kirchengast, G., Kabas, T., Leuprecht, A., Bichler, C., & Truhetz, H. (2014). WegenerNet: A pioneering high-resolution network for monitoring weather and climate. *Bulletin of the American Meteorological Society*, 95(2), 227–242. <https://doi.org/10.1175/BAMS-D-11-00161.1>
- Kottek, M., Grieser, J., Beck, C., Rudolf, B., & Rubel, F. (2006). World map of the köppen-geiger climate classification updated. *Meteorologische Zeitschrift*, 15(3), 259–263. <https://doi.org/10.1127/0941-2948/2006/0130>
- Langousis, A. (2005). *The areal reduction factor (ARF): A multifractal analysis doctoral dissertation*. Cambridge, MA: Massachusetts Institute of Technology. Retrieved from DSpace <http://dspace.mit.edu/handle/1721.1/30196>
- Lebel, T., & Laborde, J. P. (1988). A geostatistical approach for areal rainfall statistics assessment. *Stochastic Hydrology and Hydraulics*, 2(4), 245–261. <https://doi.org/10.1007/BF01544039>
- Leclerc, G., & Schaake, J. (1972). Derivation of hydrologic frequency curves (*Rep. 142*). Cambridge: Mass. Inst. of Technol.
- Lind, P., Lindstedt, D., Kjellstrom, E., & Jones, C. (2016). Spatial and temporal characteristics of summer precipitation over Central Europe in a suite of high-resolution climate models. *Journal of Climate*, 29(10), 3501–3518. <https://doi.org/10.1175/JCLI-D-15-0463.1>
- Lochbihler, K., Lenderink, G., & Siebesma, A. P. (2017). The spatial extent of rainfall events and its relation to precipitation scaling. *Geophysical Research Letters*, 44, 8629–8636. <https://doi.org/10.1002/2017GL074857>
- Ly, S., Charles, C., & Degré, A. (2011). Geostatistical interpolation of daily rainfall at catchment scale: The use of several variogram models in the Ourthe and Ambleve catchments, Belgium. *Hydrology and Earth System Sciences*, 15(7), 2259–2274. <https://doi.org/10.5194/hess-15-2259-2011>
- Marra, F., Nikolopoulos, E., Creutin, J., & Borga, M. (2016). Space–time organization of debris flows-triggering rainfall and its effect on the identification of the rainfall threshold relationship. *Journal of Hydrology*, 541(Part A), 246–255. <https://doi.org/10.1016/j.jhydrol.2015.10.010>
- McMillan, H., Krueger, T., & Freer, J. (2012). Benchmarking observational uncertainties for hydrology: Rainfall, river discharge and water quality. *Hydrological Processes*, 26(26), 4078–4111. <https://doi.org/10.1002/hyp.9384>
- Mineo, C., Ridolfi, E., Napolitano, F., & Russo, F. (2018). The areal reduction factor: A new analytical expression for the Lazio Region in central Italy. *Journal of Hydrology*, 560, 471–479. <https://doi.org/10.1016/j.jhydrol.2018.03.033>
- Mishra, A. K. (2013). Effect of rain gauge density over the accuracy of rainfall: A case study over Bangalore, India. *SpringerPlus*, 2, 311. <https://doi.org/10.1186/2193-1801-2-311>
- Mishra, V., Dominguez, F., & Lettenmaier, D. P. (2012). Urban precipitation extremes: How reliable are regional climate models? *Geophysical Research Letters*, 39, L03407. <https://doi.org/10.1029/2011GL050658>
- Moore, R. J., Jones, D. A., Cox, D. R., & Isham, V. S. (2000). Design of the HYREX raingauge network. *Hydrology and Earth System Sciences*, 4(4), 521–530. <https://doi.org/10.5194/hess-4-521-2000>
- Olsson, J., Berg, P., & Kawamura, A. (2014). Impact of RCM spatial resolution on the reproduction of local, subdaily precipitation. *Journal of Hydrometeorology*, 16(2), 534–547. <https://doi.org/10.1175/JHM-D-14-0007.1>
- O, S., Foelsche, U., Kirchengast, G., & Fuchsberger, J. (2018). Validation and correction of rainfall data from the WegenerNet high density network in southeast Austria. *Journal of Hydrology*, 556, 1110–1122. <https://doi.org/10.1016/j.jhydrol.2016.11.049>
- Pavlovic, S., Perica, S., Laurent, M. S., & Mejia, A. (2016). Intercomparison of selected fixed-area areal reduction factor methods. *Journal of Hydrology*, 537, 419–430. <https://doi.org/10.1016/j.jhydrol.2016.03.027>
- Pedersen, L., Jensen, N. E., Christensen, L. E., & Madsen, H. (2010). Quantification of the spatial variability of rainfall based on a dense network of rain gauges. *Atmospheric Research*, 95(4), 441–454. <https://doi.org/10.1016/j.atmosres.2009.11.007>
- Peleg, N., Ben-Asher, M., & Morin, E. (2013). Radar subpixel-scale rainfall variability and uncertainty: Lessons learned from observations of a dense rain-gauge network. *Hydrology and Earth System Sciences*, 17(6), 2195–2208. <https://doi.org/10.5194/hess-17-2195-2013>
- Philipp, A., Beck, C., Huth, R., & Jacobeit, J. (2016). Development and comparison of circulation type classifications using the COST 733 dataset and software. *International Journal of Climatology*, 36(7), 2673–2691. <https://doi.org/10.1002/joc.3920>
- Prein, A. F., & Gobiet, A. (2017). Impacts of uncertainties in European gridded precipitation observations on regional climate analysis. *International Journal of Climatology*, 37(1), 305–327. <https://doi.org/10.1002/joc.4706>
- Prein, A. F., Rasmussen, R. M., Ikeda, K., Liu, C., Clark, M. P., & Holland, G. J. (2017). The future intensification of hourly precipitation extremes. *Nature Climate Change*, 7(1), 48–52. <https://doi.org/10.1038/nclimate3168>
- Rogelis, M. C., & Werner, M. G. F. (2013). Spatial interpolation for real-time rainfall field estimation in areas with complex topography. *Journal of Hydrometeorology*, 14(1), 85–104. <https://doi.org/10.1175/JHM-D-11-0150.1>
- Schiemann, R., & Frei, C. (2010). How to quantify the resolution of surface climate by circulation types: An example for Alpine precipitation. *Physics and Chemistry of the Earth Parts A/B/C*, 35(9–12), 403–410. <https://doi.org/10.1016/j.pce.2009.09.005>
- Schroeder, K., & Kirchengast, G. (2018). Sensitivity of extreme precipitation to temperature: The variability of scaling factors from a regional to local perspective. *Climate Dynamics*, 50(11–12), 3981–3994. <https://doi.org/10.1007/s00382-017-3857-9>
- Seibert, P., Frank, A., & Formayer, H. (2007). Synoptic and regional patterns of heavy precipitation in Austria. *Theoretical and Applied Climatology*, 87(1–4), 139–153. <https://doi.org/10.1007/s00704-006-0198-8>
- Singer, M. B., & Michaelides, K. (2017). Deciphering the expression of climate change within the Lower Colorado River basin by stochastic simulation of convective rainfall. *Environmental Research Letters*, 12(10), 104011. <https://doi.org/10.1088/1748-9326/aa8e50>
- Sivapalan, M., & Blöschl, G. (1998). Transformation of point rainfall to areal rainfall: Intensity-duration-frequency curves. *Journal of Hydrology*, 204(1), 150–167. [https://doi.org/10.1016/S0022-1694\(97\)00117-0](https://doi.org/10.1016/S0022-1694(97)00117-0)
- Sun, Q., Miao, C., Duan, Q., Ashouri, H., Sorooshian, S., & Hsu, K.-L. (2018). A review of global precipitation data sets: Data sources, estimation, and intercomparisons. *Reviews of Geophysics*, 56, 79–107. <https://doi.org/10.1002/2017RG000574>, advanced online publication.
- Sunilkumar, K., Narayana Rao, T., & Satheshkumar, S. (2016). Assessment of small-scale variability of rainfall and multi-satellite precipitation estimates using measurements from a dense rain gauge network in Southeast India. *Hydrology and Earth System Sciences*, 20, 1719–1735. <https://doi.org/10.5194/hess-20-1719-2016>
- Sunyer, M. A., Sørup, H. J. D., Christensen, O. B., Madsen, H., Rosbjerg, D., Mikkelsen, P. S., & Arnbjerg-Nielsen, K. (2013). On the importance of observational data properties when assessing regional climate model performance of extreme precipitation. *Hydrology and Earth System Sciences*, 17(11), 4323–4337. <https://doi.org/10.5194/hess-17-4323-2013>
- Svensson, C., & Jones, D. A. (2010). Review of methods for deriving areal reduction factors. *Journal of Flood Risk Management*, 3(3), 232–245. <https://doi.org/10.1111/j.1753-318X.2010.01075.x>

# 4.1 RESEARCH ARTICLE 1: DEPENDENCE OF EXTREME CONVECTIVE PRECIPITATION INTENSITIES ON GAUGE NETWORK DENSITY



- Syed, K. H., Goodrich, D. C., Myers, D. E., & Sorooshian, S. (2003). Spatial characteristics of thunderstorm rainfall fields and their relation to runoff. *Journal of Hydrology*, 271(1), 1–21. [https://doi.org/10.1016/S0022-1694\(02\)00311-6](https://doi.org/10.1016/S0022-1694(02)00311-6)
- Tokay, A., Roche, R. J., & Bashor, P. G. (2014). An experimental study of spatial variability of rainfall. *Journal of Hydrometeorology*, 15(2), 801–812. <https://doi.org/10.1175/JHM-D-13-031.1>
- Tripathi, O. P., & Dominguez, F. (2013). Effects of spatial resolution in the simulation of daily and subdaily precipitation in the southwestern US. *Journal of Geophysical Research: Atmospheres*, 118, 7591–7605. <https://doi.org/10.1002/jgrd.50590>
- Verworn, A., & Haberlandt, U. (2011). Spatial interpolation of hourly rainfall – effect of additional information, variogram inference and storm properties. *Hydrology and Earth System Sciences*, 15, 569–584. <https://doi.org/10.5194/hess-15-569-2011>
- Villarini, G., Mandapaka, P. V., Krajewski, W. F., & Moore, R. J. (2008). Rainfall and sampling uncertainties: A rain gauge perspective. *Journal of Geophysical Research: Atmospheres*, 113, D11102. <https://doi.org/10.1029/2007JD009214>
- Westra, S., Fowler, H. J., Evans, J. P., Alexander, L. V., Berg, P., Johnson, F., et al. (2014). Future changes to the intensity and frequency of short-duration extreme rainfall. *Reviews of Geophysics*, 52, 522–555. <https://doi.org/10.1002/2014RG000464>
- Wood, S. J., Jones, D. A., & Moore, R. J. (2000). Accuracy of rainfall measurement for scales of hydrological interest. *Hydrology and Earth System Sciences*, 4(4), 531–543. <https://doi.org/10.5194/hess-4-531-2000>
- Wright, D. B., Smith, J. A., & Baeck, M. L. (2014). Critical examination of area reduction factors. *Journal of Hydrologic Engineering*, 19(4), 769–776. [https://doi.org/10.1061/\(ASCE\)HE.1943-5584.0000855](https://doi.org/10.1061/(ASCE)HE.1943-5584.0000855)
- Ye, H., Fetzer, E. J., Wong, S., & Lambriqtsen, B. H. (2017). Rapid decadal convective precipitation increase over Eurasia during the last three decades of the 20th century. *Science Advances*, 3(1). <https://doi.org/10.1126/sciadv.1600944>
- Yoon, S.-S., & Lee, B. (2017). Effects of using high-density rain gauge networks and weather radar data on urban hydrological analyses. *Water*, 9(12). <https://doi.org/10.3390/w9120931>



4.2 Research Article 2: Quantifying damage contributions  
from convective and stratiform weather types: How well do  
precipitation and discharge data indicate the risk?



Published as:

**Katharina Schroeer** and Mari R. Tye (2019). Quantifying damage contributions from convective and stratiform weather types: How well do precipitation and discharge data indicate the risk? *Journal of Flood Risk Management* 2019;12:e12491. 13 pages. DOI: 10.1111/jfr3.12491.

Original article and supporting information available at: <https://doi.org/10.1111/jfr3.12491>



## Quantifying damage contributions from convective and stratiform weather types: How well do precipitation and discharge data indicate the risk?

Katharina Schroeder<sup>1,2,4</sup>  | Mari R. Tye<sup>3</sup> 

<sup>1</sup>Wegener Center for Climate and Global Change (WEGC), University of Graz, Graz, Austria

<sup>2</sup>FWF-DK Climate Change, University of Graz, Graz, Austria

<sup>3</sup>Capacity Center for Climate & Weather Extremes, Mesoscale and Microscale Meteorology Laboratory, National Center for Atmospheric Research, Boulder, Colorado

<sup>4</sup>Now at Federal Office of Meteorology and Climatology MeteoSwiss, Zurich, Switzerland

### Correspondence

Katharina Schroeder, Wegener Center for Climate and Global Change (WEGC), University of Graz, Austria.

Email: katharina.schroeder@uni-graz.at

### Funding information

Austrian Science Fund, Grant/Award Number: W 1256-G15 (Doctoral Programme Climate Change Uncertainties, Thresholds and Coping Strategies); National Science Foundation, Grant/Award Number: NSF EaSM3 Grant 1419563

Convective precipitation is intensifying in many regions, but potential implications of shifts in precipitation types on impacts have not been quantified. Furthermore, risk assessments often focus on rare extremes, but also more frequent hydro-meteorological events burden private and public budgets. Here synoptic, hydrological, meteorological, and socio-economic data are merged to analyse 25 years of damage claims in 480 Austrian municipalities. Exceedance probabilities of discharge and precipitation associated with damage reports are calculated and compared for convective and stratiform weather patterns. During April to November, 60% of claims are reported under convective conditions. Irrespective of the weather type, most of the accumulated cost links to minor hazard levels, not only indicating that frequent events are a highly relevant expense factor, but also pointing to deficiencies in observational data. High uncertainty in damage costs attributable to extreme events demonstrates the questionable reliability of calculating low-frequency event return levels. Significant differences exist among weather types. Stratiform weather types are up to 10 times more often associated with damaging extreme discharge or precipitation, while convective weather shows the highest nuisance level contributions. The results show that changes in convective precipitation are pertinent to risk management as convective weather types have contributed significantly to damage in the past.

### KEYWORDS

convective precipitation, extreme events, natural hazard, nuisance events, vulnerability, weather types

## 1 | INTRODUCTION

Damage from extreme precipitation disrupts daily life and imposes financial burdens on private and public budgets. In Austria, damage repairs from hydro-meteorological hazards are largely supported by a tax-financed disaster fund. While fluvial flooding, often stemming from large-scale precipitation, is considered in risk assessments on the national level (BMNT, 2011), also flash floods, debris flows, and landslides frequently cause damage. These events are often caused by

intense localised convective precipitation on sub-daily time scales (Aceto, Caloiero, Pasqua, & Petrucci, 2016; Llasat, Marcos, Turco, Gilabert, & Llasat-Botija, 2016).

Contributions from convective precipitation to total damage volume are not well quantified, but knowledge of such damage potential is important because extreme convective precipitation is expected to intensify with global warming in many regions (Bao, Sherwood, Alexander, & Evans, 2017; Dai, Rasmussen, Liu, Ikeda, & Prein, 2017; Donat, Lowry, Alexander, O'Gorman, & Maher, 2016; Prein et al., 2017;

This is an open access article under the terms of the Creative Commons Attribution License, which permits use, distribution and reproduction in any medium, provided the original work is properly cited.

© 2018 The Authors. *Journal of Flood Risk Management* published by Chartered Institution of Water and Environmental Management and John Wiley & Sons Ltd.

Westra, Alexander, & Zwiers, 2012). The frequency of convective storms has increased over the mid-latitudes (Feng et al., 2016; Ye, Fetzer, Wong, & Lambriksen, 2017), and atmospheric conditions favouring severe storms are projected to increase over central-southern Europe (Púčík et al., 2017). Convective storms challenge risk assessments, because associated extreme precipitation and runoff are not well represented in gauge observations (Eggert, Berg, Haerter, Jacob, & Moseley, 2015; Lebel, Bastin, Oblet, & Creutin, 1987; Schroeder, Kirchengast & O, 2018). There is still considerable underestimation of extreme intensities in radar estimates (Kann et al., 2015; Peleg et al., 2018). Insurance data can complement sparse observations, but come with their own set of uncertainties (Grahn & Nyberg, 2017; Punge & Kunz, 2016; Wirtz, Kron, Löw, & Steuer, 2014).

Data limitations often force regional risk assessments to focus on large-scale precipitation patterns or to single out specific catchments or events (e.g., Boudou, Lang, Vinet, & Cœur, 2016). Bernet, Prasuhn, and Weingartner (2017) showed that surface water flooding away from watercourses, which is rarely considered in studies, contributes considerably to overall flood losses in Switzerland. The shares were particularly high in conjunction with local extreme rainfall intensities, while after long-duration precipitation events more fluvial flood damages occurred. This suggests that damage patterns from convective precipitation are different than from stratiform events, but little is known about these differences.

Weather types, which describe the larger-scale synoptic situation over a region, can increase confidence in the type of precipitation despite fragmentary ground observations (e.g., Prein, Holland, Rasmussen, Clark, & Tye, 2016). Weather types have been used, for example, to determine synoptic conditions favourable to landslide occurrence (Wood, Harrison, Turkington, & Reinhardt, 2016), to develop a weather based risk index for flooding and landslides in Italian regions (Messeri et al., 2015), or to identify conditions driving very rare flood events in a long historical record (De Niel, Demarée, & Willems, 2017).

Localised extreme precipitation, typical for convective weather patterns, can be perceived as rare and catastrophic from a local perspective, but the probability of occurrence increases over larger domains (e.g., Sass et al., 2012; Syed, Goodrich, Myers, & Sorooshian, 2003). Moftakhari, Agha-Kouchak, Sanders, and Matthew (2017) showed how exposure to less severe frequent coastal flooding, so-called “nuisance” events (annual exceedance probability AEP > 0.5), accumulates to financial risk similar to the risk from more extreme events (AEP < 0.05). So far, attention to inland nuisance flooding has been limited and focused on stream flow rather than precipitation (Slater & Villarini, 2016). Yet, for risk management actors such as the Austrian government, financing disaster recovery through the public disaster fund, such cumulative damage contributions are

highly relevant. Because risk measures in the form of exceedance probabilities are typically derived from daily observations, in which convective extremes are not well represented, convective precipitation is more likely to appear as nuisance events and its impacts may be misrepresented in regional risk analyses.

To understand how convective precipitation events have contributed to regional damage accumulation in the past and how this risk is reflected in annual exceedance probabilities of daily precipitation totals and river discharge levels, we analyse a large database of damage claims using weather types to distinguish between damage from convective and stratiform precipitation. The number and cost of reported damage claims, including damage caused by flooding, debris flows, and landslides, are assessed and associated hazard levels of discharge and precipitation are compared for distinctive patterns of convective and stratiform precipitation over the convective season from April to November.

## 2 | DATA AND METHODS

### 2.1 | Damage claim and municipality data

We analyse a database of 116,900 claims reported to the Austrian disaster fund (Katastrophenfonds) in 480 municipalities in southeastern Austria over 25 years (1990–2014). The data were obtained from the office of the provincial government of Styria, Austria.

The disaster fund is an ex-ante form of risk financing financed by shares of annual income and corporate tax revenues (BMF, 2016). While ~70% of this fund supports preventive measures such as torrent and avalanche control, emergency services and compensation for uninsured recovery activities after exceptional events are also covered (OECD, 2014). On average, 20–30% of damage is reimbursed, with up to 50% for building damages. Payouts are only to be used to restore functionality. The types of damage eligible for reimbursement include direct damages to buildings and inventory, private roads, meadows, harvest and livestock, forest soil and roads, but exclude cars, luxury or hobby items as well as any consequential damages such as business operation losses. Before an individual can claim excess damage from the disaster fund, insured losses must be deducted from the total loss. Unfortunately, these data are not available (c.f. Pretenthaler & Vetter, 2009). There is no compulsory hazard insurance in Austria, and insurers respond to adverse selection through restricting coverage and charging expensive premiums (Holub & Fuchs, 2009). The combination of tax-based governmental relief and adverse selection leads to low flood insurance coverage in Austria (e.g., Gruber, 2008; Hanger et al., 2017; Raschky, Schwarze, Schwindt, & Zahn, 2013). Thus, the disaster fund currently holds the most reliable data available for analysing household level natural hazard damages.



## 4.2 RESEARCH ARTICLE 2: DAMAGE CONTRIBUTIONS FROM CONVECTIVE AND STRATIFORM WEATHER TYPES

We consider claims associated with hydro-meteorological hazards (flooding, landslides, debris flows) during the warm season (1 April to 30 November), and exclude damage from avalanches, snow pressure, and earthquakes. This covers 84% of all claims in the database. The data comprise the municipality (but not exact location), date, type of damage, and claimed costs. To estimate vulnerability and exposure at the macro-scale of this analysis (c.f. Merz, Kreibich, Schwarze, & Thieken, 2010), we combine available data sets of indicators such as buildings, population, land use, and topography at the municipality level. Table 1 summarises the data used.

The municipalities are divided into three groups of primarily agrarian, alpine, and urban character using principal component and hierarchical clustering analyses (Figure 1). The capital Graz builds a fourth cluster comprised of only one municipality with high population density. Figure 2 shows the properties of the clusters. Alpine municipalities are generally the steepest and most extensive, have considerable forestry, and cover the northwestern part of the study region. Agricultural municipalities lie in the southeastern part, with a similar population density as alpine municipalities, but considerably more buildings. The urban municipalities include county towns with higher population density, many buildings and artificial surfaces, and a third of agricultural area. Each of the four groups has a similar overall population of around 300,000 inhabitants.

Figure 3 shows the number and value of damage claims per year by municipality cluster. All costs were inflation adjusted to the Austrian consumer price index, with no

further adjustments or normalizations. In total, a sum of 200 million € was claimed. A minimum claim threshold of 1,000€ superseded a model with deductibles and minimum payout sum in 2012 and so increased the official reporting threshold from approx. previous 600€. The high variability of hazard occurrence and decentralised handling of damage assessment make it difficult to quantify the effects of legislative changes. To avoid biases from the introduction of minimum reporting value, we remove all claims below 1,000€ from the sample before calculating trends. Simple trend analyses and Mann-Kendall tests show no significant trends in annual number of claims or cost, but the average cost per claim has almost doubled from the first (1990–1999) to the most recent (2006–2015) decade of observations (factor 1.9). This value only changes slightly (factor 1.8) when the extreme years 1991 and 2009 are excluded. Calculating trends including claims below 1,000€ increases the factors to 2.3 and 2.5, respectively, indicating that the introduction of the minimum reporting value explains ~20% of the increased cost per claim in the full dataset.

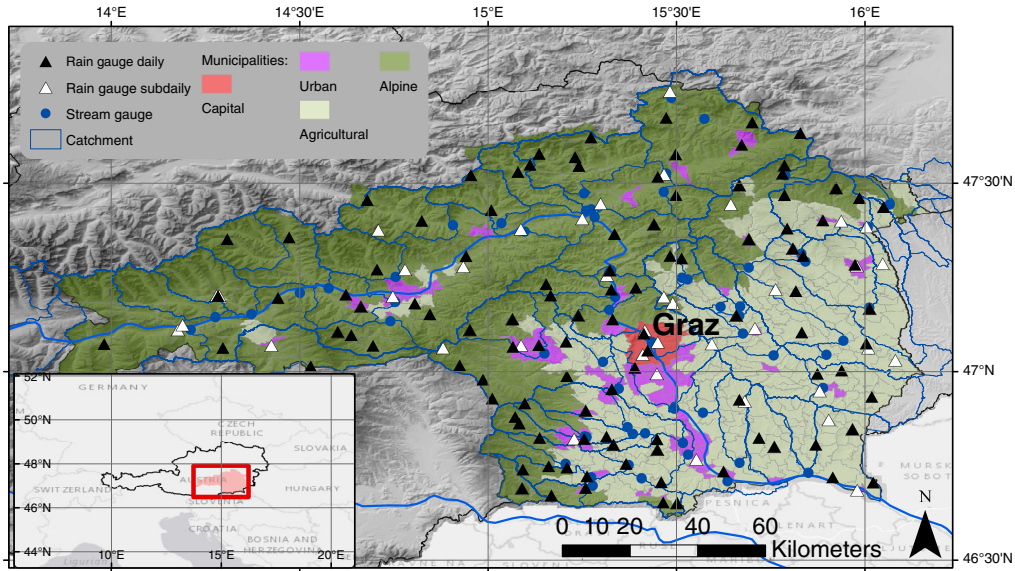
Other reasons for an increased cost/claim ratio are potential increases in value of the objects damaged or the intensity of a hazard. Increased construction and property values in flood-prone areas are often mentioned as a reason for rising flood damages, but this is not generally true as regional trends in development have to be considered (Fuchs, Keiler, & Zischg, 2015). For Styria, census data from 1991–2011 indicate the second lowest overall demographic change of all nine Austrian provinces, with decreasing population in 56% of municipalities (on average –2.6% per

TABLE 1 Summary of the data used in this study

Description	Time period analysed	Resolution	Reference/source	Data used for
Point observations of precipitation (108 daily/72 sub-daily gauges)	1990–2016	10 min/daily	Austrian national weather (ZAMG) and hydrographic (AHYD) services	Characterising precipitation in weather types
Daily discharge observations (61 gauges)	1990–2016	Daily	Austrian hydrographic service (AHYD), chyd.gv.at	Calculating exceedance probabilities of discharge levels
Weather reviews and synoptic situation descriptions	1999–2017	Daily	Austrian national weather service (ZAMG)	Classifying weather types
gpad1 gridded precipitation dataset (quality controlled)	1990–2011	Daily, 1 x 1 km	Hofstätter et al. (2015)	Validating weather type classification, calculating average daily precipitation totals for all municipalities and estimating exceedance probabilities of precipitation events
INCA nowcasting system gridded precipitation (not quality controlled)	2004–2014	15 min, 1 x 1 km	Haiden et al. (2010)	
ERA-interim reanalysis data (PSL, CAPE, geopotential, wind speed)	1979–2016	Daily	Dee et al. (2011)	Classifying weather types
Damage claims to the disaster relief fund	1990–2014 (available until 2016)	Daily	Departments of the provincial government of Styria (data.steiermark.at)	Analysing distributions among weather types and municipality clustering
Census data of the population in the Styrian municipalities	1991, 2001, 2011	10-year		Municipality clustering
Digital elevation model	2014	10 x 10 m		Municipality clustering
CORINE land cover	2000	100 x 100 m	EEA (2017) (gis.epa.ie)	Municipality clustering
Shapefile of building outlines in the study area	2016	vector data	OpenStreetMap (openstreetmap.org)	Municipality clustering

Note. See Table S1 in Appendix S1, Supporting Information for a detailed list of gauges.

# 4 EXTREME PRECIPITATION



**FIGURE 1** Study area, municipalities, gauge locations and catchments in the southeastern Alpine forelands of Austria. The shading of the municipalities denotes the group according to the cluster analysis

decade in the districts excluding Graz and Graz-Surroundings) (Federal Government of Styria, 2014). Only the district surrounding Graz experienced a net increase in population (on average +10% per decade). The dynamics of land use change in Austria are among Europe's lowest, and the rate of artificial land take (0.21% p.a., corresponding to a total of 50 km<sup>2</sup> over 2006–2012), is half that of the European average (EEA, 2017). Although changes are important on the

local scale, the magnitude of these changes does not influence the clustering of municipalities.

For the distribution of incurred damages among convective and stratiform weather types, it can be assumed that vulnerable objects are equally exposed to the different weather types in any given year. We consider both the cost and number of claims. While claim occurrence indicates exposure, the accumulated costs on a particular day and/or place signal the severity of the event and level of vulnerability.

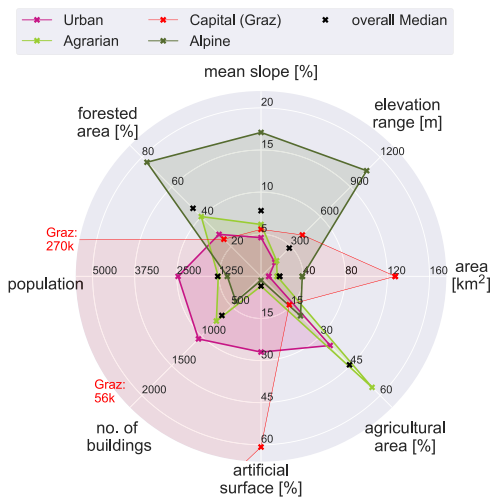


**FIGURE 2** Factors of vulnerability and exposure in the four municipality clusters

## 2.2 | Precipitation and discharge

We use several data sources for a more robust analysis of precipitation observations. Sub-daily precipitation data (10 min aggregated) and daily precipitation sums are available for 72 and 108 gauges, respectively. The gauges are operated by the Austrian weather service (ZAMG) and the

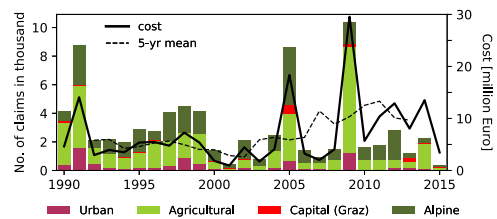


**FIGURE 3** Number of damage claims from flooding, landslides, and debris flows per year and municipality cluster (bars, left axis) and total claim value per year (black solid line, right axis) as reported to the disaster fund 1990–2015 (1 April to 30 November)

## 4.2 RESEARCH ARTICLE 2: DAMAGE CONTRIBUTIONS FROM CONVECTIVE AND STRATIFORM WEATHER TYPES

hydrographic service of Styria (Figure 1). Daily (sub-daily) records range from 1 to 27 (2 to 25) years with a median of 25 (13) years. See Tables S1–S3 in Appendix S1, Supporting Information for lengths and missing data in all station records. Rain gauge observations are used to assess sub-daily precipitation characteristics of the weather types.

Furthermore we use the gridded, quality-controlled dataset *gpard1* (daily, 1990–2011) (Hofstätter et al., 2015), and the nowcasting product INCA, which blends station and radar observations (15 min aggregated to 1 day, 2004–2014) (Haiden et al., 2010). Both products are based on ZAMG gauge observations and are provided on a 1 km x 1 km grid. Gridded data are used to estimate daily precipitation totals over all municipalities on damage days.

No trends were identified in the sub-daily precipitation data, however, studies found a decreasing trend in annual precipitation over the region (Masson & Frei, 2015). Agreement among data products is high on the daily scale, but correlations decrease towards sub-hourly observations due to the high variability on small spatio-temporal scales and storm movement. Furthermore, sub-daily extremes and small-scale phenomena are not well represented in gridded precipitation datasets (Hiebl & Frei, 2018; Schroeer, Kirchengast & O, 2018).

Average daily discharge data from gauges operated by the hydrographic service are available for 62 catchments ranging from 20 to 1,000 km<sup>2</sup> (See Tables S1 and S4 in Appendix S1 for information on individual gauge records). Each municipality is associated with the relevant stream/river catchment. Administrative boundaries largely coincide with topography so that this mapping is unambiguous. The annual exceedance probability (AEP) of the daily discharge is calculated for each stream using Gumbel extreme value distributions fitted to the seasonal maxima over all available years. Kolmogorov-Smirnov statistics support this choice for 100% of the gauges in summer, and for 99 and 92% of the gauges in spring and fall (autumn), respectively (95% confidence level). Information on anthropogenic modifications of the catchments was not available. For annual maximum daily discharge in Austrian discharge gauges, no change points were detected for the mean in the southeastern Alpine region, and significant change points in variance at two stations fall outside the study period (Villarini, Smith, Serinaldi, Ntelekos, & Schwarz, 2012). We address uncertainties in AEP by fitting the distribution to randomly selected two thirds of the data 1,000 times. The 90% confidence interval is then defined as the 5-95th percentile range of AEPs calculated from each of these bootstrapped distributions.

The same method is applied to the seasonal maxima of daily rainfall calculated for each municipality using the gridded datasets to estimate AEPs of precipitation events (Kolmogorov–Smirnov test support a Gumbel distribution for all gauges except for one in fall). We follow Mofatkhari et al. (2017) in classifying events with return intervals below

2 years as minor (AEP > 0.5), between 2 and 20 years (AEP ≤ 0.5 and AEP > 0.05) as major and ≥ 20 years (AEP ≤ 0.05) as extreme. These comparably low thresholds are justified by our interest in the cumulative effect of frequent events, the application to observed data only, and make calculations arguably more tractable, as statistical models are less sensitive to assumptions about the extreme tail behaviour (Serinaldi & Kilsby, 2014).

### 2.3 | Weather types

The spatiotemporal coverage of sub-daily precipitation observations is sparse compared to the spatiotemporal resolution of reported damages. This leads to high uncertainties when linking gauge-based sub-daily precipitation directly to damage in the municipalities. Through associating observed precipitation with larger-scale synoptic conditions, we can utilise all available information and increase confidence in the character of precipitation events under different weather patterns. We first perform a circulation type classification based on daily ERA-Interim data (1979–2016) (Dee et al., 2011) over the Greater Alpine Region (40.5–51.57°N, 3.0–20.25°E), using the COST Action 733 circulation type classification software (Philipp, Beck, Huth, & Jacobeit, 2016). The optimal classification scheme depends on the predictand (Huth, Beck, & Kucerova, 2016; Schiemann & Frei, 2010), here patterns of predominantly convective or stratiform precipitation. We apply principal component analysis and cluster analysis method (e.g., Prein et al., 2016) to sea level pressure, 700 hPa wind velocity, convective available potential energy (CAPE), and 500 hPa geopotential as indicators of atmospheric stability and seasonality, and to consider fast and slow moving systems. Codes for the synoptic situation over Austria were then collected from daily weather reports issued by the ZAMG since March 1, 1999.

Through merging the computationally identified weather classes with the weather types issued explicitly for Austria, we obtain a tailored classification of six weather types, WT1A, WT1B, WT1C, WT2, WT3, and WT4. WT1A to WT1C and WT4 are dominated by low gradient or high-pressure situations, while WT2 and WT3 predominantly contain days of south and south-westerly and north and north-westerly flows, respectively. Positive CAPE anomalies and above-average peak intensities distinguish the convective classes WT1A and WT1B occurring 1 June through 30 September. The difference is that WT1A sees low daily precipitation totals and wet spell durations mostly associated with single-cell or multi-cell storms, while extreme precipitation under WT1B is associated with disturbances and intense frontal precipitation and unstable atmospheric conditions, reaching higher precipitation totals and longer lasting events. WT1C is also dominated by low gradient situations, but CAPE and precipitation in general are lower in spring and fall. WT4 is dominated by persistent high-pressure situations and negative precipitation anomalies. Rare

precipitation events can occur in form of isolated thunderstorms on the warmest days in this class. Duration and daily precipitation totals are high in WT2, with only average peak intensities. In WT3, long wet spells, high daily precipitation totals, and low peak intensities prevail. Although dominated by large-scale and stratiform precipitation, embedded convection at the onset of the precipitation event, particularly during the summer months, does occur.

Figure 4 illustrates the frequency of each weather type during the study period and the weather-type specific extreme (98th percentile) daily precipitation totals and 10-min peak intensities and average wet spell duration (sum of 10 min intervals >0.1 mm) compared to the respective monthly percentile. These indicators were calculated from all rain gauges. WT-specific discharges are provided in Figure S1 in Appendix S1.

3 | RESULTS

3.1 | Distribution of damage claims by weather types

Figure 5 shows the frequency (% days) of each weather type and the associated damage (% total reported cost). The predominantly convective weather types WT1A and WT1B

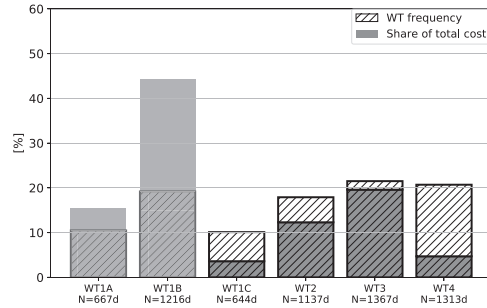


FIGURE 5 Relative frequency of days under all weather types (1990–2014, April to November) (hatched bars). Grey bars show the cumulated cost associated with each weather type relative of the total cost. Asterisks mark the relative frequency of damage reports within each weather type (number of days with reported damage divided by total number of weather type days)

show over-proportional damage shares (15 and 43%, respectively), whereas little damage is reported during WT1C and WT4. ~12% of the total cost is attributed to WT2, while the share of damage under WT3 is approximately proportional to its occurrence (~20%).

Generally, most claims are caused by flooding (~62%), followed by landslides (~20%) and debris flows (~18%).

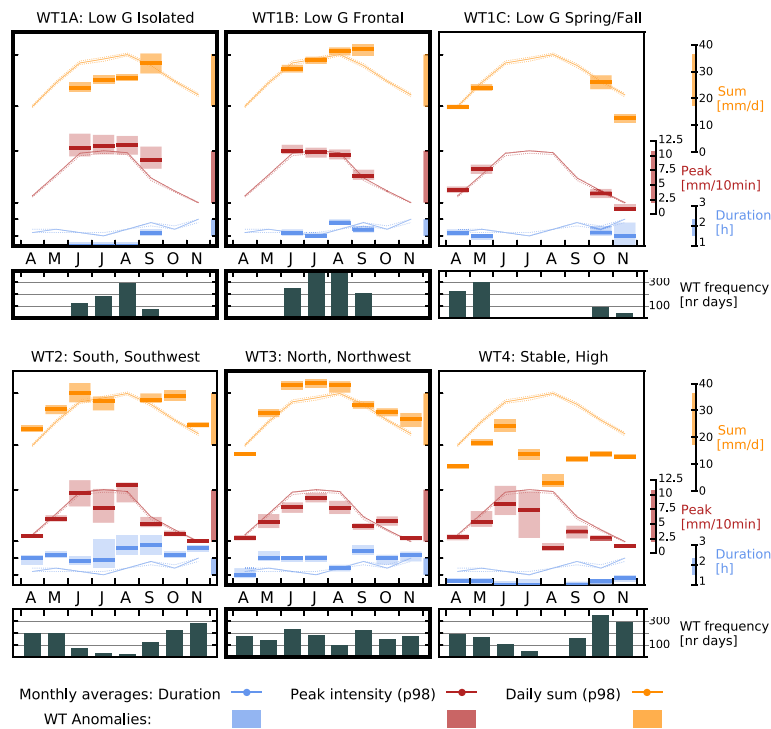


FIGURE 4 Weather type frequency (black bars, rows 2 and 4) and associated extreme precipitation (98th percentile, horizontal bars) for peak intensity (red), daily sum (yellow), and average wet spell duration (blue). Shadings show 90% confidence intervals. Full lines are identical in all panels and show the overall monthly climatological percentile values (full lines, dotted lines mark 90% confidence intervals). Note that the scales differ between colours

## 4.2 RESEARCH ARTICLE 2: DAMAGE CONTRIBUTIONS FROM CONVECTIVE AND STRATIFORM WEATHER TYPES

Figure 6 splits the claims by cause and municipality group. Graz is not included in this visualisation, because of the small total of 1,558 claims, of which ~90% are due to flooding. The breakdown shows an interesting division of the vulnerabilities of the different municipality groups to the weather types. WT1B is associated with most claims for all hazards and municipality groups except for landslides in the agricultural group. This is due to several large-scale precipitation events in the region which caused exceptional amounts of landslides under WT2 and WT3 (Hornich & Adelwöhner, 2010). Short but intense summer precipitation events under WT1A have less impact in this class, while alpine municipalities record the second largest frequency of both flood and debris flow claims in this weather type.

Precipitation processes interact with the basic topography and thus amplify vulnerabilities. While flooding can be expected anywhere in the study region, the agricultural group is prone to landslides due to its geological disposition, with over 5,000 km<sup>2</sup>, or half of the total area of the Province of Styria, classified in the highest of three landslide risk levels (Leopold, Draganits, Heiss, & Kovacs, 2013; Proske & Bauer, 2016). This part is also more directly influenced by southerly flow directions common under WT2, which occur in spring and fall when precipitation in the alpine municipalities in the higher northwestern parts can fall as snow and delay runoff. Furthermore, Alpine catchments are characterised by steep mountain topography and susceptibility to debris flows. Orography enhances convective precipitation in Alpine regions (Giorgi et al., 2016), a known trigger for debris flows.

Per capita claims in Graz and the urban municipalities are disproportionately low. Towns are usually not in steep areas prone to debris flows or landslides and most damage is caused by flooding under WT1B and WT1A. Because urban municipalities cover smaller areas, the probability of localised extreme precipitation hitting the area is smaller, yet if it

does the consequences such as extreme runoff and surface water flooding occur immediately (c.f. Roodsari & Chandler, 2017; Sass et al., 2012; Syed et al., 2003), which is why urban areas are considered to be particularly vulnerable to flash floods (Guillén, Patalano, Garcia, & Bertoni, 2017; Kermanshah, Derrible, & Berkelhammer, 2017; Mahmood, Elagib, Horn, & Saad, 2017; Pereira, Diakakis, Deligiannakis, & Zezere, 2017). On the contrary, the area exposed is much larger in agricultural and alpine municipalities, and buildings are likely located closer to the hazard processes.

### 3.2 | Annual exceedance probabilities of damage-associated river discharge and precipitation

The previous section showed disproportionately high damage under convective weather types (WT1A, WT1B) compared to the incurred damage under stratiform weather types. To find out how this risk is reflected in hazard measures, we analyse the damage contributions under estimated minor, major, and extreme precipitation and discharge events and compare the patterns from convective weather types to the most damaging non-convective weather type WT3.

The analysis of the annual exceedance probabilities (AEP) of river discharge shows considerable differences in the calculated flood risks among WT1A, WT1B, and WT3 (Figure 7). The AEP is shown separately for municipalities within catchments that were (a) not affected (no reported damage), (b) affected (1–20 damage claims), and (c) severely affected (>20 reported claims). This stratification indicates the severity of an event based on the impact and is independent of observations of precipitation or discharge.

Expectedly, AEP of discharge is always significantly lower on days with more damage claims than on days with moderate or no impact reported. However, under WT1A, AEPs only decrease slightly for moderate and high impact

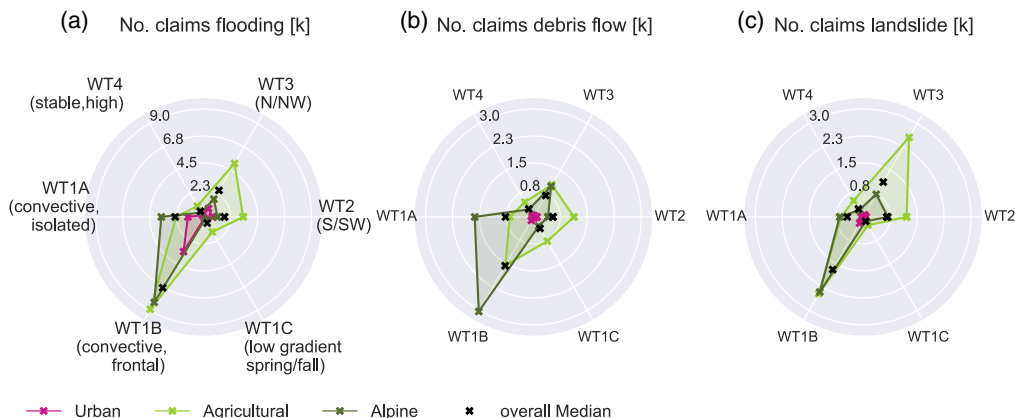


**FIGURE 6** Number of claims to the disaster fund due to (a) flooding, (b) debris flows, and (c) landslides in rural, Alpine, and urban municipalities in the different weather type groups. Graz is not included due to the small numbers in claims. Note the different axis scaling in (a) and (b, c)

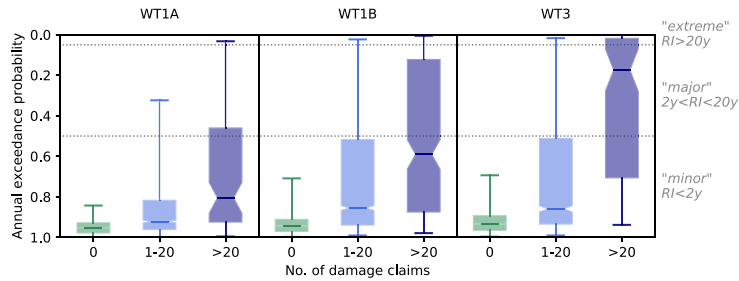


**FIGURE 7** Annual exceedance probabilities of discharge levels on days with 0, 1–20, and > 20 reported claims under the convective WT1A and WT1B and the stratiform WT3. Whiskers denote the 5–95th percentile interval. Dotted horizontal lines mark the AEP thresholds applied in this study to define minor, major, and extreme events. Corresponding recurrence intervals (RI) are also given

events. With medians in the minor flooding class, daily discharge observations rarely indicate the risk of damage under WT1A. Although discharge levels are significantly higher under WT1B, in ~50% of the incidents the AEP of the closest stream gauge does not record unusual discharge even when more than 20 damage claims are reported in the catchment. On the contrary, high impact events under the stratiform WT3 are accompanied by major and even extreme discharge more regularly.

A possible reason for this is that widespread and long-duration precipitation under WT3 allows more time for the rivers to react and the distance between damage location and stream gauge is less relevant under such conditions. In contrast, short-duration, localised convective events might not have much effect on average daily discharges. Convective rainfall intense enough to cause damage might still not precipitate a large enough volume of water to raise water levels to a major or extreme level, especially in large rivers. If, additionally, the centre of a storm is located away from a stream gauge, this effect is even stronger, as runoff may be infiltrated or intercepted by the sewer system before reaching a stream.

Overall, minor discharge levels are observed on days accounting for 42.7–52.7% of the total reported cost. 15.9–18.6% and 5–17.7% of costs coincide with major and extreme river discharge levels, respectively. Less than 1% of the total cost associated with extreme discharge occurred under WT1A, in contrast to 2.3–6.8% under WT1B and 1.3–5.9% under WT3. For ~25% of the total cost no discharge data is available for the respective catchment.

The differences in the distributions of hazard levels become more apparent when AEPs are considered relative to the weather type specific cost. Nuisance levels are associated with 69.2–73.6% of the damages under WT1A, with 41.1–52.5% under WT1B, and with only 27.3–34.8% under WT3. Likewise, 0.7–3.9% (WT1A), 5.3–15.4% (WT1B) and 6.7–22.9% (WT3) of weather type specific cost can be linked to extreme discharge.

Figure 8 shows the AEPs of discharge relative to the WT-specific cost in the different municipality groups.

Extreme discharge most frequently occurs in agricultural municipalities, particularly under WT3, where also the share of nuisance flooding is low (~20% of the cost). Also in urban municipalities, up to 20% of damage is associated with extreme discharge, albeit large uncertainty arises from the smaller sample. In alpine and urban municipalities under WT1A, daily discharge data almost never reach extreme levels. No significant differences are observed between municipality groups under WT1B.

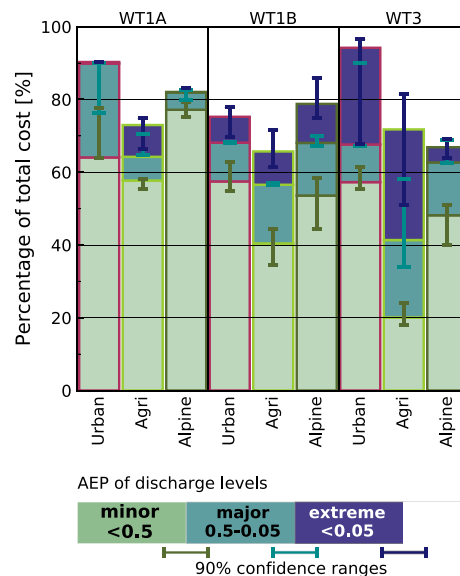


**FIGURE 8** Relative proportion of claimed loss by annual exceedance probability of river discharge in each catchment. Green (light blue, dark blue) bars indicate minor (major, extreme) discharge levels. The proportions are shown individually for the total payout sums in urban, agricultural, and alpine municipalities under weather types WT1A, WT1B, and WT3. Error bars indicate the 90% confidence intervals of the individual contributions, that is, to be interpreted as the possible upper ends of each colour band. Space is left blank where no discharge data are available. Figure after Mofiakhari et al. (2017)

## 4.2 RESEARCH ARTICLE 2: DAMAGE CONTRIBUTIONS FROM CONVECTIVE AND STRATIFORM WEATHER TYPES

The large share of cost associated with nuisance-level events suggests that streamflow is not well correlated with large parts of the damage data. This can be either because damage was caused despite low discharge levels in form of nuisance flooding or surface water flooding, or because the discharge is not correctly observed. E.g., discharges used are those associated with the day of the reported claim and do not include delayed overland runoff. Although the data do not allow for disentangling of these effects, robust differences among weather types indicate that the risk of impacts under convective WT1A and, to lesser extent, frontal convective WT1B, is particularly underestimated in daily discharge data.

Precipitation is more directly linked to surface water flooding and AEPs of daily precipitation totals might better indicate the risk from convective extremes than available discharge data. Also here, minor events contribute 63.6–73% to the overall reported cost. Major and extreme level precipitation is observed in 18.5–19.7% and 6.5–14.8%, respectively. The proportion of total cost associated with extreme daily precipitation differs between convective (WT1A: 0.7–1.1%, WT1B: 2.5–6.2%) and stratiform (WT3: 9.9–11.1%) weather types. Within the weather type specific cost, 4.0–6.9% (WT1A), 5.6–14.1% (WT1B), and 16.7–29.0% (WT3) can be linked to extreme daily precipitation.

Figure 9 shows the shares of the event magnitudes within each weather type and municipality group. Again, the agricultural municipalities see the lowest share of nuisance level events under WT3, whereas this fraction is particularly high under the isolated convective WT1A. In alpine municipalities, the group most vulnerable to WT1A, precipitation data better indicates the risk of damage than discharge data (5.9 vs. 0.1% of cost can be attributed to extreme levels of precipitation and discharge, respectively), although part of this might be due to better data coverage (2% of costs coincide with missing precipitation data).

In summary, both precipitation and discharge data agree quite well on the damage contributions under minor, major, and extreme events. For one half to two thirds of the total cost, observational data indicate only minor hazard levels, and this effect is particularly distinct in convective WTs even when major impacts were reported.

### 4 | DISCUSSION

#### 4.1 | Discussion of uncertainties and limitations

The results showed that convective weather types are associated with frequent damage claims and that associated precipitation and discharge events often do not indicate this risk. Several sources of uncertainties come into play when interpreting these results.

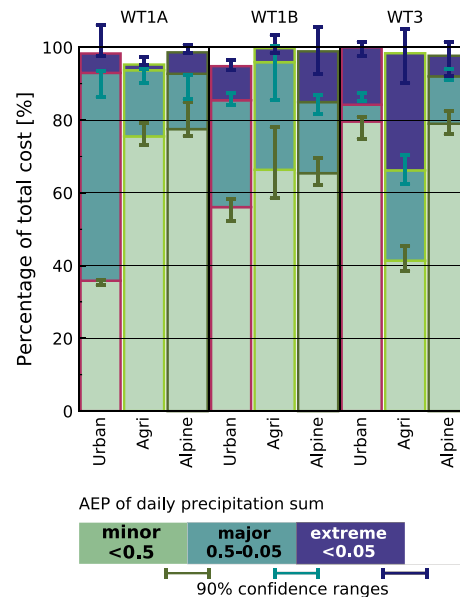


**FIGURE 9** Relative proportion of claimed loss by annual exceedance probability of daily precipitation totals in the respective municipalities. Green (light blue, dark blue) bars indicate minor (major, extreme) precipitation totals. The proportions are shown individually for the total payout sums in urban, agricultural, and Alpine municipalities under weather types WT1A, WT1B, and WT3. Error bars indicate the 90% confidence intervals of the individual contributions, that is, to be interpreted as the possible upper ends of each colour band. Overshooting error bars can thus occur due to the stacked layout. Space is left blank where no precipitation data are available. Figure after Mofkakhari et al. (2017)

The high number of damage reports that cannot be linked to significant precipitation or discharge levels indicates that extremes under WT1A and WT1B are indeed not well represented in observations. Under WT3, extremes from large-scale precipitation patterns, which can be approximated with some confidence within the study region's observation network, seem to be better captured. Still, a high share of damage can only be linked to nuisance hazard levels. The share of nuisance level events is lowest in agricultural municipalities and particularly high in alpine municipalities. This indicates that the range of explanatory power of observations is smaller in the mountainous topography with secluded valleys in the alpine municipalities.

Increasing availability of precipitation data on small spatio-temporal scales from high-resolution networks and improving radar data will help to overcome these issues in the future. To understand damage fingerprints from convective and stratiform precipitation, better information is also needed on location and eligibilities of damages, and on procedural changes in claim handling. This would allow distinguishing damage from surface water flooding away from watercourses from flooding from overflowing streams. Furthermore, weather type specific exposures could be

explicitly considered. For example, hail is associated with intense convective events (Nisi, Martius, Hering, Kunz, & Germann, 2016) and particularly with cold fronts during early summer (Schemm, Nisi, Martinov, Leuenberger, & Martius, 2016). Non-availability of hail damage data likely leads to undervaluing the damage potential from convective patterns especially in agricultural municipalities. If exposure and vulnerability are generally similar to the analysed region-wide household level data, the non-availability of these data, for example, of damages to small businesses has little effect on the presented results of relative contributions.

Large uncertainty ranges in damage cost attributable to extreme discharge events highlight the difficulty in confidently assessing low frequency return levels. This is even though the threshold for extremes of annual exceedance probability of 0.05 is comparably low and the lengths of observational data series exceed the targeted return level. This underlines how more recent concepts such as the flood peak ratio, which avoids the calculation of large return intervals by setting observed flood peaks in relation to a 10-year flood event (Czajkowski, Cunha, Michel-Kerjan, & Smith, 2016), can help the assessment of extreme flood events.

Uncertainties also arise from changes in vulnerability and exposure over time. Regarding the presented results, the main question is whether implemented actions and measures have had divergent effects with respect to convective or stratiform hazards. Exposure and vulnerabilities might be weather type specific among sectors, or for direct and indirect damages. Such differences could not be considered here and need further research. After catastrophic events in 2005, the city of Graz initialized a 65 million €, 10-year Special Programme—The Streams of Graz, investing in protection measures, retention areas, renaturalization, and educational advertising. Similarly, with expenditures of 27 million € per annum over 2000–2005, and 40 million € per annum 2005–2013, the province of Styria continuously invests in flood protection measures (Hornich, Zenz, Hammer, & Reischl, 2014). Construction projects often run for several years, and sometimes high-risk land is purchased to incorporate it into the floodplain instead of building protection measures, thus the avoided impact difficult to assess. The fact that there is no obvious indication of damage reduction in the data analysed here calls for a deeper analysis of the effectiveness and temporal dimensions of such adaptation efforts. Effects of public awareness campaigns and private adaptation are generally hard to quantify (Aerts et al., 2018), but first studies show how disastrous events trigger adaptation (Kreibich et al., 2017). So far, these studies focus on large fluvial floods. Extending this research offers an opportunity to find out how various adaptation measures are effective in reducing impacts from large-scale events and localised extremes, and stratiform or convective precipitation, respectively.

#### 4.2 | Implications for future risk assessment

Data on past losses include comprehensive information on damage from both frequent and rare events arising from convective and stratiform conditions. The large database analysed here helps to quantify the respective contributions and delivers insights into impacts related to convective precipitation events. This is important because many risk assessments, which often build on exceedance probabilities of inundation depths and coarse input data, might underestimate the risk from localised convective precipitation events as well as the cumulative effects from frequent nuisance level events.

This analysis showed that ~60% of all damage occurred under synoptic conditions favouring convective precipitation with high sub-daily intensities. For one half to two thirds of these incidents, neither the observed stream discharge nor the daily precipitation indicate this risk.

It is interesting that the contribution of extreme level events to overall damage under the predominantly stratiform WT3 (~23%) is close to the estimates of how much extreme events contribute to total exposure (~20%) in US coastal cities by Mofitakhari et al. (2017). Although the scope and setting of the studies differ, this supports the hypothesis that large-scale extremes are more easily captured in observational data and future flood risk assessments.

Hanger et al. (2017) find that “generally, governments focus more on large-scale flood protection opportunities than on incentivizing private risk-reduction behaviour”. Our results underline why focusing on large scale events is not enough to reduce impacts from extreme precipitation. Annual frequencies of weather types do not show significant changes over the study period, except for a slight increase in frequency of WT1B days (0.65 days per year, 90% confidence level). Extreme convective precipitation intensities are highly sensitive to temperature in southeastern Austria (Schroerer & Kirchengast, 2017) and are generally expected to increase with global warming (Zhang, Zwiers, Li, Wan, & Cannon, 2017). Although trends in sub-daily extreme precipitation cannot be robustly detected at this point, this means that both the frequency of convective days and the intensity of precipitation on these days could increase in the future. It is thus important to facilitate private risk-reduction behaviour to increase resilience to localised impacts and surface water flooding, against which technical measures along streams are less effective.

Most regular annual payouts of the disaster fund are spent on damage in rural and less densely populated areas. Claims per capita are much smaller in urban areas. Potential reasons for this are the smaller areas exposed and thus lower probability of an event occurring exactly here, and the fact that protection measures effectively protect a larger number of people than in dispersed settlements. Interesting differences between rural and urban areas regarding risk perception are observed also by Fuchs et al. (2017). They compare



## 4.2 RESEARCH ARTICLE 2: DAMAGE CONTRIBUTIONS FROM CONVECTIVE AND STRATIFORM WEATHER TYPES

the perception and adaptation of inhabitants of a rural region susceptible to large-scale river floods, and an urban area prone to flash floods. They find a lower individual disposition to pro-actively invest in adaptation measures in the rural population exposed to large scale events, even though several floods occurred in the recent past. What is more, state and administrative authorities were blamed for unsatisfactory levels of protection measures. The willingness to accept human behaviour and development as risk factors and to individually adapt was higher in the urban area threatened by flash floods.

Even though the different socio-cultural backgrounds must be considered, these findings relate to our results because they point towards the difficulties that may arise when developing adaptation strategies. It underlines the importance of differentiating the hazard processes as well as the socio-economic context of the exposed area. Our results emphasise that private risk reduction behaviour is important to complement publicly funded structural measures concentrating on watercourses.

In the alpine municipalities, debris flows also cause a considerable proportion of the damage. In a modelling study, Meissl et al. (2017) reveal possible implications for steep mountain catchments in Alpine environments. Continued warming reduces the days with critical antecedent soil moisture conditions but increases mobilizable dried up litter. Hence, the consequences of intensified convective precipitation extremes could lead to rarer, but more intense debris flows.

Here, we established a relationship between critical circulation types and vulnerability factors using observed data. Such an approach, for example, through assessing larger-scale trends in severe storm environments (Púčik et al., 2017), can support identifying future damage potential using climate models, where simulation of small-scale extreme precipitation is improving, but considerable uncertainties remain (e.g., Olsson, Berg, & Kawamura, 2014). However, also changes of circulation types over the Alpine region need further research and uncertainties remain particularly in summer (Rohrer, Croci-Maspoli, & Appenzeller, 2017).

### 5 | CONCLUSION

We analysed a large database of damage claims in combination with several observational hydro-meteorological datasets to identify contributions from different weather types and assess their reflection in hazard intensity measures. Observed and projected intensifications of convective precipitation and the associated high damage potential make this issue relevant to risk management activities. While at a specific location the event may be considered rare, impacts from convective storms occur more frequently at regional scales. The accumulated cost contributes significantly to the damage cost from natural hazards. Weather types indicate

the character of the hazard event even when sub-daily observations are not available at the damage location.

The present analysis showed that more than half of the damage from hydro-meteorological hazards in the warm season (1 April to 30 November) can be attributed to synoptic situations favouring convective precipitation. In 50–60% of these events, associated river discharge levels are not considered to be extreme ( $AEP < 0.05$ ). Under stratiform conditions, discharge reaches extreme levels more frequently, yet ~40% of the damage is attributed to only minor discharge levels.

The generally high proportion of minor hazard levels indicates that convective precipitation, nuisance level events, and surface water flooding all significantly burden the disaster fund. Better resolved data on discharge, precipitation, and the location of damages, are needed to accurately ascribe damages to these processes. Large uncertainty ranges in AEP of extreme events underline the difficulty of accurately estimating return levels of extreme events from limited observations.

This initial study showed that identifying the risk-prone environment through merging a “top-down” weather typing approach with ground based observational data is beneficial for data-limited analyses. It allows identifying the different natures of damaging precipitation events through their atmospheric drivers and local impacts and so improves our understanding of region- and context-specific vulnerabilities.

### ACKNOWLEDGEMENTS

This work was funded by the Austrian Science Fund (FWF) under research grant W 1256-G15 (Doctoral Programme Climate Change Uncertainties, Thresholds and Coping Strategies). We thank the offices of the Austrian Hydrographic Services and the ZAMG Austrian National Weather Service for provision of the precipitation data and the departments of the Styrian government for the provision of and information on the disaster fund data. The National Center for Atmospheric Research is sponsored by the National Science Foundation (NSF); MRT was supported by NSF EaSM3 Grant 1419563.

### ORCID

Katharina Schroeer  <https://orcid.org/0000-0002-2535-6658>

Mari R. Tye  <https://orcid.org/0000-0003-2491-1020>

### REFERENCES

- Aceto, L., Caloiero, T., Pasqua, A. A., & Petrucci, O. (2016). Analysis of damaging hydrogeological events in a Mediterranean region (Calabria). *Journal of Hydrology*, 541, 510–522. <https://doi.org/10.1016/j.jhydrol.2015.12.041>
- Aerts, J. C. J. H., Botzen, W. J., Clarke, K. C., Cutter, S. L., Hall, J. W., Merz, B., ... Kunreuther, H. (2018). Integrating human behaviour dynamics into flood disaster risk assessment. *Nature Climate Change*, 8, 193–199. <https://doi.org/10.1038/s41558-018-0085-1>

- Bao, J., Sherwood, S. C., Alexander, L. V., & Evans, J. P. (2017). Future increases in extreme precipitation exceed observed scaling rates. *Nature Climate Change*, 7, 128–132. <https://doi.org/10.1038/nclimate3201>
- Bernet, D. B., Prasuhn, V., & Weingartner, R. (2017). Surface water floods in Switzerland: What insurance claim records tell us about the damage in space and time. *Natural Hazards and Earth System Sciences*, 17, 1659–1682. <https://doi.org/10.5194/nhess-17-1659-2017>
- BMF. (2016). *Katastrophenfondsgesetz 1996. 11. Textbackslash, Bericht des Bundesministers für Finanzen. Austrian Federal Ministry of Finance*. Retrieved from [https://www.bmf.gv.at/budget/finanzbeziehungen-zu-laendern-und-gemeinden/Katastrophenfondsbericht\\_2014-2015.pdf](https://www.bmf.gv.at/budget/finanzbeziehungen-zu-laendern-und-gemeinden/Katastrophenfondsbericht_2014-2015.pdf)
- BMNT. (2011). Weiterführende Information—Hochwasser. Hochwasserzonierung Austria—HORA. Retrieved from [http://www.hora.gv.at/assets/eHORA/pdf/HORA\\_Hochwasser\\_Weiterfuehrende\\_Informationen\\_v4.pdf](http://www.hora.gv.at/assets/eHORA/pdf/HORA_Hochwasser_Weiterfuehrende_Informationen_v4.pdf)
- Boudou, M., Lang, M., Vinet, F., & Cœur, D. (2016). Comparative hazard analysis of processes leading to remarkable flash floods (France, 1930–1999). *Journal of Hydrology*, 541, Part A, 533–552. <https://doi.org/10.1016/j.jhydrol.2016.05.032>
- Czajkowski, J., Cunha, L. K., Michel-Kerjan, E., & Smith, J. A. (2016). Toward economic flood loss characterization via hazard simulation. *Environmental Research Letters*, 11, 084006. <https://doi.org/10.1088/1748-9326/11/8/084006>
- Dai, A., Rasmussen, R. M., Liu, C., Ikeda, K., & Prein, A. F. (2017). A new mechanism for warm-season precipitation response to global warming based on convection-permitting simulations. *Climate Dynamics*, 1–26. <https://doi.org/10.1007/s00382-017-3787-6>
- De Niel, J., Demarée, G., & Willems, P. (2017). Weather typing-based flood frequency analysis verified for exceptional historical events of past 500 years along the Meuse river. *Water Resources Research*, 53, 8459–8474. <https://doi.org/10.1002/2017WR020803>
- Dee, D. P., Uppala, S.M., Simmons, A.J., Berrisford, P., Poli, P., Kobayashi, ... Vitart, F. (2011). The ERA-interim reanalysis: Configuration and performance of the data assimilation system. *Quarterly Journal of the Royal Meteorological Society*, 137, 553–597. <https://doi.org/10.1002/qj.828>
- Donat, M. G., Lowry, A. L., Alexander, L. V., O’Gorman, P. A., & Maher, N. (2016). More extreme precipitation in the world’s dry and wet regions. *Nature Climate Change*, 6, 508–513. <https://doi.org/10.1038/nclimate2941>
- EEA. (2017). Austria. Country fact sheet Land cover 2012. Retrieved from [https://www.eea.europa.eu/themes/landuse/land-cover-country-fact-sheets/at-austria-landcover-2012.pdf/at\\_download/file](https://www.eea.europa.eu/themes/landuse/land-cover-country-fact-sheets/at-austria-landcover-2012.pdf/at_download/file)
- Eggert, B., Berg, P., Haerter, J. O., Jacob, D., & Moseley, C. (2015). Temporal and spatial scaling impacts on extreme precipitation. *Atmospheric Chemistry and Physics*, 15, 5957–5971. <https://doi.org/10.5194/acp-15-5957-2015>
- Federal Government of Styria. (2014). Registerzählung 2011—Bevölkerung, Haushalte, Familien. *Steirische Statistiken*, Federal Government of Styria, Abteilung 7 Landes- und Gemeindeentwicklung, Referat Statistik und Geoinformation. Retrieved from [http://www.landesentwicklung.steiermark.at/cms/dokumente/12658765\\_142970621/9db939fc/Publikation%201-2014-Internet.pdf](http://www.landesentwicklung.steiermark.at/cms/dokumente/12658765_142970621/9db939fc/Publikation%201-2014-Internet.pdf)
- Feng, Z., Leung, L. R., Hagos, S., Houze, R. A., Burleyson, C. D., & Balaguru, K. (2016). More frequent intense and long-lived storms dominate the springtime trend in central US rainfall. *Nature Communications*, 7, 13429. <https://doi.org/10.1038/ncomms13429>
- Fuchs, S., Karagiorgos, K., Kitikidou, K., Maris, F., Paparizos, S., & Thaler, T. (2017). Flood risk perception and adaptation capacity: A contribution to the socio-hydrology debate. *Hydrology and Earth System Sciences*, 21, 3183–3198. <https://doi.org/10.5194/hess-21-3183-2017>
- Fuchs, S., Keiler, M., & Zischg, A. (2015). A spatiotemporal multi-hazard exposure assessment based on property data. *Natural Hazards and Earth System Sciences*, 15, 2127–2142. <https://doi.org/10.5194/nhess-15-2127-2015>
- Giorgi, F., Torma, C., Coppola, E., Ban, N., Schar, C., & Somot, S. (2016). Enhanced summer convective rainfall at alpine high elevations in response to climate warming. *Nature Geoscience*, 9, 584–589. <https://doi.org/10.1038/ngeo2761>
- Grähn, T., & Nyberg, L. (2017). Assessment of pluvial flood exposure and vulnerability of residential areas. *International Journal of Disaster Risk Reduction*, 21, 367–375. <https://doi.org/10.1016/j.ijdrr.2017.01.016>
- Gruber, M. (2008). Alternative solutions for public and private catastrophe funding in Austria. *Natural Hazards and Earth System Sciences*, 8, 603–616. <https://doi.org/10.5194/nhess-8-603-2008>
- Guillén, N. F., Patalano, A., García, C. M., & Berton, J. C. (2017). Use of LSPIV in assessing urban flash flood vulnerability. *Natural Hazards*, 87, 383–394. <https://doi.org/10.1007/s11069-017-2768-8>
- Haiden, T., Kann, A., Wittmann, C., Pistotnik, G., Bica, B., & Gruber, C. (2010). The integrated Nowcasting through comprehensive analysis (INCA) system and its validation over the eastern alpine region. *Weather and Forecasting*, 26, 166–183. <https://doi.org/10.1175/2010WAF2222451.1>
- Hanger, S., Linnerooth-Bayer, J., Surminski, S., Nenciu-Posner, C., Lorant, A., Ionescu, R., & Patt, A. (2017). Insurance, public assistance, and household flood risk reduction: A comparative study of Austria, England, and Romania. *Risk Analysis*, 38, 680–693. <https://doi.org/10.1111/risa.12881>
- Hiebl, J., & Frei, C. (2018). Daily precipitation grids for Austria since 1961—Development and evaluation of a spatial dataset for hydroclimatic monitoring and modelling. *Theoretical and Applied Climatology*, 132, 327–345. <https://doi.org/10.1007/s00704-017-2093-x>
- Hofstätter, M., Jacobeit, J., Homann, M., Lexer, A., Chimani, B., Philipp, A., ... Ganekind, M. (2015). WETRAX—Weather patterns, cyclone tracks and related precipitation extremes. *Grossflächige Starkniederschläge im Klimawandel in Mitteleuropa. Projektendbericht. Geographica Augustana*, 19, 239.
- Holub, M., & Fuchs, S. (2009). Mitigating mountain hazards in Austria – Legislation, risk transfer, and awareness building. *Natural Hazards and Earth System Sciences*, 9, 523–537. <https://doi.org/10.5194/nhess-9-523-2009>
- Hornich, R., & Adelwöhrer, R. (2010). Landslides in Styria in 2009. *Geomechanics and Tunneling*, 3, 455–461. <https://doi.org/10.1002/geot.201000042>
- Hornich, R., G. Zenz, A. Hammer, & M. Reischl. (2014). HORST—HochwasserRisikomanagement Steiermark. *Wasserland Steiermark*, Vol. 02Z034436 of, Federal state government of Styria, Austria, 4–8.
- Huth, R., Beck, C., & Kucerova, M. (2016). Synoptic-climatological evaluation of the classifications of atmospheric circulation patterns over Europe. *International Journal of Climatology*, 36, 2710–2726. <https://doi.org/10.1002/joc.4546>
- Kann, A., Meirold-Mautner, I., Schmid, F., Kirchengast, G., Fuchsberger, J., Meyer, V., ... Bica, B. (2015). Evaluation of high-resolution precipitation analyses using a dense station network. *Hydrology and Earth System Sciences*, 19, 1547–1559. <https://doi.org/10.5194/hess-19-1547-2015>
- Kermanshah, A., Derrible, S., & Berkelhammer, M. (2017). Using climate models to estimate urban vulnerability to flash floods. *Journal of Applied Meteorology and Climatology*, 56, 2637–2650. <https://doi.org/10.1175/JAMC-D-17-0083.1>
- Kreibich, H., Di Baldassarre, G., Vorogushyn, S., Aerts, J.C.J.H., Apel, H., Aronica, G.T., ... Merz, B. (2017). Adaptation to flood risk: Results of international paired flood event studies. *Earths Future*, 5, 953–965. <https://doi.org/10.1002/2017EF000606>
- Lebel, T., Bastin, G., Oblad, C., & Creutin, J. D. (1987). On the accuracy of areal rainfall estimation: A case study. *Water Resources Research*, 23, 2123–2134. <https://doi.org/10.1029/WR023i011p02123>
- Leopold, P., Draganits, E., Heiss, G., & Kovacs, E. (2013). A geotechnical explanation for the transition from creep to slides in the Alpine foreland. In C. Margottini, P. Canuti, & K. Sassa (Eds.), *Landslide science and practice: Volume 4: Global environmental change* (pp. 75–78). Berlin, Heidelberg: Springer.
- Llasat, M. C., Marcos, R., Turco, M., Gilabert, J., & Llasat-Botija, M. (2016). Trends in flash flood events versus convective precipitation in the Mediterranean region: The case of Catalonia. *Journal of Hydrology*, 541, 24–37. <https://doi.org/10.1016/j.jhydrol.2016.05.040>
- Mahmood, M. I., Elagib, N. A., Horn, F., & Saad, S. A. G. (2017). Lessons learned from Khartoum flash flood impacts: An integrated assessment. *Science of the Total Environment*, 601, 1031–1045. <https://doi.org/10.1016/j.scitotenv.2017.05.260>
- Masson, D., & Frei, C. (2015). Long-term variations and trends of mesoscale precipitation in the Alps: Recalculation and update for 1901–2008. *International Journal of Climatology*, 36, 492–500. <https://doi.org/10.1002/joc.4343>
- Meissl, G., Formayer, H., Klebinder, K., Kerl, F., Schoeberl, F., Geitner, C., ... Bronstert, A. (2017). Climate change effects on hydrological system conditions influencing generation of storm runoff in small Alpine catchments. *Hydrological Processes*, 31, 1314–1330. <https://doi.org/10.1002/hyp.11104>
- Merz, B., Kreibich, H., Schwarze, R., & Thieken, A. (2010). Review article: Assessment of economic flood damage. *Natural Hazards and Earth System Sciences*, 10, 1697–1724. <https://doi.org/10.5194/nhess-10-1697-2010>

## 4.2 RESEARCH ARTICLE 2: DAMAGE CONTRIBUTIONS FROM CONVECTIVE AND STRATIFORM WEATHER TYPES

- Messeri, A., Morabito, M., Messeri, G., Brandani, G., Petralli, M., Natali, F., ... Orlandini, S. (2015). Weather-related flood and landslide damage: A risk index for Italian regions. *PLoS One*, *10*, e0144468. <https://doi.org/10.1371/journal.pone.0144468>
- Moftakhari, H. R., AghaKouchak, A., Sanders, B. F., & Matthew, R. A. (2017). Cumulative hazard: The case of nuisance flooding. *Earths Future*, *5*, 214–223. <https://doi.org/10.1002/2016EF000494>
- Nisi, L., Martius, O., Hering, A., Kunz, M., & Germann, U. (2016). Spatial and temporal distribution of hailstorms in the Alpine region: A long-term, high resolution, radar-based analysis. *Quarterly Journal of the Royal Meteorological Society*, *142*, 1590–1604. <https://doi.org/10.1002/qj.2771>
- OECD. (2014). *OECD reviews of risk management. Policies boosting resilience through innovative risk governance*. Paris: OECD Publishing.
- Olsson, J., Berg, P., & Kawamura, A. (2014). Impact of RCM spatial resolution on the reproduction of local, subdaily precipitation. *Journal of Hydrometeorology*, *16*, 534–547. <https://doi.org/10.1175/JHM-D-14-0007.1>
- Peleg, N., Marra, F., Faticchi, S., Paschalis, A., Molnar, P., & Burlando, P. (2018). Spatial variability of extreme rainfall at radar subpixel scale. *Journal of Hydrology*, *556*, 922–933. <https://doi.org/10.1016/j.jhydrol.2016.05.033>
- Pereira, S., Diakakis, M., Deligiannakis, G., & Zezere, J. L. (2017). Comparing flood mortality in Portugal and Greece (Western and eastern Mediterranean). *International Journal of Disaster Risk Reduction*, *22*, 147–157. <https://doi.org/10.1016/j.ijdrr.2017.03.007>
- Philipp, A., Beck, C., Huth, R., & Jacobsen, J. (2016). Development and comparison of circulation type classifications using the COST 733 dataset and software. *International Journal of Climatology*, *36*, 2673–2691. <https://doi.org/10.1002/joc.3920>
- Prein, A. F., Holland, G. J., Rasmussen, R. M., Clark, M. P., & Tye, M. R. (2016). Running dry: The U.S. Southwest's drift into a drier climate state. *Geophysical Research Letters*, *43*, 1272–1279. <https://doi.org/10.1002/2015GL066727>
- Prein, A. F., Rasmussen, R. M., Ikeda, K., Liu, C., Clark, M. P., & Holland, G. J. (2017). The future intensification of hourly precipitation extremes. *Nature Climate Change*, *7*, 48–52. <https://doi.org/10.1038/nclimate3168>
- Pretenthaler, F., & Vetter, N. (2009). In F. Pretenthaler & H. Albrecher (Eds.), *Hochwasser und dessen Versicherung in Österreich* (pp. 14–28). Wien: Verlag Österreichische Akademie der Wissenschaften.
- Proske, H., & Bauer, C. (2016). Indicative hazard maps for landslides in Styria; Austria. *Acta Geobalcanica*, *2*, 93–101. <https://doi.org/10.18509/AGB.2016.10>
- Pučík, T., Groenemeijer, P., Radler, A.T., Tijssen, L., Nikulin, G., Prein, A.F., ... Teichmann, C. (2017). Future changes in European severe convection environments in a regional climate model ensemble. *Journal of Climate*, *30*, 6771–6794. <https://doi.org/10.1175/JCLI-D-16-0777.1>
- Punge, H. J., & Kunz, M. (2016). Hail observations and hailstorm characteristics in Europe: A review. *Atmospheric Research*, *176*, 159–184. <https://doi.org/10.1016/j.atmosres.2016.02.012>
- Raschky, P. A., Schwarze, R., Schwindt, M., & Zahn, F. (2013). Uncertainty of governmental relief and the crowding out of flood insurance. *Environmental and Resource Economics*, *54*, 179–200. <https://doi.org/10.1007/s10640-012-9586-y>
- Rohrer, M., Croci-Maspoli, M., & Appenzeller, C. (2017). Climate change and circulation types in the Alpine region. *Meteorologische Zeitschrift*, *26*, 83–92. <https://doi.org/10.1127/metz/2016/0681>
- Roodsari, B. K., & Chandler, D. G. (2017). Distribution of surface imperviousness in small urban catchments predicts runoff peak flows and stream flashiness. *Hydrological Processes*, *31*, 2990–3002. <https://doi.org/10.1002/hyp.11230>
- Sass, O., Heel, M., Leistner, I., Stoeger, F., Wetzel, K.-F., & Friedmann, A. (2012). Disturbance, geomorphic processes and recovery of wildfire slopes in North Tyrol. *Earth Surface Processes and Landforms*, *37*, 883–894. <https://doi.org/10.1002/esp.3221>
- Schemm, S., Nisi, L., Martinov, A., Leuenberger, D., & Martius, O. (2016). On the link between cold fronts and hail in Switzerland. *Atmospheric Science Letters*, *17*, 315–325. <https://doi.org/10.1002/asl.660>
- Schiemann, R., & Frei, C. (2010). How to quantify the resolution of surface climate by circulation types: An example for alpine precipitation. *Physics and Chemistry of the Earth Parts ABC*, *35*, 403–410. <https://doi.org/10.1016/j.pce.2009.09.005>
- Schroeder, K., & Kirchengast, G. (2017). Sensitivity of extreme precipitation to temperature: The variability of scaling factors from a regional to local perspective. *Climate Dynamics*, *50*(11–12), 3981–3994. <https://doi.org/10.1007/s00382-017-3857-9>
- Schroeder, K., Kirchengast, G. & O. S. (2018). Strong dependence of extreme convective precipitation intensities on gauge network density. *Geophysical Research Letters*. *Early View*, pp. 11. <https://doi.org/10.1029/2018GL077994>
- Serinaldi, F., & Kilsby, C. G. (2014). Rainfall extremes: Toward reconciliation after the battle of distributions. *Water Resources Research*, *50*, 336–352. <https://doi.org/10.1002/2013WR014211>
- Slater, L. J., & Villarini, G. (2016). Recent trends in U.S. flood risk. *Geophysical Research Letters*, *43*, 1–9. <https://doi.org/10.1002/2016GL071199>
- Syed, K. H., Goodrich, D. C., Myers, D. E., & Sorooshian, S. (2003). Spatial characteristics of thunderstorm rainfall fields and their relation to runoff. *Journal of Hydrology*, *271*, 1–21. [https://doi.org/10.1016/S0022-1694\(02\)00311-6](https://doi.org/10.1016/S0022-1694(02)00311-6)
- Villarini, G., Smith, J. A., Serinaldi, F., Ntelekos, A. A., & Schwarz, U. (2012). Analyses of extreme flooding in Austria over the period 1951–2006. *International Journal of Climatology*, *32*, 1178–1192. <https://doi.org/10.1002/joc.2331>
- Westra, S., Alexander, L. V., & Zwiari, F. W. (2012). Global increasing trends in annual maximum daily precipitation. *Journal of Climate*, *26*, 3904–3918. <https://doi.org/10.1175/JCLI-D-12-00502.1>
- Wirtz, A., Kron, W., Löw, P., & Steuer, M. (2014). The need for data: Natural disasters and the challenges of database management. *Natural Hazards*, *70*, 135–157. <https://doi.org/10.1007/s11069-012-0312-4>
- Wood, J. L., Harrison, S., Turkington, T. A. R., & Reinhardt, L. (2016). Landslides and synoptic weather trends in the European Alps. *Climatic Change*, *136*, 297–308. <https://doi.org/10.1007/s10584-016-1623-3>
- Ye, H., Fetzer, E. J., Wong, S., & Lambrigtsen, B. H. (2017). Rapid decadal convective precipitation increase over Eurasia during the last three decades of the 20th century. *Science Advances*, *3*, e1600944. <https://doi.org/10.1126/sciadv.1600944>
- Zhang, X., Zwiari, F. W., Li, G., Wan, H., & Cannon, A. J. (2017). Complexity in estimating past and future extreme short-duration rainfall. *Nature Geoscience*, *10*, 255–259. <https://doi.org/10.1038/ngeo2911>

### SUPPORTING INFORMATION

Additional supporting information may be found online in the Supporting Information section at the end of the article.

**How to cite this article:** Schroeder K, Tye MR. Quantifying damage contributions from convective and stratiform weather types: How well do precipitation and discharge data indicate the risk? *J Flood Risk Management*. 2019;12:e12491. <https://doi.org/10.1111/jfr3.12491>



4.3 Research Article 3: Sensitivity of extreme precipitation to  
temperature: the variability of scaling factors from a  
regional to local perspective

Published as:

**Katharina Schroeer** and Gottfried Kirchengast (2018). Sensitivity of extreme precipitation to temperature: the variability of scaling factors from a regional to local perspective. *Climate Dynamics* **50**, pages 3981–3994. DOI: 10.1007/s00382-017-3857-9.

Original article available at: <https://doi.org/10.1007/s00382-017-3857-9>





## Sensitivity of extreme precipitation to temperature: the variability of scaling factors from a regional to local perspective

K. Schroeer<sup>1,2</sup> · G. Kirchengast<sup>1,2,3</sup>

Received: 7 December 2016 / Accepted: 10 August 2017 / Published online: 9 September 2017  
© The Author(s) 2017. This article is an open access publication

**Abstract** Potential increases in extreme rainfall induced hazards in a warming climate have motivated studies to link precipitation intensities to temperature. Increases exceeding the Clausius–Clapeyron (CC) rate of  $6\text{--}7\%/^{\circ}\text{C}^{-1}$  are seen in short-duration, convective, high-percentile rainfall at mid latitudes, but the rates of change cease or revert at regionally variable threshold temperatures due to moisture limitations. It is unclear, however, what these findings mean in term of the actual risk of extreme precipitation on a regional to local scale. When conditioning precipitation intensities on local temperatures, key influences on the scaling relationship such as from the annual cycle and regional weather patterns need better understanding. Here we analyze these influences, using sub-hourly to daily precipitation data from a dense network of 189 stations in south-eastern Austria. We find that the temperature sensitivities in the mountainous western region are lower than in the eastern lowlands. This is due to the different weather patterns that cause extreme precipitation in these regions. Sub-hourly and hourly intensities intensify at super-CC and CC-rates, respectively, up to temperatures of about  $17^{\circ}\text{C}$ . However, we also find that, because of the regional and seasonal variability of the precipitation intensities, a smaller scaling factor can imply a larger absolute change in intensity. Our insights underline that temperature precipitation scaling requires careful

interpretation of the intent and setting of the study. When this is considered, conditional scaling factors can help to better understand which influences control the intensification of rainfall with temperature on a regional scale.

**Keywords** Precipitation · Temperature · Alps · Climate · Variability · Risk · Intensity

### 1 Introduction

Hydro-meteorological hazards induced by extreme precipitation pose considerable risk to communities. Thus, statements on possible changes of extreme precipitation are delicate information for politicians, urban planners, farmers, and others who need to manage the risk from climate and weather extremes. However, knowledge gaps exist especially on regional to local scales due to the complex precipitation generating processes, the high natural variability of rainfall, and because data are often not available in sufficient resolution, length, or quality (Alexander 2016; Prein and Gobiet 2016; Contractor et al. 2015).

In recent years, an increasing number of studies has built on the physically based expectation that extreme precipitation intensity changes with temperature following the Clausius–Clapeyron (CC) equation, which describes the water holding capacity of the atmosphere. Thus, an increase in rainfall intensity of  $6\text{--}7\%/^{\circ}\text{C}^{-1}$  (CC-rate) is expected, given constant relative humidity. The concept and recent developments have been reviewed by Westra et al. (2014) and O’Gorman (2015). Three major aspects can be summarized.

First, convective extreme precipitation intensities at sub-daily scales have been found to increase at rates up to about double the CC-rate in both observations and models over the mid-latitudes, whereas intensities on the daily scale

✉ K. Schroeer  
katharina.schroeer@uni-graz.at

<sup>1</sup> Wegener Center for Climate and Global Change (WEGC), University of Graz, Graz, Austria

<sup>2</sup> FWF-DK Climate Change, University of Graz, Graz, Austria

<sup>3</sup> Institute for Geophysics, Astrophysics, and Meteorology (IGAM), Institute of Physics, University of Graz, Graz, Austria

and those associated with stratiform precipitation mostly increase at approximately the CC-rate (Ivancic and Shaw 2016; Ban et al. 2015; Berg and Haerter 2013; Lenderink and van Meijgaard 2009; Haerter and Berg 2009). The high scaling rates have been attributed to both a shift from stratiform to convective precipitation, and an intensification of the convective process itself (Moseley et al. 2016; Attema et al. 2014; Loriaux et al. 2013; Berg et al. 2013).

Second, a decline or reversal of extreme intensities takes place at regionally varying threshold temperatures when the environmental conditions shift from a moist to dry regime and suppress a further intensification of rainfall (Prein et al. 2017; Chan et al. 2016; Drobinski et al. 2016).

Third, connecting local temperature-precipitation relationships to global warming is controversial (IPCC 2013, p. 626) and the available studies differ in scope. Some analyze a single rain gauge (Formayer and Fritz 2016), others assess regional (e.g., Molnar et al. 2015; Wasko and Sharma 2015), or global station networks (e.g., Wang et al. 2017; O’Gorman 2015). Zhang et al. (2017) differentiate studies that detect long-term trends in precipitation intensities with global warming (e.g., Barbero et al. 2017), and studies that establish regional scaling relationships based on conditional quantiles (e.g., Drobinski et al. 2016). In the first case, thermodynamic effects and the Earth’s energy budget are considered to be the dominant factors. In the latter, the variable dynamic conditions throughout the annual cycle become increasingly influential. Furthermore, the cooling effect of precipitation on local temperatures might significantly influence the scaling rates especially for larger-scale precipitation events (Bao et al. 2017).

Here we analyze the variability of the temperature precipitation relationship at the regional to local scale, deliberately considering how the annual cycle and weather systems affect the sensitivity of the statistical scaling factors on the sub-hourly, the hourly and the daily scale. Thus the aim of this study is not to analyze trends in rainfall extremes, but to gain deeper insight into the controls of the spatio-temporal variability of scaling factors on a regional level and to address the implications for interpreting the results. We use sub-hourly rainfall data from a very dense regional station network over south-eastern Austria, filling a gap between the aforementioned single station studies and considerably sparser station networks on national scales.

The study region presents an interesting setting from both a climatological and a socio-economic viewpoint. The geographic location transitions from high Alpine terrain in the north-west of the region to lower-elevation forelands in the south-east, where a strong warming trend with a substantial increase in heat days has been observed over the last decades (Kabas et al. 2011). Moisture advection from the Mediterranean Sea and orographic lifting provide essential ingredients for extreme precipitation events on the southern Alpine

slopes (Cassola et al. 2016; Panziera et al. 2015; Schicker et al. 2010; Sodemann and Zubler 2010) and lows over the Mediterranean moving northeastward ( $\nabla b$ -cyclone tracks) regularly result in excessive rain and large-scale flooding in the southern and south-eastern Alpine region (Volosciuk et al. 2016; Messmer et al. 2015; Hofstaetter and Chimani 2012).

Furthermore, small-scale flash flooding caused by local, short-term extremely intense convective rainfall has destroyed human livelihood in the past, where for the most destructive events, rainfall depths of 100–600 mm have been reconstructed (hydroConsult GmbH 2011; Schocklitsch 1914; Forchheimer 1913). One of the top three Central European one-day precipitation records occurred here (Munzar et al. 2011). The area is densely populated and the terrain favors debris flows and landslides. The local agriculture with vineyard and fruit cultivation is vulnerable to short-term extreme precipitation and hailstorms especially during the summer half year.

We assess the temperature sensitivity of the maximum (10-min) peak and maximum hourly rainfall intensity within observed rainfall events, as well as daily rainfall sums during the summer half year (April to October). The questions we strive to answer here are: (1) Which factors control the spatial and temporal variability seen in the temperature sensitivities on a regional scale? (2) How applicable and useful is the scaling approach on the regional to local scale considering regional climate variability? (3) What do scaling factors tell us about changes in absolute rainfall intensities?

The paper is structured as follows. The data and methods used are described in Sects. 2 and 3, respectively. We report and discuss the spatial, seasonal, and storm-type variability of scaling factors in Sects. 4.1 and 4.2, and link them to actual rainfall amounts in Sect. 4.3 to assess how the temperature sensitivities can be interpreted from a regional to local impact scale perspective. Concluding arguments are given in Sect. 5.

## 2 Data

Our study area comprises the south-eastern Alpine foreland region of Austria south of the main Alpine ridge (Fig. 1). Southerly flow and weak gradient situations with convective precipitation during the summer months are the dominant patterns associated with extreme daily precipitation sums in the eastern part. In the southern- and westernmost part, the heaviest precipitation days occur during “Southern Stau” situations and peak in October (Seibert et al. 2006).

We use sub-daily precipitation data from 77 semi-automated weather stations of the Austrian meteorological service (ZAMG) and from 112 rain gauges provided by five provincial administrations of the Austrian hydrographic



# 4.3 RESEARCH ARTICLE 3: SENSITIVITY OF EXTREME PRECIPITATION TO TEMPERATURE FROM A REGIONAL TO LOCAL PERSPECTIVE

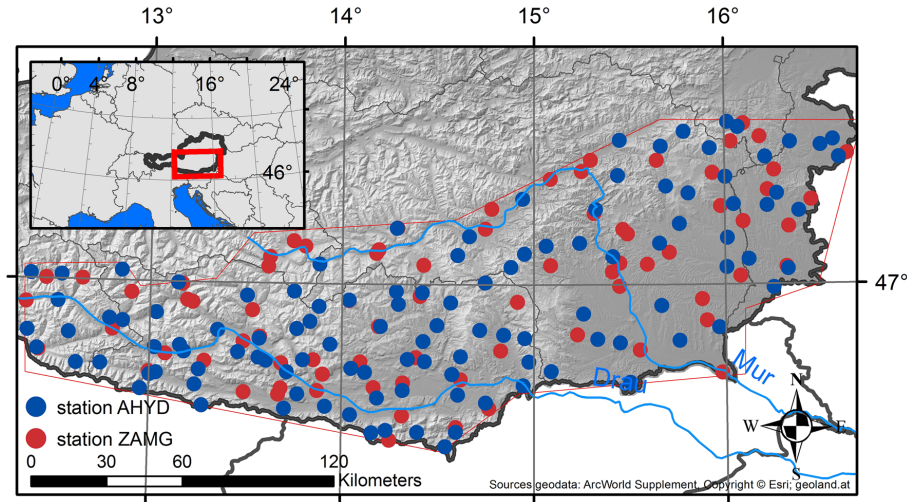


**Fig. 1** Austrian south-eastern Alpine foreland region (red polygon) and precipitation measurement stations used in the analysis. Observations of additional atmospheric variables (temperature, humidity) are

available for most stations operated by the Austrian meteorological service ZAMG (red). Stations operated by the Austrian hydrographic service AHYD (blue) provide precipitation data only

service (AHYD), both delivering 0.1 mm resolution in rainfall amount. This yields a total number of 189 stations, with record lengths from 1 to 58 years (median: 14 years), ending November 2014. The mean distance to the nearest neighboring station is ~6 km. 1–5 min aggregated precipitation at AHYD stations was summed up to match the 10 minute aggregated precipitation reported at ZAMG stations. The data are cut to our focus season defined as the period from 1st April to 31st October.

The average amount of missing data is 1.4%, with 15 stations reporting a higher fraction of over 15%. These 15 stations are not excluded from the analysis, because they are amongst the stations with the longest records (20 years on average) and a detailed inspection showed that periods of missing data are due to long coherent out-of-service periods. As no time series or trend analysis is done in this study, we decided to use all existing information on plausible events. Since previous quality control of the data varied with the provider, all station series were double-checked for data gaps and inconsistencies.

Extreme outliers (events exceeding the 99.95th percentile) were analyzed case-by-case and only removed from the statistical analysis if they could not be justified to be physically plausible. For this, we analyzed the rainfall records at the station where the event was recorded and at the five closest neighboring stations from 12 h before until 12 h after the event. We checked the records for suspicious values (e.g., 99 and similar, several identical values

in a row, sudden breaks), and in addition investigated weather review reports issued by the ZAMG documenting exceptional rainfall events, and hydrographical year books issued by the Austrian Federal Ministry of Agriculture, Forestry, Environment and Water Management, which contain dates and record rainfall amounts, water levels and runoff at AHYD gauges. As a result, 41 out of 153 outlier events were excluded from the sample.

Because temperature measurements are not available for every precipitation station, the daily average and maximum temperature of the days of and preceding a precipitation event were interpolated for all station locations from the high quality 1 × 1 km SPARTACUS (Hiebl and Frei 2016) and INCA (Haiden et al. 2010) gridded temperature data products (INCA to extend the SPARTACUS dataset from 2011 to 2014). We used inverse distance-weighted horizontal interpolation and a standard vertical temperature lapse rate (−6.5 K/km). Single station temperature time series used for validation showed very good agreement of the interpolated and directly observed temperatures, confirming the adequacy of this approach.

### 3 Methods

We estimate the temperature sensitivity of extreme precipitation on an event basis rather than from single observations. This has been done by several other authors (Wasko and Sharma 2015; Molnar et al. 2015; Gaál et al. 2014)

and prevents double counting of dependent observations within the same storm. Note that this considers only the temporal dependence; if the same storm moves over more than one station, it repeatedly enters the sample.

We first define periods of continuous rainfall as rainfall events, where each dry interval separates two rainfall events. For each day, we save the number and duration of events, the total number of wet observations, the daily precipitation sum and rain rate (total sum divided by the number of wet observations). We consider only the highest 10-min amount as maximum peak intensity (MPI) and the highest hourly amount as maximum hour intensity (MHI). This way, we only pair each daily mean temperature once, while keeping the information on how concentrated or dispersed the total daily rainfall was distributed over the day.

In addition, we performed a circulation type classification (CTC) based on daily ERA-Interim data (1979–2016, Dee et al. 2011) over the Greater Alpine Region (40.5–51.57°N, 3.0–20.25°E), using the COST Action 733 CTC software (Philipp et al. 2016). We apply a principal component analysis and cluster analysis with 27 circulation types (CTs), which has been shown to perform best in explaining Alpine precipitation variability (Schiemann and Frei 2010). In addition to sea level pressure, we include data of convective available potential energy as indicator of atmospheric stability and seasonality, 700 hPa wind velocity to consider fast and slow moving systems, and 500 hPa geopotential.

Since we are primarily interested in summertime convective precipitation as well as in keeping samples large enough for robust statistical analyses, it is not expedient to continue with 27 CTs. Hence we classify each given day as either falling into a summer convective CT or not. This is done by visual inspection of the anomaly plots of the variables used, the frequency of occurrence, and precipitation anomalies of the CTs (using ZAMG GPARD-1 1 × 1 km daily gridded precipitation data over Austria, Hofstätter et al. 2015).

Maximum hour and maximum peak intensities (MHI and MPI), as well as the daily precipitation sums (DPS) are paired with the daily mean temperature of the day of event onset ( $T_{\text{mean}}$ ). Days with an average daily temperature below 5 °C were dismissed to exclude snow events. We alternatively calculated the temperature sensitivities for the daily rain rate, for the daily maximum temperature, as well as for the mean and maximum temperature of the day prior to event onset in order to exclude cooling due to the event itself, but the scaling results did not show significant differences to the results obtained from  $T_{\text{mean}}$ . Similar low sensitivities against some variation in temperature choice were found by Lenderink and van Meijgaard (2009) and Lepore et al. (2015).

We also calculated the scaling rates for dew point temperatures (dpT), as they are a more immediate indicator

of the available moisture (Lenderink and Meijgaard 2010), and compared them to the results for  $T_{\text{mean}}$ . Data were only available for a reduced sample of ZAMG stations. The change rates for the 98th percentile were not significantly different for dpT as compared to  $T_{\text{mean}}$ , while the moderate intensities showed higher dpT sensitivities.

We calculate the scaling factors that describe the percentage change in precipitation intensity per degree of daily mean temperature using quantile regression. In contrast to ordinary least squares regression, quantile regression estimates the influence of the independent variable on a selected conditional quantile of the dependent variable instead of just on the mean (see, e.g., McMillen 2012). Quantile regression thus gives a more comprehensive picture of the influence of temperature on the distribution of precipitation intensities. We fit the quantile regression model for each event sample of interest to the logarithmic precipitation as a function of mean temperature, similar to Wasko et al. (2015),

$$\ln(P) = \beta_0^q + \beta_1^q T, \quad (1)$$

where  $P$  is the event precipitation intensity (MHI, MPI, or DPS),  $q$  is the target quantile, and  $T$  the daily mean temperature of the event onset day. Based on the linear-slope regression coefficient  $\beta_1^q$  obtained from this fit, the scaling factor (SF) as the rate of change of precipitation with temperature is then estimated as

$$\text{SF} [\%/^\circ\text{C}] = (\Delta P / \Delta T) = 100 \cdot (e^{\beta_1} - 1). \quad (2)$$

The significance of a regression coefficient  $\beta_1^{q_e}$ , where  $q_e$  is the quantile of interest (e.g., the 98th percentile), is estimated to be most robust and distinct if it not only deviates from zero with 95% confidence, but if the 95% confidence interval of  $\beta_1^{q_e}$  does not overlap with the one of  $\beta_1^{q_{\text{med}}}$ , where  $q_{\text{med}}$  is the median (50th percentile). The method is also more robust against outliers and allows a more straightforward reporting of the statistical uncertainties than the more common temperature binning approach (e.g., studies reviewed in Westra et al. 2014).

Quantile regression is a linear method, and therefore non-linearities in the data are not considered (which is also the case when a linear regression is fit to binned percentiles). However, in sensitivity tests, in which we cut off the data at different temperatures at the lower and higher ends of the temperature range, we found that the decrease of intensities at the highest temperatures primarily manifests itself in large uncertainty ranges in in these areas, while the overall scaling factor remains robust. This is due the smaller sample sizes at the highest temperatures. Thus, the uncertainty ranges deliver an important indicator of the robustness of the regression. To account for non-linearities in a more explicit

### 4.3 RESEARCH ARTICLE 3: SENSITIVITY OF EXTREME PRECIPITATION TO TEMPERATURE FROM A REGIONAL TO LOCAL PERSPECTIVE

**Fig. 2** Scaling factors (SFs) of station event precipitation intensity with daily mean temperature for the 98th percentile. Results for the maximum peak intensities (MPI, *top panel*), maximum hourly intensities (MHI, *center panel*), and daily precipitation sums (DPS, *lower panel*) are shown. *Plus symbols (+)* indicate that the SF is sensitivity significantly different from zero, *circles (o)* indicate that the SFs of the 98th percentile is also significantly different from the 50th percentile (median). The size of the *circle symbols* indicates the length of the station record as summarized in the legend

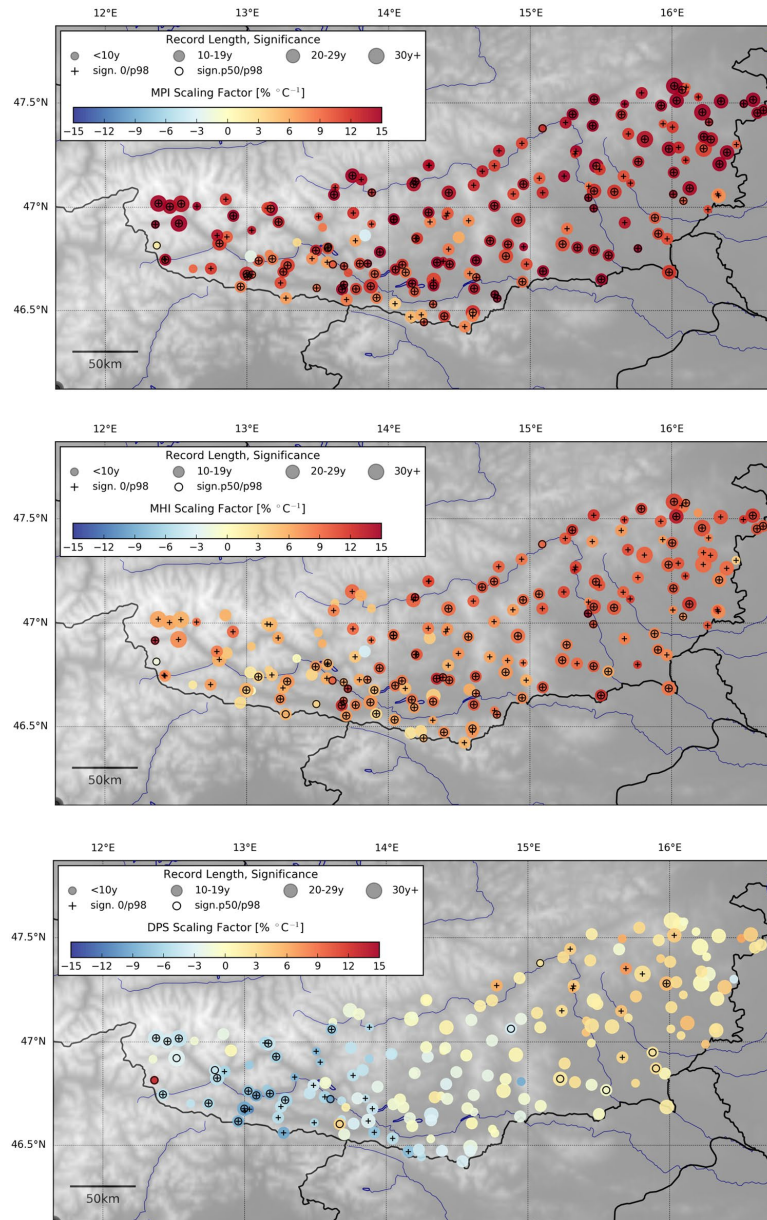


**Table 1** Summary characteristics of the station scaling factors (results for 98th percentile)

	Mean SF	Stdev	Min	25%	75%	Max	Avg. 95% CI	Avg. 98th percentile
MPI	12.2	3.5	-3.1	20.2	10.6	14.3	$\pm 3.5$	8.1 mm, $\sigma = 6.6$ mm
MHI	8.9	2.8	3.6	7.3	10.6	19.0	$\pm 3.3$	16.0 mm, $\sigma = 10$ mm
DPS	-1.4	3.9	-11.4	12.8	-3.8	1.8	$\pm 2.8$	52.0 mm, $\sigma = 30$ mm
Rain rate	10.7	2.8	-5.2	19.6	9.0	12.3	$\pm 3.6$	1.7 mm/h, $\sigma = 0.7$ mm/10 min

The values in all columns except the first and last one are in units [%/°C]

way, we calculated the scaling rates in moving windows over the temperature range (see Sect. 4.3).

## 4 Results and discussion

### 4.1 Spatial variability and regional patterns of scaling factors

Figure 2 and Table 1 show the 98th percentile station event scaling factors (SFs) for maximum peak intensity (MPI), maximum hour intensity (MHI), the daily precipitation sum (DPS), and the average rain rate (mm/h, Table 1 only) of the entire event sample.

With an average SF of 12%/°C, the MPIs increase with daily mean temperature at rates that exceed the CC-rate and that are significantly higher than those for moderate intensities (50th percentile) at the majority of the stations. The MHIs increase closer to the CC-rate at 9% on average, but a spatial partition emerges with higher/lower SFs in the eastern/western part of the study region, respectively. The higher sensitivity of the 10 min peak intensity compared to the hourly peak intensity is robust throughout our analysis. This is interesting, because even though most studies see scaling rates increase when the time scales decrease from daily to sub-hourly resolution, findings on super-CC scaling on the sub-hourly scale have been inconclusive (Molnar et al. 2015, and review by Westra et al. 2014). The SFs of the DPS show a bipolar pattern with SFs around 3% in the eastern part and negative SFs around -10% in the western part.

We calculated the station SFs for each summer month individually, for the MPI, MHI, DPS, and rain rates (not separately shown). We find that the MPI sensitivities generally show the most consistent scaling at CC-to-super-CC rates throughout the year, especially in the eastern region. In the west, super-CC scaling prevails, but several stations show non-significant or even negative scaling especially in April and October. For the MHI, positive scaling at approximately the CC-rate is consistent in the east, whereas in the west, the picture is inconclusive. Here, negative SFs prevail in April, rise towards CC-rates in September for almost all stations, and become negative again in October at several stations. The bipolar pattern of the SFs of the DPS is consistent throughout

the year, although the transition from negative to positive SFs is located farther west in April, May, and June.

The regional and seasonal patterns of SFs indicate that regional scale temperature sensitivity depends on weather patterns and the climatology of the region. The eastern part of the study region is located at lower elevations and the average daily mean temperatures are higher than in the mountainous and high Alpine western part throughout the year. Climatologically, the days of heaviest precipitation in the eastern region are predominantly convective and occur during July and August under weak-pressure-gradient synoptic situations. In the south western part, the heaviest precipitation days culminate in October during 'Southern Stau' conditions, when moist air masses from the Mediterranean are lifted at the Karavanks and Carnic Alps, often resulting in persistent and intense precipitation (Pretenthaler et al. 2010; Seibert et al. 2006).

This helps to explain the low and negative SFs in the south-western part of our study region, since in these situations, the moisture content of the advected air mass is driven by warm Mediterranean SSTs, while local temperatures are cooler especially in the fall season. In addition, the daily mean temperature during long and persistent rainfall events is likely to be more affected by the rainfall events itself than it is for short events (Bao et al. 2017). The eastern part is largely shielded from 'Southern Stau' events, the highest extremes occur during shorter convective events during the warm summer months and are less affected by cooling effects due to the event itself, which can explain the higher SFs in this region.

It is apparent that despite the regional patterns, some neighboring stations show large differences in SFs. This underlines that deriving regional temperature sensitivities from a single station is problematic. Especially in mountainous regions, station altitude and temperature range could in part account for differences of scaling factors in nearby stations. However, in a simple linear regression analysis, we find no statistically significant influence of the station altitude on the SFs. We do find a weakly significant positive effect of the station temperature range on its MHI SF, explaining about 15% of the variability, but not on the MPI SF.

The spatial variability and pattern of scaling rates presented here are consistent with results from Molnar et al.

### 4.3 RESEARCH ARTICLE 3: SENSITIVITY OF EXTREME PRECIPITATION TO TEMPERATURE FROM A REGIONAL TO LOCAL PERSPECTIVE

(2015), who, for 59 rain gauges over Switzerland, found that stations in pre-Alpine areas show higher SFs than high Alpine regions and valleys. The analysis of the considerably denser rain gauge network used here robustly confirms the influence of regional weather patterns on SF in a mountainous region.

#### 4.2 Seasonal and storm type patterns of scaling factors

Climatological precipitation over the Alpine area generally reaches its maximum in the warmer summer/fall season and its minimum in the cold winter season (Frei and Schär 1998). Scaling factors conditioned on the local absolute temperatures are therefore always governed by the annual cycle, and hence are of limited suitability to assess the effect of global warming on extreme precipitation intensities (see Zhang et al. 2017 for a more detailed discussion). Still, it is highly worthwhile to look at conditional SFs in order to quantify the extent to which the annual cycle and weather patterns govern the local temperature-scaling relationship and to assess under which temperature conditions intense rainfall is most likely to occur.

The previous section showed that rainfall intensities and temperatures are not spatially independent, and pooling all stations over the study region conceals higher scaling rates particularly in the east (see Fig. 3). We thus separate the western and eastern parts of the study region by the 15°E meridian. The mixing effect over diverging temperature ranges might also play a role in mountain regions due to the substantial vertical temperature gradients. However, we do not further account for these effects here.

As displayed in Fig. 3, MPIs show the highest scaling rates, ranging from 2–12%, with MHIs being 1–2% lower on average, while the DPS SFs are mostly negative. The MPI and MHI extreme intensities (98th percentile)

increase faster with temperature than the moderate intensities (50th percentile) during May–September in the western region and during April–October in the eastern region. For the daily sums, the difference between the moderate and extreme daily sums is only significant in the eastern region. Here, the moderate daily sums decrease by 4–7%/°C, while the extreme daily sums only decrease at about 0–2%/°C.

Inspecting the distribution of rainfall events and temperature in the subsamples (not shown) helps to understand the variability driven by the differences in regional climatology as described above. A possible explanation for diverging scaling rates in moderate and extreme DPS is the concentrated nature of convective storms that dominate extreme precipitation in the east. When it rains on a hot summer day, it pours. The shorter and more concentrated a rainfall event, the less difference there is between the MPI, MHI, and the DPS. Hence, the DPS from extremely intense rainfall events do not decrease as significantly with temperature as the moderate DPS. In the western part, extreme DPS occur at cooler temperatures and events last longer. In addition, the rainfall sums are larger than in the east, and it is therefore harder to preserve high scaling rates (see Sect. 4.3 for discussion).

Furthermore, the MPI sensitivities are significantly lower in July and September. The analysis of the scatter plots of the underlying temperature-precipitation distributions in these months (not shown) indicate extremes that are higher and more evenly distributed over the temperature range than in other months. This is because the temperature range is shifted to the right and the extreme intensities decrease over the hottest temperatures. Moisture limitations might inhibit larger scaling factors at these temperatures (see Westra et al. 2014), however, data on relative humidity are only available

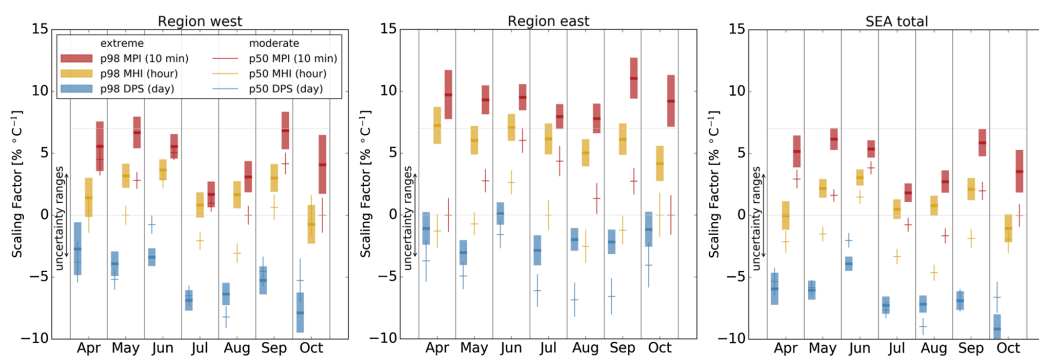


**Fig. 3** Monthly scaling factors (SFs) for the 50th (*thin lines*) and 98th (*fat lines*) percentiles of maximum peak intensities (MPI, *red*), maximum hour intensities (MHI, *yellow*), and daily precipitation

sums (DPS, *blue*). The vertical spread of the lines denote the 95% confidence interval of the SF

for the ZAMG stations and cannot sufficiently prove this general assumption.

In addition to rainfall intensity, event duration is an important factor of the damage potential of extreme precipitation. Convective showers in the mid-latitudes are usually short and intense, whereas extreme stratiform precipitation events accumulate large sums at lower intensities over longer durations. Short events, however, occur frequently and under all weather conditions in our sample.

In order to assess whether the temperature sensitivity of summertime convective precipitation is different from other days, we separated those days from our sample that fall within a circulation type (CT) associated with convective conditions over the Alpine domain. Note that this is not a classification of the rainfall type in individual events, but of the large-scale synoptic situation over the Alps. In addition, the samples were conditioned on the total duration of non-zero rainfall (0.2–2, 2–5, 5–24 h), indicating the overall 'wetness' of the day when an event occurred. Figure 4 shows the results for the subsamples.

CC- to super-CC scaling is apparent on days with short rainfall events over the entire region. In the east, the SFs for MPI and DPS diverge in autumn, which is due to an increasing influence of events yielding high total sums at lower

temperatures and rain rates. In the west, the proximity of MPI and DPS SFs indicate that both the daily sums and the peak intensities increase with temperature.

The convective CT sample isolates the hottest days during high summer. The temperature sensitivities during June, July, and August (JJA) are lower than for the other CTs. In the east region, daily mean temperatures reach up to 27 °C, while extreme rainfall intensities start to decline from ~24 °C upwards. In September, the mean temperatures generally do not exceed ~24 °C anymore and the higher SFs indicate a robust increase of extreme intensities in convective CTs. In the western region, daily mean temperatures in JJA rarely exceed ~24 °C. Extreme rainfall intensities, however, start to decline already at ~20 °C. This indicates that the reversal of extremes as described in, e.g., Prein et al. (2017) is location specific even on this regional scale.

On the wetter days in July, SFs during nonconvective-CTs are only about 2–3%/°C. Again, the distribution of temperature and precipitation suggests that  $T_{\text{mean}}$  in July rarely falls below 10 °C, and high precipitation intensities occur over the entire temperature range, decreasing at its high end, resulting in low SFs. This decrease of the highest intensities at the highest temperatures is less pronounced in June and September, and in addition, fewer extreme intensities are

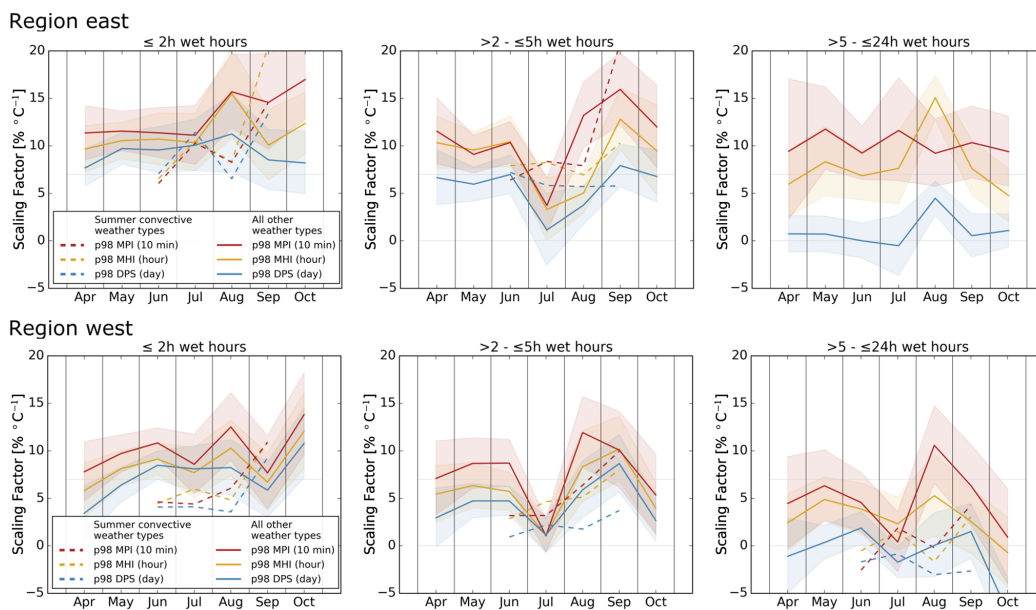


**Fig. 4** Monthly scaling factors in the east and west region (upper and lower row, respectively) for the 98th percentile of maximum peak intensities (MPI, red), maximum hour intensities (MHI, yellow), and daily precipitation sums (DPS, blue) on days with a total maximum

of two wet hours (left), 2–5 wet hours (middle), and 5–24 wet hours (right). SFs for days under summer convective synoptic conditions are shown separately (dashed lines, Jun–Sep). The shaded areas denote the 95% confidence interval of the SFs

### 4.3 RESEARCH ARTICLE 3: SENSITIVITY OF EXTREME PRECIPITATION TO TEMPERATURE FROM A REGIONAL TO LOCAL PERSPECTIVE

observed at cooler temperatures, which leads to a steeper increase and a higher SF. Further research on the synoptic patterns and atmospheric conditions that inhibit or foster the intensification of extreme intensities in the warmest summer months is needed to explain the differences in SFs.

#### 4.3 How regional scaling factors relate to absolute rainfall intensities

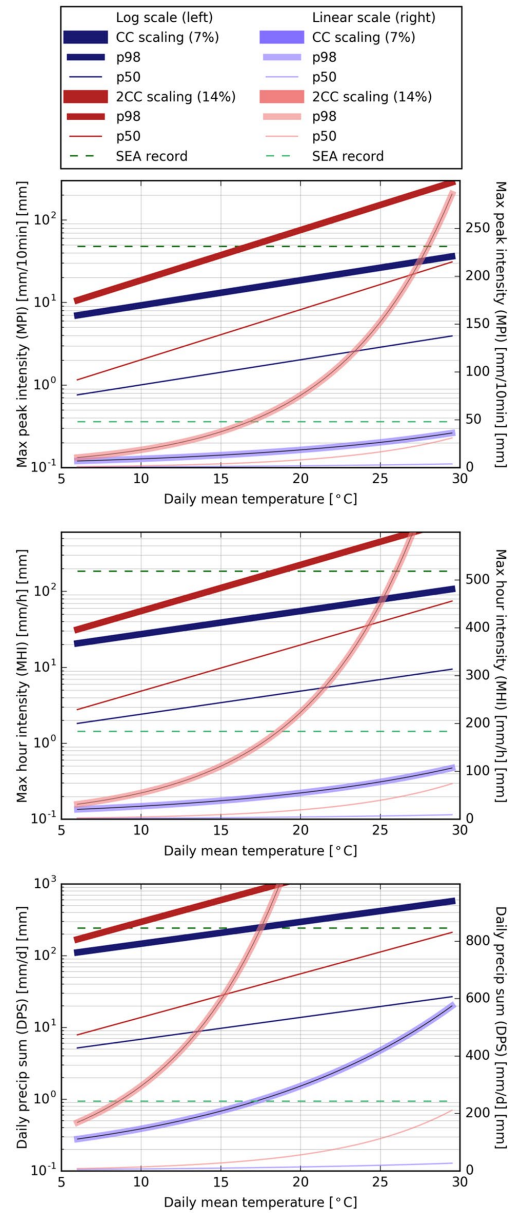
Risk from extreme precipitation is either posed through high intensity rainfall over short times, causing sudden and small scale flash flooding, or through persistent precipitation leading to slower-onset but larger-scale flooding. We have shown that the temperature sensitivity of extreme precipitation, defined as the 98th percentile of event maximum intensities on the 10 minute, the hourly and the daily scale, vary with the station location, the time of the year, and the prevailing weather patterns. The magnitude of a scaling factor, however, does not provide any information on the magnitude of the actual rainfall intensity.

Figure 5 shows four graphs of CC- and super-CC-rates for the MPI, MHI, and DPS 50th and 98th percentile, respectively. The graphs are initialized at the respective percentile value estimated for the 5–7 °C  $T_{mean}$  bin. By means of the highest observed rainfall intensities over the study area, we illustrate how the scaling rates relate to absolute amounts of precipitation intensity.

Whether a scaling rate implies a high absolute change in rainfall intensity depends on the magnitudes of the scaling rate, the rainfall intensity, and the temperature. For the 98th percentile MPI, a CC-rate can be perpetuated up to daily mean temperatures above 30 °C before traversing the threshold of the current record rainfall amount. The same holds true for a super-CC rate in the case of the much smaller 50th percentile MPI.

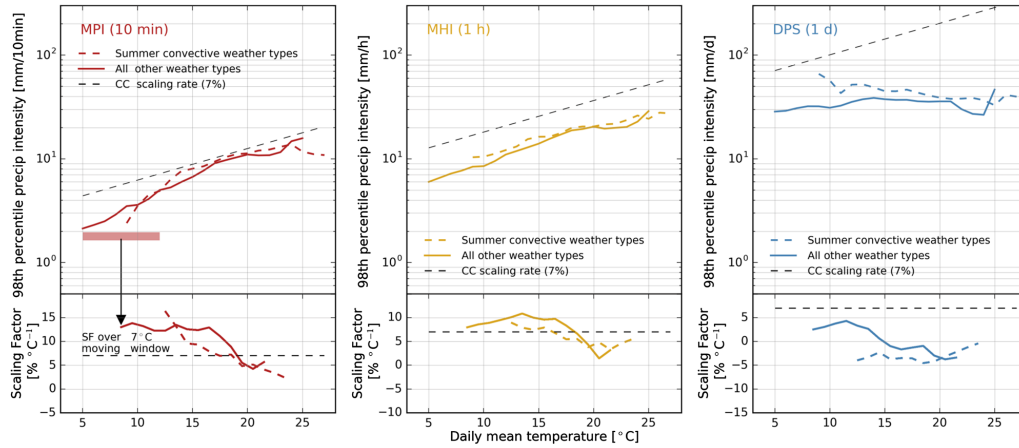
This changes drastically when either the absolute rainfall intensities increase, or the scaling factor is higher. For example, super-CC scaling in MPI from our graph (Fig. 5, top) would imply record intensities beyond daily mean temperature of ~16–17 °C. For scaling in the DPS (Fig. 5, bottom), the threshold temperatures to reach the record are ~16 °C for CC- and ~8 °C for super-CC scaling, respectively.

Furthermore, a low scaling factor in high rainfall intensities implies a larger absolute change than a high scaling factor in low rainfall intensities. Even though the scaling factors in the western region—or on days with long rainfall durations—are lower than they are in the eastern region—or on days with short rainfall events—, the extremes do significantly increase with temperature during the summer months. At around 20 °C, for example, a 4% increase in a long event MHI (~50 mm) implies an additional 2 mm per degree; at the same time, an 8% increase in a short event MHI (~20 mm) means an additional 1.6 mm per degree. That



**Fig. 5** CC (blue) and super-CC (2CC, red) scaling rates, originating from the 50th (thin lines) and 98th (fat lines) percentile values calculated for the 5–7 °C daily  $T_{mean}$  bin. The panels show maximum peak intensities (MPI, top), maximum hour intensities (MHI, middle), and daily precipitation sums (DPS, bottom) on a log-scale (left ordinate) and linear scale (right ordinate); the legend box on top identifies the individual cases. Actual MPI, MHI, and DPS rainfall records over the SEA study region are shown as green dashed lines

Region east



Region west

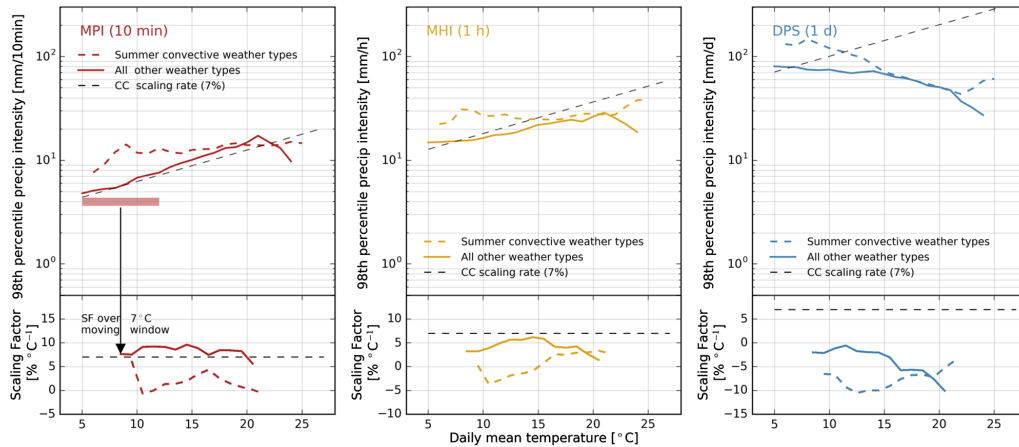


**Fig. 6** Absolute 98th percentile values (*upper panels in both rows*) of the maximum peak intensities (MPI, *left, red*), maximum hour intensities (MHI, *middle, yellow*), and daily precipitation sums (DPS, *right, blue*) for the east and west region. The *lower panels* in both rows show the corresponding scaling factors calculated over 7 °C

moving windows (as indicated in the *left panels*). Note that the scales for the scaling factors vary for MPI, MHI, and DPS. Both percentiles and scaling factors are shown for summertime convective synoptic situations (*dashed*) and all other synoptic conditions (*solid*), with CC-rates shown as reference lines (*black dashed*)

is, even though the MHI in longer and larger scale rainfall events scales lower, the flood risk might increase considerably if the event occurs in warmer temperature conditions.

Our findings also demonstrate that the change rate for a given percentile (e.g., 98th) should only be compared under consideration of the underlying temperature and precipitation data, because the actual percentile values may vary

significantly, with major implications for the resulting scaling factor.

Figure 6 shows a comparison of the actual 98th percentile values of rainfall intensity calculated for 2 °C bins containing at least 100 events. To visualize non-linear dependencies in the data and to get a better understanding how the SFs relate to the absolute rainfall intensities, we calculated



the SFs for sub-samples using a 7 °C moving window over the range of daily mean temperatures. The window width of 7 °C yielded the most robust SFs when trading off the event sample size and a sufficiently large temperature spread over which the regression could be calculated. We find this approach more informative than splitting the event sample only once at the estimated threshold temperature at which the scaling turns from positive to negative (Wasko and Sharma 2015).

The illustrations of Fig. 6 summarize the findings of the spatial and seasonal analysis of the scaling factors and their relation to absolute rainfall. The temperature sensitivities are highest for the MPI, lower for the MHI, and lowest for the DPS. The highest SFs are seen between about 10–15 °C, after which they start to decline.

The temperature sensitivity under summertime convective conditions is lower than on other days until approx. 20 °C. These convective days are characterized by warmer temperatures and overall higher extreme precipitation intensities. Extreme convective precipitation in the generally cooler western region occurs at lower local daily mean temperatures than in the eastern region.

Orographic enhancement of convection in mountainous regions is one reason for the strong intensities at lower temperatures occurring in the western region. This is supported by recent regional climate models, which show that global warming likely intensifies Alpine summer convective precipitation (Giorgi et al. 2016). Generally, SFs are lower and extreme percentiles are higher in the western region. The 98th percentile MPIs start to decrease around 24 and 20 °C in the eastern and western regions, respectively. However, the data on events at the highest ends of the temperature distributions are too sparse to calculate robust percentiles and SFs.

The peak intensities of small scale, short convective showers, which contribute the largest share of events in this high temperature range, might be underrepresented in the data due to the limited spatial coverage of the observation network (Kann et al. 2015; Jones 2014), adding uncertainty to the analysis of the scaling relationship at these temperatures. It is likely that humidity constraints contribute to the inhibition of further intensification of the extreme intensities. Data on relative humidity, however, is only available for approx. one third of the stations and thus moisture conditions could not be robustly assessed. Data in the subsample for which humidity could be analyzed indicate lower relative humidity on days with the most extreme intensities as compared to days with moderate precipitation, pointing to a potential moisture limitation. However, further research is needed to test this assumption in our study region. Recent contributions to the literature by Loriaux et al. (2016a) and Loriaux et al. (2016b) demonstrate that considering relative humidity alone is not sufficient to explain the intensification

of extreme precipitation. Through including atmospheric control factors such as large scale moisture convergence and atmospheric stability, they deliver valuable contributions to process understanding.

## 5 Summary and concluding remarks

We have analyzed the temperature sensitivities of extreme daily, hourly and sub-hourly (10-min) precipitation intensities of rainfall events over a dense network of 189 rain gauges in the south-eastern Alpine foreland region of Austria. Scaling factors conditioned on local temperatures require a different interpretation than scaling factors that assess the precipitation response to global warming, as seasonal weather patterns and the annual cycle outweigh the thermodynamic response. We looked at the spatial and seasonal patterns of the temperature sensitivities to assess these implications. Linking the scaling rates to actual changes in rainfall amounts enables new insights for the adequate interpretation of temperature sensitivity from an impact-perspective. We find several distinct aspects of scaling behavior over the study region.

First, the maximum 10-min peak intensities (MPI) significantly and strongly increase with temperature at super-CC rates at most of the stations, whereas peak hourly intensities (MHI) do so at weaker rates around the CC-rate, and daily precipitation sums (DPS) decrease with temperature.

Second, the temperature sensitivities are higher in the generally warmer eastern parts of the study region, where extreme precipitation is associated with short, convective rainfall events during summer and low gradient synoptic conditions with high shares of locally recycled moisture (Bisselink and Dolman 2008). Extremes here rarely occur in cold temperature conditions. In contrast, the scaling factors in the western part of the study region are lower. Extreme precipitation occurs when Mediterranean moisture is advected and lifted at the southern slopes of the Alps. Thus the moisture is not locally sourced, and local temperatures might be less indicative of the sensitivity (Zhang et al. 2017). Also, the cooling effect of large scale events might play a role here (Bao et al. 2017), as well as the orographic amplification of precipitation and generally cooler temperatures in the Alpine environment.

Third, the temperature sensitivities are higher for short duration rainfall as compared to long duration events in both regions. This implies that the peak event intensities on the hourly and sub-hourly scale in long rainfall events increase slower with temperature than peak event intensities in short rainfall events. An explanation for these differences is again the variability of weather patterns, but this time within the respective regions. Further research on how the temperature sensitivities look like in different weather types, might thus

reveal valuable insight into the dynamic controls of the temperature precipitation scaling on a regional to local scale.

The salient seasonal and spatial variability in the scaling factors that we found underlines the difficulty to compare scaling factors among different studies. The confrontation with actual rainfall amounts showed that the sample size and the magnitude of a specific percentile are crucial parameters of a given rainfall change rate.

From a risk assessment perspective, it is furthermore important to note that a statistically defined extreme event can deviate from what is considered an extreme event in practice. For example, high scaling factors at low daily mean temperatures do not necessarily imply large absolute changes in precipitation intensity, while even moderate scaling factors at high temperatures may have substantial consequences in terms of accumulated rainfall.

It is often justifiably argued that the local temperature is not an appropriate choice for temperature precipitation scaling, since the moisture uptake often occurs in regions and at temperatures far away from the point of precipitation. Through taking into account these dynamic factors by isolating, e.g., weak gradient synoptic situations with mainly local moisture recycling from other events, regional temperature sensitivities can however deliver useful insights into how the thermodynamic and dynamic factors play together in controlling the change of precipitation intensities with temperature in specific seasons and regions.

**Acknowledgements** Open access funding provided by Austrian Science Fund (FWF). The study was funded by the FWF-DK Climate Change of the Austrian Science Fund (FWF Doctoral Programme No. W 1256-G15; <http://dk-climate-change.uni-graz.at>). The interdisciplinary faculty and students of this doctoral programme are thanked for discussion and comments during the study and A. Prein, M. Tye (NCAR Boulder), and C. Unterberger for valuable comments on earlier versions of the manuscript. We thank the offices of the Austrian Hydrographic Service and the Austrian National Weather Service ZAMG for provision of the precipitation data and for complementary meteorological data.

**Open Access** This article is distributed under the terms of the Creative Commons Attribution 4.0 International License (<http://creativecommons.org/licenses/by/4.0/>), which permits unrestricted use, distribution, and reproduction in any medium, provided you give appropriate credit to the original author(s) and the source, provide a link to the Creative Commons license, and indicate if changes were made.

## References

- Alexander LV (2016) Global observed long-term changes in temperature and precipitation extremes: a review of progress and limitations in IPCC assessments and beyond. *Weather Clim Extrem* 11:4–16. doi:10.1016/j.wace.2015.10.007
- Attema JJ, Loriaux JM, Lenderink G (2014) Extreme precipitation response to climate perturbations in an atmospheric mesoscale model. *Environ Res Lett* 9(1):014003. doi:10.1088/1748-9326/9/1/014003
- Ban N, Schmidli J, Schär C (2015) Heavy precipitation in a changing climate: Does short-term summer precipitation increase faster? *Geophys Res Lett* 42(4):1165–1172. doi:10.1002/2014GL062588
- Bao J, Sherwood SC, Alexander LV, Evans JP (2017) Future increases in extreme precipitation exceed observed scaling rates. *Nat Clim Change* 7(2):128–132. doi:10.1038/nclimate3201
- Barbero R, Fowler HJ, Lenderink G, Blenkinsop S (2017) Is the intensification of precipitation extremes with global warming better detected at hourly than daily resolutions? *Geophys Res Lett* 44(2):974983. doi:10.1002/2016GL071917
- Berg P, Haerter JO (2013) Unexpected increase in precipitation intensity with temperature—a result of mixing of precipitation types? *Atmos Res* 119:56–61. doi:10.1016/j.atmosres.2011.05.012
- Berg P, Moseley C, Haerter JO (2013) Strong increase in convective precipitation in response to higher temperatures. *Nat Geosci* 6(3):181–185. doi:10.1038/ngeo1731
- Bisselink B, Dolman AJ (2008) Precipitation recycling: moisture sources over Europe using ERA-40 Data. *J Hydrometeorol* 9(5):1073–1083. doi:10.1175/2008JHM962.1
- Cassola F, Ferrari F, Mazzino A, Miglietta MM (2016) The role of the sea on the flash floods events over Liguria (northwestern Italy). *Geophys Res Lett* 43(7):3534–3542. doi:10.1002/2016GL068265
- Chan SC, Kendon EJ, Roberts NM, Fowler HJ, Blenkinsop S (2016) Downturn in scaling of UK extreme rainfall with temperature for future hottest days. *Nat Geosci* 9(1):24–28. doi:10.1038/ngeo2596
- Contractor S, Alexander LV, Donat MG, Herold N (2015) How well do gridded datasets of observed daily precipitation compare over Australia? *Advances in Meteorology* p 325718. doi:10.1155/2015/325718
- Dee DP, Uppala SM, Simmons AJ, Berrisford P, Poli P, Kobayashi S, Andrae U, Balmaseda MA, Balsamo G, Bauer P, Bechtold P, Beljaars ACM, van de Berg L, Bidlot J, Bormann N, Delsol C, Dragani R, Fuentes M, Geer AJ, Haimberger L, Healy SB, Hersbach H, Hölm EV, Isaksen L, Källberg P, Köhler M, Matricardi M, McNally AP, Monge-Sanz BM, Morcrette JJ, Park BK, Peubey C, de Rosnay P, Tavolato C, Thépaut JN, Vitart F (2011) The era-interim reanalysis: configuration and performance of the data assimilation system. *Quart J R Meteorol Soc* 137(656):553–597. doi:10.1002/qj.828
- Drobinski P, Alonzo B, Bastin S, Da Silva N, Muller C (2016) Scaling of precipitation extremes with temperature in the French Mediterranean region: what explains the hook shape? *J Geophys Res Atmos* 121(7):3100–3119. doi:10.1002/2015JD023497
- Drobinski P, Silva ND, Panthou G, Bastin S, Muller C, Ahrens B, Borga M, Conte D, Fosser G, Giorgi F, Güttler I, Kotroni V, Li L, Morin E, Önal B, Quintana-Segui P, Romera R, Torma CZ (2016) Scaling precipitation extremes with temperature in the Mediterranean: past climate assessment and projection in anthropogenic scenarios. *Climate Dynamics* pp 1–21. doi:10.1007/s00382-016-3083-x
- Forchheimer P (1913) Der Wolkenbruch im Grazer Hügelland vom 16. Juli 1913. *Sitzungsberichte der Kaiserlichen Akademie der Wissenschaften in Wien, mathematisch-naturw Klasse, Abt 2a* 122:2100–2109
- Formayer H, Fritz A (2016) Temperature dependency of hourly precipitation intensities—surface versus cloud layer temperature. *Int J Climatol* 37(1):1–10. doi:10.1002/joc.4678
- Frei C, Schär C (1998) A precipitation climatology of the Alps from high-resolution rain-gauge observations. *Int J Climatol* 18(8):873–900. doi:10.1002/(SICI)1097-0088(19980630)18:8<873::AID-JOC255>3.0.CO;2-9
- Gaál L, Molnar P, Szolgay J (2014) Selection of intense rainfall events based on intensity thresholds and lightning data in Switzerland. *Hydrol Earth Syst Sci* 18(5):1561–1573. doi:10.5194/hess-18-1561-2014

# 4.3 RESEARCH ARTICLE 3: SENSITIVITY OF EXTREME PRECIPITATION TO TEMPERATURE FROM A REGIONAL TO LOCAL PERSPECTIVE

- Giorgi F, Torma C, Coppola E, Ban N, Schar C, Somot S (2016) Enhanced summer convective rainfall at Alpine high elevations in response to climate warming. *Nature Geoscience* 9(8):2016/07/11/online, DOI: 10.1038/NCEO2761, wOS:000382137900013
- Haerter JO, Berg P (2009) Unexpected rise in extreme precipitation caused by a shift in rain type? *Nat Geosci* 2(6):372–373. doi:10.1038/ngeo523
- Haiden T, Kann A, Wittmann C, Pistotnik G, Bica B, Gruber C (2010) The integrated nowcasting through comprehensive analysis (INCA) system and its validation over the eastern Alpine region. *Weather Forecast* 26(2):166–183. doi:10.1175/2010WAF2222451.1
- Hiebl J, Frei C (2016) Daily temperature grids for Austria since 1961—concept, creation and applicability. *Theor Appl Climatol* 124(1–2):161–178. doi:10.1007/s00704-015-1411-4
- Hofstaetter M, Chimani B (2012) Van Bebber’s cyclone tracks at 700 hPa in the Eastern Alps for 1961–2002 and their comparison to Circulation Type Classifications. *Meteorologische Zeitschrift* 21(5):459–473. doi:10.1127/0941-2948/2012/0473
- Hofstätter M, Jacobeit J, Homann M, Lexer A, Chimani B, Philipp A, Beck C, Ganekind M (2015) WETRAX - Weather patterns, cyclone tracks and related precipitation extremes. *Grossflächige Starkniederschläge im Klimawandel in Mitteleuropa*. Projektendbericht, Geographica Augustana, p 19
- hydroConsult GmbH (2011) Hochwasserdokumentation Wölzertal 7.7.2011. Tech. rep., Amt der Steiermärkischen Landesregierung FA19B
- IPCC (2013) *Climate Change 2013: The Physical Science Basis. Contribution of Working Group I to the Fifth Assessment Report of the Intergovernmental Panel on Climate Change*. Cambridge University Press, Cambridge, United Kingdom and New York, NY, USA. doi:10.1017/CBO9781107415324
- Ivancic TJ, Shaw SB (2016) A U.S.-based analysis of the ability of the Clausius–Clapeyron relationship to explain changes in extreme rainfall with changing temperature. *Journal of Geophysical Research: Atmospheres* 121(7):30663078, doi:10.1002/2015JD024288
- Jones JAA (2014) *Global hydrology: processes, resources and environmental management*. Routledge, London
- Kabas T, Foelsche U, Kirchengast G (2011) Seasonal and annual trends of temperature and precipitation within 1951/1971–2007 in south-eastern Styria, Austria. *Meteorologische Zeitschrift* 20(3):277–289. doi:10.1127/0941-2948/2011/0233
- Kann A, Meirold-Mautner I, Schmid F, Kirchengast G, Fuchsberger J, Meyer V, Tächler L, Bica B (2015) Evaluation of high-resolution precipitation analyses using a dense station network. *Hydrol Earth Syst Sci* 19(3):1547–1559. doi:10.5194/hess-19-1547-2015
- Lenderink G, van Meijgaard E (2009) Unexpected rise in extreme precipitation caused by a shift in rain type? *Nat Geosci* 2(6):373–373. doi:10.1038/ngeo524
- Lenderink G, Ev Meijgaard (2010) Linking increases in hourly precipitation extremes to atmospheric temperature and moisture changes. *Environ Res Lett* 5(2):025208. doi:10.1088/1748-9326/5/2/025208
- Lepore C, Veneziano D, Molini A (2015) Temperature and CAPE dependence of rainfall extremes in the eastern United States. *Geophys Res Lett* 42(1):74–83. doi:10.1002/2014GL062247
- Loriaux JM, Lenderink G, De Roode SR, Siebesma AP (2013) Understanding convective extreme precipitation scaling using observations and an entraining plume model. *J Atmos Sci* 70(11):3641–3655. doi:10.1175/JAS-D-12-0317.1
- Loriaux JM, Lenderink G, Siebesma AP (2016a) Large-scale controls on extreme precipitation. *J Clim* 30(3):955–968. doi:10.1175/JCLI-D-16-0381.1
- Loriaux JM, Lenderink G, Siebesma AP (2016b) Peak precipitation intensity in relation to atmospheric conditions and large-scale forcing at midlatitudes. *J Geophys Res Atmos* 121(10):5471–5487. doi:10.1002/2015JD024274
- McMillen DP (2012) *Quantile regression for spatial data*. Springer-Verlag, Berlin
- Messmer M, Gomez-Navarro JJ, Raible CC (2015) Climatology of Vb cyclones, physical mechanisms and their impact on extreme precipitation over Central Europe. *Earth Syst Dyn* 6(2):541–553. doi:10.5194/esd-6-541-2015
- Molnar P, Faticchi S, Gaál L, Szolgay J, Burlando P (2015) Storm type effects on super Clausius–Clapeyron scaling of intense rainstorm properties with air temperature. *Hydrol Earth Syst Sci* 19(4):1753–1766. doi:10.5194/hess-19-1753-2015
- Moseley C, Hohenegger C, Berg P, Haerter JO (2016) Intensification of convective extremes driven by cloud-cloud interaction. *Nat Geosci* 9(10):748–752. doi:10.1038/ngeo2789
- Munzar J, Ondracek S, Auer I (2011) Central European one-day precipitation records. *Moravian Geograph Rep* 19(1):32–40
- O’Gorman PA (2015) Precipitation extremes under climate change. *Curr Clim Change Rep* 1(2):49–59. doi:10.1007/s40641-015-0009-3
- Panziera L, James CN, Germann U (2015) Mesoscale organization and structure of orographic precipitation producing flash floods in the Lago Maggiore region. *Quart J R Meteorol Soc* 141(686):224–248. doi:10.1002/qj.2351
- Philipp A, Beck C, Huth R, Jacobeit J (2016) Development and comparison of circulation type classifications using the COST 733 dataset and software. *Int J Climatol* 36(7):2673–2691. doi:10.1002/joc.3920
- Prein AF, Gobiet A (2016) Impacts of uncertainties in European gridded precipitation observations on regional climate analysis. *Int J Climatol* 37(1):305–327. doi:10.1002/joc.4706
- Prein AF, Rasmussen RM, Ikeda K, Liu C, Clark MP, Holland GJ (2017) The future intensification of hourly precipitation extremes. *Nat Clim Change* 7(1):48–52. doi:10.1038/nclimate3168
- Pretenthaler F, Podesser A, Pilger H (2010) *KlimaAtlas Steiermark. Periode 1971–2000. Eine anwenderorientierte Klimatographie. No. 4 in Studien zum Klimawandel in Österreich. ÖAW*
- Schicker I, Radanovics S, Seibert P (2010) Origin and transport of Mediterranean moisture and air. *Atmos Chem Phys* 10(11):5089–5105. doi:10.5194/acp-10-5089-2010
- Schiemann R, Frei C (2010) How to quantify the resolution of surface climate by circulation types: an example for Alpine precipitation. *Phys Chem Earth, Parts A/B/C* 35(9–12):403–410. doi:10.1016/j.pce.2009.09.005
- Schocklitsch A (1914) Die Hochwasserkatastrophe in Graz am 16. Juli 1913. *Zeitschrift des Österreichischen Ingenieur- und Architekten-Vereines* 27:511–518
- Seibert P, Frank A, Formayer H (2006) Synoptic and regional patterns of heavy precipitation in Austria. *Theor Appl Climatol* 87(1–4):139–153. doi:10.1007/s00704-006-0198-8
- Sodemann H, Zubler E (2010) Seasonal and inter-annual variability of the moisture sources for Alpine precipitation during 1995–2002. *Int J Climatol* 30(7):947–961. doi:10.1002/joc.1932
- Volosciuk C, Maraun D, Semenov VA, Tilinina N, Gulev SK, Latif M (2016) Rising mediterranean sea surface temperatures amplify extreme summer precipitation in central Europe. *Sci Rep* 6:32450. doi:10.1038/srep32450
- Wang G, Wang D, Trenberth KE, Erfanian A, Yu M, Bosilovich MG, Parr DT (2017) The peak structure and future changes of the relationships between extreme precipitation and temperature. *Nat Clim Change* 7(4):268–274. doi:10.1038/nclimate3239
- Wasko C, Sharma A (2015) Steeper temporal distribution of rain intensity at higher temperatures within Australian storms. *Nat Geosci* 8(7):527–529. doi:10.1038/ngeo2456
- Wasko C, Sharma A, Johnson F (2015) Does storm duration modulate the extreme precipitation-temperature scaling relationship?

## 4 EXTREME PRECIPITATION

3994

K. Schroeer, G. Kirchengast

- Geophysical Research Letters 42(20):2015GL066274. doi:[10.1002/2015GL066274](https://doi.org/10.1002/2015GL066274)
- Westra S, Fowler HJ, Evans JP, Alexander LV, Berg P, Johnson F, Kendon EJ, Lenderink G, Roberts NM (2014) Future changes to the intensity and frequency of short-duration extreme rainfall. *Rev Geophys* 52(3):522–555. doi:[10.1002/2014RG000464](https://doi.org/10.1002/2014RG000464)
- Zhang X, Zwiers FW, Li G, Wan H, Cannon AJ (2017) Complexity in estimating past and future extreme short-duration rainfall. *Nat Geosci* 10(4):255–259. doi:[10.1038/ngeo2911](https://doi.org/10.1038/ngeo2911)

## 5 DISCUSSION AND CONCLUSIONS

This thesis shows that extreme convective precipitation events (ECPEs) in the southeastern Alpine forelands are a highly relevant atmospheric phenomenon. Taking an integrative perspective on the character and impacts of ECPEs, it considers observational uncertainty, societal risk, and patterns of temperature sensitivity associated with extreme precipitation events. The findings can be of use not only to researchers, but also, for example, to risk managers, who have great interest in reducing the risk from ECPEs. This risk has been notoriously hard to quantify, because high resolution observations are largely missing. Thanks to several high resolution, gauge-based precipitation datasets in the study region, a detailed analysis of extreme precipitation is possible on the sub-daily to sub-hourly scale. In addition, a weather typing approach helps to identify convective and stratiform precipitation patterns. Individual and physically plausible events are identified from the observations prior to subsequent pairing with other data. This allows a targeted and robust analysis considering also the duration, and mean or peak intensities of the storms.

Research Article 1 reveals that the loss of information on short-duration extreme intensities with increasing inter-station distances can be empirically quantified using the very high resolution research rain gauge network WegenerNet Feldbach region climate station network (WegenerNet) (*Schroeer et al.*, 2018). The results (see Section 4.1.3) show that event maximum area precipitation estimates exponentially decrease with lower network densities. It is complemented here that discrepancies among the WegenerNet and the networks operated by *Zentralanstalt für Meteorologie und Klimatologie* (ZAMG) and *Hydrographischer Dienst Österreich* / Austrian Hydrographic Service (AHYD) are more relevant for area- rather than point-scale precipitation. They arise from two sources. First, when point measurements are interpolated onto a grid, the strong spatial gradients in ECPEs lead to rapidly declining area precipitation estimates with increasing inter-station distances. This is shown in Figure 4.1.5 of Research Article 1. Second, given the observation period is long enough, and the area considered is climati-

cally homogeneous, a gauge in a lower-density network will likely at some point be hit by a ECPEs and thus sample a representative maximum event intensity. Figure 5.1 illustrates this. The distributions represent the event maximum precipitation intensities in 527 ECPEs events in the southeastern Alpine forelands (see Section 4.1.2) sampled with high-density WegenerNet on the one hand and with low-density ZAMG and AHYD networks on the other. The rug plots at the top of the panels show that the most extreme samples are indeed roughly in the same order of magnitude in both networks. However, the WegenerNet observes medium to high intensities significantly more often, indicating that lower density networks underestimate the frequency of ECPEs. The underestimation of the regional frequency in low-density networks can be expected to be less severe for area-covering stratiform precipitation events, which will be recorded by one or more gauges with much higher probability, while ECPEs falling in between gauges may remain completely unobserved.

Given that ground-based and space-borne radar technology can deliver essential information on the spatial scales of precipitation (*Belachsen et al., 2017; Eggert et al., 2015; Lochbihler et al., 2017*), the question arises as to whether the underestimation of ECPEs can be alleviated using radar data. Very large discrepancies and uncertainties result from the fundamentally differing observation modes of radar quantitative precipitation estimate (QPE) as opposed to rain gauge measurements. Other types of sensors are employed, and the final precipitation estimate is integrated over different temporal and spatial scales (*Foehn et al., 2018; Gabella et al., 2017*). Several precipitation products have been developed that merge ground-based gauge observations and radar QPE in order to obtain spatially coherent precipitation fields (e.g., the product *CombiPrecip* for Switzerland (*Sideris et al., 2014*) or the *INCA* system for Austria (*Haiden et al., 2010*)). These products improve earlier gridded precipitation products (e.g., *Panziera et al., 2018*) and generally more accurate runoff simulations can be achieved using the adjusted precipitation data as input to hydrological models (*Antonetti and Zappa, 2018; Bernet et al., 2018*). However, convective events with extreme localized precipitation are still not accurately captured because of too sparse rain gauge coverage (*Kann et al., 2015; Sideris et al., 2014*). This becomes evident in flood modelling as particularly runoff simulations for short and intense precipitation events still hinge on the resolution of the underlying station network (*Antonetti and Zappa, 2018*). With improving technology, radar QPE will increasingly be used outside the forecasting rooms and likely be given more weight in climatological

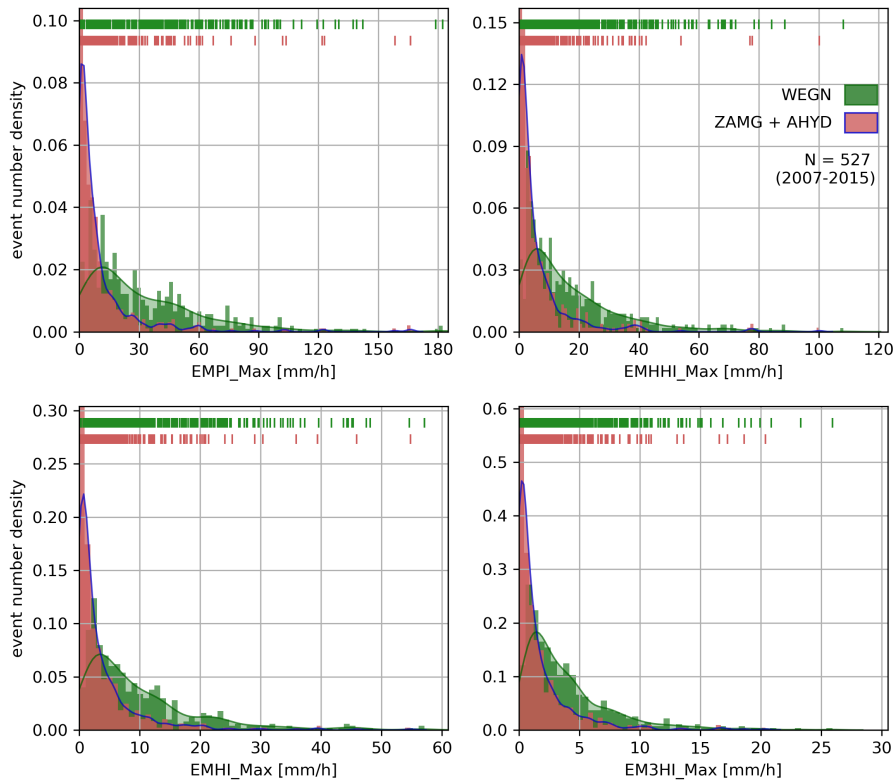


Figure 5.1: Histograms and kernel density estimates of the event maximum precipitation intensities sampled by WegenerNet (green) and ZAMG and AHYD (red-blue) rain gauges for the sample of ECPEs analyzed in Research Article 1. ZAMG and AHYD gauges within 5 km of the WegenerNet are considered and the same 527 events were sampled for all distributions. Rug plots on top of the panels indicate the maximum intensities of individual events. From top left to bottom right panel the distributions are shown for 10 min (EMPI\_Max), half-hourly (EMHHI\_Max), hourly (EMHI\_Max), and 3-hourly (EM3HI\_Max) time integration, respectively.

datasets. However, for the time being rain gauge observation networks serve as undisputed ground reference and are a prerequisite to adequate representation of ECPEs.

Very highly resolved precipitation observations, such as weather radars and networks like WegenerNet, are expensive to initialize and operate. An area-covering deployment on a larger scale is therefore currently neither practical nor feasible. Experiments on the small scale can serve as cornerstones through quantifying how much and how often ECPEs are actually underestimated in lower-density networks. The empirical relationships of maximum event intensities on gauge spacing presented in Research Article 1 can serve such purpose.

A major challenge will be to find means and techniques to transfer findings dis-

covered at the local scale to datasets at larger scales. This is essential because these datasets are used by a large number of users from science to practice, and developing standardized ways to incorporate uncertainty information will provide downstream applications with radically improved information. A prerequisite to upscaling the extreme precipitation–station density relationship derived from the WegenerNet observations is to test and validate the magnitudes of undersampling also in other regions. Streamflow data and hydrological models can provide useful tools to assess and compare the effects of spatial precipitation estimates and storm intensity by means of analyzing the generated runoff (*Syed et al.*, 2003).

As simulations from Convection Permitting Climate Models (CPM) become increasingly available, accurate estimates of convective precipitation undersampling in observations is crucial information to validate CPM output. Hence, an interesting exercise will be to compare the empirically derived scaling rates to their model equivalents calculated from CPM area precipitation estimates at increasing model resolution.

Historical data are subject to uncertainties and cannot be interpreted as unfiltered *observed truth*. Increasing awareness of this has initialized several efforts to better represent those uncertainties. For example, observational datasets are reprocessed to include uncertainty from underlying gauge densities, although on much larger, pan-European scale (*Cornes et al.*, 2018). The need for climatological consistency is acknowledged also through developing regional reanalysis ensembles for Europe using the numerical weather prediction model COSMO (*Bach et al.*, 2016). Furthermore, hourly precipitation observations are now more systematically collected and transferable quality control routines are developed (*Blenkinsop et al.*, 2018). Data can so be used to derive sub-daily precipitation datasets on the national scale, which are consistent also with the larger-scale climatology (*Lewis et al.*, 2018). This is a major step towards better hydrological modelling of flooding caused by sub-daily extremes.

*Lewis et al.* (2018) conclude their study by saying that “[s]ome key prerequisites for generating a probabilistic rainfall product would be to gain a better understanding of the uncertainties associated with the hourly gauge data (for example undercatch)”. The scaling relationships of maximum event intensities found for ECPEs present empirically quantified estimates of such uncertainty (Research Article 1). It needs to be further explored how these findings can be combined with methods of stochastic storm generation (e.g., *Singer et al.*, 2018) and precipitation disaggregation techniques (e.g., *Müller and Haberlandt*, 2018) used in hydraulic



modelling. This could cross-fertilize the incorporation of undersampling uncertainties of localized extreme precipitation to applications at the larger scale, e.g., to model ECPEs-specific exposure.

Research Article 2 demonstrated that precipitation observed with ZAMG and AHYD rain gauge networks is insufficient to characterize the risk from ECPEs in the southeastern Alpine forelands (*Schroeer and Tye, 2019*). For weather types characteristic to isolated, very localized convective storms, available observations often did not even record any extreme precipitation or discharge quantities. This exemplifies some of the difficulties that result from sparse observations and consequential undersampling of localized ECPEs for downstream risk analysis. These results, together with results from Research Article 1, indicate that infrastructure and agricultural assets are more often exposed to extreme convective rain rates than traditional rain gauge observation networks suggest.

The weather type analysis shows that approximately 60 % of all analyzed damage<sup>1</sup> in 480 southeastern Austrian municipalities were reported to the national disaster fund under convective weather types. The fact that those damages are often not captured in precipitation observations is an important constraint to using precipitation observations to define thresholds. Often, the sensitivity of a system to trigger an event of some kind is inferred from relating event data to precipitation observations and identifying a critical threshold, e.g., for damage occurrence (e.g., *Cortès et al., 2018*), or debris flow initialization (*Marra et al., 2017; Segoni et al., 2018*). Especially if the event is sensitive to highly intense precipitation on small spatiotemporal scales, identified thresholds might be inaccurate.

Research Article 2 further shows that damage from events of smaller magnitude accumulates to significant financial burdens. *Moftakhari et al. (2018)* argue that defining a category of so-called nuisance flooding (NF) provides a useful concept to consider the consequences of high-frequency, low-magnitude events. They state that “[a]lthough individual NF events are not expected to lead to disaster declarations, defining NF offers the potential for providing Federal [sic] funding for major cumulative impacts resulting from chronic NF”. The high damage shares where no significantly high precipitation or runoff levels are observed indicate that nuisance-level events causing minor damages are a relevant phenomenon also in the Alpine region. Further research is needed, however, to distinguish true nuisance flooding from cases where high hazard levels are just not accurately represented

---

<sup>1</sup>The considered damage includes claims associated with hydro-meteorological hazards flooding, landslides, and debris flows during 1 April–30 November from 1990–2015

in observations. As underestimation of observed rainfall is of particular concern under convective conditions, the relations of ECPEs and nuisance level events are particularly interesting. In order to better understand nuisance level events in the Alpine region, the different types of hazards (e.g., rainwater intrusion, surface water floods, flash floods, river floods) need better understanding.

It is furthermore essential to analyze the vulnerabilities towards ECPEs related hazards. The differences in damage numbers under the different weather types and among municipality groups indicate that there are distinct patterns of susceptibility for both ECPEs and large-scale precipitation events. Analyzing the complex chains of interaction of hazard and vulnerabilities is key to understanding impacts from natural hazards (*AghaKouchak et al.*, 2018; *Sillmann et al.*, 2018). This reaches from precipitation to runoff generation, and from identifying exposed areas to understanding highly variable socio-economic vulnerabilities. A deeper analysis of the drivers of risk, however, is currently hampered by the lack of high resolution data. Uncertainties regarding patterns of vulnerability likely exceed the factor of precipitation uncertainty, and include many facets such as the vulnerability of buildings (*Ettlinger et al.*, 2016; *Fuchs et al.*, 2015), dynamic adaptation effects (*Aerts et al.*, 2018; *Kreibich et al.*, 2017), and even adverse impacts from structural protection measures (*Di Baldassarre et al.*, 2018; *Mård et al.*, 2018).

These studies demonstrate the high level on which risk analyses are already done. However, the small scales of localized extreme precipitation make it inherently difficult to compile the data necessary to disentangle the factors of risk on scales beyond case study examples, although some progress has been made. Responding to the need for better data on regional scales, *Amponsah et al.* (2018) provide a dataset which includes comprehensive data of flash flood events in the Mediterranean region in order to facilitate research on various aspects of the rainfall to runoff process. To advance our understanding of the risk from ECPEs, combining the weather type approach applied here with building-level vulnerabilities (e.g., *Fuchs et al.*, 2015) and address-based distinction of surface water floods (e.g., *Bernet et al.*, 2017) pose challenging, but promising directions for future research.

The urgency to better understand the risk from ECPEs is augmented by the fact that extreme convective precipitation is generally expected to increase with global climate change (see Chapter 2) and that observed sub-daily rain rates in extreme precipitation events in southeastern Austria are strongly and posi-

tively related to temperature. This is shown in Research Article 3 (*Schroeer and Kirchengast, 2018*). First and foremost, however, it is crucial to understand and acknowledge the fundamentally different approaches that go by the name of temperature-precipitation scaling, or temperature sensitivity of precipitation (T/P-scaling) (see Section 2.2.3) that are rarely explicitly discussed in the literature (e.g., by *Wang et al., 2017; Zhang et al., 2017*). Research Article 3 contributes to the debate in two ways. First, it reveals and discusses the regional and seasonal patterns that govern the scaling rates at the regional-to-local level. These exemplify the contribution of circulation patterns and highlight common misinterpretations when deriving climate change effects from instantaneous local scaling rates, i.e., from regressing same-day precipitation and temperature observations. Second, it works out the relevance of the absolute scale of precipitation changes (c.f. Figure 4.3.5). This is a facet often overlooked by the physical science community but highly relevant from an impact perspective. Depending on the temperature range and definition of extreme (e.g., whether a high percentile is calculated including or excluding dry observations (*Schär et al., 2016*)), a high T/P-scaling rate is not necessarily related to high absolute increases.

Although no temporal trends were considered in the analysis, the strong positive scaling rates indicate potential for precipitation extremes to become more intense as temperatures continue to rise with global climate change. In general, scaling rates refer to the intensity and not the frequency of extreme events, however, both are relevant factors. Thermodynamics constrain the atmospheric water vapor availability, but dynamic processes direct large scale moisture transport and influence local relative humidity and precipitation efficiency. While both forcings are implicit in scaling rates derived from observations, expectations based on the Clausius-Clapeyron (CC) equation are limited to the thermodynamic component. Further research is thus needed on how patterns of large-scale circulation now and in the future interact with storm initialization to fully understand the potential for changes in extreme precipitation at the regional-to-local scale.

In summary, this thesis showed that the risk from ECPEs is substantial in the southeastern Alpine forelands and several sources of uncertainty were identified. These are related to observing ECPEs using rain gauge networks, but uncertainty also exists with regard to societies' vulnerability and ability to cope with such events. It is empirically substantiated that rain gauge spacing of 10 km and more cannot accurately resolve the scales of intense precipitation from ECPEs; as a consequence, event maximum area precipitation intensities are strongly underestimated when

derived from such networks. The damage potential of ECPEs is demonstrated to be significant, as events under convective weather types are associated with approximately two thirds of all damage claims during April–November. The high local temperature sensitivities of sub-hourly precipitation intensities in ECPEs indicate the potential that risk from ECPEs might increase in the future. Spatio-temporal patterns of T/P-scaling attest the importance of dynamic processes on the precipitation response to warmer temperatures and underline the need for better understanding.

The identified uncertainties have consequences for other fields such as hydrology and risk management, because the risk from such events might be underestimated. Not only scientists, but also practitioners will profit from further exploring the role of ECPEs. All aspects explored in this thesis will immensely benefit from better and higher resolved data. The weather type classes applied comprise convective precipitation under different atmospheric flow patterns for the purpose of an initial discrimination of precipitation types. However, a more detailed and process-based analysis of the atmospheric patterns will help to understand which processes in particular are important drivers of ECPEs. Such patterns can then be analyzed also in climate models to infer potential future developments.

It is further argued in this thesis that the goal of T/P-scaling studies should not be to prove the CC equation through obtaining a rate as close as possible to CC scaling. Instead, the goal should be to better understand the drivers and processes that determine the character and frequency of extreme precipitation events. This applies both to what we have to expect in present times, and to how patterns might change in the future. While isolating CC scaling from other factors can be one step in achieving this, other factors such as potential shifts in seasonality of extreme events also need to be considered (*Brönnimann et al.*, 2018).

In order to fully comprehend regional-to-local sensitivities of extreme precipitation to climate change as well as to understand the risk from extreme precipitation events to society, dynamical and feedback processes of both physical and socio-economic systems need to be analyzed across scales. An integrative perspective on both the hazard and the impacts, as propounded on the example of ECPEs in this thesis, presents a promising approach to achieve this.

# APPENDIX

## A.1 Supplementary Information Research Article 1



**Supplementary information to Schroeer, K. and Tye, M.R.: Quantifying damage contributions from convective and stratiform weather types: how well do precipitation and discharge data indicate the risk?**

**Contents:**

1. **Figure 1:** Discharge anomalies associated with weather types
2. **Table S1:** Summary statistics of gauge records
3. **Table S2:** Information rain gauges (sub-daily precipitation)
4. **Table S3:** Information rain gauges (daily precipitation)
5. **Table S4:** Information stream gauges (daily observations)

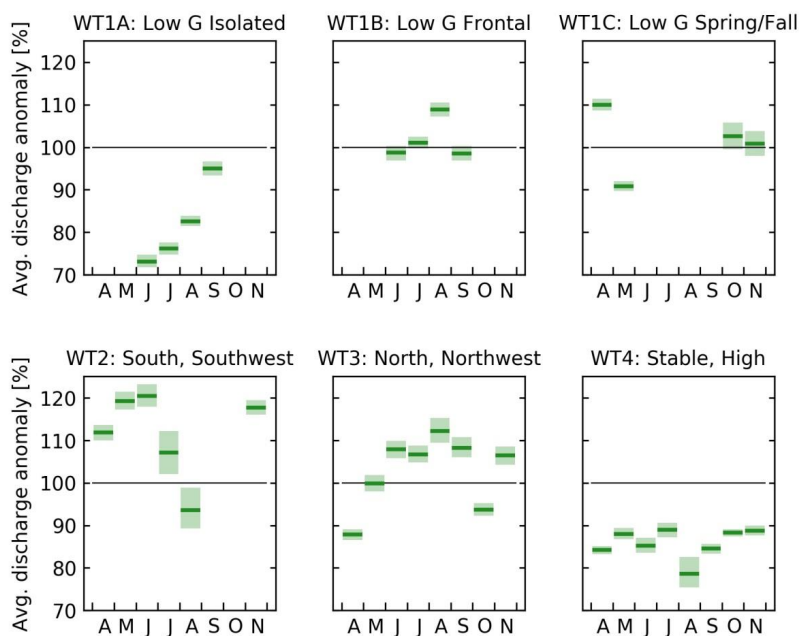


Figure 1: Average monthly discharge anomalies associated with the different weather types over all stream gauges. Horizontal green lines show the average weather-type specific deviation from the long-term climatological mean (horizontal black lines); green boxes denote the 90% confidence intervals of the sample means.

## APPENDIX

Table S 1: Summary statistics of gauge records

	<b>Number gauges</b>	<b>Median record length</b>	<b>Record lengths 5th and 95<sup>th</sup> percentile</b>	<b>Median Missing data study period</b>	<b>Missing data study period 5th and 95th percentile</b>
Sub-daily precipitation	72	13	[6.2, 22.3]	0.4	[0.0, 6.6]
Daily precipitation	108	40	[17, 114]	0.0	[0.0, 4.0]
Stream gauges	61	40	[20, 63]	0.0	[0.0, 0.0]



Table S 2: Information rain gauges (sub-daily precipitation)

	First observation	Last observation	Record length (years)	Missing data during study period (1990-2015) [%]	Provider	Lat	Lon
1	1992-08-29 00:10:00	2014-12-26 23:50:00	22.3	6.3	ZAMG	46.69	15.98
2	1992-08-29 00:10:00	2014-12-26 23:50:00	22.3	1.8	ZAMG	47.11	14.18
3	1992-08-29 00:10:00	2014-12-26 23:50:00	22.3	1.7	ZAMG	47.07	15.59
4	1992-08-29 00:10:00	2014-12-26 23:50:00	22.3	1.6	ZAMG	47.08	15.45
5	1993-02-16 13:30:00	2014-12-26 23:50:00	21.9	3.3	ZAMG	47.20	15.47
6	1993-07-29 11:10:00	2014-12-26 23:50:00	21.4	1.8	ZAMG	47.07	14.42
7	1994-10-24 13:30:00	2014-12-26 23:50:00	20.2	1.6	ZAMG	46.82	15.23
8	1994-10-24 13:10:00	2014-12-26 23:50:00	20.2	1.2	ZAMG	47.28	15.98
9	1997-02-17 12:40:00	2014-12-26 23:50:00	17.9	1	ZAMG	47.45	15.30
10	1997-09-01 00:10:00	2014-12-26 23:50:00	17.3	0.5	ZAMG	47.20	14.75
11	1999-08-16 09:30:00	2014-12-26 23:50:00	15.4	0.4	ZAMG	46.95	15.88
12	2001-11-08 16:10:00	2014-12-26 23:50:00	13.1	0.9	ZAMG	47.27	14.78
13	2002-07-31 14:20:00	2014-12-26 23:50:00	12.4	0.7	ZAMG	47.18	15.49
14	2003-04-08 16:10:00	2014-12-26 23:50:00	11.7	0.4	ZAMG	46.87	15.90
15	2003-11-03 12:10:00	2014-12-26 23:50:00	11.2	0.3	ZAMG	46.77	15.55
16	2004-10-28 14:50:00	2014-12-26 23:50:00	10.2	3.6	ZAMG	47.41	15.25
17	2004-10-31 20:10:00	2014-12-26 23:50:00	10.2	3.3	ZAMG	47.07	15.09
18	2004-11-09 12:10:00	2014-12-26 23:50:00	10.1	1	ZAMG	47.44	15.64
19	2007-05-09 10:00:00	2014-12-26 23:50:00	7.6	2	ZAMG	47.03	16.08
20	2007-05-08 08:40:00	2014-12-26 23:50:00	7.6	0.3	ZAMG	47.12	15.71
21	2007-07-20 17:00:00	2014-12-26 23:50:00	7.4	0.9	ZAMG	47.20	14.29
22	2007-07-24 12:00:00	2014-12-26 23:50:00	7.4	0.1	ZAMG	47.12	14.19
23	2007-11-07 10:00:00	2014-12-26 23:50:00	7.1	0.2	ZAMG	47.05	15.41
24	2008-09-05 14:50:00	2014-12-26 23:50:00	6.3	0.4	ZAMG	47.26	15.31
25	2008-08-25 12:30:00	2014-12-26 23:50:00	6.3	0.3	ZAMG	46.99	15.45
26	2008-11-10 15:40:00	2014-12-26 23:50:00	6.1	0.4	ZAMG	47.40	15.94
27	2012-10-04 13:20:00	2014-12-26 23:50:00	2.2	0.6	ZAMG	47.38	15.09
28	1982-06-01 07:00:00	2015-01-28 06:20:00	32.7	6.5	AHYD	47.33	15.81
29	1990-04-04 08:00:00	2015-01-01 00:00:00	24.8	24.4	AHYD	47.57	14.24
30	1999-01-01 07:00:00	2014-12-30 23:50:00	16	8.3	AHYD	46.65	15.50
31	1999-06-19 08:00:00	2015-01-27 23:50:00	15.6	0.1	AHYD	47.48	14.53
32	2000-01-01 07:00:00	2014-12-30 23:50:00	15	6.7	AHYD	47.14	15.06
33	2000-01-01 07:00:00	2015-01-01 06:50:00	15	1.7	AHYD	47.35	15.69
34	2000-01-01 07:00:00	2014-12-30 23:50:00	15	0.6	AHYD	46.81	15.33
35	2000-01-01 07:00:00	2014-12-30 23:50:00	15	0.1	AHYD	47.38	14.71
36	2000-01-01 07:00:00	2014-12-30 23:50:00	15	0	AHYD	47.06	14.88
37	2000-01-01 07:00:00	2015-01-01 06:50:00	15	0	AHYD	47.17	16.01
38	2000-01-01 07:00:00	2014-12-30 23:50:00	15	0	AHYD	46.90	15.26
39	2000-01-01 07:00:00	2015-01-01 06:50:00	15	0	AHYD	47.38	16.00
40	2000-07-01 07:00:00	2015-01-01 06:50:00	14.5	0.1	AHYD	47.49	15.92
41	2000-08-01 00:00:00	2014-12-30 23:50:00	14.4	0.1	AHYD	47.55	15.79
42	2000-08-01 00:00:00	2014-12-30 23:50:00	14.4	0	AHYD	47.15	15.24
43	2001-01-01 07:00:00	2014-12-30 23:50:00	14	0	AHYD	47.52	15.47
44	2001-01-01 07:00:00	2014-12-30 23:50:00	14	0	AHYD	46.79	15.45
45	2001-01-01 07:00:00	2014-12-30 23:50:00	14	0	AHYD	46.69	15.09
46	2001-01-01 07:00:00	2015-01-01 06:50:00	14	0	AHYD	47.22	15.76

## APPENDIX

47	2000-01-02 07:00:00	2013-06-20 13:10:00	13.5	0	AHYD	47.11	14.95
48	2001-10-01 07:00:00	2015-01-27 23:50:00	13.3	0	AHYD	47.74	15.48
49	2001-07-26 11:10:00	2014-10-16 06:50:00	13.2	3.2	AHYD	47.61	14.85
50	2002-01-01 07:00:00	2014-12-30 23:50:00	13	4.4	AHYD	47.20	14.28
51	2002-01-02 00:00:00	2014-12-30 23:50:00	13	0.4	AHYD	47.28	14.93
52	2002-01-01 07:00:00	2015-01-01 06:50:00	13	0	AHYD	46.85	15.97
53	2002-06-19 08:00:00	2015-01-18 10:40:00	12.6	0.6	AHYD	47.38	14.12
54	2002-06-19 08:00:00	2015-01-27 23:50:00	12.6	0.1	AHYD	47.51	14.83
55	2003-07-17 17:10:00	2014-12-30 12:50:00	11.5	0	AHYD	47.41	13.89
56	2003-10-01 00:00:00	2015-01-01 06:50:00	11.3	0	AHYD	46.92	15.68
57	2003-12-31 07:00:00	2014-12-30 23:50:00	11	0.2	AHYD	47.39	15.44
58	2003-12-31 07:00:00	2014-12-30 23:50:00	11	0	AHYD	47.17	14.66
59	2004-01-01 07:00:00	2015-01-01 06:50:00	11	0	AHYD	47.15	15.66
60	2004-01-01 07:00:00	2015-01-01 06:50:00	11	0	AHYD	47.29	16.05
61	2004-04-30 07:00:00	2014-12-30 23:50:00	10.7	0	AHYD	47.27	15.32
62	2004-10-01 07:00:00	2014-12-30 23:50:00	10.3	1.4	AHYD	47.11	14.60
63	2005-06-19 08:00:00	2015-01-27 23:50:00	9.6	0.1	AHYD	47.43	14.49
64	2005-07-01 07:00:00	2015-01-01 00:00:00	9.5	10.5	AHYD	47.66	14.98
65	2005-11-01 07:00:00	2014-12-30 23:50:00	9.2	0.7	AHYD	46.80	15.76
66	2005-12-31 07:00:00	2015-01-01 06:50:00	9	0.5	AHYD	47.06	16.01
67	2006-01-01 07:00:00	2015-01-01 00:00:00	9	0	AHYD	47.39	13.66
68	2006-06-19 08:00:00	2015-01-27 23:50:00	8.6	0	AHYD	47.59	14.63
69	2007-01-01 07:00:00	2014-12-30 23:50:00	8	0.4	AHYD	46.92	13.88
70	2007-09-17 13:50:00	2014-12-30 23:50:00	7.3	0	AHYD	47.11	15.42
71	2010-01-01 07:00:00	2015-01-01 06:50:00	5	0	AHYD	47.49	15.67
72	2010-11-16 15:40:00	2015-01-01 00:00:00	4.1	0	AHYD	47.37	13.72

Table S 3: Information rain gauges (daily precipitation). List includes 72 gauges from Table S 2, but record lengths are given for the daily observation records. Daily observations are available from an additional 80 rain gauges.

	First observation	Last observation	Record length (years)	Missing data during study period (1990-2015) [%]	Provider	Lat	Lon
1	1983-05-01 00:00:00	2017-02-07 00:00:00	33.8	0.3	ZAMG	47.55	15.24
2	1999-04-01 00:00:00	2017-02-07 00:00:00	17.9	0.8	ZAMG	47.63	15.83
3	2000-09-30 00:00:00	2017-02-06 00:00:00	16.4	0.3	ZAMG	47.52	14.95
4	2008-09-08 00:00:00	2017-02-07 00:00:00	8.4	0	ZAMG	47.60	15.67
5	1900-01-00 00:00:00	2014-12-31 00:00:00	115.1	0	AHYD	46.90	15.26
6	1901-01-01 00:00:00	2014-12-31 00:00:00	114.1	14.3	AHYD	46.93	15.67
7	1901-01-01 00:00:00	2014-12-31 00:00:00	114.1	5.3	AHYD	47.27	15.32
8	1901-01-01 00:00:00	2014-12-31 00:00:00	114.1	4	AHYD	47.22	15.39
9	1901-01-01 00:00:00	2014-12-31 00:00:00	114.1	0	AHYD	46.79	15.45
10	1901-01-01 00:00:00	2014-12-31 00:00:00	114.1	0	AHYD	47.17	16.01
11	1901-01-01 00:00:00	2014-12-31 00:00:00	114.1	0	AHYD	47.46	14.68
12	1901-01-01 00:00:00	2014-12-31 00:00:00	114.1	0	AHYD	46.82	15.45
13	1901-01-01 00:00:00	2014-12-31 00:00:00	114.1	0	AHYD	47.10	15.83
14	1901-01-01 00:00:00	2014-12-31 00:00:00	114.1	0	AHYD	47.07	14.69
15	1901-01-01 00:00:00	2014-12-31 00:00:00	114.1	0	AHYD	46.69	15.26
16	1901-01-01 00:00:00	2014-12-31 00:00:00	114.1	0	AHYD	47.06	14.30
17	1901-01-01 00:00:00	2014-12-31 00:00:00	114.1	0	AHYD	47.02	14.92
18	1901-01-01 00:00:00	2014-12-31 00:00:00	114.1	0	AHYD	46.99	15.21
19	1901-01-01 00:00:00	2014-12-31 00:00:00	114.1	0	AHYD	47.07	15.07
20	1901-01-01 00:00:00	2014-12-31 00:00:00	114.1	0	AHYD	46.81	15.87
21	1901-01-01 00:00:00	2014-12-31 00:00:00	114.1	0	AHYD	47.53	15.78
22	1901-01-01 00:00:00	2014-12-31 00:00:00	114.1	0	AHYD	47.36	14.47
23	1901-01-01 00:00:00	2014-12-31 00:00:00	114.1	0	AHYD	47.20	14.44
24	1901-01-01 00:00:00	2014-12-31 00:00:00	114.1	0	AHYD	47.67	15.47
25	1901-01-01 00:00:00	2014-12-31 00:00:00	114.1	0	AHYD	47.47	15.50
26	1901-01-01 00:00:00	2014-12-31 00:00:00	114.1	0	AHYD	47.53	15.08
27	1901-01-01 00:00:00	2014-12-31 00:00:00	114.1	0	AHYD	47.58	15.50
28	1901-01-01 00:00:00	2014-12-31 00:00:00	114.1	0	AHYD	47.28	15.97
29	1901-01-01 00:00:00	2014-12-31 00:00:00	114.1	0	AHYD	47.47	15.79
30	1901-01-01 00:00:00	2014-12-31 00:00:00	114.1	0	AHYD	47.21	15.82
31	1901-01-01 00:00:00	2014-12-31 00:00:00	114.1	0	AHYD	47.40	15.89
32	1902-01-01 00:00:00	2014-12-31 00:00:00	113.1	0	AHYD	47.40	14.82
33	1901-01-01 00:00:00	2006-04-30 00:00:00	105.4	0	AHYD	47.31	14.94
34	1913-01-01 00:00:00	2014-12-31 00:00:00	102.1	0	AHYD	47.27	14.71
35	1927-07-01 00:00:00	2014-12-31 00:00:00	87.6	0	AHYD	47.43	15.01
36	1929-06-01 00:00:00	2014-12-31 00:00:00	85.6	0	AHYD	46.80	15.76
37	1930-01-01 00:00:00	2014-12-31 00:00:00	85.1	0	AHYD	46.98	14.99
38	1930-01-01 00:00:00	2014-12-31 00:00:00	85.1	0	AHYD	46.93	15.01
39	1933-01-01 00:00:00	2014-12-31 00:00:00	82.1	0	AHYD	47.15	15.24
40	1936-01-01 00:00:00	2014-12-31 00:00:00	79.1	0	AHYD	46.65	15.46
41	1946-01-01 00:00:00	2014-12-31 00:00:00	69	0	AHYD	47.10	15.41

## APPENDIX

42	1947-03-01 00:00:00	2014-12-31 00:00:00	67.9	0	AHYD	47.17	14.66
43	1947-07-01 00:00:00	2014-12-31 00:00:00	67.5	0	AHYD	47.39	15.44
44	1948-01-01 00:00:00	2014-12-31 00:00:00	67	1.7	AHYD	47.01	14.53
45	1951-11-01 00:00:00	2014-12-31 00:00:00	63.2	0	AHYD	46.95	15.33
46	1952-01-01 00:00:00	2014-12-31 00:00:00	63	0	AHYD	47.66	15.70
47	1954-08-01 00:00:00	2014-12-31 00:00:00	60.5	4	AHYD	46.75	15.16
48	1955-01-01 00:00:00	2014-12-31 00:00:00	60	0	AHYD	46.71	16.02
49	1955-11-01 00:00:00	2014-12-31 00:00:00	59.2	0	AHYD	47.00	15.94
50	1971-01-01 00:00:00	2014-12-31 00:00:00	44	4	AHYD	47.11	14.60
51	1971-01-01 00:00:00	2014-12-31 00:00:00	44	0	AHYD	47.14	15.33
52	1971-01-01 00:00:00	2014-12-31 00:00:00	44	0	AHYD	47.44	16.05
53	1971-01-01 00:00:00	2014-12-31 00:00:00	44	0	AHYD	46.72	15.91
54	1961-01-01 00:00:00	2003-01-31 00:00:00	42.1	0	AHYD	47.20	14.28
55	1974-01-01 00:00:00	2014-12-31 00:00:00	41	0	AHYD	47.07	15.13
56	1974-07-01 00:00:00	2014-12-31 00:00:00	40.5	0	AHYD	47.07	13.98
57	1961-01-01 00:00:00	2001-01-31 00:00:00	40.1	9	AHYD	47.58	15.14
58	1975-01-01 00:00:00	2014-12-31 00:00:00	40	0	AHYD	46.74	15.62
59	1975-01-01 00:00:00	2014-12-31 00:00:00	40	0	AHYD	47.31	15.84
60	1975-01-01 00:00:00	2014-12-31 00:00:00	40	0	AHYD	47.38	15.79
61	1975-01-01 00:00:00	2014-12-31 00:00:00	40	0	AHYD	46.93	16.02
62	1977-01-01 00:00:00	2014-12-31 00:00:00	38	0	AHYD	47.07	16.00
63	1977-05-01 00:00:00	2014-12-31 00:00:00	37.7	0	AHYD	46.72	15.26
64	1971-01-01 00:00:00	2008-06-30 00:00:00	37.5	0	AHYD	47.35	14.31
65	1979-01-01 00:00:00	2014-12-31 00:00:00	36	0	AHYD	47.23	15.15
66	1980-01-01 00:00:00	2014-12-31 00:00:00	35	0	AHYD	47.08	15.21
67	1981-01-01 00:00:00	2014-12-31 00:00:00	34	0	AHYD	47.30	15.51
68	1981-01-01 00:00:00	2014-12-31 00:00:00	34	0	AHYD	46.82	15.72
69	1957-07-01 00:00:00	1990-12-31 00:00:00	33.5	0	AHYD	47.57	15.23
70	1982-01-01 00:00:00	2014-12-31 00:00:00	33	0	AHYD	47.46	15.99
71	1984-01-01 00:00:00	2014-12-31 00:00:00	32.7	0	AHYD	47.33	15.81
72	1971-01-01 00:00:00	2002-12-31 00:00:00	32	1.9	AHYD	46.85	15.97
73	1984-01-01 00:00:00	2014-12-31 00:00:00	31	0	AHYD	46.69	15.09
74	1984-01-01 00:00:00	2014-12-31 00:00:00	31	0	AHYD	47.20	15.17
75	1984-01-01 00:00:00	2014-12-31 00:00:00	31	0	AHYD	46.75	15.21
76	1984-01-01 00:00:00	2014-12-31 00:00:00	31	0	AHYD	46.67	15.17
77	1985-01-01 00:00:00	2014-12-31 00:00:00	30	12	AHYD	46.82	15.14
78	1975-01-01 00:00:00	2004-12-31 00:00:00	30	0	AHYD	46.76	15.37
79	1985-01-01 00:00:00	2014-12-31 00:00:00	30	0	AHYD	46.86	15.08
80	1986-10-01 00:00:00	2014-12-31 00:00:00	28.3	0	AHYD	46.83	15.31
81	1987-01-01 00:00:00	2014-12-31 00:00:00	28	0	AHYD	46.71	15.46
82	1987-01-01 00:00:00	2014-12-31 00:00:00	28	0	AHYD	46.92	15.10
83	1988-01-01 00:00:00	2014-12-31 00:00:00	27	0	AHYD	47.31	15.48
84	1988-01-01 00:00:00	2014-12-31 00:00:00	27	0	AHYD	46.74	15.09
85	1988-01-01 00:00:00	2014-12-31 00:00:00	27	0	AHYD	47.18	14.81
86	1990-01-01 00:00:00	2014-12-31 00:00:00	25	0	AHYD	47.49	15.67
87	1990-01-01 00:00:00	2014-12-31 00:00:00	25	0	AHYD	46.99	15.87
88	1991-01-01 00:00:00	2014-12-31 00:00:00	24	0	AHYD	47.11	14.95
89	1991-01-01 00:00:00	2014-12-31 00:00:00	24	0	AHYD	47.01	15.39
90	1991-01-01 00:00:00	2014-12-31 00:00:00	24	0	AHYD	47.37	15.34
91	1991-01-01 00:00:00	2014-12-31 00:00:00	24	0	AHYD	47.55	15.11
92	1994-01-01 00:00:00	2014-12-31 00:00:00	21	0	AHYD	46.65	15.50
93	1994-01-01 00:00:00	2014-12-31 00:00:00	21	0	AHYD	47.14	15.06
94	1994-01-01 00:00:00	2014-12-31 00:00:00	21	0	AHYD	47.22	15.33
95	1994-01-01 00:00:00	2014-12-31 00:00:00	21	0	AHYD	46.88	15.07
96	1994-01-01 00:00:00	2014-12-31 00:00:00	21	0	AHYD	46.82	15.25
97	1994-01-01 00:00:00	2014-12-31 00:00:00	21	0	AHYD	47.10	14.64
98	1994-01-01 00:00:00	2014-12-31 00:00:00	21	0	AHYD	47.15	14.85
99	1996-01-01 00:00:00	2014-12-31 00:00:00	19	0	AHYD	47.15	15.66
100	1997-01-01 00:00:00	2014-12-31 00:00:00	18	0	AHYD	47.35	15.69
101	1998-01-01 00:00:00	2014-12-31 00:00:00	17	0	AHYD	46.81	15.33

102	1998-01-01 00:00:00	2014-12-31 00:00:00	17	0	AHYD	46.92	13.88
103	1998-01-01 00:00:00	2014-12-31 00:00:00	17	0	AHYD	47.06	15.42
104	1998-01-01 00:00:00	2014-12-31 00:00:00	17	0	AHYD	47.20	14.62
105	1998-01-01 00:00:00	2014-12-31 00:00:00	17	0	AHYD	47.62	15.27
106	1999-03-01 00:00:00	2014-12-31 00:00:00	15.8	14.2	AHYD	47.49	15.92
107	1994-01-01 00:00:00	2002-02-28 00:00:00	14.4	0	AHYD	47.55	15.79
108	2011-12-01 00:00:00	2014-12-31 00:00:00	14	0	AHYD	47.52	15.45

Table S 4: Information stream gauges (daily observations)

	First observation	Last observation	Record length (years)	Missing data during study period (1990-2015) [%]	Provider	Lat	Lon
1	1951-01-01 00:00:00	2014-12-31 00:00:00	64	0	AHYD	47.21	14.54
2	1951-01-01 00:00:00	2013-12-30 00:00:00	63	0	AHYD	47.02	16.14
3	1951-01-01 00:00:00	2013-12-30 00:00:00	63	0	AHYD	46.96	15.89
4	1951-01-01 00:00:00	2013-12-30 00:00:00	63	0	AHYD	47.22	14.58
5	1951-01-01 00:00:00	2013-12-30 00:00:00	63	0	AHYD	47.38	15.09
6	1951-01-01 00:00:00	2013-12-30 00:00:00	63	0	AHYD	47.47	15.25
7	1951-01-01 00:00:00	2013-12-30 00:00:00	63	0	AHYD	46.96	15.35
8	1951-01-01 00:00:00	2013-12-30 00:00:00	63	0	AHYD	46.76	15.21
9	1951-01-01 00:00:00	2013-12-30 00:00:00	63	0	AHYD	46.72	15.27
10	1951-01-01 00:00:00	2013-12-30 00:00:00	63	0	AHYD	46.78	15.53
11	1961-01-01 00:00:00	2013-12-30 00:00:00	53	0	AHYD	47.21	16.09
12	1961-01-01 00:00:00	2013-12-30 00:00:00	53	0	AHYD	47.17	16.01
13	1961-01-01 00:00:00	2013-12-30 00:00:00	53	0	AHYD	47.28	15.69
14	1961-01-01 00:00:00	2013-12-30 00:00:00	53	0	AHYD	47.08	15.94
15	1961-01-01 00:00:00	2013-12-30 00:00:00	53	0	AHYD	47.11	14.21
16	1961-01-01 00:00:00	2013-12-30 00:00:00	53	0	AHYD	47.43	15.26
17	1961-01-01 00:00:00	2013-12-30 00:00:00	53	0	AHYD	46.81	15.52
18	1966-01-01 00:00:00	2014-12-31 00:00:00	49	0	AHYD	47.03	15.45
19	1966-01-01 00:00:00	2013-12-30 00:00:00	48	0	AHYD	47.18	15.67
20	1966-01-01 00:00:00	2013-12-30 00:00:00	48	0	AHYD	47.38	16.00
21	1966-01-01 00:00:00	2013-12-30 00:00:00	48	0	AHYD	47.19	14.75
22	1966-01-01 00:00:00	2013-12-30 00:00:00	48	0	AHYD	47.39	14.91
23	1966-01-01 00:00:00	2013-12-30 00:00:00	48	0	AHYD	47.39	15.03
24	1966-01-01 00:00:00	2013-12-30 00:00:00	48	0	AHYD	47.53	15.47
25	1966-01-01 00:00:00	2013-12-30 00:00:00	48	0	AHYD	47.05	15.15
26	1967-01-01 00:00:00	2013-12-30 00:00:00	47	0	AHYD	47.41	15.28
27	1968-01-01 00:00:00	2013-12-30 00:00:00	46	0	AHYD	47.04	15.76
28	1969-01-01 00:00:00	2013-12-30 00:00:00	45	0	AHYD	46.76	15.67
29	1971-01-01 00:00:00	2013-12-30 00:00:00	43	0	AHYD	47.43	15.27
30	1972-01-01 00:00:00	2013-12-30 00:00:00	42	0	AHYD	47.25	15.51
31	1974-01-01 00:00:00	2013-12-30 00:00:00	40	0	AHYD	46.71	15.79
32	1976-01-01 00:00:00	2013-12-30 00:00:00	38	0	AHYD	46.73	15.85
33	1977-01-01 00:00:00	2013-12-30 00:00:00	37	0	AHYD	47.29	16.09
34	1979-01-01 00:00:00	2013-12-30 00:00:00	35	0	AHYD	46.99	16.21
35	1980-01-01 00:00:00	2013-12-30 00:00:00	34	0	AHYD	47.17	15.62

## APPENDIX

36	1981-01-01 00:00:00	2013-12-30 00:00:00	33	0	AHYD	47.31	15.83
37	1981-01-01 00:00:00	2013-12-30 00:00:00	33	0	AHYD	47.29	15.84
38	1981-01-01 00:00:00	2013-12-30 00:00:00	33	0	AHYD	47.20	15.34
39	1982-01-01 00:00:00	2013-12-30 00:00:00	32	0	AHYD	46.72	15.41
40	1982-01-01 00:00:00	2013-12-30 00:00:00	32	0	AHYD	46.83	15.26
41	1982-01-01 00:00:00	2013-12-30 00:00:00	32	0	AHYD	47.33	16.05
42	1982-01-01 00:00:00	2013-12-30 00:00:00	32	0	AHYD	47.25	15.52
43	1984-01-01 00:00:00	2013-12-30 00:00:00	30	0	AHYD	47.15	15.67
44	1987-01-01 00:00:00	2013-12-30 00:00:00	27	4.7	AHYD	47.52	15.79
45	1987-01-01 00:00:00	2013-12-30 00:00:00	27	0	AHYD	47.37	16.12
46	1987-01-01 00:00:00	2013-12-30 00:00:00	27	0	AHYD	47.13	14.74
47	1987-01-01 00:00:00	2013-12-30 00:00:00	27	0	AHYD	47.16	15.32
48	1989-01-01 00:00:00	2013-12-30 00:00:00	25	0	AHYD	46.84	15.38
49	1989-01-01 00:00:00	2013-12-30 00:00:00	25	0	AHYD	46.83	15.26
50	1990-01-01 00:00:00	2013-12-30 00:00:00	24	0	AHYD	46.85	15.37
51	1990-01-01 00:00:00	2013-12-30 00:00:00	24	0	AHYD	46.90	15.49
52	1991-01-01 00:00:00	2013-12-30 00:00:00	23	0	AHYD	46.93	16.16
53	1991-01-01 00:00:00	2013-12-30 00:00:00	23	0	AHYD	47.48	15.47
54	1991-01-01 00:00:00	2013-12-30 00:00:00	23	0	AHYD	47.10	15.68
55	1993-01-01 00:00:00	2013-12-30 00:00:00	21	0	AHYD	46.89	15.57
56	1993-01-01 00:00:00	2013-12-30 00:00:00	21	0	AHYD	46.75	15.37
57	1994-01-01 00:00:00	2013-12-30 00:00:00	20	0	AHYD	47.25	14.76
58	1994-01-01 00:00:00	2013-12-30 00:00:00	20	0	AHYD	46.70	15.27
59	1995-01-01 00:00:00	2013-12-30 00:00:00	19	0	AHYD	47.03	15.30
60	2000-06-20 00:00:00	2013-12-30 00:00:00	13.5	0	AHYD	47.14	14.28
61	2003-09-02 00:00:00	2013-12-30 00:00:00	10.3	0	AHYD	47.15	14.37

## A.2 Supplementary Information Research Article 2





## Supplementary information to Schroeer, K. and Tye, M.R.: Quantifying damage contributions from convective and stratiform weather types: how well do precipitation and discharge data indicate the risk?

### Contents:

1. **Figure S1:** Discharge anomalies associated with weather types
2. **Figure S2:** Distribution of claims by municipality group and weather type, full sample
2. **Table S1:** Summary statistics of gauge records
3. **Table S2:** Information rain gauges (sub-daily precipitation)
4. **Table S3:** Information rain gauges (daily precipitation)
5. **Table S4:** Information stream gauges (daily observations)

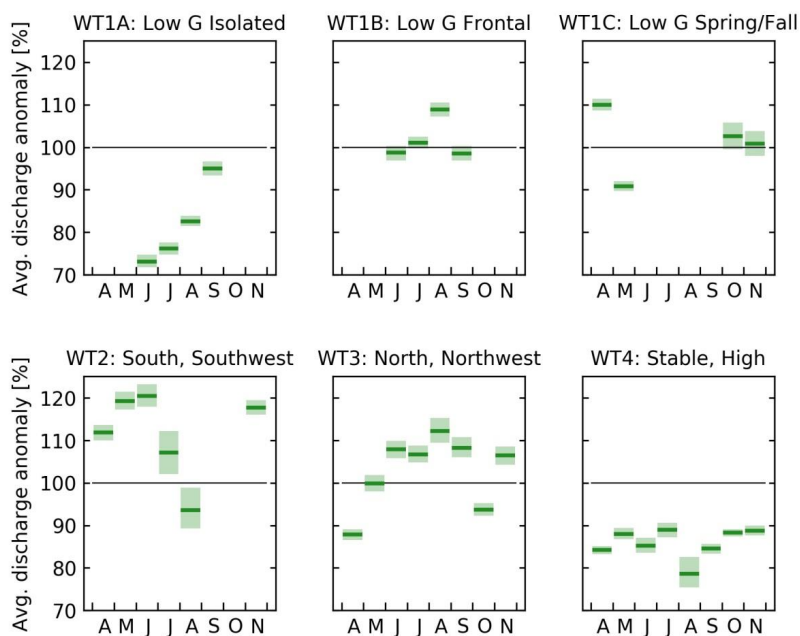


Figure 1: Average monthly discharge anomalies associated with the different weather types over all stream gauges. Horizontal green lines show the average weather-type specific deviation from the long-term climatological mean (horizontal black lines); green boxes denote the 90% confidence intervals of the sample means.

## APPENDIX

Table S 1: Summary statistics of gauge records

	<b>Number gauges</b>	<b>Median record length</b>	<b>Record lengths 5th and 95<sup>th</sup> percentile</b>	<b>Median Missing data study period</b>	<b>Missing data study period 5th and 95th percentile</b>
Sub-daily precipitation	72	13	[6.2, 22.3]	0.4	[0.0, 6.6]
Daily precipitation	108	40	[17, 114]	0.0	[0.0, 4.0]
Stream gauges	61	40	[20, 63]	0.0	[0.0, 0.0]

Table S 2: Information rain gauges (sub-daily precipitation)

	First observation	Last observation	Record length (years)	Missing data during study period (1990-2015) [%]	Provider	Lat	Lon
1	1992-08-29 00:10:00	2014-12-26 23:50:00	22.3	6.3	ZAMG	46.69	15.98
2	1992-08-29 00:10:00	2014-12-26 23:50:00	22.3	1.8	ZAMG	47.11	14.18
3	1992-08-29 00:10:00	2014-12-26 23:50:00	22.3	1.7	ZAMG	47.07	15.59
4	1992-08-29 00:10:00	2014-12-26 23:50:00	22.3	1.6	ZAMG	47.08	15.45
5	1993-02-16 13:30:00	2014-12-26 23:50:00	21.9	3.3	ZAMG	47.20	15.47
6	1993-07-29 11:10:00	2014-12-26 23:50:00	21.4	1.8	ZAMG	47.07	14.42
7	1994-10-24 13:30:00	2014-12-26 23:50:00	20.2	1.6	ZAMG	46.82	15.23
8	1994-10-24 13:10:00	2014-12-26 23:50:00	20.2	1.2	ZAMG	47.28	15.98
9	1997-02-17 12:40:00	2014-12-26 23:50:00	17.9	1	ZAMG	47.45	15.30
10	1997-09-01 00:10:00	2014-12-26 23:50:00	17.3	0.5	ZAMG	47.20	14.75
11	1999-08-16 09:30:00	2014-12-26 23:50:00	15.4	0.4	ZAMG	46.95	15.88
12	2001-11-08 16:10:00	2014-12-26 23:50:00	13.1	0.9	ZAMG	47.27	14.78
13	2002-07-31 14:20:00	2014-12-26 23:50:00	12.4	0.7	ZAMG	47.18	15.49
14	2003-04-08 16:10:00	2014-12-26 23:50:00	11.7	0.4	ZAMG	46.87	15.90
15	2003-11-03 12:10:00	2014-12-26 23:50:00	11.2	0.3	ZAMG	46.77	15.55
16	2004-10-28 14:50:00	2014-12-26 23:50:00	10.2	3.6	ZAMG	47.41	15.25
17	2004-10-31 20:10:00	2014-12-26 23:50:00	10.2	3.3	ZAMG	47.07	15.09
18	2004-11-09 12:10:00	2014-12-26 23:50:00	10.1	1	ZAMG	47.44	15.64
19	2007-05-09 10:00:00	2014-12-26 23:50:00	7.6	2	ZAMG	47.03	16.08
20	2007-05-08 08:40:00	2014-12-26 23:50:00	7.6	0.3	ZAMG	47.12	15.71
21	2007-07-20 17:00:00	2014-12-26 23:50:00	7.4	0.9	ZAMG	47.20	14.29
22	2007-07-24 12:00:00	2014-12-26 23:50:00	7.4	0.1	ZAMG	47.12	14.19
23	2007-11-07 10:00:00	2014-12-26 23:50:00	7.1	0.2	ZAMG	47.05	15.41
24	2008-09-05 14:50:00	2014-12-26 23:50:00	6.3	0.4	ZAMG	47.26	15.31
25	2008-08-25 12:30:00	2014-12-26 23:50:00	6.3	0.3	ZAMG	46.99	15.45
26	2008-11-10 15:40:00	2014-12-26 23:50:00	6.1	0.4	ZAMG	47.40	15.94
27	2012-10-04 13:20:00	2014-12-26 23:50:00	2.2	0.6	ZAMG	47.38	15.09
28	1982-06-01 07:00:00	2015-01-28 06:20:00	32.7	6.5	AHYD	47.33	15.81
29	1990-04-04 08:00:00	2015-01-01 00:00:00	24.8	24.4	AHYD	47.57	14.24
30	1999-01-01 07:00:00	2014-12-30 23:50:00	16	8.3	AHYD	46.65	15.50
31	1999-06-19 08:00:00	2015-01-27 23:50:00	15.6	0.1	AHYD	47.48	14.53
32	2000-01-01 07:00:00	2014-12-30 23:50:00	15	6.7	AHYD	47.14	15.06
33	2000-01-01 07:00:00	2015-01-01 06:50:00	15	1.7	AHYD	47.35	15.69
34	2000-01-01 07:00:00	2014-12-30 23:50:00	15	0.6	AHYD	46.81	15.33
35	2000-01-01 07:00:00	2014-12-30 23:50:00	15	0.1	AHYD	47.38	14.71
36	2000-01-01 07:00:00	2014-12-30 23:50:00	15	0	AHYD	47.06	14.88
37	2000-01-01 07:00:00	2015-01-01 06:50:00	15	0	AHYD	47.17	16.01
38	2000-01-01 07:00:00	2014-12-30 23:50:00	15	0	AHYD	46.90	15.26
39	2000-01-01 07:00:00	2015-01-01 06:50:00	15	0	AHYD	47.38	16.00
40	2000-07-01 07:00:00	2015-01-01 06:50:00	14.5	0.1	AHYD	47.49	15.92
41	2000-08-01 00:00:00	2014-12-30 23:50:00	14.4	0.1	AHYD	47.55	15.79
42	2000-08-01 00:00:00	2014-12-30 23:50:00	14.4	0	AHYD	47.15	15.24
43	2001-01-01 07:00:00	2014-12-30 23:50:00	14	0	AHYD	47.52	15.47
44	2001-01-01 07:00:00	2014-12-30 23:50:00	14	0	AHYD	46.79	15.45
45	2001-01-01 07:00:00	2014-12-30 23:50:00	14	0	AHYD	46.69	15.09
46	2001-01-01 07:00:00	2015-01-01 06:50:00	14	0	AHYD	47.22	15.76

## APPENDIX

47	2000-01-02 07:00:00	2013-06-20 13:10:00	13.5	0	AHYD	47.11	14.95
48	2001-10-01 07:00:00	2015-01-27 23:50:00	13.3	0	AHYD	47.74	15.48
49	2001-07-26 11:10:00	2014-10-16 06:50:00	13.2	3.2	AHYD	47.61	14.85
50	2002-01-01 07:00:00	2014-12-30 23:50:00	13	4.4	AHYD	47.20	14.28
51	2002-01-02 00:00:00	2014-12-30 23:50:00	13	0.4	AHYD	47.28	14.93
52	2002-01-01 07:00:00	2015-01-01 06:50:00	13	0	AHYD	46.85	15.97
53	2002-06-19 08:00:00	2015-01-18 10:40:00	12.6	0.6	AHYD	47.38	14.12
54	2002-06-19 08:00:00	2015-01-27 23:50:00	12.6	0.1	AHYD	47.51	14.83
55	2003-07-17 17:10:00	2014-12-30 12:50:00	11.5	0	AHYD	47.41	13.89
56	2003-10-01 00:00:00	2015-01-01 06:50:00	11.3	0	AHYD	46.92	15.68
57	2003-12-31 07:00:00	2014-12-30 23:50:00	11	0.2	AHYD	47.39	15.44
58	2003-12-31 07:00:00	2014-12-30 23:50:00	11	0	AHYD	47.17	14.66
59	2004-01-01 07:00:00	2015-01-01 06:50:00	11	0	AHYD	47.15	15.66
60	2004-01-01 07:00:00	2015-01-01 06:50:00	11	0	AHYD	47.29	16.05
61	2004-04-30 07:00:00	2014-12-30 23:50:00	10.7	0	AHYD	47.27	15.32
62	2004-10-01 07:00:00	2014-12-30 23:50:00	10.3	1.4	AHYD	47.11	14.60
63	2005-06-19 08:00:00	2015-01-27 23:50:00	9.6	0.1	AHYD	47.43	14.49
64	2005-07-01 07:00:00	2015-01-01 00:00:00	9.5	10.5	AHYD	47.66	14.98
65	2005-11-01 07:00:00	2014-12-30 23:50:00	9.2	0.7	AHYD	46.80	15.76
66	2005-12-31 07:00:00	2015-01-01 06:50:00	9	0.5	AHYD	47.06	16.01
67	2006-01-01 07:00:00	2015-01-01 00:00:00	9	0	AHYD	47.39	13.66
68	2006-06-19 08:00:00	2015-01-27 23:50:00	8.6	0	AHYD	47.59	14.63
69	2007-01-01 07:00:00	2014-12-30 23:50:00	8	0.4	AHYD	46.92	13.88
70	2007-09-17 13:50:00	2014-12-30 23:50:00	7.3	0	AHYD	47.11	15.42
71	2010-01-01 07:00:00	2015-01-01 06:50:00	5	0	AHYD	47.49	15.67
72	2010-11-16 15:40:00	2015-01-01 00:00:00	4.1	0	AHYD	47.37	13.72

Table S 3: Information rain gauges (daily precipitation). List includes 72 gauges from Table S 2, but record lengths are given for the daily observation records. Daily observations are available from an additional 80 rain gauges.

	First observation	Last observation	Record length (years)	Missing data during study period (1990-2015) [%]	Provider	Lat	Lon
1	1983-05-01 00:00:00	2017-02-07 00:00:00	33.8	0.3	ZAMG	47.55	15.24
2	1999-04-01 00:00:00	2017-02-07 00:00:00	17.9	0.8	ZAMG	47.63	15.83
3	2000-09-30 00:00:00	2017-02-06 00:00:00	16.4	0.3	ZAMG	47.52	14.95
4	2008-09-08 00:00:00	2017-02-07 00:00:00	8.4	0	ZAMG	47.60	15.67
5	1900-01-00 00:00:00	2014-12-31 00:00:00	115.1	0	AHYD	46.90	15.26
6	1901-01-01 00:00:00	2014-12-31 00:00:00	114.1	14.3	AHYD	46.93	15.67
7	1901-01-01 00:00:00	2014-12-31 00:00:00	114.1	5.3	AHYD	47.27	15.32
8	1901-01-01 00:00:00	2014-12-31 00:00:00	114.1	4	AHYD	47.22	15.39
9	1901-01-01 00:00:00	2014-12-31 00:00:00	114.1	0	AHYD	46.79	15.45
10	1901-01-01 00:00:00	2014-12-31 00:00:00	114.1	0	AHYD	47.17	16.01
11	1901-01-01 00:00:00	2014-12-31 00:00:00	114.1	0	AHYD	47.46	14.68
12	1901-01-01 00:00:00	2014-12-31 00:00:00	114.1	0	AHYD	46.82	15.45
13	1901-01-01 00:00:00	2014-12-31 00:00:00	114.1	0	AHYD	47.10	15.83
14	1901-01-01 00:00:00	2014-12-31 00:00:00	114.1	0	AHYD	47.07	14.69
15	1901-01-01 00:00:00	2014-12-31 00:00:00	114.1	0	AHYD	46.69	15.26
16	1901-01-01 00:00:00	2014-12-31 00:00:00	114.1	0	AHYD	47.06	14.30
17	1901-01-01 00:00:00	2014-12-31 00:00:00	114.1	0	AHYD	47.02	14.92
18	1901-01-01 00:00:00	2014-12-31 00:00:00	114.1	0	AHYD	46.99	15.21
19	1901-01-01 00:00:00	2014-12-31 00:00:00	114.1	0	AHYD	47.07	15.07
20	1901-01-01 00:00:00	2014-12-31 00:00:00	114.1	0	AHYD	46.81	15.87
21	1901-01-01 00:00:00	2014-12-31 00:00:00	114.1	0	AHYD	47.53	15.78
22	1901-01-01 00:00:00	2014-12-31 00:00:00	114.1	0	AHYD	47.36	14.47
23	1901-01-01 00:00:00	2014-12-31 00:00:00	114.1	0	AHYD	47.20	14.44
24	1901-01-01 00:00:00	2014-12-31 00:00:00	114.1	0	AHYD	47.67	15.47
25	1901-01-01 00:00:00	2014-12-31 00:00:00	114.1	0	AHYD	47.47	15.50
26	1901-01-01 00:00:00	2014-12-31 00:00:00	114.1	0	AHYD	47.53	15.08
27	1901-01-01 00:00:00	2014-12-31 00:00:00	114.1	0	AHYD	47.58	15.50
28	1901-01-01 00:00:00	2014-12-31 00:00:00	114.1	0	AHYD	47.28	15.97
29	1901-01-01 00:00:00	2014-12-31 00:00:00	114.1	0	AHYD	47.47	15.79
30	1901-01-01 00:00:00	2014-12-31 00:00:00	114.1	0	AHYD	47.21	15.82
31	1901-01-01 00:00:00	2014-12-31 00:00:00	114.1	0	AHYD	47.40	15.89
32	1902-01-01 00:00:00	2014-12-31 00:00:00	113.1	0	AHYD	47.40	14.82
33	1901-01-01 00:00:00	2006-04-30 00:00:00	105.4	0	AHYD	47.31	14.94
34	1913-01-01 00:00:00	2014-12-31 00:00:00	102.1	0	AHYD	47.27	14.71
35	1927-07-01 00:00:00	2014-12-31 00:00:00	87.6	0	AHYD	47.43	15.01
36	1929-06-01 00:00:00	2014-12-31 00:00:00	85.6	0	AHYD	46.80	15.76
37	1930-01-01 00:00:00	2014-12-31 00:00:00	85.1	0	AHYD	46.98	14.99
38	1930-01-01 00:00:00	2014-12-31 00:00:00	85.1	0	AHYD	46.93	15.01
39	1933-01-01 00:00:00	2014-12-31 00:00:00	82.1	0	AHYD	47.15	15.24
40	1936-01-01 00:00:00	2014-12-31 00:00:00	79.1	0	AHYD	46.65	15.46
41	1946-01-01 00:00:00	2014-12-31 00:00:00	69	0	AHYD	47.10	15.41

## APPENDIX

42	1947-03-01 00:00:00	2014-12-31 00:00:00	67.9	0	AHYD	47.17	14.66
43	1947-07-01 00:00:00	2014-12-31 00:00:00	67.5	0	AHYD	47.39	15.44
44	1948-01-01 00:00:00	2014-12-31 00:00:00	67	1.7	AHYD	47.01	14.53
45	1951-11-01 00:00:00	2014-12-31 00:00:00	63.2	0	AHYD	46.95	15.33
46	1952-01-01 00:00:00	2014-12-31 00:00:00	63	0	AHYD	47.66	15.70
47	1954-08-01 00:00:00	2014-12-31 00:00:00	60.5	4	AHYD	46.75	15.16
48	1955-01-01 00:00:00	2014-12-31 00:00:00	60	0	AHYD	46.71	16.02
49	1955-11-01 00:00:00	2014-12-31 00:00:00	59.2	0	AHYD	47.00	15.94
50	1971-01-01 00:00:00	2014-12-31 00:00:00	44	4	AHYD	47.11	14.60
51	1971-01-01 00:00:00	2014-12-31 00:00:00	44	0	AHYD	47.14	15.33
52	1971-01-01 00:00:00	2014-12-31 00:00:00	44	0	AHYD	47.44	16.05
53	1971-01-01 00:00:00	2014-12-31 00:00:00	44	0	AHYD	46.72	15.91
54	1961-01-01 00:00:00	2003-01-31 00:00:00	42.1	0	AHYD	47.20	14.28
55	1974-01-01 00:00:00	2014-12-31 00:00:00	41	0	AHYD	47.07	15.13
56	1974-07-01 00:00:00	2014-12-31 00:00:00	40.5	0	AHYD	47.07	13.98
57	1961-01-01 00:00:00	2001-01-31 00:00:00	40.1	9	AHYD	47.58	15.14
58	1975-01-01 00:00:00	2014-12-31 00:00:00	40	0	AHYD	46.74	15.62
59	1975-01-01 00:00:00	2014-12-31 00:00:00	40	0	AHYD	47.31	15.84
60	1975-01-01 00:00:00	2014-12-31 00:00:00	40	0	AHYD	47.38	15.79
61	1975-01-01 00:00:00	2014-12-31 00:00:00	40	0	AHYD	46.93	16.02
62	1977-01-01 00:00:00	2014-12-31 00:00:00	38	0	AHYD	47.07	16.00
63	1977-05-01 00:00:00	2014-12-31 00:00:00	37.7	0	AHYD	46.72	15.26
64	1971-01-01 00:00:00	2008-06-30 00:00:00	37.5	0	AHYD	47.35	14.31
65	1979-01-01 00:00:00	2014-12-31 00:00:00	36	0	AHYD	47.23	15.15
66	1980-01-01 00:00:00	2014-12-31 00:00:00	35	0	AHYD	47.08	15.21
67	1981-01-01 00:00:00	2014-12-31 00:00:00	34	0	AHYD	47.30	15.51
68	1981-01-01 00:00:00	2014-12-31 00:00:00	34	0	AHYD	46.82	15.72
69	1957-07-01 00:00:00	1990-12-31 00:00:00	33.5	0	AHYD	47.57	15.23
70	1982-01-01 00:00:00	2014-12-31 00:00:00	33	0	AHYD	47.46	15.99
71	1984-01-01 00:00:00	2014-12-31 00:00:00	32.7	0	AHYD	47.33	15.81
72	1971-01-01 00:00:00	2002-12-31 00:00:00	32	1.9	AHYD	46.85	15.97
73	1984-01-01 00:00:00	2014-12-31 00:00:00	31	0	AHYD	46.69	15.09
74	1984-01-01 00:00:00	2014-12-31 00:00:00	31	0	AHYD	47.20	15.17
75	1984-01-01 00:00:00	2014-12-31 00:00:00	31	0	AHYD	46.75	15.21
76	1984-01-01 00:00:00	2014-12-31 00:00:00	31	0	AHYD	46.67	15.17
77	1985-01-01 00:00:00	2014-12-31 00:00:00	30	12	AHYD	46.82	15.14
78	1975-01-01 00:00:00	2004-12-31 00:00:00	30	0	AHYD	46.76	15.37
79	1985-01-01 00:00:00	2014-12-31 00:00:00	30	0	AHYD	46.86	15.08
80	1986-10-01 00:00:00	2014-12-31 00:00:00	28.3	0	AHYD	46.83	15.31
81	1987-01-01 00:00:00	2014-12-31 00:00:00	28	0	AHYD	46.71	15.46
82	1987-01-01 00:00:00	2014-12-31 00:00:00	28	0	AHYD	46.92	15.10
83	1988-01-01 00:00:00	2014-12-31 00:00:00	27	0	AHYD	47.31	15.48
84	1988-01-01 00:00:00	2014-12-31 00:00:00	27	0	AHYD	46.74	15.09
85	1988-01-01 00:00:00	2014-12-31 00:00:00	27	0	AHYD	47.18	14.81
86	1990-01-01 00:00:00	2014-12-31 00:00:00	25	0	AHYD	47.49	15.67
87	1990-01-01 00:00:00	2014-12-31 00:00:00	25	0	AHYD	46.99	15.87
88	1991-01-01 00:00:00	2014-12-31 00:00:00	24	0	AHYD	47.11	14.95
89	1991-01-01 00:00:00	2014-12-31 00:00:00	24	0	AHYD	47.01	15.39
90	1991-01-01 00:00:00	2014-12-31 00:00:00	24	0	AHYD	47.37	15.34
91	1991-01-01 00:00:00	2014-12-31 00:00:00	24	0	AHYD	47.55	15.11
92	1994-01-01 00:00:00	2014-12-31 00:00:00	21	0	AHYD	46.65	15.50
93	1994-01-01 00:00:00	2014-12-31 00:00:00	21	0	AHYD	47.14	15.06
94	1994-01-01 00:00:00	2014-12-31 00:00:00	21	0	AHYD	47.22	15.33
95	1994-01-01 00:00:00	2014-12-31 00:00:00	21	0	AHYD	46.88	15.07
96	1994-01-01 00:00:00	2014-12-31 00:00:00	21	0	AHYD	46.82	15.25
97	1994-01-01 00:00:00	2014-12-31 00:00:00	21	0	AHYD	47.10	14.64
98	1994-01-01 00:00:00	2014-12-31 00:00:00	21	0	AHYD	47.15	14.85
99	1996-01-01 00:00:00	2014-12-31 00:00:00	19	0	AHYD	47.15	15.66
100	1997-01-01 00:00:00	2014-12-31 00:00:00	18	0	AHYD	47.35	15.69
101	1998-01-01 00:00:00	2014-12-31 00:00:00	17	0	AHYD	46.81	15.33

102	1998-01-01 00:00:00	2014-12-31 00:00:00	17	0	AHYD	46.92	13.88
103	1998-01-01 00:00:00	2014-12-31 00:00:00	17	0	AHYD	47.06	15.42
104	1998-01-01 00:00:00	2014-12-31 00:00:00	17	0	AHYD	47.20	14.62
105	1998-01-01 00:00:00	2014-12-31 00:00:00	17	0	AHYD	47.62	15.27
106	1999-03-01 00:00:00	2014-12-31 00:00:00	15.8	14.2	AHYD	47.49	15.92
107	1994-01-01 00:00:00	2002-02-28 00:00:00	14.4	0	AHYD	47.55	15.79
108	2011-12-01 00:00:00	2014-12-31 00:00:00	14	0	AHYD	47.52	15.45

Table S 4: Information stream gauges (daily observations)

	First observation	Last observation	Record length (years)	Missing data during study period (1990-2015) [%]	Provider	Lat	Lon
1	1951-01-01 00:00:00	2014-12-31 00:00:00	64	0	AHYD	47.21	14.54
2	1951-01-01 00:00:00	2013-12-30 00:00:00	63	0	AHYD	47.02	16.14
3	1951-01-01 00:00:00	2013-12-30 00:00:00	63	0	AHYD	46.96	15.89
4	1951-01-01 00:00:00	2013-12-30 00:00:00	63	0	AHYD	47.22	14.58
5	1951-01-01 00:00:00	2013-12-30 00:00:00	63	0	AHYD	47.38	15.09
6	1951-01-01 00:00:00	2013-12-30 00:00:00	63	0	AHYD	47.47	15.25
7	1951-01-01 00:00:00	2013-12-30 00:00:00	63	0	AHYD	46.96	15.35
8	1951-01-01 00:00:00	2013-12-30 00:00:00	63	0	AHYD	46.76	15.21
9	1951-01-01 00:00:00	2013-12-30 00:00:00	63	0	AHYD	46.72	15.27
10	1951-01-01 00:00:00	2013-12-30 00:00:00	63	0	AHYD	46.78	15.53
11	1961-01-01 00:00:00	2013-12-30 00:00:00	53	0	AHYD	47.21	16.09
12	1961-01-01 00:00:00	2013-12-30 00:00:00	53	0	AHYD	47.17	16.01
13	1961-01-01 00:00:00	2013-12-30 00:00:00	53	0	AHYD	47.28	15.69
14	1961-01-01 00:00:00	2013-12-30 00:00:00	53	0	AHYD	47.08	15.94
15	1961-01-01 00:00:00	2013-12-30 00:00:00	53	0	AHYD	47.11	14.21
16	1961-01-01 00:00:00	2013-12-30 00:00:00	53	0	AHYD	47.43	15.26
17	1961-01-01 00:00:00	2013-12-30 00:00:00	53	0	AHYD	46.81	15.52
18	1966-01-01 00:00:00	2014-12-31 00:00:00	49	0	AHYD	47.03	15.45
19	1966-01-01 00:00:00	2013-12-30 00:00:00	48	0	AHYD	47.18	15.67
20	1966-01-01 00:00:00	2013-12-30 00:00:00	48	0	AHYD	47.38	16.00
21	1966-01-01 00:00:00	2013-12-30 00:00:00	48	0	AHYD	47.19	14.75
22	1966-01-01 00:00:00	2013-12-30 00:00:00	48	0	AHYD	47.39	14.91
23	1966-01-01 00:00:00	2013-12-30 00:00:00	48	0	AHYD	47.39	15.03
24	1966-01-01 00:00:00	2013-12-30 00:00:00	48	0	AHYD	47.53	15.47
25	1966-01-01 00:00:00	2013-12-30 00:00:00	48	0	AHYD	47.05	15.15
26	1967-01-01 00:00:00	2013-12-30 00:00:00	47	0	AHYD	47.41	15.28
27	1968-01-01 00:00:00	2013-12-30 00:00:00	46	0	AHYD	47.04	15.76
28	1969-01-01 00:00:00	2013-12-30 00:00:00	45	0	AHYD	46.76	15.67
29	1971-01-01 00:00:00	2013-12-30 00:00:00	43	0	AHYD	47.43	15.27
30	1972-01-01 00:00:00	2013-12-30 00:00:00	42	0	AHYD	47.25	15.51
31	1974-01-01 00:00:00	2013-12-30 00:00:00	40	0	AHYD	46.71	15.79
32	1976-01-01 00:00:00	2013-12-30 00:00:00	38	0	AHYD	46.73	15.85
33	1977-01-01 00:00:00	2013-12-30 00:00:00	37	0	AHYD	47.29	16.09
34	1979-01-01 00:00:00	2013-12-30 00:00:00	35	0	AHYD	46.99	16.21
35	1980-01-01 00:00:00	2013-12-30 00:00:00	34	0	AHYD	47.17	15.62

## APPENDIX

36	1981-01-01 00:00:00	2013-12-30 00:00:00	33	0	AHYD	47.31	15.83
37	1981-01-01 00:00:00	2013-12-30 00:00:00	33	0	AHYD	47.29	15.84
38	1981-01-01 00:00:00	2013-12-30 00:00:00	33	0	AHYD	47.20	15.34
39	1982-01-01 00:00:00	2013-12-30 00:00:00	32	0	AHYD	46.72	15.41
40	1982-01-01 00:00:00	2013-12-30 00:00:00	32	0	AHYD	46.83	15.26
41	1982-01-01 00:00:00	2013-12-30 00:00:00	32	0	AHYD	47.33	16.05
42	1982-01-01 00:00:00	2013-12-30 00:00:00	32	0	AHYD	47.25	15.52
43	1984-01-01 00:00:00	2013-12-30 00:00:00	30	0	AHYD	47.15	15.67
44	1987-01-01 00:00:00	2013-12-30 00:00:00	27	4.7	AHYD	47.52	15.79
45	1987-01-01 00:00:00	2013-12-30 00:00:00	27	0	AHYD	47.37	16.12
46	1987-01-01 00:00:00	2013-12-30 00:00:00	27	0	AHYD	47.13	14.74
47	1987-01-01 00:00:00	2013-12-30 00:00:00	27	0	AHYD	47.16	15.32
48	1989-01-01 00:00:00	2013-12-30 00:00:00	25	0	AHYD	46.84	15.38
49	1989-01-01 00:00:00	2013-12-30 00:00:00	25	0	AHYD	46.83	15.26
50	1990-01-01 00:00:00	2013-12-30 00:00:00	24	0	AHYD	46.85	15.37
51	1990-01-01 00:00:00	2013-12-30 00:00:00	24	0	AHYD	46.90	15.49
52	1991-01-01 00:00:00	2013-12-30 00:00:00	23	0	AHYD	46.93	16.16
53	1991-01-01 00:00:00	2013-12-30 00:00:00	23	0	AHYD	47.48	15.47
54	1991-01-01 00:00:00	2013-12-30 00:00:00	23	0	AHYD	47.10	15.68
55	1993-01-01 00:00:00	2013-12-30 00:00:00	21	0	AHYD	46.89	15.57
56	1993-01-01 00:00:00	2013-12-30 00:00:00	21	0	AHYD	46.75	15.37
57	1994-01-01 00:00:00	2013-12-30 00:00:00	20	0	AHYD	47.25	14.76
58	1994-01-01 00:00:00	2013-12-30 00:00:00	20	0	AHYD	46.70	15.27
59	1995-01-01 00:00:00	2013-12-30 00:00:00	19	0	AHYD	47.03	15.30
60	2000-06-20 00:00:00	2013-12-30 00:00:00	13.5	0	AHYD	47.14	14.28
61	2003-09-02 00:00:00	2013-12-30 00:00:00	10.3	0	AHYD	47.15	14.37



# FIGURES

2.1	Risk framework in the context of processes and data analyzed in this thesis. . . . .	10
3.1	Study area in the Austrian southeastern Alpine forelands and data layers . . . . .	23
4.1.1	Study area and rain gauge locations in southeastern Austria . . . .	41
4.1.2	Examples of sampled convective events over the study region . . . .	42
4.1.3	Schematic description of the fishnet-windowed triangular mesh (FWTM) subnetwork sampling method . . . . .	42
4.1.4	Correlogram (spatial correlation) and root-mean-square deviation of precipitation . . . . .	44
4.1.5	Observed and power law fits of precipitation intensities in extreme convective events depending on network density . . . . .	45
4.2.1	Study area, municipalities, gauge locations and catchments in the southeastern Alpine forelands of Austria . . . . .	56
4.2.2	Factors of vulnerability and exposure in the four municipality clusters . . . . .	56
4.2.3	Number of damage claims from flooding, landslides, and debris flows per year and municipality cluster . . . . .	56
4.2.4	Weather type frequency, associated extreme precipitation and average wet spell duration . . . . .	58
4.2.5	Relative frequency and cumulated cost associated with each weather type relative to the total cost . . . . .	58
4.2.6	Number of claims due to flooding, debris flows, and landslides in rural, alpine, and urban municipalities in the different weather type groups . . . . .	59
4.2.7	Annual exceedance probabilities of discharge levels on days with 0, 1–20, and >20 reported claims under convective and stratiform weather types . . . . .	60

## FIGURES

4.2.8	Relative proportion of claimed loss by annual exceedance probability of river discharge in each catchment . . . . .	60
4.2.9	Relative proportion of claimed loss by annual exceedance probability of daily precipitation totals in the respective municipalities . . . . .	61
4.3.1	Austrian south-eastern Alpine foreland region and precipitation measurement stations used in the analysis . . . . .	71
4.3.2	Scaling factors of station event precipitation intensity with daily mean temperature for the 98 <sup>th</sup> percentile . . . . .	73
4.3.3	Monthly scaling factors for the 50 <sup>th</sup> and 98 <sup>th</sup> percentiles of maximum peak and hour intensities and daily precipitation sums . . . . .	75
4.3.4	Monthly scaling factors in the east and west region for the 98 <sup>th</sup> percentile of maximum peak and hour intensities and daily precipitation sums . . . . .	76
4.3.5	CC and super-CC scaling rates, originating from the 50 <sup>th</sup> and 98 <sup>th</sup> percentile values calculated for the 5 % °C <sup>-1</sup> to 7 % °C <sup>-1</sup> daily T <sub>mean</sub> bin . . . . .	77
4.3.6	Absolute 98 <sup>th</sup> percentile values of the maximum peak and hour intensities and daily precipitation sums for the east and west region . . . . .	78
5.1	Event maximum precipitation intensities sampled by WEGN and ZAMG + AHYD station networks . . . . .	85

# TABLES

3.1 Properties and usage of data used in the research articles . . . . .	26
3.2 Qualitative description of results from the sensitivity tests comparing the estimated annual exceedance probability (AEP) using generalized extreme value distribution (GEV) versus GEV type-I (Gumbel) fitted to annual seasonal maximum daily precipitation amount (sRX1D) and annual seasonal maximum daily discharge (sQX1D) for the empirically observed events of magnitude $z$ . . . . .	34
4.1 Summary of the data used in this study . . . . .	55
4.2 Summary characteristics of the station scaling factors for the 98 <sup>th</sup> percentile . . . . .	74



## REFERENCES

- Aalbers, E. E., G. Lenderink, E. van Meijgaard, and B. J. J. M. van den Hurk (2018), Local-scale changes in mean and heavy precipitation in Western Europe, climate change or internal variability?, *Climate Dynamics*, *50*(11), 4745–4766, doi:10.1007/s00382-017-3901-9.
- Aerts, J. C. J. H., W. J. Botzen, K. C. Clarke, S. L. Cutter, J. W. Hall, B. Merz, E. Michel-Kerjan, J. Mysiak, S. Surminski, and H. Kunreuther (2018), Integrating human behaviour dynamics into flood disaster risk assessment, *Nature Climate Change*, *8*(3), 193–199, doi:10.1038/s41558-018-0085-1.
- AghaKouchak, A., L. Huning, F. Chiang, M. Sadegh, F. Vahedifard, O. Mazdiyasn, H. Moftakhari, and I. Mallakpour (2018), How do natural hazards cascade to cause disasters?, *Nature*, *561*, 458–460, doi:10.1038/d41586-018-06783-6.
- Alexander, L., and C. Tebaldi (2012), Climate and weather extremes: observations, modelling and projections., *The Future of the World's Climate*, pp. 253–288, 2nd edition. A. Henderson-Sellers and K. McGuffie, Eds., Elsevier.
- Alexander, L. V. (2016), Global observed long-term changes in temperature and precipitation extremes: A review of progress and limitations in IPCC assessments and beyond, *Weather and Climate Extremes*, *11*, 4–16, doi:10.1016/j.wace.2015.10.007.
- Ali, H., and V. Mishra (2018), Contributions of dynamic and thermodynamic scaling in subdaily precipitation extremes in india, *Geophysical Research Letters*, *45*(5), 2352–2361, doi:10.1002/2018GL077065.
- Allen, J. T. (2018), Climate change and severe thunderstorms, *Oxford Research Encyclopedias: Climate Science*, p. 67pp, doi:10.1093/acrefore/9780190228620.013.62.
- Allen, J. T., M. K. Tippett, and A. H. Sobel (2015), An empirical model relating US monthly hail occurrence to large-scale meteorological environ-

- ment, *Journal of Advances In Modeling Earth Systems*, 7(1), 226–243, doi:10.1002/2014MS000397.
- Allen, M. R., and W. J. Ingram (2002), Constraints on future changes in climate and the hydrologic cycle, *Nature*, 419(6903), 224–232, doi:10.1038/nature01092.
- American Meteorological Society (2018), Glossary of Meteorology, [Available online at <http://glossary.ametsoc.org/wiki>, 2018-08-15].
- Amponsah, W., P.-A. Ayrál, B. Boudevillain, C. Bouvier, I. Braud, P. Brunet, G. Delrieu, J.-F. Didon-Lescot, E. Gaume, L. Lebouc, L. Marchi, F. Marra, E. Morin, G. Nord, O. Payrastre, D. Zoccatelli, and M. Borga (2018), Integrated high-resolution dataset of high-intensity European and mediterranean flash floods, *Earth System Science Data*, 10(4), 1783–1794, doi:10.5194/essd-10-1783-2018.
- Antonetti, M., and M. Zappa (2018), How can expert knowledge increase the realism of conceptual hydrological models? A case study based on the concept of dominant runoff process in the Swiss Pre-Alps, *Hydrology and Earth System Sciences*, 22(8), 4425–4447, doi:10.5194/hess-22-4425-2018.
- Auer, I., R. Böhm, A. Jurković, A. Orlik, R. Potzmann, W. Schöner, M. Ungersböck, M. Brunetti, T. Nanni, M. Maugeri, K. Briffa, P. Jones, D. Efthymiadis, O. Mestre, J.-M. Moisselin, M. Begert, R. Brazdil, O. Bochnicek, T. Cegnar, M. Gajić-čapka, K. Zaninović, Majstorović, S. Szalai, T. Szentimrey, and L. Mercalli (2005), A new instrumental precipitation dataset for the greater Alpine region for the period 1800–2002, *International Journal of Climatology*, 25(2), 139–166, doi:10.1002/joc.1135.
- Bach, L., C. Schraff, J. D. Keller, and A. Hense (2016), Towards a probabilistic regional reanalysis system for Europe: evaluation of precipitation from experiments, *Tellus Series A—Dynamic Meteorology and Oceanography*, 68(1), 32,209, doi:10.3402/tellusa.v68.32209.
- Ban, N., J. Schmidli, and C. Schär (2014), Evaluation of the convection-resolving regional climate modeling approach in decade-long simulations, *Journal of Geophysical Research: Atmospheres*, 119(13), 7889–7907, doi:10.1002/2014JD021478.

- Ban, N., J. Schmidli, and C. Schär (2015), Heavy precipitation in a changing climate: Does short-term summer precipitation increase faster?, *Geophysical Research Letters*, *42*(4), 1165–1172, doi:10.1002/2014GL062588.
- Bao, J., S. C. Sherwood, L. V. Alexander, and J. P. Evans (2017a), Future increases in extreme precipitation exceed observed scaling rates, *Nature Climate Change*, *7*(2), 128–132, doi:10.1038/nclimate3201.
- Bao, J., S. C. Sherwood, M. Colin, and V. Dixit (2017b), The robust relationship between extreme precipitation and convective organization in idealized numerical modeling simulations, *Journal of Advances in Modeling Earth Systems*, *9*(6), 2291–2303, doi:10.1002/2017MS001125.
- Bao, J., S. C. Sherwood, L. V. Alexander, and J. P. Evans (2018), Comments on “Temperature-extreme precipitation scaling: a two-way causality?”, *International Journal of Climatology*, *38*(12), 4661–4663, doi:10.1002/joc.5665.
- Barbero, R., S. Westra, G. Lenderink, and H. J. Fowler (2017), Temperature-extreme precipitation scaling: a two-way causality?, *International Journal of Climatology*, *38*(S1), e1274–e1279, doi:10.1002/joc.5370.
- Beck, H. E., N. Vergopolan, M. Pan, V. Levizzani, A. I. J. M. van Dijk, G. P. Weedon, L. Brocca, F. Pappenberger, G. J. Huffman, and E. F. Wood (2017), Global-scale evaluation of 22 precipitation datasets using gauge observations and hydrological modeling, *Hydrology and Earth System Sciences*, *21*(12), 6201–6217, doi:10.5194/hess-21-6201-2017.
- Becker, A., P. Finger, A. Meyer-Christoffer, B. Rudolf, K. Schamm, U. Schneider, and M. Ziese (2013), A description of the global land-surface precipitation data products of the Global Precipitation Climatology Centre with sample applications including centennial (trend) analysis from 1901–present, *Earth System Science Data*, *5*(1), 71–99, doi:10.5194/essd-5-71-2013.
- Belachsen, I., F. Marra, N. Peleg, and E. Morin (2017), Convective rainfall in a dry climate: relations with synoptic systems and flash-flood generation in the Dead Sea region, *Hydrology and Earth System Sciences*, *21*(10), 5165–5180, doi:10.5194/hess-21-5165-2017.
- Berg, P., and J. O. Haerter (2013), Unexpected increase in precipitation intensity with temperature - A result of mixing of precipitation types?, *Atmospheric Research*, *119*, 56–61, doi:10.1016/j.atmosres.2011.05.012.

- Berg, P., C. Moseley, and J. O. Haerter (2013), Strong increase in convective precipitation in response to higher temperatures, *Nature Geoscience*, *6*(3), 181–185, doi:10.1038/ngeo1731.
- Bernet, D. B., V. Prasuhn, and R. Weingartner (2017), Surface water floods in Switzerland: What insurance claim records tell us about the damage in space and time, *Natural Hazards and Earth System Sciences*, *17*(9), 1659–1682, doi:10.5194/nhess-17-1659-2017.
- Bernet, D. B., A. P. Zischg, V. Prasuhn, and R. Weingartner (2018), Modeling the extent of surface water floods in rural areas: Lessons learned from the application of various uncalibrated models, *Environmental Modelling & Software*, *109*, 134–151, doi:10.1016/j.envsoft.2018.08.005.
- Blenkinsop, S., H. J. Fowler, R. Barbero, S. C. Chan, S. B. Guerreiro, E. Kendon, G. Lenderink, E. Lewis, X.-F. Li, S. Westra, L. Alexander, R. P. Allan, P. Berg, R. J. H. Dunn, M. Ekström, J. P. Evans, G. Holland, R. Jones, E. Kjellström, A. Klein-Tank, D. Lettenmaier, V. Mishra, A. F. Prein, J. Sheffield, and M. R. Tye (2018), The INTENSE Project: Using observations and models to understand the past, present and future of sub-daily rainfall extremes, *Advances in Science and Research*, *15*, 117–126, doi:10.5194/asr-15-117-2018.
- Bloeschl, G., J. Hall, J. Parajka, R. A. P. Perdigao, B. Merz, B. Arheimer, G. T. Aronica, A. Bilibashi, O. Bonacci, M. Borga, I. Canjevac, A. Castellarin, G. B. Chirico, P. Claps, K. Fiala, N. Frolova, L. Gorbachova, A. Gul, J. Hannaford, S. Harrigan, M. Kireeva, A. Kiss, T. R. Kjeldsen, S. Kohnova, J. J. Koskela, O. Ledvinka, N. Macdonald, M. Mavrova-Guirguinova, L. Mediero, R. Merz, P. Molnar, A. Montanari, C. Murphy, M. Osuch, V. Ovcharuk, I. Radevski, M. Rogger, J. L. Salinas, E. Sauquet, M. Sraj, J. Szolgay, A. Viglione, E. Volpi, D. Wilson, K. Zaimi, and N. Zivkovic (2017), Changing climate shifts timing of european floods, *Science*, *357*(6351), 588–590, doi:10.1126/science.aan2506.
- Brönnimann, S., J. Rajczak, E. M. Fischer, C. C. Raible, M. Rohrer, and C. Schär (2018), Changing seasonality of moderate and extreme precipitation events in the Alps, *Natural Hazards and Earth System Sciences*, *18*(7), 2047–2056, doi:10.5194/nhess-18-2047-2018.
- Bronstert, A., A. Agarwal, B. Boessenkool, I. Crisologo, M. Fischer, M. Heistermann, L. Koehn-Reich, J. Andres Lopez-Tarazon, T. Moran, U. Ozturk,



- C. Reinhardt-Imjela, and D. Wendi (2018), Forensic hydro-meteorological analysis of an extreme flash flood: The 2016-05-29 event in Braunsbach, SW Germany, *Science of the Total Environment*, *630*, 977–991, doi:10.1016/j.scitotenv.2018.02.241.
- CCCA (2016), Endbericht ÖKS15 – Klimaszenarien für Österreich – Daten – Methoden – Klimaanalyse, Version 1., *Tech. rep.*, Climate Change Centre Austria CCCA, PID: <https://hdl.handle.net/20.500.11756/06edd0c9>. [October 27, 2018].
- Cecinati, F., M. A. Rico-Ramirez, G. B. M. Heuvelink, and D. Han (2017), Representing radar rainfall uncertainty with ensembles based on a time-variant geostatistical error modelling approach, *Journal of Hydrology*, *548*, 391–405, doi:10.1016/j.jhydrol.2017.02.053.
- Chan, S. C., E. J. Kendon, N. M. Roberts, H. J. Fowler, and S. Blenkinsop (2016), Downturn in scaling of UK extreme rainfall with temperature for future hottest days, *Nature Geoscience*, *9*(1), 24–28, doi:10.1038/ngeo2596.
- Chan, S. C., E. J. Kendon, N. Roberts, S. Blenkinsop, and H. J. Fowler (2018), Large-scale predictors for extreme hourly precipitation events in convection-permitting climate simulations, *Journal of Climate*, *31*(6), 2115–2131, doi:10.1175/JCLI-D-17-0404.1.
- Chen, M., W. Shi, P. Xie, V. B. S. Silva, V. E. Kousky, R. Wayne Higgins, and J. E. Janowiak (2008), Assessing objective techniques for gauge-based analyses of global daily precipitation, *Journal of Geophysical Research: Atmospheres*, *113*(D4), D04,110, doi:10.1029/2007JD009132.
- Coles, S. (2001), *An Introduction to Statistical Modeling of Extreme Values*, 209 pp., Springer-Verlag, London, doi:10.1007/978-1-4471-3675-0.
- Cornes, R. C., G. van der Schrier, E. J. M. van den Besselaar, and P. D. Jones (2018), An ensemble version of the E–OBS temperature and precipitation data sets, *Journal of Geophysical Research-Atmospheres*, *123*(17), 9391–9409, doi:10.1029/2017JD028200.
- Cortès, M., M. C. Llasat, J. Gilabert, M. Llasat-Botija, M. Turco, R. Marcos, J. P. Martín Vide, and L. Falcón (2018), Towards a better understanding of the evolution of the flood risk in Mediterranean urban areas: the case of Barcelona, *Natural Hazards*, *93*(1), 39–60, doi:10.1007/s11069-017-3014-0.

- Cortès, M., M. Turco, M. Llasat-Botija, and M. C. Llasat (2018), The relationship between precipitation and insurance data for floods in a Mediterranean region (northeast Spain), *Natural Hazards and Earth System Sciences*, 18(3), 857–868, doi:10.5194/nhess-18-857-2018.
- Dai, A., R. M. Rasmussen, C. Liu, K. Ikeda, and A. F. Prein (2017), A new mechanism for warm-season precipitation response to global warming based on convection-permitting simulations, *Climate Dynamics*, pp. 1–26, doi:10.1007/s00382-017-3787-6, advanced online publication.
- Dee, D. P., S. M. Uppala, A. J. Simmons, P. Berrisford, P. Poli, S. Kobayashi, U. Andrae, M. A. Balmaseda, G. Balsamo, P. Bauer, P. Bechtold, A. C. M. Beljaars, L. van de Berg, J. Bidlot, N. Bormann, C. Delsol, R. Dragani, M. Fuentes, A. J. Geer, L. Haimberger, S. B. Healy, H. Hersbach, E. V. Hölm, L. Isaksen, P. Kållberg, M. Köhler, M. Matricardi, A. P. McNally, B. M. Monge-Sanz, J.-J. Morcrette, B.-K. Park, C. Peubey, P. de Rosnay, C. Tavolato, J.-N. Thépaut, and F. Vitart (2011), The ERA-Interim reanalysis: Configuration and performance of the data assimilation system, *Quarterly Journal of the Royal Meteorological Society*, 137(656), 553–597, doi:10.1002/qj.828.
- Di Baldassarre, G., H. Kreibich, S. Vorogushyn, J. Aerts, K. Arnbjerg-Nielsen, M. Barendrecht, P. Bates, M. Borga, W. Botzen, P. Bubeck, B. De Marchi, C. Llasat, M. Mazzoleni, D. Molinari, E. Mondino, J. Mård, O. Petrucci, A. Scolobig, A. Viglione, and P. J. Ward (2018), HESS opinions: An interdisciplinary research agenda to explore the unintended consequences of structural flood protection, *Hydrology and Earth System Sciences Discussions*, 2018, 1–11, doi:10.5194/hess-2018-333.
- Dittus, A. J., D. J. Karoly, M. G. Donat, S. C. Lewis, and L. V. Alexander (2018), Understanding the role of sea surface temperature-forcing for variability in global temperature and precipitation extremes, *Weather and Climate Extremes*, 21, 1–9, doi:doi.org/10.1016/j.wace.2018.06.002.
- Drobinski, P., B. Alonzo, S. Bastin, N. Da Silva, and C. Muller (2016), Scaling of precipitation extremes with temperature in the French Mediterranean region: What explains the hook shape?, *Journal of Geophysical Research-Atmospheres*, 121(7), 3100–3119, doi:10.1002/2015JD023497.
- Duethmann, D., and G. Blöschl (2018), Why has catchment evaporation increased

in the past 40 years? A data-based study in Austria, *Hydrology and Earth System Sciences*, 22(10), 5143–5158, doi:10.5194/hess-22-5143-2018.

Easterling, D. R., G. A. Meehl, C. Parmesan, S. A. Changnon, T. R. Karl, and L. O. Mearns (2000), Climate extremes: Observations, modeling, and impacts, *Science*, 289(5487), 2068–2074, doi:10.1126/science.289.5487.2068.

Eggert, B., P. Berg, J. O. Haerter, D. Jacob, and C. Moseley (2015), Temporal and spatial scaling impacts on extreme precipitation, *Atmospheric Chemistry and Physics*, 15(10), 5957–5971, doi:10.5194/acp-15-5957-2015.

Ettinger, S., L. Mounaud, C. Magill, A.-F. Yao-Lafourcade, J.-C. Thouret, V. Manville, C. Negulescu, G. Zuccaro, D. De Gregorio, S. Nardone, J. A. L. Uchuchoque, A. Arguedas, L. Macedo, and N. Manrique Llerena (2016), Building vulnerability to hydro-geomorphic hazards: Estimating damage probability from qualitative vulnerability assessment using logistic regression, *Journal of Hydrology*, 541, 563–581, doi:10.1016/j.jhydrol.2015.04.017.

Fischer, E., and R. Knutti (2016), Observed heavy precipitation increase confirms theory and early models, *Nature Climate Change*, 6, 986–991, doi:10.1038/nclimate3110.

Foehn, A., J. G. Hernández, B. Schaeffli, and G. D. Cesare (2018), Spatial interpolation of precipitation from multiple rain gauge networks and weather radar data for operational applications in alpine catchments, *Journal of Hydrology*, 563, 1092–1110, doi:10.1016/j.jhydrol.2018.05.027.

Formayer, H., and A. Fritz (2016), Temperature dependency of hourly precipitation intensities – surface versus cloud layer temperature, *International Journal of Climatology*, 37(1), 1–10, doi:10.1002/joc.4678.

Fuchs, S., M. Keiler, and A. Zischg (2015), A spatiotemporal multi-hazard exposure assessment based on property data, *Natural Hazards and Earth System Sciences*, 15(9), 2127–2142, doi:10.5194/nhess-15-2127-2015.

Furl, C., D. Ghebreyesus, and H. O. Sharif (2018), Assessment of the performance of satellite-based precipitation products for flood events across diverse spatial scales using GSSHA modeling system, *Geosciences*, 8(6), 191, doi:10.3390/geosciences8060191.

- Gabella, M., P. Speirs, U. Hamann, U. Germann, and A. Berne (2017), Measurement of precipitation in the Alps using dual-polarization C-Band ground-based radars, the GPM spaceborne Ku-Band radar, and rain gauges, *Remote Sensing*, *9*(11), doi:10.3390/rs9111147.
- Garsaball, E. C., and H. Markov (2017), Climate change: are building codes keeping up? a case study on hurricanes in the caribbean, *Proceedings of the Institution of Civil Engineers-Forensic Engineering*, *170*(2), 67–71, doi:10.1680/jfoen.16.00034.
- Gensini, V. A., and J. T. Allen (2018), US hail frequency and the global wind oscillation, *Geophysical Research Letters*, *45*(3), 1611–1620, doi:10.1002/2017GL076822.
- Gilleland, E., and R. W. Katz (2016), extremes 2.0: An extreme value analysis package in r, *Journal of Statistical Software*, *72*(8), 1–39, doi:10.18637/jss.v072.i08.
- Goodrich, D. C., T. O. Keefer, C. L. Unkrich, M. H. Nichols, H. B. Osborn, J. J. Stone, and J. R. Smith (2008), Long-term precipitation database, Walnut Gulch Experimental Watershed, Arizona, United States, *Water Resources Research*, *44*(5), W05S04, doi:10.1029/2006WR005782.
- Gubler, S., S. Hunziker, M. Begert, M. Croci-Maspoli, T. Konzelmann, S. Brönnimann, C. Schwierz, C. Oria, and G. Rosas (2017), The influence of station density on climate data homogenization, *International Journal of Climatology*, *37*(13), 4670–4683, doi:10.1002/joc.5114.
- Guerreiro, S. B., H. J. Fowler, R. Barbero, S. Westra, G. Lenderink, S. Blenkinsop, E. Lewis, and X.-F. Li (2018), Detection of continental-scale intensification of hourly rainfall extremes, *Nature Climate Change*, *8*(9), 803–807, doi:10.1038/s41558-018-0245-3.
- Haerter, J. O., P. Berg, and C. Moseley (2017), Precipitation onset as the temporal reference in convective self-organization, *Geophysical Research Letters*, *44*(12), 6450–6459, doi:10.1002/2017GL073342.
- Haiden, T., A. Kann, C. Wittmann, G. Pistotnik, B. Bica, and C. Gruber (2010), The integrated nowcasting through comprehensive analysis (INCA) system and its validation over the eastern Alpine region, *Weather and Forecasting*, *26*(2), 166–183, doi:10.1175/2010WAF2222451.1.

- Handler, S. L., and C. R. Homeyer (2018), Radar-observed bulk microphysics of midlatitude leading-line trailing-stratiform mesoscale convective systems, *Journal of Applied Meteorology and Climatology*, 57(10), 2231–2248, doi:10.1175/JAMC-D-18-0030.1.
- Hardwick Jones, R., S. Westra, and A. Sharma (2010), Observed relationships between extreme sub-daily precipitation, surface temperature, and relative humidity, *Geophysical Research Letters*, 37(22), doi:10.1029/2010GL045081.
- Held, I. M., and B. J. Soden (2006), Robust responses of the hydrological cycle to global warming, *Journal of Climate*, 19(21), 5686–5699, doi:10.1175/JCLI3990.1.
- Herrera, S., S. Kotlarski, P. M. M. Soares, R. M. Cardoso, A. Jacewski, J. M. Gutiérrez, and D. Maraun (2018), Uncertainty in gridded precipitation products: Influence of station density, interpolation method and grid resolution, *International Journal of Climatology*, doi:10.1002/joc.5878, advanced online publication.
- Hiebl, J., and C. Frei (2016), Daily temperature grids for Austria since 1961 – concept, creation and applicability, *Theoretical and Applied Climatology*, 124(1-2), 161–178, doi:10.1007/s00704-015-1411-4.
- Hoffmann, P. (2018), Enhanced seasonal predictability of the summer mean temperature in Central Europe favored by new dominant weather patterns, *Climate Dynamics*, 50(7-8), 2799–2812, doi:10.1007/s00382-017-3772-0.
- Hofstaetter, M., A. Lexer, M. Homann, and G. Bloeschl (2018), Large-scale heavy precipitation over central Europe and the role of atmospheric cyclone track types, *International Journal of Climatology*, 38(1), e497–e517, doi:10.1002/joc.5386.
- Hohmann, C., G. Kirchengast, and S. Birk (2018), Alpine foreland running drier? Sensitivity of a drought vulnerable catchment to changes in climate, land use, and water management, *Climatic Change*, 147(1), 179–193, doi:10.1007/s10584-017-2121-y.
- Hooshyar, M., D. Wang, S. Kim, S. C. Medeiros, and S. C. Hagen (2015), Valley and channel networks extraction based on local topographic curvature and k-means clustering of contours, *Water Resources Research*, 52(10), 8081–8102, doi:10.1002/2015WR018479.

- Huntington, T. G. (2006), Evidence for intensification of the global water cycle: Review and synthesis, *Journal of Hydrology*, *319*(1), 83–95, doi:10.1016/j.jhydrol.2005.07.003.
- hydroConsult GmbH (2011), Hochwasserdokumentation Wölzertal 7.7.2011, *Tech. rep.*, Amt der Steiermärkischen Landesregierung FA19B.
- IPCC (2013), *Climate Change 2013: The Physical Science Basis. Contribution of Working Group I to the Fifth Assessment Report of the Intergovernmental Panel on Climate Change*, Cambridge University Press, Cambridge, United Kingdom and New York, NY, USA, doi:10.1017/CBO9781107415324.
- Isotta, F. A., C. Frei, V. Weilguni, M. Perčec Tadić, P. Lassègues, B. Rudolf, V. Pavan, C. Cacciamani, G. Antolini, S. M. Ratto, M. Munari, S. Micheletti, V. Bonati, C. Lussana, C. Ronchi, E. Panettieri, G. Marigo, and G. Vertačnik (2014), The climate of daily precipitation in the Alps: Development and analysis of a high-resolution grid dataset from pan-Alpine rain-gauge data, *International Journal of Climatology*, *34*(5), 1657–1675, doi:10.1002/joc.3794.
- Jurgilevich, A., A. Rasanen, F. Groundstroem, and S. Juhola (2017), A systematic review of dynamics in climate risk and vulnerability assessments, *Environmental Research Letters*, *12*(1), 013,002, doi:10.1088/1748-9326/aa5508.
- Kabas, T., U. Foelsche, and G. Kirchengast (2011), Seasonal and annual trends of temperature and precipitation within 1951/1971–2007 in south-eastern Styria, Austria, *Meteorologische Zeitschrift*, *20*(3), 277–289, doi:10.1127/0941-2948/2011/0233.
- Kann, A., I. Meirold-Mautner, F. Schmid, G. Kirchengast, J. Fuchsberger, V. Meyer, L. Tächler, and B. Bica (2015), Evaluation of high-resolution precipitation analyses using a dense station network, *Hydrology and Earth System Sciences*, *19*(3), 1547–1559, doi:10.5194/hess-19-1547-2015.
- Kendon, E. J., N. Ban, N. M. Roberts, H. J. Fowler, M. J. Roberts, S. C. Chan, J. P. Evans, G. Fosser, and J. M. Wilkinson (2016), Do convection-permitting regional climate models improve projections of future precipitation change?, *Bulletin of the American Meteorological Society*, *98*, 79–93, doi:10.1175/BAMS-D-15-0004.1.
- Kirchengast, G., T. Kabas, A. Leuprecht, C. Bichler, and H. Truhetz (2014), WegenerNet: A pioneering high-resolution network for monitoring weather and

climate, *Bulletin of the American Meteorological Society*, 95(2), 227–242, doi:10.1175/BAMS-D-11-00161.1.

Koenker, R. (2005), *Quantile regression*, Cambridge University Press, New York.

Kotlarski, S., P. Szabó, S. Herrera, O. Ráty, K. Keuler, P. M. Soares, R. M. Cardoso, T. Bosshard, C. Pagé, F. Boberg, J. M. Gutiérrez, F. A. Isotta, A. Jaczewski, F. Kreienkamp, M. A. Liniger, C. Lussana, and K. Pianko-Kluczyńska (2017), Observational uncertainty and regional climate model evaluation: a pan-European perspective, *International Journal of Climatology*, doi:10.1002/joc.5249, advanced online publication.

Koutsoyiannis, D. (2004), On the appropriateness of the gumbel distribution for modelling extreme rainfall (solicited), in *Hydrological Risk: recent advances in peak river flow modelling, prediction and real-time forecasting. Assessment of the impacts of land-use and climate changes*, edited by A. Brath, A. Montanari, and E. Toth, pp. 303–319, Editoriale Bios, Castrolibero, Italy, doi:10.13140/RG.2.1.3811.6080.

Kreibich, H., G. Di Baldassarre, S. Vorogushyn, J. C. J. H. Aerts, H. Apel, G. T. Aronica, K. Arnbjerg-Nielsen, L. M. Bouwer, P. Bubeck, T. Caloiero, D. T. Chinh, M. Cortés, A. K. Gain, V. Giampá, C. Kuhlicke, Z. W. Kundzewicz, M. C. Llasat, J. Mørd, P. Matczak, M. Mazzoleni, D. Molinari, N. V. Dung, O. Petrucci, K. Schröter, K. Slager, A. H. Thielen, P. J. Ward, and B. Merz (2017), Adaptation to flood risk: Results of international paired flood event studies, *Earth's Future*, 5(6), 953–965, doi:10.1002/2017EF000606.

Laudan, J., V. Roezer, T. Sieg, K. Vogel, and A. H. Thielen (2017), Damage assessment in Braunsbach 2016: data collection and analysis for an improved understanding of damaging processes during flash floods, *Natural Hazards and Earth System Sciences*, 17(12), 2163–2179, doi:10.5194/nhess-17-2163-2017.

Lenderink, G., and H. J. Fowler (2017), Understanding rainfall extremes, *Nature Climate Change*, 7(6), 391–393, doi:10.1038/nclimate3305.

Lenderink, G., and E. van Meijgaard (2009), Unexpected rise in extreme precipitation caused by a shift in rain type?, *Nature Geoscience*, 2(6), 373–373, doi:10.1038/ngeo524.

- Lenderink, G., R. Barbero, S. Westra, and H. J. Fowler (2018), Reply to comments on “Temperature-extreme precipitation scaling: a two-way causality?”, *International Journal of Climatology*, *38*(12), 4664–4666, doi:10.1002/joc.5799.
- Lewis, E., N. Quinn, S. Blenkinsop, H. J. Fowler, J. Freer, M. Tanguy, O. Hitt, G. Coxon, P. Bates, and R. Woods (2018), A rule based quality control method for hourly rainfall data and a 1-km resolution gridded hourly rainfall dataset for Great Britain: CEH-GEAR1hr, *Journal of Hydrology*, *564*, 930–943, doi:10.1016/j.jhydrol.2018.07.034.
- Lochbihler, K., G. Lenderink, and A. P. Siebesma (2017), The spatial extent of rainfall events and its relation to precipitation scaling, *Geophysical Research Letters*, *44*(16), 8629–8636, doi:10.1002/2017GL074857.
- Loriaux, J. M., G. Lenderink, S. R. De Roode, and A. P. Siebesma (2013), Understanding convective extreme precipitation scaling using observations and an entraining plume model, *Journal of the Atmospheric Sciences*, *70*(11), 3641–3655, doi:10.1175/JAS-D-12-0317.1.
- Loriaux, J. M., G. Lenderink, and A. P. Siebesma (2016a), Large-scale controls on extreme precipitation, *Journal of Climate*, *30*(3), 955–968, doi:10.1175/JCLI-D-16-0381.1.
- Loriaux, J. M., G. Lenderink, and A. P. Siebesma (2016b), Peak precipitation intensity in relation to atmospheric conditions and large-scale forcing at mid-latitudes, *Journal of Geophysical Research: Atmospheres*, *121*(10), 5471–5487, doi:10.1002/2015JD024274.
- Madonna, E., D. Ginsbourger, and O. Martius (2018), A poisson regression approach to model monthly hail occurrence in Northern Switzerland using large-scale environmental variables, *Atmospheric Research*, *203*, 261–274, doi:10.1016/j.atmosres.2017.11.024.
- Mård, J., G. Di Baldassarre, and M. Mazzoleni (2018), Nighttime light data reveal how flood protection shapes human proximity to rivers, *Science Advances*, *4*(8), doi:10.1126/sciadv.aar5779.
- Marra, F., and E. Morin (2018), Autocorrelation structure of convective rainfall in semiarid-arid climate derived from high-resolution X-band radar estimates, *Atmospheric Research*, *200*, 126–138, doi:10.1016/j.atmosres.2017.09.020.



- Marra, F., E. Destro, E. I. Nikolopoulos, D. Zoccatelli, J. D. Creutin, F. Guzzetti, and M. Borga (2017), Impact of rainfall spatial aggregation on the identification of debris flow occurrence thresholds, *Hydrology and Earth System Sciences*, *21*(9), 4525–4532, doi:10.5194/hess-21-4525-2017.
- McKinnon, K. A., and C. Deser (2018), Internal variability and regional climate trends in an observational large ensemble, *Journal of Climate*, *31*(17), 6783–6802, doi:10.1175/JCLI-D-17-0901.1.
- Messori, A., M. Morabito, G. Messori, G. Brandani, M. Petralli, F. Natali, D. Griffoni, A. Crisci, G. Gensini, and S. Orlandini (2015), Weather-related flood and landslide damage: A risk index for Italian regions, *Plos One*, *10*(12), e0144468, doi:10.1371/journal.pone.0144468.
- Mishra, V., J. M. Wallace, and D. P. Lettenmaier (2012), Relationship between hourly extreme precipitation and local air temperature in the United States, *Geophysical Research Letters*, *39*(16), L16,403, doi:10.1029/2012GL052790.
- Moftakhari, H. R., A. AghaKouchak, B. F. Sanders, and R. A. Matthew (2017), Cumulative hazard: The case of nuisance flooding, *Earth's Future*, *5*(2), 214–223, doi:10.1002/2016EF000494.
- Moftakhari, H. R., A. AghaKouchak, B. F. Sanders, M. Allaire, and R. A. Matthew (2018), What is nuisance flooding? Defining and monitoring an emerging challenge, *Water Resources Research*, *54*(7), 4218–4227, doi:10.1029/2018WR022828.
- Mohr, S., M. Kunz, and B. Geyer (2015), Hail potential in Europe based on a regional climate model hindcast, *Geophysical Research Letters*, *42*(24), 10,904–10,912, doi:10.1002/2015GL067118.
- Molnar, P., S. Fatichi, L. Gaál, J. Szolgay, and P. Burlando (2015), Storm type effects on super Clausius-Clapeyron scaling of intense rainstorm properties with air temperature, *Hydrology and Earth System Sciences*, *19*(4), 1753–1766, doi:10.5194/hess-19-1753-2015.
- Morss, R. E., O. V. Wilhelmi, G. A. Meehl, and L. Dilling (2011), Improving societal outcomes of extreme weather in a changing climate: An integrated perspective, in *Annual Review of Environment and Resources*, VOL 36, *Annual Review of Environment and Resources*, vol. 36, edited by A. Gadgil

- and D. Liverman, pp. 1–25, Annual Reviews, Palo Alto, CA, USA, doi:10.1146/annurev-environ-060809-100145.
- Moseley, C., C. Hohenegger, P. Berg, and J. O. Haerter (2016), Intensification of convective extremes driven by cloud-cloud interaction, *Nature Geoscience*, *9*(10), 748–752, doi:10.1038/ngeo2789.
- Mroz, K., A. Battaglia, T. J. Lang, S. Tanelli, and G. F. Sacco (2018), Global precipitation measuring dual-frequency precipitation radar observations of hailstorm vertical structure: Current capabilities and drawbacks, *Journal of Applied Meteorology and Climatology*, *57*(9), 2161–2178, doi:10.1175/JAMC-D-18-0020.1.
- Muller, C., and P. O’Gorman (2011), An energetic perspective on the regional response of precipitation to climate change, *Nature Climate Change*, *1*, 266–271, doi:10.1038/nclimate1169.
- Müller, H., and U. Haberlandt (2018), Temporal rainfall disaggregation using a multiplicative cascade model for spatial application in urban hydrology, *Journal of Hydrology*, *556*, 847–864, doi:10.1016/j.jhydrol.2016.01.031.
- Nie, J., A. H. Sobel, D. A. Shaevitz, and S. Wang (2018), Dynamic amplification of extreme precipitation sensitivity, *Proceedings of the National Academy of Sciences*, doi:10.1073/pnas.1800357115, advanced online publication.
- Nilsen, I. B., J. H. Stagge, and L. M. Tallaksen (2017), A probabilistic approach for attributing temperature changes to synoptic type frequency, *International Journal of Climatology*, *37*(6), 2990–3002, doi:10.1002/joc.4894.
- Nisi, L., O. Martius, A. Hering, M. Kunz, and U. Germann (2016), Spatial and temporal distribution of hailstorms in the Alpine region: A long-term, high resolution, radar-based analysis, *Quarterly Journal of the Royal Meteorological Society*, *142*(697), 1590–1604, doi:10.1002/qj.2771.
- O, S., U. Foelsche, G. Kirchengast, and J. Fuchsberger (2018), Validation and correction of rainfall data from the WegenerNet high density network in southeast Austria, *Journal of Hydrology*, *556*, 1110–1122, doi:10.1016/j.jhydrol.2016.11.049.
- O’Gorman, P. A. (2015), Precipitation extremes under climate change, *Current Climate Change Reports*, *1*(2), 49–59, doi:10.1007/s40641-015-0009-3.

- O’Gorman, P. A., and T. Schneider (2009a), Scaling of precipitation extremes over a wide range of climates simulated with an idealized GCM, *Journal of Climate*, *22*(21), 5676–5685, doi:10.1175/2009JCLI2701.1.
- O’Gorman, P. A., and T. Schneider (2009b), The physical basis for increases in precipitation extremes in simulations of 21st-century climate change, *Proceedings of the National Academy of Sciences*, *106*(35), 14,773–14,777, doi:10.1073/pnas.0907610106.
- Panziera, L., M. Gabella, U. Germann, and O. Martins (2018), A 12-year radar-based climatology of daily and sub-daily extreme precipitation over the Swiss Alps, *International Journal of Climatology*, *38*(10), 3749–3769, doi:10.1002/joc.5528.
- Peleg, N., F. Marra, S. Fatichi, A. Paschalis, P. Molnar, and P. Burlando (2016), Spatial variability of extreme rainfall at radar subpixel scale, *Journal of Hydrology*, doi:10.1016/j.jhydrol.2016.05.033.
- Peleg, N., F. Marra, S. Fatichi, P. Molnar, E. Morin, A. Sharma, and P. Burlando (2018), Intensification of convective rain cells at warmer temperatures observed from high-resolution weather radar data, *Journal of Hydrometeorology*, *19*(4), 715–726, doi:10.1175/JHM-D-17-0158.1.
- Pendergrass, A. G. (2018), What precipitation is extreme?, *Science*, *360*(6393), 1072–1073, doi:10.1126/science.aat1871.
- Pendergrass, A. G., and E. P. Gerber (2016), The rain is askew: Two idealized models relating vertical velocity and precipitation distributions in a warming world, *Journal of Climate*, *29*(18), 6445–6462, doi:10.1175/JCLI-D-16-0097.1.
- Pendergrass, A. G., and D. L. Hartmann (2014), Changes in the distribution of rain frequency and intensity in response to global warming, *Journal of Climate*, *27*(22), 8372–8383, doi:10.1175/JCLI-D-14-00183.1.
- Pendergrass, A. G., K. A. Reed, and B. Medeiros (2016), The link between extreme precipitation and convective organization in a warming climate: Global radiative-convective equilibrium simulations, *Geophysical Research Letters*, *43*(21), 445–452, doi:10.1002/2016GL071285.

- Pendergrass, A. G., R. Knutti, F. Lehner, and B. M. Sanderson (2017), Precipitation variability increases in a warmer climate, *Scientific Reports*, 7, doi:10.1038/s41598-017-17966-y, Article Nr. 17966.
- Perez-Morales, A., S. Gil-Guirado, and J. Olcina-Cantos (2018), Housing bubbles and the increase of flood exposure. Failures in flood risk management on the Spanish south-eastern coast (1975–2013), *Journal of Flood Risk Management*, 11(1), S302–S313, doi:10.1111/jfr3.12207.
- Pfahl, S., P. O’Gorman, and E. Fischer (2017), Understanding the regional pattern of projected future changes in extreme precipitation, *Nature Climate Change*, 7, 423–427, doi:10.1038/nclimate3287.
- Philipp, A., C. Beck, R. Huth, and J. Jacobeit (2016), Development and comparison of circulation type classifications using the COST 733 dataset and software, *International Journal of Climatology*, 36(7), 2673–2691, doi:10.1002/joc.3920.
- Phillips, R. C., S. Z. Samadi, and M. E. Meadows (2018), How extreme was the October 2015 flood in the Carolinas? An assessment of flood frequency analysis and distribution tails, *Journal of Hydrology*, 562, 648–663, doi:10.1016/j.jhydrol.2018.05.035.
- Prein, A. F., and A. Gobiet (2017), Impacts of uncertainties in European gridded precipitation observations on regional climate analysis, *International Journal of Climatology*, 37(1), 305–327, doi:10.1002/joc.4706.
- Prein, A. F., W. Langhans, G. Fosser, A. Ferrone, N. Ban, K. Goergen, M. Keller, M. Tölle, O. Gutjahr, F. Feser, E. Brisson, S. Kollet, J. Schmidli, N. P. M. van Lipzig, and R. Leung (2015), A review on regional convection-permitting climate modeling: Demonstrations, prospects, and challenges, *Reviews of Geophysics*, 53(2), 323–361, doi:10.1002/2014RG000475.
- Prein, A. F., G. J. Holland, R. M. Rasmussen, M. P. Clark, and M. R. Tye (2016), Running dry: The U.S. Southwest’s drift into a drier climate state, *Geophysical Research Letters*, 43(3), 1272–1279, doi:10.1002/2015GL066727.
- Prein, A. F., C. Liu, K. Ikeda, S. B. Trier, R. M. Rasmussen, G. J. Holland, and M. P. Clark (2017a), Increased rainfall volume from future convective storms in the US, *Nature Climate Change*, 7(12), 880–884, doi:10.1038/s41558-017-0007-7.

- Prein, A. F., R. M. Rasmussen, K. Ikeda, C. Liu, M. P. Clark, and G. J. Holland (2017b), The future intensification of hourly precipitation extremes, *Nature Climate Change*, 7(1), 48–52, doi:10.1038/nclimate3168.
- Schär, C., N. Ban, E. M. Fischer, J. Rajczak, J. Schmidli, C. Frei, F. Giorgi, T. R. Karl, E. J. Kendon, A. M. G. K. Tank, P. A. O’Gorman, J. Sillmann, X. Zhang, and F. W. Zwiers (2016), Percentile indices for assessing changes in heavy precipitation events, *Climatic Change*, 137(1), 201–216, doi:10.1007/s10584-016-1669-2.
- Scherrer, S. C., E. M. Fischer, R. Posselt, M. A. Liniger, M. Croci-Maspoli, and R. Knutti (2016), Emerging trends in heavy precipitation and hot temperature extremes in Switzerland, *Journal of Geophysical Research: Atmospheres*, 121(6), 2626–2637, doi:10.1002/2015JD024634.
- Schiemann, R., and C. Frei (2010), How to quantify the resolution of surface climate by circulation types: An example for Alpine precipitation, *Physics and Chemistry of the Earth, Parts A/B/C*, 35(9-12), 403–410, doi:10.1016/j.pce.2009.09.005.
- Schroerer, K., and G. Kirchengast (2018), Sensitivity of extreme precipitation to temperature: the variability of scaling factors from a regional to local perspective, *Climate Dynamics*, 50(11), 3981–3994, doi:10.1007/s00382-017-3857-9.
- Schroerer, K., and M. R. Tye (2019), Quantifying damage contributions from convective and stratiform weather types: How well do precipitation and discharge data indicate the risk?, *Journal of Flood Risk Management*, 2019;12:e12491, e12,491, doi:10.1111/jfr3.12491.
- Schroerer, K., G. Kirchengast, and S. O (2018), Strong dependence of extreme convective precipitation intensities on gauge network density, *Geophysical Research Letters*, 45(16), 8253–8263, doi:10.1029/2018GL077994.
- Segoni, S., L. Piciullo, and S. L. Gariano (2018), A review of the recent literature on rainfall thresholds for landslide occurrence, *Landslides*, 15(8), 1483–1501, doi:10.1007/s10346-018-0966-4.
- Seibert, P., A. Frank, and H. Formayer (2006), Synoptic and regional patterns of heavy precipitation in Austria, *Theoretical and Applied Climatology*, 87(1-4), 139–153, doi:10.1007/s00704-006-0198-8.

- Sharghi, E., V. Nourani, S. Soleimani, and F. Sadikoglu (2018), Application of different clustering approaches to hydroclimatological catchment regionalization in mountainous regions, a case study in Utah State, *Journal of Mountain Science*, *15*(3), 461–484, doi:10.1007/s11629-017-4454-4.
- Sideris, I. V., M. Gabella, R. Erdin, and U. Germann (2014), Real-time radar-rain-gauge merging using spatio-temporal co-kriging with external drift in the alpine terrain of Switzerland, *Quarterly Journal of the Royal Meteorological Society*, *140*(680), 1097–1111, doi:10.1002/qj.2188.
- Sillmann, J., S. Russo, S. Sippel, and K. Alnes (2018), From hazard to risk, *Bulletin of the American Meteorological Society*, *99*(8), 1689–1693, doi:10.1175/BAMS-D-17-0327.1.
- Singer, M. B., K. Michaelides, and D. E. J. Hobley (2018), STORM 1.0: a simple, flexible, and parsimonious stochastic rainfall generator for simulating climate and climate change, *Geoscientific Model Development*, *11*(9), 3713–3726, doi:10.5194/gmd-11-3713-2018.
- Singleton, A., and R. Toumi (2012), Super-Clausius-Clapeyron scaling of rainfall in a model squall line, *Quarterly Journal of the Royal Meteorological Society*, *139*(671), 334–339, doi:10.1002/qj.1919.
- Spekkers, M., V. Roezer, A. Thielen, M.-C. ten Veldhuis, and H. Kreibich (2017), A comparative survey of the impacts of extreme rainfall in two international case studies, *Natural Hazards and Earth System Sciences*, *17*(8), 1337–1355, doi:10.5194/nhess-17-1337-2017.
- Storch, H. v., and F. W. Zwiers (1999), *Statistical Analysis in Climate Research*, Cambridge University Press, Cambridge, United Kingdom, doi:10.1017/CBO9780511612336.
- Strader, S. M., W. S. Ashley, T. J. Pingel, and A. J. Kremenec (2017a), Observed and projected changes in United States tornado exposure, *Weather Climate and Society*, *9*(2), 109–123, doi:10.1175/WCAS-D-16-0041.1.
- Strader, S. M., W. S. Ashley, T. J. Pingel, and A. J. Kremenec (2017b), Projected 21st century changes in tornado exposure, risk, and disaster potential, *Climatic Change*, *141*(2), 301–313, doi:10.1007/s10584-017-1905-4.

- Sun, Q., C. Miao, Q. Duan, H. Ashouri, S. Sorooshian, and K.-L. Hsu (2018), A review of global precipitation datasets: data sources, estimation, and intercomparisons, *Reviews of Geophysics*, *46*, 79–107, doi:10.1002/2017RG000574.
- Svensson, C., and D. A. Jones (2010), Review of methods for deriving areal reduction factors, *Journal of Flood Risk Management*, *3*(3), 232–245, doi:10.1111/j.1753-318X.2010.01075.x.
- Syed, K. H., D. C. Goodrich, D. E. Myers, and S. Sorooshian (2003), Spatial characteristics of thunderstorm rainfall fields and their relation to runoff, *Journal of Hydrology*, *271*(1), 1–21, doi:10.1016/S0022-1694(02)00311-6.
- Tandon, N. F., X. Zhang, and A. H. Sobel (2018), Understanding the dynamics of future changes in extreme precipitation intensity, *Geophysical Research Letters*, *45*(6), 2870–2878, doi:10.1002/2017GL076361.
- Towler, E., B. Rajagopalan, E. Gilleland, R. S. Summers, D. Yates, and R. W. Katz (2010), Modeling hydrologic and water quality extremes in a changing climate: A statistical approach based on extreme value theory, *Water Resources Research*, *46*, doi:10.1029/2009WR008876.
- Trenberth, K. E., A. Dai, R. M. Rasmussen, and D. B. Parsons (2003), The changing character of precipitation, *Bulletin of the American Meteorological Society*, *84*(9), 1205–1218, doi:10.1175/BAMS-84-9-1205.
- Trigg, M. A., C. E. Birch, J. C. Neal, P. D. Bates, A. Smith, C. C. Sampson, D. Yamazaki, Y. Hirabayashi, F. Pappenberger, E. Dutra, P. J. Ward, H. C. Winsemius, P. Salamon, F. Dottori, R. Rudari, M. S. Kappes, A. L. Simpson, G. Hadzilacos, and T. J. Fewtrell (2016), The credibility challenge for global fluvial flood risk analysis, *Environmental Research Letters*, *11*(9), 094,014.
- Unterberger, C. (2018), How flood damages to public infrastructure affect municipal budget indicators, *Economics of Disasters and Climate Change*, *2*(1), 5–20, doi:10.1007/s41885-017-0015-0.
- Unterberger, C., P. Hudson, W. W. Botzen, K. Schroeer, and K. W. Steininger (2019), Future public sector flood risk and risk sharing arrangements: An assessment for Austria, *Ecological Economics*, *156*, 153–163, doi:10.1016/j.ecolecon.2018.09.019.

- Vallorani, R., G. Bartolini, G. Betti, A. Crisci, B. Gozzini, D. Grifoni, M. Iannucilli, A. Messeri, G. Messeri, M. Morabito, and G. Maracchi (2017), Circulation type classifications for temperature and precipitation stratification in Italy, *International Journal of Climatology*, *38*(2), 915–931, doi:10.1002/joc.5219.
- Veneziano, D., and A. Langousis (2005), The areal reduction factor: A multifractal analysis, *Water Resources Research*, *41*(7), W07,008, doi:10.1029/2004WR003765.
- Villarini, G., and L. J. Slater (2018), Examination of changes in annual maximum gauge height in the Continental United States using quantile regression, *Journal of Hydrologic Engineering*, *23*(3), 06017,010, doi:10.1061/(ASCE)HE.1943-5584.0001620.
- Villarini, G., J. A. Smith, M. L. Baeck, R. Vitolo, D. B. Stephenson, and W. F. Krajewski (2011), On the frequency of heavy rainfall for the Midwest of the United States, *Journal of Hydrology*, *400*(1-2), 103–120, doi:10.1016/j.jhydrol.2011.01.027.
- Villarini, G., B.-C. Seo, F. Serinaldi, and W. F. Krajewski (2014), Spatial and temporal modeling of radar rainfall uncertainties, *ATMOSPHERIC RESEARCH*, *135*, 91–101, doi:10.1016/j.atmosres.2013.09.007.
- Wang, G., D. Wang, K. E. Trenberth, A. Erfanian, M. Yu, M. G. Bosilovich, and D. T. Parr (2017), The peak structure and future changes of the relationships between extreme precipitation and temperature, *Nature Climate Change*, *7*(4), 268–274, doi:10.1038/nclimate3239.
- Wang, Y., B. Geerts, and C. Liu (2018), A 30-year convection-permitting regional climate simulation over the interior western United States. Part I: Validation, *International Journal of Climatology*, *38*(9), 3684–3704, doi:10.1002/joc.5527.
- Wasko, C., and A. Sharma (2014), Quantile regression for investigating scaling of extreme precipitation with temperature, *Water Resources Research*, *50*(4), 3608–3614, doi:10.1002/2013WR015194.
- Wasko, C., and A. Sharma (2015), Steeper temporal distribution of rain intensity at higher temperatures within Australian storms, *Nature Geoscience*, *8*(7), 527–529, doi:10.1038/ngeo2456.



- Wasko, C., A. Sharma, and F. Johnson (2015), Does storm duration modulate the extreme precipitation-temperature scaling relationship?, *Geophysical Research Letters*, *42*(20), 2015GL066,274, doi:10.1002/2015GL066274.
- Wasko, C., A. Sharma, and S. Westra (2016), Reduced spatial extent of extreme storms at higher temperatures, *Geophysical Research Letters*, *43*(8), 4026–4032, doi:10.1002/2016GL068509.
- Wasko, C., W. Tang Lu, and R. Mehrotra (2018), Relationship of extreme precipitation, dry-bulb temperature, and dew point temperature across Australia, *Environmental Research Letters*, *13*, doi:10.1088/1748-9326/aad135, advanced online publication.
- Westra, S., H. J. Fowler, J. P. Evans, L. V. Alexander, P. Berg, F. Johnson, E. J. Kendon, G. Lenderink, and N. M. Roberts (2014), Future changes to the intensity and frequency of short-duration extreme rainfall, *Reviews of Geophysics*, *52*(3), 522–555, doi:10.1002/2014RG000464.
- Willner, S. N., A. Levermann, F. Zhao, and K. Frieler (2018), Adaptation required to preserve future high-end river flood risk at present levels, *Science Advances*, *4*(1), doi:10.1126/sciadv.aao1914.
- Wood, J. L., S. Harrison, T. a. R. Turkington, and L. Reinhardt (2016), Landslides and synoptic weather trends in the European Alps, *Climatic Change*, *136*(2), 297–308, doi:10.1007/s10584-016-1623-3.
- World Climate Research Program (2018), WCRP Coupled Model Intercomparison Project (CMIP), [Available online at <https://www.wcrp-climate.org/wgcm-cmip>, 25.09.2018].
- Ye, H., E. J. Fetzer, S. Wong, and B. H. Lambriksen (2017), Rapid decadal convective precipitation increase over Eurasia during the last three decades of the 20th century, *Science Advances*, *3*(1), doi:10.1126/sciadv.1600944.
- Zhang, X., L. Alexander, G. C. Hegerl, P. Jones, A. K. Tank, T. C. Peterson, B. Trewin, and F. W. Zwiers (2012), Indices for monitoring changes in extremes based on daily temperature and precipitation data, *Wiley Interdisciplinary Reviews: Climate Change*, *2*(6), 851–870, doi:10.1002/wcc.147.

Zhang, X., F. W. Zwiers, G. Li, H. Wan, and A. J. Cannon (2017), Complexity in estimating past and future extreme short-duration rainfall, *Nature Geoscience*, *10*(4), 255–259, doi:10.1038/ngeo2911.

Zittis, G. (2017), Observed rainfall trends and precipitation uncertainty in the vicinity of the Mediterranean, Middle East and North Africa, *Theoretical and Applied Climatology*, *134*(3–4), 1207–1230, doi:10.1007/s00704-017-2333-0.



*Abstract:*

Research on extreme convective precipitation events (ECPEs) is crucial to avoid damage and to better understand the climate system, but a lack of area-covering long-term measurements of the short-lived and localized storms hamper climatological analyses. This thesis explores uncertainties associated with ECPEs in the Austrian south-eastern Alpine forelands using sub-daily rain and stream gauge observations as well as damage data. Additional variables are used to define weather types and socioeconomic vulnerabilities. Different analytic and statistical methods are applied to quantify sampling biases and temperature sensitivities as well as damage contributions from ECPEs.

Using a novel technique to systematically thin out the 1.4 km × 1.4 km WegenerNet Feldbach region climate station network (WegenerNet), it is demonstrated that conventional rain gauge networks lead to severe underestimation of extreme area rainfall in convective storms. The rate of underestimation follows a power law with exponent -0.5 over inter-station distances from 1 km to 30 km. It is shown that damage reported to the Austrian disaster fund under convective weather types is systematically less correlated with precipitation extremes, as compared to stratiform weather systems. These findings are particularly relevant, as higher daily mean temperature has been shown to robustly correlate with an increase in precipitation extremes. This indicates that ECPEs might become more intense with climate warming; however, temporal trends and the role of dynamic processes need further research.

The thesis underlines the need for high resolution observations and strategies to implement sampling uncertainties into model evaluation and risk reduction strategies, as ECPEs significantly contribute to total damage and the risk from such events will likely increase.

*Zum Inhalt:*

Um das Klimasystem besser zu verstehen und Unwetterschäden zu begrenzen, ist die Erforschung kleinräumiger konvektiver Starkniederschlagsereignisse (KSNE) essenziell. Ein Mangel flächendeckender und lange zurückreichender Aufzeichnungen erschwert die Analyse dieser räumlich wie zeitlich hoch variablen Ereignisse.

Diese Dissertation erforscht KSNE im südöstlichen Alpenvorraum Österreichs und mit ihnen verbundene Unsicherheiten. Hierzu werden unter-tägliche Niederschlagsmessungen, Schadensmeldungen und Daten zur Bestimmung von Wetterlagen und sozioökonomischen Vulnerabilitäten mittels verschiedener analytischer und statistischer Methoden ausgewertet. Ein innovativer Ansatz dünnt das Klimastationsnetzwerk WegenerNet systematisch aus und kann so nachweisen, dass konventionelle Messnetze eine Unterschätzung der maximalen Flächenniederschläge von KSNE erheblich begünstigen. Darüber hinaus wird gezeigt, dass Schäden, die während konvektiver Wetterlagen gemeldet werden, systematisch seltener mit extremen Niederschlagsmessungen in Zusammenhang gebracht werden können, als Schäden, die bei Wetterlagen mit flächigem Niederschlag auftreten. Die Ergebnisse sind besonders relevant, weil unter-stündliche bis unter-tägliche Niederschlagsextreme robust und stark positiv mit der Lufttemperatur in Zusammenhang stehen. KSNE könnten daher mit fortschreitendem Klimawandel und einhergehender Erwärmung intensiver werden, wobei zeitliche Trends und die Rolle dynamischer Prozesse weiterhin von vielen Unsicherheiten geprägt sind.

Insgesamt zeigen die Ergebnisse dieser Dissertation, wie wichtig hochaufgelöste Beobachtungsdaten sind, um Strategien zu entwickeln, mithilfe derer Messunsicherheiten bei der Modellevaluierung und in der Naturgefahrenprävention besser berücksichtigt werden können. Vor dem Hintergrund steigender Durchschnittstemperaturen und einer wahrscheinlichen Zunahme der Intensität von KSNE ist dies besonders relevant.